

LOW MASS STARS WITH MASS LOSS
AND LOW-LUMINOSITY
CARBON STAR FORMATION

thesis by

Arnold I. Boothroyd

In Partial Fulfillment of the Requirements

For the Degree of

Doctor of Philosophy

California Institute of Technology

Pasadena, California

1987

(Submitted May 22, 1987)

ACKNOWLEDGEMENTS

It is a pleasure to express my gratitude to Dr. I.-J. Sackmann for patient encouragement, guidance and instruction, as well as to Professors R. D. Blandford, C. A. Barnes, S. E. Koonin, and S. C. Frautschi for their encouragement and support. I am also grateful to Professors S. C. Frautschi, J. Morgan, and A. Albee for the teaching assistantships that provided my financial support (and for a special grant for the final term). I have benefitted from valuable discussions with Professors W. A. Fowler, J. R. Mould, C. Rolfs, V. Weidemann, Z. Barkat, D. Sugimoto, K. Nomoto, I. Iben, Jr., R. A. Malaney, and P. Huber; my thanks are also due to Drs. W. Huebner, N. H. Magee, Jr., and J. Keady at Los Alamos for supplying the latest stellar opacity tables. Finally, I would like to thank all the inhabitants of the W. K. Kellogg Radiation Laboratory, who have made this such an enjoyable place to do research.

ABSTRACT

The effects of large carbon enrichments in static stellar envelopes were investigated, using new Los Alamos opacities (including low-temperature carbon and molecular opacities) and including carbon ionizations. To search for the production of low-mass, low-luminosity carbon stars, *detailed stellar evolutionary computations* were carried out for a grid of low-mass stars of two different metallicities. The stars were evolved from the main sequence through all intermediate stages and through helium shell flashes on the asymptotic giant branch. The effects of the latest nuclear reaction rates, the new Los Alamos opacities, Reimers-type wind mass loss, and detailed treatment of convection and semiconvection were investigated. Two low-luminosity carbon stars were achieved, in excellent agreement with observations. Conditions favoring dredge-up (and thus carbon star production) include a reasonably large convective mixing length, low metallicity, relatively large envelope mass, and high flash strength. Mass loss was of major importance, tending to oppose dredge-up; the total mass loss amounts inferred from observations suffice to prevent formation of high-mass, high-luminosity carbon stars.

Composition dependence of the important and widely-used $M_c - L$, $M_c - T_b$, and $M_c - \tau_{if}$ relations at low core mass was obtained; the first two of these *differed significantly* from extrapolations from higher-mass stars. The flash strength $L_{\text{He}}^{\text{max}}$ was *not* found to obey any such relation; this renders suspect certain computational short-cuts frequently used in the literature.

CONTENTS

ACKNOWLEDGEMENTS.....	ii
ABSTRACT	iii
INTRODUCTION	1
<i>a) Stellar Evolution and the Carbon Star Mystery.....</i>	1
<i>b) Thesis Organization.....</i>	6
CHAPTER 1. Carbon-Enriched Stellar Envelopes: Nuclei of Planetary Nebulae and R Coronae Borealis Stars	10
ABSTRACT	10
I. INTRODUCTION	11
II. METHODS	14
<i>a) Carbon Opacities.....</i>	15
<i>b) Carbon Ionization Effects.....</i>	18
III. RESULTS AND DISCUSSION	20
<i>a) Ionizations.....</i>	20
<i>b) Carbon Opacity Effects.....</i>	21
<i>c) Carbon-rich vs. Normal Envelopes.....</i>	24
i) Resulting Run of Opacity.....	24
ii) Convection	26
iii) Shifts Across the H-R Diagram.....	28
<i>d) Carbon Mimics Hydrogen.....</i>	29
IV. SUMMARY AND SUGGESTIONS	30

REFERENCES.....	33
TABLES	36
FIGURE CAPTIONS	38
FIGURES	41
CHAPTER 2. Paper I: Flash-Driven Luminosity and Radius	
Variations for Low Mass Stars.....	54
ABSTRACT	54
I. INTRODUCTION	55
II. COMPUTATIONAL DETAILS.....	56
III. RESULTS AND DISCUSSION	58
REFERENCES.....	65
TABLES	67
FIGURE CAPTIONS	70
FIGURES	72
CHAPTER 3. Paper II: The Core Mass–Luminosity Relation	
for Low Mass Stars.....	83
ABSTRACT	83
I. INTRODUCTION	84
II. PREVIOUS WORK	87
III. COMPUTATIONAL DETAILS OF THE PRESENT WORK.....	94
IV. RESULTS AND DISCUSSION.....	97
<i>a) The $M_c - L$ Relation on the Red Giant Branch.....</i>	<i>97</i>
<i>b) The $M_c - L$ Relation on the Asymptotic Giant Branch.....</i>	<i>99</i>

V. CONCLUSIONS	107
REFERENCES	109
FIGURE CAPTIONS	111
FIGURES	113

CHAPTER 4. Paper III: The Production of Low Mass Carbon

Stars	122
ABSTRACT	122
I. INTRODUCTION	125
II. METHODS AND COMPUTATIONAL DETAILS	128
<i>a) General Program Organization</i>	130
<i>b) Nuclear Reaction Handling and Reaction Rates</i>	136
<i>c) Convection and Semiconvection Handling</i>	142
<i>d) Mass Loss</i>	148
III. RESULTS AND DISCUSSION	149
<i>a) Pre-Asymptotic Giant Branch Evolution</i>	149
<i>b) Helium Shell Flashes on the Asymptotic Giant Branch</i>	157
i) The First Flash	158
ii) The Growth of the Flash Strength	160
iii) Mass Loss During the Shell Flash Stage	162
iv) The Core Mass–Base Temperature Relation for Flash-Driven Convection	168
v) Composition of the Flash-Produced Carbon Pocket	170
vi) The Core Mass–Interflash Period Relation	172

c) *Carbon Star Production: Conditions for Dredge-up*.....173

REFERENCES 187

TABLES 193

FIGURE CAPRIONS 198

FIGURES..... 202

CHAPTER 5. On the Origin of the Solar System s-Process

Abundances 221

ABSTRACT 221

I. INTRODUCTION 222

II. THE $M_c - T_b$ RELATION FOR AGB STARS 224

III. s-PROCESS ABUNDANCE CALCULATIONS 226

IV. DISCUSSION 229

REFERENCES 232

TABLE 235

FIGURE CAPTIONS 236

FIGURES..... 237

CHAPTER 6. Neutron Exposures in Time-dependent Stellar

Convective Regions 239

ABSTRACT 239

I. INTRODUCTION 239

II. STELLAR MODEL AND CONVECTIVE DIFFUSION..... 242

III. CONCLUSIONS 247

REFERENCES 248

FIGURE CAPTIONS	251
FIGURES.....	252
CHAPTER 7. SUMMARY AND CONCLUSIONS.....	254

INTRODUCTION

a) Stellar Evolution and the Carbon Star Mystery

A star's lifetime is mostly quiet and serene; but it is punctuated by periods of more violent and interesting behavior. The stars under consideration here are of relatively low mass, namely between 0.8 and 3.0 solar masses (M_{\odot}), so they do not end up as supernovae; but they do go through episodes of by no means insignificant violence. During some of these episodes, heavier elements (including carbon) produced by nucleosynthesis in the stellar interior can be dredged up to the surface. This results in enrichment of the interstellar medium, since mass loss (via a continuous stellar wind or a short-lived "superwind") eventually ejects into space all but the central core of the star. (Note that in the context of astrophysics the term "metals" refers to all elements heavier than helium, and it is used in this sense hereafter.)

A low mass star, between $0.8 M_{\odot}$ and $3.0 M_{\odot}$, starts out by burning hydrogen in its core. This first stage, referred to as the main sequence (MS), is the longest stage in the star's lifetime, as well as the least eventful. The star spends from a couple of hundred million years (for a $3 M_{\odot}$ star) to over ten billion years (for a $0.8 M_{\odot}$ star) just sitting there, growing only slightly more luminous as time passes.

At the end of the main sequence stage, when the hydrogen in the core has been exhausted, things happen much more quickly. The star expands, its surface getting cooler and redder, and climbs the red giant branch (RGB) on a timescale

of only millions of years. During this stage of its life, the star is burning hydrogen in a shell around the hydrogen-exhausted core, growing steadily more luminous but only slightly cooler. This stage is terminated when helium ignites in the core. For stars of mass greater than about $2.5 M_{\odot}$, the ignition is uneventful; but for stars of lower mass, ignition does not take place until the core has been compressed into degenerate matter, and is correspondingly very violent: it is referred to as the helium core flash. In either case, the star zips back down the red giant branch, becoming somewhat hotter and much less luminous, before settling down quietly on the horizontal branch.

During the horizontal branch (HB) stage, the star burns helium in its core, and hydrogen in a surrounding shell. The surface grows slowly hotter (bluer), then cooler (redder) again, while the luminosity remains nearly constant. The horizontal branch timescale is between about a half and a tenth of the main sequence lifetime. Eventually, the core helium is exhausted, and helium burns in a shell around a degenerate core composed mostly of carbon and oxygen. The hydrogen-burning shell is extinguished, and the star grows cooler and more luminous in a manner similar to the red giant stage (and with a similar timescale).

When the helium-burning shell comes close to the hydrogen-helium discontinuity left by the hydrogen-burning shell, the hydrogen-burning shell reignites, and the star begins the asymptotic giant branch (AGB) stage. This stage is characterized by double-shell burning (both a hydrogen and a helium shell), and by helium shell flashes (also called thermal pulses). Helium shell flashes are a violent repetitive nuclear runaway phenomenon. The flash begins as the helium-burning shell becomes

unstable, burning more and more strongly. The star's surface luminosity is between 10^3 and 10^4 solar luminosities (L_{\odot}); but, on a timescale that shortens to days, even to hours, the helium-burning shell grows to generate energy at a rate of $10^6 L_{\odot}$ to $10^8 L_{\odot}$. The effect at the star's surface is relatively small; almost all this energy goes into causing expansion of the intershell zone. This expansion extinguishes the hydrogen-burning shell, and eventually quenches the flash. The flash energy generation causes a convective region to form, reaching from the helium-burning shell up to a point near the hydrogen-burning shell, and thus mixing upward the products of flash nucleosynthesis: carbon, a bit of oxygen, and in some cases small but significant amounts of heavy elements produced by *s*-process nucleosynthesis (i.e., by neutron absorption, starting with iron). The carbon-enriched region thus formed is referred to as the "carbon pocket." As the flash dies down, over a period of decades to centuries, the flash-driven intershell convective region disappears, but expansion continues for some time; and as the outer regions of the star expand, the convective envelope (which reaches from the surface down to a point not too far outside the hydrogen shell) reaches even deeper into the star (in terms of mass: if one looked at events in terms of radius, one would say that the expansion pushed deeper mass layers of the star out into the envelope convective zone). At this stage, in some cases the envelope convective region reaches deep enough to mix part of the carbon pocket to the surface: this is known as "classical" carbon dredge-up. Eventually the star contracts again, and the hydrogen-burning shell eventually reignites. The interflash period prior to the next flash lasts from thousands to hundreds of thousands of years; during this time, the hydrogen-burning shell produces the major

portion of the star's luminosity.

The asymptotic giant branch stage is terminated when mass loss has removed virtually all of the star's envelope (above the burning shells). The star quickly moves to the left in the Hertzsprung-Russell diagram, on a time scale of hundreds to thousands of years: the surface temperature grows very hot, while the luminosity remains nearly constant. A star in this stage of evolution is usually observed to be the nucleus of a planetary nebulae, as the surrounding shell of lost mass is ionized by the star's ultraviolet radiation. The star subsequently cools and dims, becoming a white dwarf.

A "carbon star" is defined as a star whose surface contains more carbon atoms than oxygen atoms (i.e., ratio by number $n(\text{C})/n(\text{O}) > 1$, which corresponds approximately to $C > \frac{3}{4}O$ in terms of the fractions *by mass* of carbon C and oxygen O at the star's surface). This definition originates from observations: in a cool star (i.e., with effective temperature of a few thousand K) which has $n(\text{C})/n(\text{O}) > 1$, not all the carbon at the surface is locked up in carbon monoxide (CO); some carbon is left over to form molecules such as CH and CN . The presence of spectral features due to these molecules thus signals a carbon star to an observer. It should be noted that there is several times more oxygen than carbon in the interstellar medium (from which stars form), and thus the surface of a carbon star must somehow have become enriched in carbon (or depleted in oxygen) relative to its initial composition. Since carbon stars are observed to lie at the high luminosities and low effective (surface) temperatures characteristic of AGB stars, the natural choice

of mechanism for carbon star production is carbon dredge-up due to helium shell flashes on the AGB.

For a number of years, there was a discrepancy between theoretical models of carbon star production and the carbon star observations. The observations indicate that carbon stars exist only at relatively low luminosities: the luminosity distribution of carbon stars is confined approximately to the range in bolometric magnitude brighter than $M_{\text{bol}} \sim -3.5$ but dimmer than $M_{\text{bol}} \sim -6$, which corresponds to the range $3.3 \lesssim \log(L/L_{\odot}) \lesssim 4.3$ in the surface luminosity L (relative to the solar luminosity L_{\odot}). Where the ages of carbon stars can be determined observationally, they are such as to imply relatively small initial stellar masses, $M_i \lesssim 4 M_{\odot}$. On the other hand, theoretical stellar evolutionary runs only found carbon dredged up to the surface for stars of higher mass ($M_i \gtrsim 5 M_{\odot}$), and only at higher luminosities (brighter than $M_{\text{bol}} \sim -6$).

Recently, part of the discrepancy has been removed, when several factors were pointed out that indicated that might prevent the relatively high-mass stars from ever encountering helium shell flashes. Observations indicated that mass loss might be sufficiently extensive that higher-mass stars would lose their entire envelopes before ever reaching the shell flash stage; and there were theoretical indications that previous estimates of the critical stellar mass (above which the star's core mass is large enough that carbon ignites quietly in the center and the shell flash regime is avoided) were overestimates: instead of 9 or 10 M_{\odot} , this limit might lie rather lower, perhaps at 5 or 6 M_{\odot} , eliminating the possibility of carbon star formation at

higher masses. In addition, there were a few reports of dredge-up being found at low stellar mass and luminosity, but these were isolated stellar models that had been generated in a rather ad hoc manner. These reports were the motivation for this thesis: the purpose being to evolve systematically a self-consistent grid of low-mass stars from well-understood initial main sequence models through the intermediate evolutionary stages and through a number of flashes on the AGB in order to search for the production of low-mass carbon stars. A strong additional motivation was provided by the fact that a number of important and widely-used AGB relations, particularly the core mass–luminosity relation, had never been investigated for low-mass stars, only extrapolation from higher-mass stars being available. Stars of low metallicity were considered (of relevance to the extensive Magellanic Cloud carbon star observations), as well as stars of solar metallicity.

b) Thesis Organization

This thesis is divided into six chapters, each comprising a section of the work written up as a paper, plus a seventh chapter comprising a summary of the conclusions presented in the first six chapters.

Chapter 1 reports the results of an investigation of the effects of strong carbon enrichment on stellar envelopes. The results were obtained using a static stellar envelope computation program. It was necessary to make extensive modifications to the original Paczyński envelope program, to enable it to handle the effects due to carbon and to improve the accuracy of the physics inputs. The program modifications and running (and of course debugging) were performed by myself, with some

guidance from I.-J. Sackmann as to what needed to be done; the paper (reporting and interpreting the results) was written in collaboration with I.-J. Sackmann.

Chapters 2 through 4 report the results of the full evolutionary computations performed to search for carbon stars. The program used to do this was based on the Paczyński stellar evolution program, but my revisions and additions now comprise about 85% of the program. A very careful rezoning routine had to be added, in order to obtain the numerical accuracy needed to follow correctly the extremely violent helium shell flashes and the even the helium core flash. A major effort had to be made to create a routine to handle convection and *semiconvection* in detail (but without excessive use of CPU time): in order to handle all the possibilities inherent in mixing due to semiconvection and convective overshoot, this routine turned out to be the largest and most complex in the entire program. Including mass loss (via a parameterized stellar wind) turned out to be non-trivial, though less difficult than some other additions. Numerous modifications and additions were necessary to solve problems of numerical non-convergence that can arise from many different sources. One such problem area was the fitting of the stellar to the outer boundary condition, originally obtained from a pre-computed three-dimensional grid of stellar envelopes; a prohibitively fine grid spacing was necessary at low temperatures. Envelope computation was therefore consolidated with the main stellar evolution program, and routines created to enable the program to choose *automatically* the appropriate grid spacing and compute envelopes of the correct composition, luminosity, effective temperature, and mass. Other additions include up-to-date nuclear reaction rates (including more reactions), correct handling of carbon, nitrogen, and

oxygen abundances, carbon and molecular opacities, *thermodynamic effects* of carbon and oxygen ionizations, and a number of other modifications and additions coming under the general heading of improved accuracy in representing the input physics and modelling stellar events. All of this algorithm design and implementation was my work. (It should be noted that the program is rather large: a listing of it comprises nearly as many pages as this thesis, perhaps more if the auxiliary programs that prepare tables of opacities, nuclear rates, and thermodynamic quantities are included.) I performed many of the stellar evolutionary runs, other runs being followed by I.-J. Sackmann: it should be noted that these runs involve not only following and interpreting stellar events in the huge amounts of output generated by the program, but also watching for fairly subtle indications (besides the blatant instances of non-convergence) that some particular event is being handled with less than the requisite accuracy (requiring further program modifications). Chapters 2 and 3 were written largely in collaboration with I.-J. Sackmann, while I wrote Chapter 4 myself (with discussion and suggestions from I.-J. Sackmann, of course). The most important results of the thesis are discussed in Chapters 3 and 4.

Chapters 5 and 6 are included largely for the sake of completeness, since I made significant contributions to the work reported therein but the largest portion of the work was performed by others. These chapters report on the associated *s*-process nucleosynthesis during helium shell flashes. The $T_b - M_c$ relation reported in Chapter 5 is due mostly to results of the stellar evolutionary runs described in the previous chapters, but the *s*-process nucleosynthesis calculations were performed by R. A. Malaney, who also did most of the writing of the paper comprising Chapter 5.

In Chapter 6, the necessary time-dependent grid of stellar quantities comes from one of my stellar evolutionary runs, and I contributed significantly to the *algorithm* that was used to Monte Carlo the motion of a particle in a convective region in a physically self-consistent manner; but the Monte Carlo *computations* and the writing of the paper comprising Chapter 6 were done by R. A. Malaney and M. J. Savage.

CHAPTER 1.

Carbon-Enriched Stellar Envelopes: Nuclei of Planetary Nebulae and R Coronae Borealis Stars

I.-Juliana Sackmann and Arnold I. Boothroyd

W. K. Kellogg Radiation Laboratory 106-38

California Institute of Technology, Pasadena, CA 91125

ABSTRACT

Envelopes rich in carbon were computed, taking envelope carbon opacities into account that were hitherto unavailable. All effects of carbon partial ionizations were fully included. We investigated stars with envelope carbon content $XC = 0.1$ and $XC = 0.31$ (fraction by weight), and compared them to stars of normal composition. We investigated R Coronae Borealis stars and nuclei of planetary nebulae, considering high-luminosity objects of $\log(L/L_{\odot}) = 4.1$, of total stellar mass $0.815 M_{\odot}$, and ranging in effective temperature from $\log T_e = 3.5$ to 5.3 .

Below $6000K$ carbon *increased* the opacity, due to molecular effects. The opacity peak around $10^4 K$ was *dramatically reduced* due to carbon enrichment. From $2 \times 10^4 K$ to $3 \times 10^5 K$, carbon *reduced* the opacity by a *small* amount. Above $3 \times 10^5 K$, carbon *increased* the opacity by about 20%. Carbon did not change the depth of convection in temperature,

although in some cases it did drive convection considerably *deeper* in mass, at a fixed T_e . Carbon shifted stars considerably to the blue in the H-R diagram, leading to a considerably *shallower* convection in mass, for stars at a fixed envelope mass. Computationally, carbon could be simulated by an equal mass of hydrogen, for $XC \lesssim 0.1$.

For red giants with *small* envelope masses, carbon molecular opacities can considerably change the envelope structure and the depth of convection in mass. Carbon molecular opacities must be known reliably.

Subject Headings: nebulae: planetary — opacities — stars: abundances
— stars: atmospheres — stars: carbon — stars:
R Coronae Borealis

I. INTRODUCTION

In the last decade, a large number of carbon stars have been observed in our galaxy and in the Large and Small Magellanic Clouds (see, e.g., Blanco, McCarthy, and Blanco 1980; Bessell, Wood, and Evans 1983). These observations show that carbon enrichment exists in the surface layers of stars. Theoretical computations have shown that large amounts of carbon must exist in the deep interior of stars during late evolutionary stages. However, no theoretical work has been undertaken to investigate the consequences of carbon enrichment on the *envelope* structure. There was no strong motivation for this until recently, because no mechanism existed for transporting *large* amounts of carbon to the surface. The dredge-up phenomenon discovered by Iben (1975) and verified by many subsequent investigations

(e.g., Sugimoto and Nomoto 1975; Fujimoto, Nomoto, and Sugimoto 1976; Iben 1976; Sackmann 1976; Paczyński 1977) does bring a significant amount of carbon to the surface, so as to produce $C/O > 1$ (where C/O refers to the number ratio of carbon to oxygen). This dredge-up phenomenon takes place for masses larger than $5 M_{\odot}$ for Population I stars and is driven by the helium shell flashes. Due to the dilution in a massive envelope, XC (the proportion by weight of *added* carbon) remains small. However, mass loss during the red giant stage will reduce considerably the mass of the envelope. A new flash mixing is then created (Sackmann 1980): it is very similar to the dredge-up phenomenon, but permits large enrichment of carbon. The red giant remnant has a mass roughly of order $1 M_{\odot}$, of which the envelope comprises only a very small fraction. There is no deep convective envelope, only a shallow surface convection zone due to the hydrogen and helium ionizations. Due to the small envelope mass, however, the flash-driven expansion can be large enough that the shallow surface convection reaches down into the intershell carbon pocket. The dilution now is small, and *large* carbon enrichment can take place. It seems plausible that $XC \sim 0.1$ can be attained with this mechanism.

Hydrogen-deficient carbon stars (HdC stars) and, in particular, R Coronae Borealis stars (hereafter referred to as R CrB stars) are carbon stars of a rather special type. Observations indicate essentially no hydrogen at their surface, but strong carbon enrichment: some may have XC of order 0.1 (see, e.g., Searle 1961; Danziger 1965; Warner 1967; Orlov and Rodríguez 1974; Hunger, Schönberner, and Steenbock 1982; Cottrell and Lambert 1982). They are very luminous stars of various spectral types across a wide range of the H-R diagram. Recently, knots of gas

in the unusual planetary nebulae Abell 30 and Abell 78 have also been discovered to be carbon-rich and hydrogen depleted (Jacoby and Ford 1983). Their carbon abundance, though highly uncertain, could also be as high as $X_C \sim 0.1$. (Note that planetary nebulae are frequently somewhat carbon-enriched, with $C/O > 1$ [Aller and Czyzak 1983; French 1983]. It is possible for the central star [nucleus] to be more carbon-rich than the nebula.)

Even though such huge carbon enrichments are known to exist, no envelope structure computations for such objects have taken fully into account carbon opacities and other carbon effects. The problem was that no carbon opacity tables for envelope temperatures were available. However, previously unavailable carbon-rich opacity tables have kindly been supplied by Huebner (1976) and Magee (1984) of the Los Alamos Opacity Group. The carbon opacity changes ∇_{rad} (where $\nabla \equiv d \ln T / d \ln P$). Via its internal energy contribution, carbon also changes ∇_{ad} . Thus carbon can affect convection, defined by $\nabla_{\text{rad}} > \nabla_{\text{ad}}$ (where “rad” refers to radiative and “ad” to adiabatic conditions). Carbon also changes the equation of state, as its six partial ionizations change the mean molecular weight μ . It was the aim of this paper to take all of the above mentioned carbon effects fully into account and to investigate possible changes in the resulting envelopes. In particular, we wished to investigate whether the presence of carbon would drive the convective envelope deeper in mass, thereby dredging up more carbon, and thus leading to enhanced mixing.

II. METHODS

All envelopes presented in this paper were computed for a star of total mass $0.815 M_{\odot}$; unless otherwise stated, the star's luminosity was $\log(L/L_{\odot}) = 4.1$. The envelopes were computed using a program similar to that described by Paczyński (1969), which includes a simple gray atmosphere model. The main modifications involved use of carbon opacities and consideration of carbon ionization effects as described below. The maximum integration step size was reduced by about a factor of four from that of Paczyński (1969), so that

$$\begin{aligned} \frac{\Delta(M - M_r)}{M - M_r} &\leq 0.15, & \frac{\Delta T}{T} &\leq 0.05, \\ \frac{\Delta \rho}{\rho} &\leq 0.15, & \frac{\Delta r}{r} &\leq 0.05, & \frac{\Delta \tau}{\tau} &\leq 0.1, \end{aligned} \tag{1}$$

for mass $M - M_r$ (i.e., measured downward from the surface), temperature T , density ρ , radius r , and optical depth τ (where the restriction on $\Delta \tau$ is only applied for $\tau < \frac{2}{3}$). Thus on the order of two hundred steps were required for an envelope, which was integrated down to the inner boundary condition. Since we did not have interior models consistent with the envelopes, we chose the inner boundary of the envelope to occur at the point where the temperature reached $T = 2 \times 10^6 K$ (a reasonable compromise between the requirement of complete ionization and the requirement that the gravitational energy generation be negligible). Note that our envelope mass, M_{env} , is *not* the conventional envelope mass (which is defined as $M_e = M - M_c$, where M is the total mass and M_c the core mass of the star). The difference is small for envelopes having low effective temperatures; but for high

effective temperatures ($\log T_e \sim 5$), there can be an order of magnitude difference between these two definitions of the envelope mass. In all of the envelopes, a value of $\alpha = 1.0$ was assumed, where $\alpha \equiv l/H_p$ is the ratio of the convective mixing length l to the pressure scale height H_p .

Note that throughout the remainder of the paper, unless specified otherwise, quantities are given in the following units: stellar masses, envelope masses, convective masses, luminosities, and radii are given in solar units (M_\odot , L_\odot , and R_\odot respectively); temperatures T are in degrees Kelvin (K), and other quantities are in c.g.s. units.

a) Carbon Opacities

The Los Alamos Opacity Group supplies tables of the Rosseland mean opacity κ as a function of density ρ and temperature T . These have been calculated in a self-consistent way in four stages, or generations. Generation I opacities are those calculated prior to 1965 (see Cox and Stewart 1965). Generation II opacities are those calculated subsequently with an improved computer code (see Cox and Stewart 1969, 1970*a, b*). Generation III opacities are those calculated with further improvements, yielding changes of order 10% from generation II (see Cox and Tabor 1976). Generation IV opacities are those calculated including molecular opacities at low temperatures ($T < 10^4 K$); they are otherwise the same as generation III (see Meyer-Hofmeister 1982). Table 1 demonstrates that including molecular opacities can cause more than an order of magnitude increase in the opacities at low temperatures.

Huebner (1976) kindly provided opacity tables for eleven mixes (including eight carbon-rich mixes) from the Los Alamos Astrophysical Opacity Library. These mixes all had metal content $Z = 0.03$, where Z here is the mass fraction of the usual spectrum of elements heavier than helium, including the usual amount of carbon. Over and above the normal amount of carbon contained in Z , there is an *added* carbon content, whose mass fraction has been denoted XC . (As usual, X and Y are the hydrogen and helium mass fractions, respectively.) These mixes were labeled A, B, or C for hydrogen contents of $X = 0, 0.3, \text{ or } 0.7$, respectively; they were sub-labeled 1, 2, 3, 4, or 5 for added carbon contents of $XC = 0, 0.2, 0.4, 0.6, \text{ or } 0.97$, respectively. Thus, for example, mix C-1 refers to a normal mix, with $XC = 0$, $X = 0.70$, $Y = 0.27$, and $Z = 0.03$, while mix B-2 is hydrogen-depleted and carbon-rich, with $XC = 0.20$, $X = 0.30$, $Y = 0.47$, and $Z = 0.03$. The opacity table for any required mix was interpolated in composition from the above eleven mixes (as described below).

The above tables only provided opacities for temperatures $T \geq 1.2 \times 10^4 K$. Low-temperature opacities (of generation IV, with molecular effects included) were obtained from two sources. Published opacity tables down to $T = 2320K$ were available (Meyer-Hofmeister 1982) for four mixes containing no extra carbon: (1) $X = 0.7, Z = 0.02$; (2) $X = 0, Z = 0.02$; (3) $X = 0.76, Z = 0.001$; and (4) $X = 0, Z = 0.001$. A relatively small extrapolation in $\log Z$ (and a small adjustment, linear in X , for the case $X = 0.7$) yielded low-temperature continuations for the opacity tables of mixes A-1 and C-1. Also, at Huebner's suggestion, Magee (1984) kindly

supplied us with unpublished opacity tables down to $T = 3000\text{ K}$ for a carbon-rich mix. For our purposes, we considered it reasonable to specify this mix as $XC = 0.067$, $X = 0$, $Y = 0.903$, and $Z = 0.03$. Extrapolation in $\log(Z + XC)$ yielded a low-temperature continuation for the opacity table of mix A-2.

The molecular opacities available from Meyer-Hofmeister and Magee are both Los Alamos opacity calculations. They include both molecular and atomic cross sections, as well as broadening due to turbulence. (Thermal and collisional broadening are also included, but are less important than turbulence broadening.) The opacities due to the following molecules were included: H^- , H_2 , H_2^+ , H_2^- , H_2O , N_2 , CO , and CN . In addition, the following molecules were also included in the equation of state, but their opacities were *not* included: OH , C_2 , O_2 , NO , CO_2 , NO_2 , and CH . It should be noted that low-temperature opacities for carbon-rich mixes are somewhat uncertain, particularly when both carbon and hydrogen are present, since oscillator strengths for some molecules have never been measured. For example, the importance of the (estimated) molecular opacity of HCN in atmospheres of very low-temperature carbon stars has been demonstrated by Eriksson *et al.* (1984). Kurucz (1984) has made extensive calculations of unmeasured oscillator strengths, and was in the process of attempting to use them to calculate low-temperature opacities as of the date of his communication with us. Sharp is collaborating with Huebner (1984) to include more molecules. Improved molecular opacities are thus expected to become available in the future.

Low-temperature opacities for mixes B-1, B-2, and C-2 were obtained by interpolation from mixes A-1, A-2, and C-1. Low-temperature opacities for mixes

A-3, A-4, and A-5 were set equal to those of mix A-2; low-temperature opacities for mixes B-3 and B-4 were set equal to those of mix B-2. For densities typical of our envelopes at these low temperatures (i.e., $\rho \lesssim 10^{-9}$ g cm $^{-3}$), only minor modifications were necessary to fit these opacities smoothly to the higher-temperature tables at $T = 1.2 \times 10^4$ K.

The eleven mixes described above form the basis for our calculations: the opacities for any particular envelope composition were obtained by interpolation among these mixes. The interpolation in hydrogen content X was always linear. The interpolation in carbon content XC was linear for $XC > 0.2$; for $XC < 0.2$, the interpolation was linear in $\log(Z + XC)$.

b) Carbon Ionization Effects

The treatment described in Paczyński (1969) was modified to take all the carbon ionizations into account. The Saha Equation was used to compute the number densities of the ionization stages of hydrogen, helium, and carbon, and the number density of electrons. It should be noted here that, due to the presence of carbon, it is not possible to use a “full ionization approximation” for any temperature below $T = 2 \times 10^6$ K (unlike Paczyński 1969).

At low temperatures, the partition function $u_r^{(i)}$ of an ionization stage r of the i^{th} type of atom is equal to the degeneracy $g_{r,0}^{(i)}$ of the ground state of that ionization stage. At higher temperatures, this may no longer be true: there may be

a significant contribution from excited states. The partition function is given by

$$u_r^{(i)} = g_{r,0}^{(i)} + \sum_{j=1}^{j_{\max}} g_{r,j}^{(i)} \exp\left(-\frac{\Delta E_{r,j}^{(i)}}{k_B T}\right), \quad (2)$$

where $g_{r,j}^{(i)}$ is the degeneracy of the j^{th} excited state, $\Delta E_{r,j}^{(i)}$ is its excitation energy above the ground state, and j_{\max} is the point at which the sum is terminated. The sum must be terminated, since it diverges; the choice of a proper termination point j_{\max} , however, is not completely trivial. It is reasonable to terminate the sum when the excited states merge with the “depressed” continuum, or when the size in space of the wave function of the excited state exceeds the average volume available for an atom (Cox and Giuli 1968). To reduce computation time, however, we chose to consider as few excited states as possible. The lowest excited states, with the smallest excitation energies, have the smallest exponents in their Boltzmann factors, and so give the largest contributions. We include the first three excited states of C I, the first two excited states of C II and C III, and the first excited state of C IV. (Actually, it would probably have been sufficiently accurate to include only the first excited state of each of these.) The effect on the partition functions is shown in Figure 1. It was not necessary to consider any excited states for hydrogen, helium, C V, or C VI.

As described in Paczyński (1969), required derivatives of the pressure and the internal energy can be computed numerically. The pressure is given by the sum of the radiation pressure P_r and the gas pressure P_g . The internal energy has contributions from the kinetic energy of ions and electrons, from the photons in the radiation field, from the ionization energy involved in creating the ions, and from

the excitation energy of those excited states which have a significant occupation.

Thus, the internal energy per unit mass is given by

$$U = \frac{3}{2} \frac{P_g}{\rho} + 3 \frac{P_r}{\rho} + \frac{1}{\rho} \sum_i \sum_{r=2}^{\mathcal{Z}_i+1} N_r^{(i)} \left[\sum_{s=1}^{r-1} E_s^{(i)} + \sum_{j=1}^{j_{\max}} \Delta E_{r,j}^{(i)} \frac{g_{r,j}^{(i)} \exp(-\Delta E_{r,j}^{(i)}/k_B T)}{u_r^{(i)}} \right], \quad (3)$$

where $N_r^{(i)}$ is the number density of the r^{th} ionization stage of the i^{th} type of atom (which has atomic number \mathcal{Z}_i), $E_s^{(i)}$ is the ionization energy of the s^{th} stage, and k_B is Boltzmann's constant (note that $r = 1$ refers to the neutral atom). Once they had been computed, the pressure and internal energy were used as described in Paczyński (1969) in the envelope integration program.

III. RESULTS AND DISCUSSION

a) Ionizations

Figure 1 shows the temperature at which ionizations of hydrogen, helium, and carbon take place. Hydrogen is 50% ionized at $\log T = 3.97$. For He I and He II, 50% ionization occurs at $\log T = 4.17$ and $\log T = 4.53$, respectively. The first four ionization stages of carbon tend to mimic those of hydrogen and helium: C I is 50% ionized at $\log T = 3.85$ —a similar temperature to that of H I, though slightly cooler. For C II, 50% ionization occurs at $\log T = 4.22$ —similar to He I. For C III and C IV, the temperatures of 50% ionization are $\log T = 4.45$ and $\log T = 4.61$, respectively—similar to He II. For C V and C VI, 50% ionization occurs at $\log T = 5.44$ and $\log T = 5.60$, respectively. These last two ionizations are close together and have

no counterpart in hydrogen and helium ionizations. (As will be shown later, they also have little or no effect on the envelope structure.)

Figure 1 also shows the partition functions of the first four ionization stages of carbon (see eq. [2] for definition). As is well known, for hydrogen and helium the partition functions can be considered constant (for H I, $u_I = 2$; for He I, $u_I = 1$; and for He II, $u_{II} = 2$). For carbon, the partition functions were calculated as described in Section II*b*. Figure 1 shows that the partition functions of C I, C II, C III, and C IV are not constant. For C I and C II, the deviations from constancy are relatively minor, of order 20%. For C III and C IV, the partition functions vary by a factor of 2. For C V and C VI, the partition functions are approximately constant ($u_V = 1$ and $u_{VI} = 2$); they are therefore not included in Figure 1.

b) Carbon Opacity Effects

Table 2 shows that the presence of carbon *reduces* the opacity at almost all values of density ρ and temperature T encountered in an envelope. The typical effect is of the order of 20%, although near $10^4 K$ the reduction can be as much as a factor of 10. There are, however, two small ranges in (ρ, T) where carbon *increases* the opacity. One range is at the high- T , high- ρ end of the envelopes (i.e., the bottom of the envelopes). There, as may be seen from Table 2, carbon can increase the opacity by as much as a factor of 2. However, for the densities and temperatures typical of our envelopes (roughly indicated by the dots in Table 2), this effect was only of the order of 20%, even after the reinforcement due to the slight density increase (at a given temperature) caused by carbon. Iben and Renzini (1982*a, b*)

showed this opacity increase can lead to a semiconvective zone, transporting carbon out and hydrogen in. The other range where carbon increases the opacity is at very low temperatures ($T < 10^4 K$: see Table 2). Here the increase can be as much as a factor of 3. However, the carbon opacities are uncertain in this region, since here the opacity is dominated by molecular opacities which are incompletely known.

One can begin to understand why carbon reduces the opacity by considering the following (highly simplified) argument: The bound-free opacity (per unit mass) of a given element i at a frequency ν is given by

$$\kappa_i(\nu) = \frac{a_{\text{bf}}^{(i)} N_{i,n}}{A_i m_{\text{H}}}, \quad (4)$$

where $a_{\text{bf}}^{(i)}$ is the bound-free absorption coefficient per bound electron, $N_{i,n}$ is the number of bound electrons in the n^{th} orbital, A_i is the atomic weight, and m_{H} is the mass of the hydrogen atom. In the hydrogenic approximation, the bound-free absorption coefficient may be written as

$$a_{\text{bf}}^{(i)} \approx \left(\frac{64\pi^4 m_e e^{10}}{3^{3/2} c h^6} \right) \frac{Z_i'^4 g(\nu)}{n^5 \nu^3}, \quad (5)$$

where Z_i' is the effective charge seen by the electrons in the n^{th} orbital and $g(\nu)$ is the Gaunt factor, a quantum-mechanical correction of order unity (see Schwarzschild 1958, p. 63). (It should be noted that the bound-free absorption coefficient is zero for photons whose energy is smaller than the ionization energy of the relevant ionization stage of the atom.) The Rosseland mean opacity κ is defined by

$$\frac{1}{\kappa} = \frac{\int_0^\infty \frac{1}{\kappa(\nu)} \frac{\partial B_\nu(T)}{\partial T} d\nu}{\int_0^\infty \frac{\partial B_\nu(T)}{\partial T} d\nu} \equiv \int_0^\infty \frac{1}{\kappa(\nu)} W(u) du, \quad (6)$$

where $B_\nu(T)$ is the Planck function, $W(u)$ is its normalized temperature derivative, and $u = h\nu/k_B T$. However, even without performing this integral, one can obtain a rough estimate of the ratio of the opacity of a unit mass of carbon relative to that of a unit mass of hydrogen from the ratio

$$\frac{\kappa_C(\nu)}{\kappa_H(\nu)} \approx \frac{a_{\text{bf}}^{(\text{C})} A_{\text{H}} N_{\text{C},n}}{a_{\text{bf}}^{(\text{H})} A_{\text{C}} N_{\text{H},n}} \approx \frac{\mathcal{Z}'_{\text{C}}{}^4 n_{\text{H}}^5 A_{\text{H}} N_{\text{C},n}}{\mathcal{Z}'_{\text{H}}{}^4 n_{\text{C}}^5 A_{\text{C}} N_{\text{H},n}}. \quad (7)$$

For a temperature of order 10^4 K, this ratio becomes

$$\frac{\kappa_C(\nu)}{\kappa_H(\nu)} \approx \frac{11}{1} \cdot \frac{1}{32} \cdot \frac{1}{12} \cdot \frac{4}{1} \approx \frac{1}{9}. \quad (8)$$

It is indeed the case that the bound-free opacity of carbon at this temperature is roughly an order of magnitude smaller than that of hydrogen, as estimated from the opacities supplied by Huebner (1976).

As mentioned earlier, the molecular opacities are still poorly known. Including carbon molecules can increase or decrease the low-temperature opacities by orders of magnitude (Huebner 1984). We therefore tried to investigate this effect by artificially varying the low-temperature opacity. We varied the opacity κ by a factor of $f_T = 10$ or $f_T = 0.1$ at $\log T = 3.3$ (i.e., setting $\kappa_{\text{new}} = f_T \times \kappa_{\text{old}}$), while leaving κ unchanged at $\log T = 4.0$. In between these two “boundary” temperatures, $\log f_T$ varied linearly with $\log T$. For $f_T = 10$, the envelope mass was reduced by a factor of 2, at $\log T_e = 3.584$ and $\log L = 4.318$. For $f_T = 0.1$, the envelope mass was increased by a factor of 2. The above investigation was carried out before we received any carbon molecular opacities. All other results presented in this paper were obtained using the opacity tables described in Section IIa: for carbon-rich mixes, the low-temperature opacities were derived from the tables provided by Magee (1984), which included carbon molecular opacities.

c) Carbon-rich vs. Normal Envelopes

We considered four different chemical compositions. Case *a* is our normal mix, with $X = 0.70$, $Y = 0.27$, $Z = 0.03$, and no added carbon, namely $XC = 0$. (Note that Z contributes a small amount of carbon, namely 14% of Z by weight.) Case *b* is a carbon-enriched mix, with $XC = 0.10$, $X = 0.56$, $Y = 0.31$, and $Z = 0.03$. Case *c* is an extreme carbon-enriched case, with $XC = 0.31$, $X = 0.27$, $Y = 0.39$, and $Z = 0.03$. Case *d* is an R Coronae Borealis type mix, with $XC = 0.10$, $X = 0$, $Y = 0.87$, and $Z = 0.03$.

i) Resulting Run of Opacity

Figures 2 and 3 refer to envelopes computed for the same luminosity and effective temperature ($\log L = 4.1$ and $\log T_e = 3.584$), comparing the three carbon-rich cases with the normal case. Figure 2*a* displays the resulting run of opacity as a function of temperature in the envelope. The most striking feature is the reduction of the opacity peak around $\log T = 4$ in the carbon-rich envelopes, relative to the normal envelope. The predominant cause of this reduction is not the increase in the carbon content, but the accompanying decrease in the hydrogen content. Relative to the normal case *a*, cases *b*, *c*, and *d* were reduced by factors of 2, 6, and 100, respectively.

Another striking feature of Figure 2*a* is the presence of three opacity peaks for case *d*, the R CrB envelope. The peak around $\log T = 3.85$ is due to the ionization of C I (just as, in cases *a*, *b*, and *c*, the peak around $\log T = 4$ was due to the ionization

of hydrogen). The peak around $\log T = 4.2$ is due to the ionization of He I, with a few percent contribution from C II. The peak around $\log T = 4.65$ is due to the ionization of He II, with perhaps a minor contribution from C III and C IV. The ionizations of C V and C VI have no visible effect on the opacity. The reason why higher ionizations have less effect on the opacity than lower ionizations can be understood by considering equations (5) and (6) above. The weight function $W(u)$ in equation (6) is given by

$$W(u) = \frac{15}{4\pi^4} \frac{u^4 \exp(-u)}{[1 - \exp(-u)]^2}. \quad (9)$$

Thus $W(u)$ has a maximum at $u \approx 4$, i.e., at $h\nu \approx 4k_B T$, and drops off rapidly for increasing ν . However, $a_{\text{bf}}(\nu)$ is zero for $\nu < \nu_0$, where $h\nu_0$ is the ionization energy. At the ionization temperature, $h\nu_0 \approx 18k_B T$; thus both $W(u)$ and $\kappa_{\text{bf}}(\nu)$ fall off rapidly with ν , and so $\kappa_{\text{bf}}(\nu_0)$ makes the major contribution to the Rosseland mean opacity κ . The weight function $W(u_0)$ is much the same for all ionizations, since $u_0 \equiv h\nu_0/k_B T$ is approximately equal to 18 for all ionizations. However, due to the factor $1/\nu^3$ in a_{bf} , the value of $\kappa_{\text{bf}}(\nu_0)$ is much smaller for higher ionizations, which have higher ionization energies and thus larger ν_0 values. Thus higher ionizations contribute less to the bound-free opacity.

Yet another striking feature in Figure 2a is the near-equality of the run of opacity for $\log T \geq 4.3$ for all four cases. For a given (ρ, T) , the opacity is smaller for the carbon-rich mixes, as discussed in Section IIIb. However, the density is increased for the carbon-rich envelopes, as may be seen in Figure 2b. These two opposing effects tend to cancel, leaving the resulting run of opacity nearly unchanged

over this temperature range. Also apparent in Figure 2a is the *increase* of opacity in the carbon-rich envelopes at the high-temperature and low-temperature ends. (Note however that mix *d* has a lower opacity at the high-temperature end than the normal mix *a*; this is again compensated by the higher density, to leave the resulting run of opacity unchanged.) The different opacities at $\log T \leq 3.7$ are caused by molecular effects, which are somewhat uncertain.

ii) Convection

In Figure 3, we examine the effects of carbon on convection in the *red giant* envelope. Here, it turns out that carbon has relatively little effect. The reason is that without carbon, for our normal mix, convection reaches down from the surface to the point where the temperature is $\log T \approx 4.7$. As shown in Figure 2a, at this temperature carbon does not change the opacity very much, so that ∇_{rad} is not affected much. Figure 3 shows that carbon ionizations do cause dips in ∇_{ad} , at nearly the same temperatures as the dips caused by hydrogen and helium; however, at $\log T \approx 4.7$ there is no ionization taking place to change ∇_{ad} . Thus the temperature at which ∇_{rad} and ∇_{ad} cross remains nearly unchanged, and convection always reaches down to a temperature of $\log T \approx 4.7$. (It should be noted that the temperature at the bottom of convection is also independent of the envelope effective temperature, for these stars.) However, if the (ρ, T) profile is different for the different mixes, then the convective mass and the total envelope mass are changed by the addition of carbon. For $\log T_e = 3.584$, cases *a*, *b*, and *c* have similar (ρ, T) profiles (see Figure 2b) and thus have similar envelope and convective masses.

However, case *d* has a significantly different (ρ, T) profile, with a higher density at all temperatures in the envelope; its envelope mass and its convective mass are larger than those of the normal case *a* by a factor of 5.

For mixes *a*, *b*, *c*, and *d*, envelopes were computed for a large number of effective temperatures reaching all across the H-R diagram (from $\log T_e = 3.5$ to 5.3), but at the same luminosity ($\log L = 4.1$) and the same stellar mass ($M = 0.815 M_\odot$). This was done to investigate the effects of carbon on the envelopes of R CrB stars and on nuclei of planetary nebulae—stars evolving at constant luminosity from the red giant branch to the blue across the H-R diagram.

In contrast with the red giant case, in the middle of the H-R diagram (i.e., with effective temperatures $\log T_e \sim 4$) carbon enrichment has a *considerable* effect, as may be seen from the convective masses and envelope masses shown in Figure 4. As in the red giant case, convection always reaches down to $\log T \approx 4.7$. However, when compared at the same T_e , envelopes with increased amounts of carbon have an increased total envelope mass, and also an increased convective mass (e.g., a factor of 4 from case *a* to case *b* at $\log T_e = 4.0$). On the other hand, if one compares envelopes at the same total envelope mass, an increased amount of carbon produces an increased T_e and thus a *decreased* convective envelope mass (e.g., a factor of 6 from case *a* to case *b* at $M_{\text{env}} = 5.3 \times 10^{-5} M_\odot$: case *a* has $\log T_e = 4.0$ and case *b* has $\log T_e \simeq 4.28$). Note that the convective mass becomes a much smaller fraction of the envelope mass as one increases T_e , as one would expect, since a smaller fraction of the envelope has $\log T < 4.7$. No convection is present in envelopes located far to the blue in the H-R diagram, i.e., with $\log T_e \gtrsim 4.7$.

Although the *bottom* of the convective region is relatively well established, this is *not* true of the *top* of the convective region. It is well known that the mixing length theory of convection breaks down near the photospheric layers. The bifurcation near $\log T_e = 4.0$ shown in Figures 4a and 4b splits the convective region into two separate zones: the upper zone is associated with H I ionization, the lower with He II ionization. However, the bifurcation is in the region where convection would be expected to be present, due to He I ionization. Since the bifurcation takes place near the photosphere, it is likely to be a spurious effect.

iii) Shifts Across the H-R Diagram

As shown in Figure 5, one striking result is that dumping carbon into an envelope has very little effect, over much of the H-R diagram. Cases *a* and *b* are nearly identical for stars redder than $\log T_e = 3.8$ or bluer than $\log T_e = 4.5$. However, for a star in the “middle” range of the H-R diagram ($3.8 \lesssim \log T_e \lesssim 4.5$), the star can be shifted to the blue by a *considerable* amount (as much as $\Delta \log T_e \sim 0.3$) as one changes the mix from *a* ($XC = 0$ and $X = 0.7$) to *b* ($XC = 0.1$ and $X = 0.56$) while holding the envelope mass constant. As one dumps in still more carbon, i.e., as one changes the mix from *a* ($XC = 0$ and $X = 0.7$) to *c* ($XC = 0.31$ and $X = 0.27$), the shift toward the blue is even larger (as much as $\Delta \log T_e \sim 0.6$). There is also a wider range in the H-R diagram where the envelopes differ significantly ($3.7 \lesssim \log T_e \lesssim 4.8$).

The difference between the normal case *a* and the R CrB case *d* is *immense* everywhere in the H-R diagram except for extremely high effective temperatures

($\log T_e \gtrsim 5$). For a red giant envelope at $\log T_e = 3.5$, the R CrB mix yields an envelope mass $M_{\text{env}} = 0.043 M_{\odot}$, which is four times the mass one obtains with a normal mix at that effective temperature. Alternatively, one can say that, at *constant* envelope mass, the R CrB envelope is shifted to the blue by $\Delta \log T_e \approx 0.1$ here. The largest shifts, in the “middle” range of the H-R diagram, can be as much as $\Delta \log T_e \sim 0.8$ (at a fixed envelope mass). This extremely large shift, however, is not due to the presence of carbon, but rather due to the absence of hydrogen.

d) Carbon Mimics Hydrogen

We constructed envelopes where we replaced a given amount of hydrogen by an equal amount, by weight, of carbon. The results are presented in Figure 6.

Comparing curves *a* to *e* and *g* to *d*, one notices in each case that the two curves are nearly identical, even though one has replaced some of the hydrogen by carbon. For the former, the largest difference in the envelope mass is 20% (at $\log T_e \sim 4$), while for the latter the largest difference is 30%. This demonstrates that for stars of *small envelope mass*, a “small” amount of carbon (up to $XC \sim 0.1$) can be simulated by an equal mass of hydrogen, as far as the *envelope mass* and *envelope structure* are concerned. However, with more carbon, say $XC = 0.3$, this no longer holds true, as may be seen by comparing curve *f* to curve *a*.

There seems to be a certain saturation effect when one adds carbon without changing the amount of hydrogen (i.e., replaces *helium* with carbon). As one increases the carbon content from $XC = 0$ to $XC = 0.1$ the envelope changes significantly (compare curves *d* and *j*). Adding still more carbon, to yield $XC = 0.3$,

results in little further change (compare curves *h* and *d*). Adding yet more carbon results in essentially *no* further change.

IV. SUMMARY AND SUGGESTIONS

The first four *ionizations* of carbon behave like those of hydrogen and helium, while the last two have no appreciable effect (C I \leftrightarrow H I, C II \leftrightarrow He I, C III and C IV \leftrightarrow He II; C V and C VI have no counterparts but also have little effect). The *opacity* of carbon is slightly less than that of hydrogen, but somewhat more than that of helium, over most of the (ρ, T) range encountered in an envelope. If one considers an initially normal hydrogen-rich envelope where one mixes in carbon and helium from nucleosynthesis below, the resulting mix has the following property: the input opacity for the envelope calculations is *reduced* over most of the (ρ, T) range encountered in the envelope, but is *increased* at the surface and bottom layers of the envelope. At the surface, the opacity is increased due to molecular opacities which are still not completely determined. For red giants with small envelope mass, the envelope mass and convective mass are quite sensitive to these molecular opacities, which thus must be reliably known. More calculations need to be performed to take molecular opacities correctly into account. At the bottom of the envelope, the opacity increase can lead to semiconvection as found by Iben and Renzini (1982*a, b*).

In reference to our aim of investigating possible enhanced mixing due to the presence of carbon, the results are somewhat inconclusive. We found that, at a fixed T_e , the presence of carbon can lead to a significantly *deeper* convective *mixing*; however, at a fixed total envelope mass, the presence of carbon can considerably it

reduce the convective mixing. Which of these opposing effects dominates can only be determined from complete stellar evolutionary models. We intend to resolve this uncertainty in our next evolutionary calculations. However, a final conclusion cannot be made with certainty until carbon molecular opacities are more firmly established.

There is one sensitive region in the H-R diagram where carbon *enrichment* in the envelope makes a *large* difference. For an envelope with an effective temperature $\log T_e \sim 4$, carbon enrichment *shifts* a star considerably toward the *blue* in the H-R diagram when one holds the envelope mass constant. For $XC = 0.1$, this blueward shift can be as large as $\Delta \log T_e \sim 0.3$, i.e., a shift from an early F-type to an early B-type star. This large shift occurs primarily for the following reason: as carbon enrichment occurs, there is a simultaneous helium enrichment too. Thus the hydrogen depletion ($\Delta X = -0.14$) is larger than the carbon enrichment ($\Delta XC = 0.1$), and the two cannot fully compensate for each other. In this middle part of the H-R diagram, a small change in envelope mass corresponds to a large change in envelope effective temperature: this accounts for the sensitivity of this region to small composition changes.

R CrB type carbon stars have a much bluer location in the H-R diagram when compared to stars of normal composition, at the *same luminosity* and the *same envelope mass*. This difference can be as much as $\Delta \log T_e \sim 0.8$. This theoretical blueward shift cannot easily be verified observationally, since observations do not yield a star's envelope mass. This blueward shift would, however, have a significant

effect on the production of R CrB stars as suggested by Iben *et al.* (1983). As their star was cooling down toward becoming a white dwarf, they encountered a strong final flash that shifted it upward and to the right in the H-R diagram, almost back to the position of the red giant branch, before it moved back parallel to its original blueward path and started to cool down again. They suggested that such a flash might cause the ejection of the tiny remaining hydrogen-rich envelope, resulting in an R CrB type surface composition. If this were the case, our results for R CrB type envelopes suggest that the track subsequent to the final flash might reach considerably less far toward the red. The dramatic difference between normal and R CrB envelopes is not due to the enrichment of carbon, but rather due to the depletion of hydrogen.

There seems to exist a *saturation* effect in the envelope structure as one adds carbon at the expense of *helium*, provided one holds the *hydrogen* content constant. After one has reached $XC = 0.1$, not too much additional change in the envelope structure occurs as one adds further amounts of carbon. This remains true even up to “wild” carbon enrichments of $XC = 0.3$ and $XC = 0.7$.

For these stars of *low envelope mass*, a wonderful simplification exists: it carbon mimics hydrogen. If one adds a “small” amount of carbon to an envelope ($XC \leq 0.1$), it leads to very nearly the same envelope *structure* as if one had added the same amount of hydrogen, by weight. The change in envelope mass is 30% at the most, and usually less than 10%. If one is satisfied by this accuracy in the envelope structure, this result enables one to cut down immensely on *envelope* computations:

carbon need not be included explicitly there. One need not include the carbon opacity tables. One need not include the six ionizations of carbon. One need not include its internal energy (which affects ∇_{ad}), etc. (Of course, the simplification discussed here applies only to obtaining the *structure* of such a low-mass envelope.) For example, it is a wonderful asset when applied to obtaining the outer boundary condition for interior calculations. It becomes even more dramatic if one encounters a time-variable envelope composition (e.g., as flash produced carbon is mixed into the envelope). A large change in the envelope mix of both carbon and hydrogen can now be reduced to a more easily computable change in hydrogen only.

We wish to express our gratitude to Professors Roger Blandford, Charles A. Barnes, and Steven E. Koonin for their helpfulness, and to Professors Steven C. Frautschi and James J. Morgan for financial support. One of us (A. I. B.) wishes to thank Professors Daiichiro Sugimoto, Ken'ichi Nomoto, and Icko Iben, Jr., for helpful discussions. We are especially indebted to Dr. Walter Huebner for supplying us with his opacity calculations in advance of publication, and to Professor Volker Weidemann for wonderful discussions and helpful comments.

REFERENCES

- Aller, L. H., and Czyzak, S. J. 1983, *Ap. J. Suppl.*, **51**, 211.
Bessell, M. S., Wood, P. R., and Evans, T. L. 1983, *M. N. R. A. S.*, **202**, 59.
Blanco, V. M., McCarthy, M. F., and Blanco, B. M. 1980, *Ap. J.*, **242**, 938.

- Cottrell, P. L., and Lambert, D. L. 1982, *Ap. J.*, **261**, 595.
- Cox, J. P., and Giuli, R. T. 1968, *Principles of Stellar Structure* (New York: Gordon and Breach).
- Cox, A. N., and Stewart, J. N. 1965, *Ap. J. Suppl.*, **11**, 22.
- . 1969, *Scientific Information of the Astronomical Council, USSR Academy of Sciences*, Vol. **15**.
- . 1970a, *Ap. J. Suppl.*, **19**, 243.
- . 1970b, *Ap. J. Suppl.*, **19**, 261.
- Cox, A. N., and Tabor, J. E. 1976, *Ap. J. Suppl.*, **31**, 271.
- Danziger, I. J. 1965, *M. N. R. A. S.*, **130**, 199.
- Eriksson, K., Gustafsson, B., Jørgensen, U. G., and Nordlund, Å. 1984, *Astron. Astrophys.*, **132**, 37.
- French, H. B. 1983, *Ap. J.*, **273**, 214.
- Fujimoto, M. Y., Nomoto, K., Sugimoto, D. 1976, *Pub. Astr. Soc. Japan*, **29**, 89.
- Huebner, W. F. 1976, private communication.
- . 1984, private communication.
- Hunger, K., Schönberner, D., and Steenbock, W. 1982, *Astron. Astrophys.*, **107**, 93.
- Iben, I., Jr. 1975, *Ap. J.*, **196**, 525.
- . 1976, *Ap. J.*, **208**, 165.
- Iben, I., Jr., and Renzini, A. 1982a, *Ap. J. (Letters)*, **259**, L79.
- . 1982b, *Ap. J. (Letters)*, **263**, L23.
- Iben, I., Jr., Kaler, J. B., Truran, J. W., and Renzini, A. 1983, *Ap. J.*, **264**, 605.
- Jacoby, G. H., and Ford, H. C. 1983, *Ap. J.*, **266**, 298.

Kurucz, B. 1984, private communication.

Magee, N. H., Jr. 1984, private communication.

Meyer-Hofmeister, E. 1982, in *Landolt-Börnstein: Numerical Data and Functional Relationships in Science and Technology, New Series*, ed. K.-H. Hellwege, Group VI: *Astronomy, Astrophysics, and Space Research*, Vol. 2, *Astronomy and Astrophysics*, Subvol. b, *Stars and Star Clusters*, ed. K. Schaifers and H. H. Voigt (New York: Springer-Verlag), p. 152.

Orlov, M. Ya., and Rodríguez, M. H. 1974, *Astron. Astrophys.*, **31**, 203.

Paczyński, B. 1969, *Acta Astr.*, **19**, 1.

———. 1977, *Ap. J.*, **214**, 812.

Sackmann, I.-J. 1976, preprint OAP-463.

———. 1980, *Ap. J. (Letters)*, **241**, L37.

Schwarzschild, M. 1958, *Structure and Evolution of the Stars* (Princeton: Princeton University Press), p. 63.

Searle, L. 1961, *Ap. J.*, **133**, 531.

Sugimoto, D., and Nomoto, K. 1975, *Pub. Astr. Soc. Japan*, **27**, 197.

Warner, B. 1967, *M. N. R. A. S.*, **137**, 119.

Table 1

Effects of Molecules on Opacities

log ρ	Generation	Opacities κ for values of log T			
		3.3	3.5	3.7	3.9
-12	(new) IV	0.0025	0.0031	0.0032	0.49
	(old) II	0.000033	0.000049	0.0023	0.40
-10	(new) IV	0.0046	0.0031	0.0039	0.91
	(old) II	0.0019	0.000079	0.0012	0.83
-8	(new) IV	0.0092	0.0073	0.031	3.1
	(old) II	0.0023	0.00087	0.011	2.1

Note.—Rosseland mean opacities κ for low densities ρ and temperatures T . Generation IV opacities, which include the opacity due to molecular lines, are much larger at low temperatures than generation II opacities, which do not. (Generation III opacities do not differ much from generation II opacities.)

Table 2

Opacity Comparison: C-rich Mix vs. Normal Mix

log ρ	Mix	Opacities κ for values of log T								
		3.6	3.8	4.0	4.2	4.5	5.0	5.5	6.0	6.3
-12	C-rich	0.0062	0.021	0.11						
	normal	0.0034	0.026	0.96						
-11	C-rich	0.0066	0.024	0.12	0.26					
	normal	0.0033	0.027	1.55	0.41					
-10	C-rich	0.011	0.055	0.60	0.68	0.40				
	normal	0.0033	0.035	4.7	1.1	0.55				
-9	C-rich	0.015	0.095	2.9	3.1	1.1	0.30			
	normal	0.0046	0.065	14.	6.6	1.3	0.40			
-8	C-rich			27.	20.	5.9	0.56	0.25		
	normal			28.	61.	7.8	0.69	0.34		
-7	C-rich					51.	2.6	0.32		
	normal					81.	2.7	0.40		
-6	C-rich						24.	0.76	0.28	
	normal						22.	0.76	0.35	
-5	C-rich							3.8	0.39	0.27
	normal							2.9	0.38	0.34
-4	C-rich								0.92	0.36
	normal								0.61	0.39
-3	C-rich								6.2	0.85
	normal								2.4	0.66

Note.—Rosseland mean opacities κ for typical envelope (ρ, T) values; the dots indicate roughly the run of density for our envelopes. Carbon *increases* the opacity in the (ρ, T) ranges to the lower left of the lines, but *decreases* the opacity elsewhere. C-rich mix *c* has $XC = 0.31$, $X = 0.27$; normal mix *a* has $XC = 0$, $X = 0.70$.

FIGURE CAPTIONS

Fig. 1.—The degree of ionization for hydrogen, helium, and carbon as a function of temperature T . The quantity $N^{(i)}$ refers to the total number density of the i^{th} element; $N_r^{(i)}$ refers to the number density of its r^{th} stage of ionization (where $r = 1$ refers to the neutral atom). The partition functions u_r for the first four ionization stages of carbon are also shown, up to the highest temperatures at which their respective ionization stages exist in significant amounts (see Section IIb for discussion of partition functions).

Fig. 2.—(a) Run of opacity κ as a function of temperature T in four envelopes of different chemical composition, at the same luminosity ($\log L = 4.1$) and effective temperature ($\log T_e = 3.584$). Mix *a* (dotted) is our normal composition: $X_C = 0$, $X = 0.70$, $Y = 0.27$, $Z = 0.03$. Mix *b* (solid) is carbon-enriched: $X_C = 0.10$, $X = 0.56$, $Y = 0.31$, $Z = 0.03$. Mix *c* (dashed) is an *extreme* carbon-enriched case: $X_C = 0.31$, $X = 0.27$, $Y = 0.39$, $Z = 0.03$. Mix *d* (solid) is an R CrB-type composition: $X_C = 0.10$, $X = 0$, $Y = 0.87$, $Z = 0.03$. (b) Run of density ρ as a function of temperature T for the same four envelopes.

Fig. 3.—Convection for the four envelopes of Fig. 2. The adiabatic and radiative temperature gradients (∇_{ad} and ∇_{rad} , respectively) are given as a function of the temperature T . The convective regions (defined by $\nabla_{\text{rad}} > \nabla_{\text{ad}}$) are indicated by “curly” regions, and the mass from the surface to the bottom of convection is given. The dips in ∇_{ad} are caused by the partial ionizations of hydrogen, helium,

and carbon. Panels (a), (b), (c), and (d) refer to the mixes *a*, *b*, *c*, and *d*, respectively (as defined in Fig. 2). Note that in all four cases convection reaches down to the same temperature, $\log T \simeq 4.7$.

Fig. 4.—Convection in the envelope, across the H-R diagram. The ordinate, $M - M_r$, gives the mass measured from the surface down, where the surface refers to an optical depth $\tau = 0$; the abscissa gives the effective temperature T_e . Convection is indicated by “curly” regions. The lower solid line indicates the bottom of the envelope (arbitrarily defined by $T = 2 \times 10^6 K$). The *top* of the convective region is shown by dashed lines, to emphasize the uncertainties in the mixing length theory of convection there (see text). Panels (a), (b), (c), and (d) refer to mixes *a*, *b*, *c*, and *d*, respectively (as defined in Fig. 2).

Fig. 5.—Envelope mass M_{env} as a function of envelope effective temperature T_e at constant luminosity ($\log L = 4.1$) for the four *mixes* of Fig. 2. The envelope mass is here defined unconventionally, as the mass exterior to the point where the temperature reaches $T = 2 \times 10^6 K$.

Fig. 6.—Effect on envelope mass M_{env} of replacing carbon with hydrogen, as a function of envelope temperature T_e . The envelope mass is defined as in Fig. 4. Curve *a* (solid): normal mix, with $XC = 0$, $X = 0.7$; curve *e* (dashed): $XC = 0.1$, $X = 0.6$; curve *f* (dotted): $XC = 0.3$, $X = 0.4$. Curve *d* (dashed): R CrB mix, with $XC = 0.1$, $X = 0$; curve *g* (solid): $XC = 0$, $X = 0.1$. To illustrate carbon “saturation” effect: curve *h* (dotted): $XC = 0.3$, $X = 0$; curve *j* (dot-dashed):

helium envelope, with $X_C = 0$, $X = 0$ (compare with curve d). Note that all mixes have $Z = 0.03$.

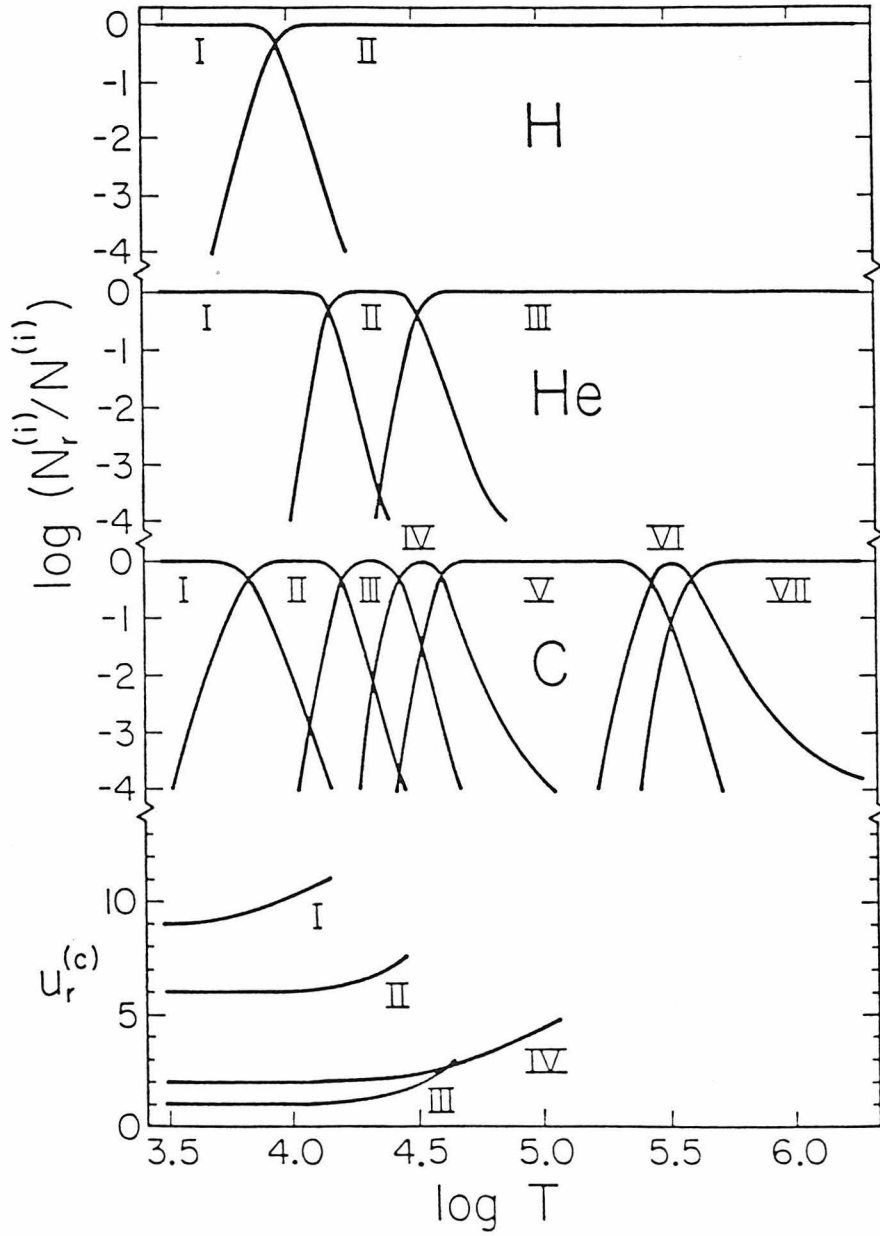


FIG. 1

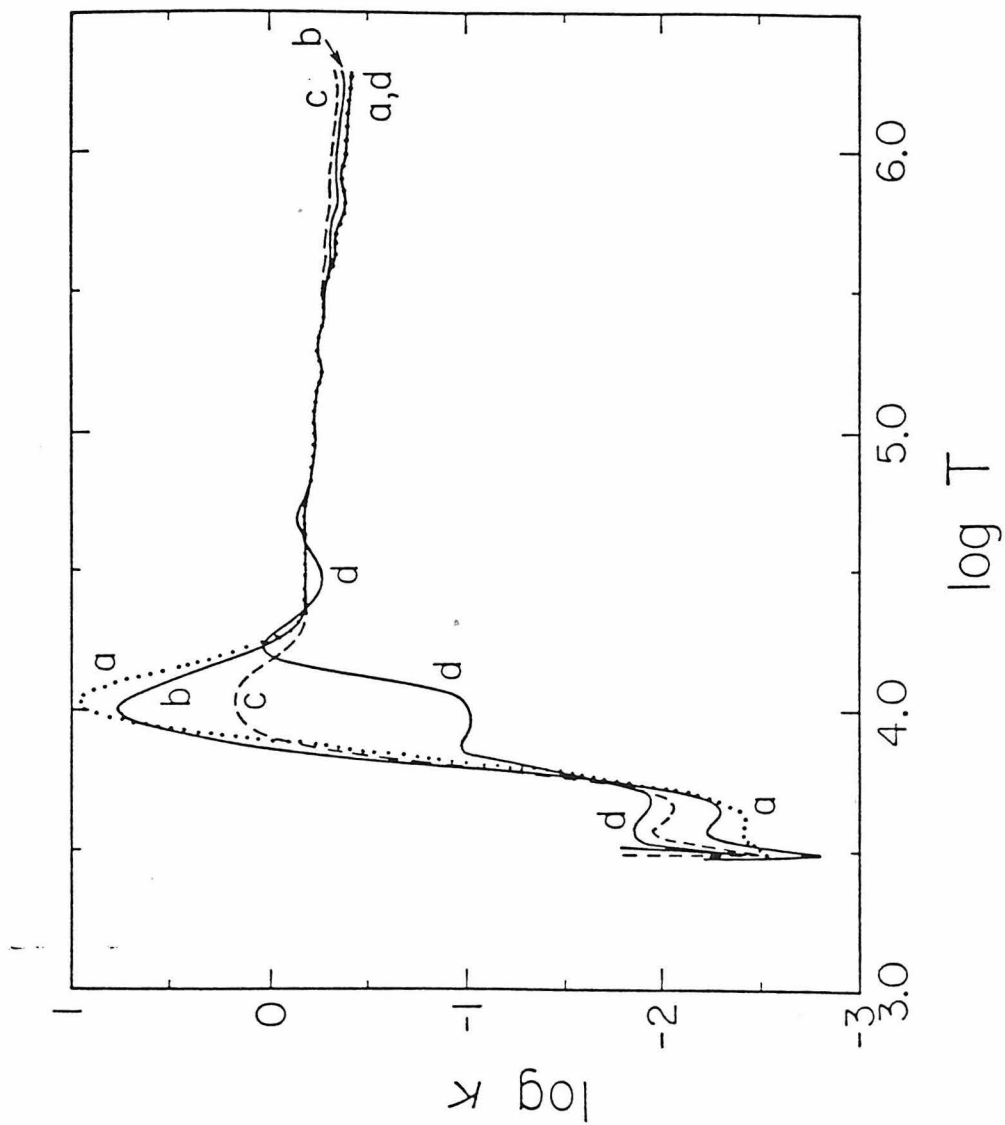


FIG. 2a

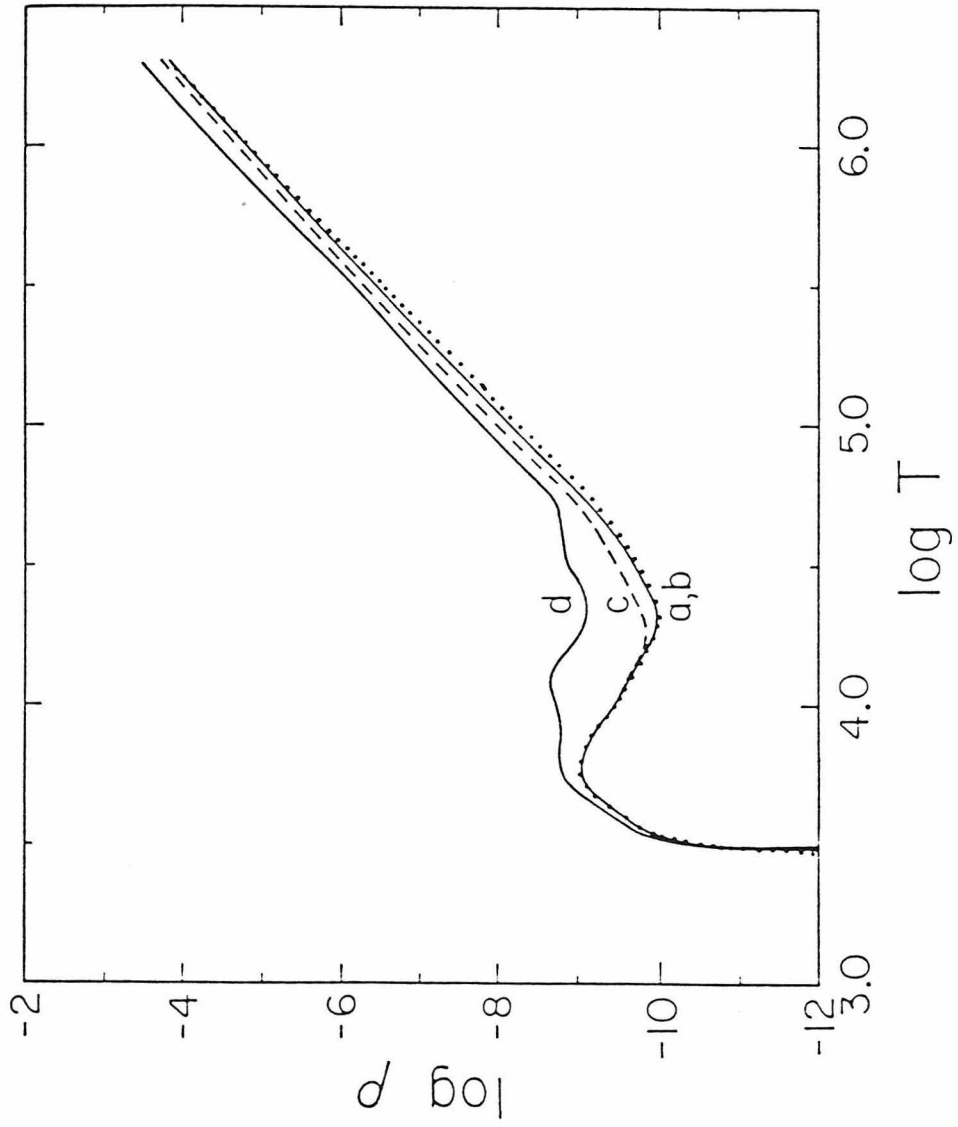


FIG. 2b

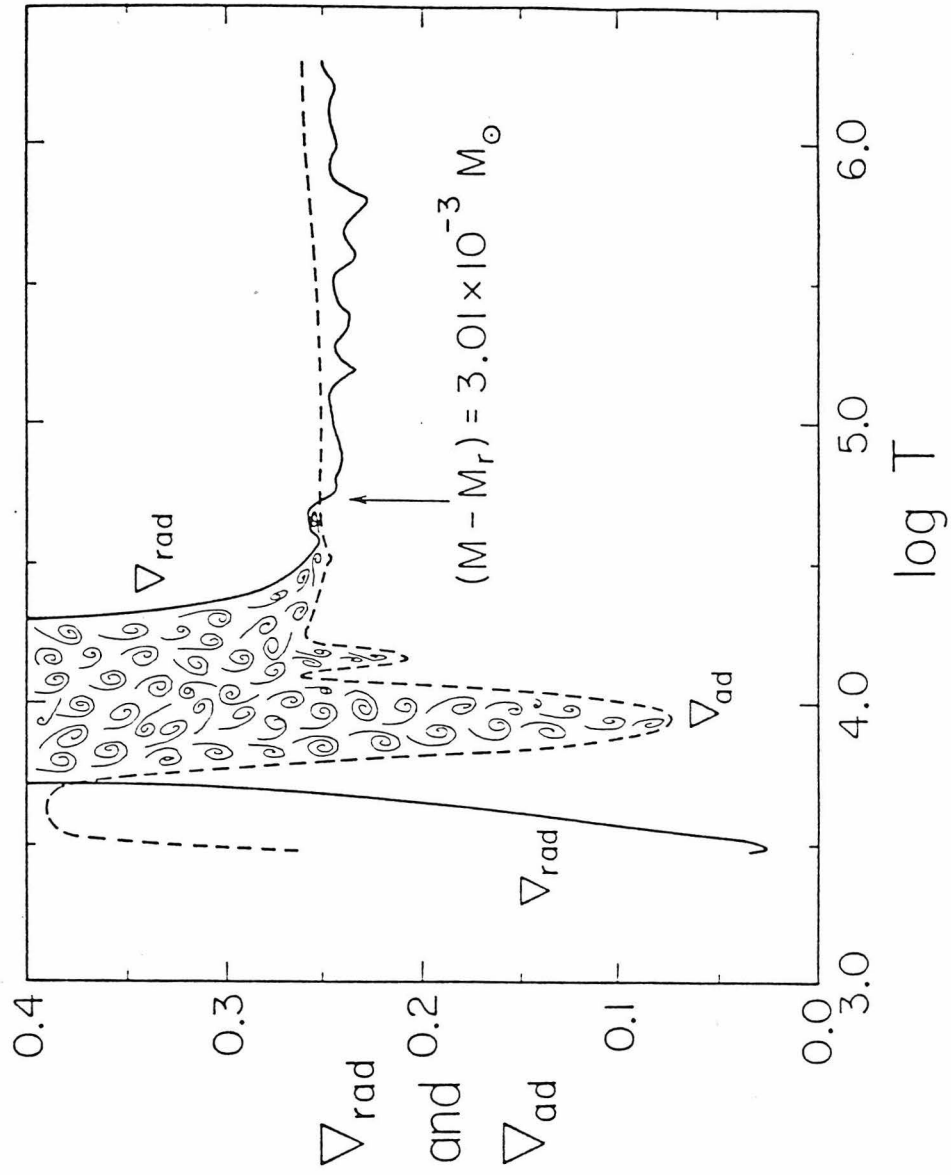


FIG. 3 α

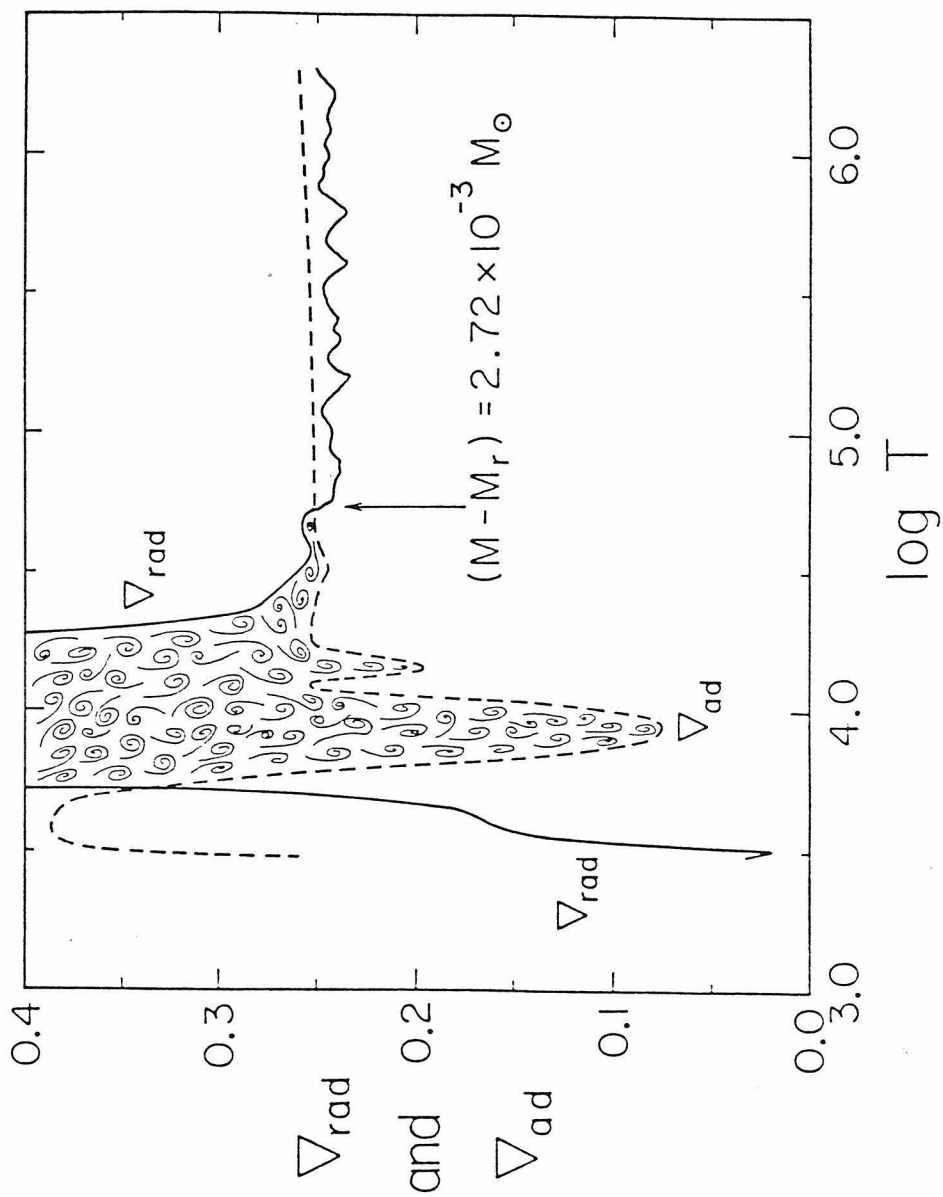


FIG. 3b

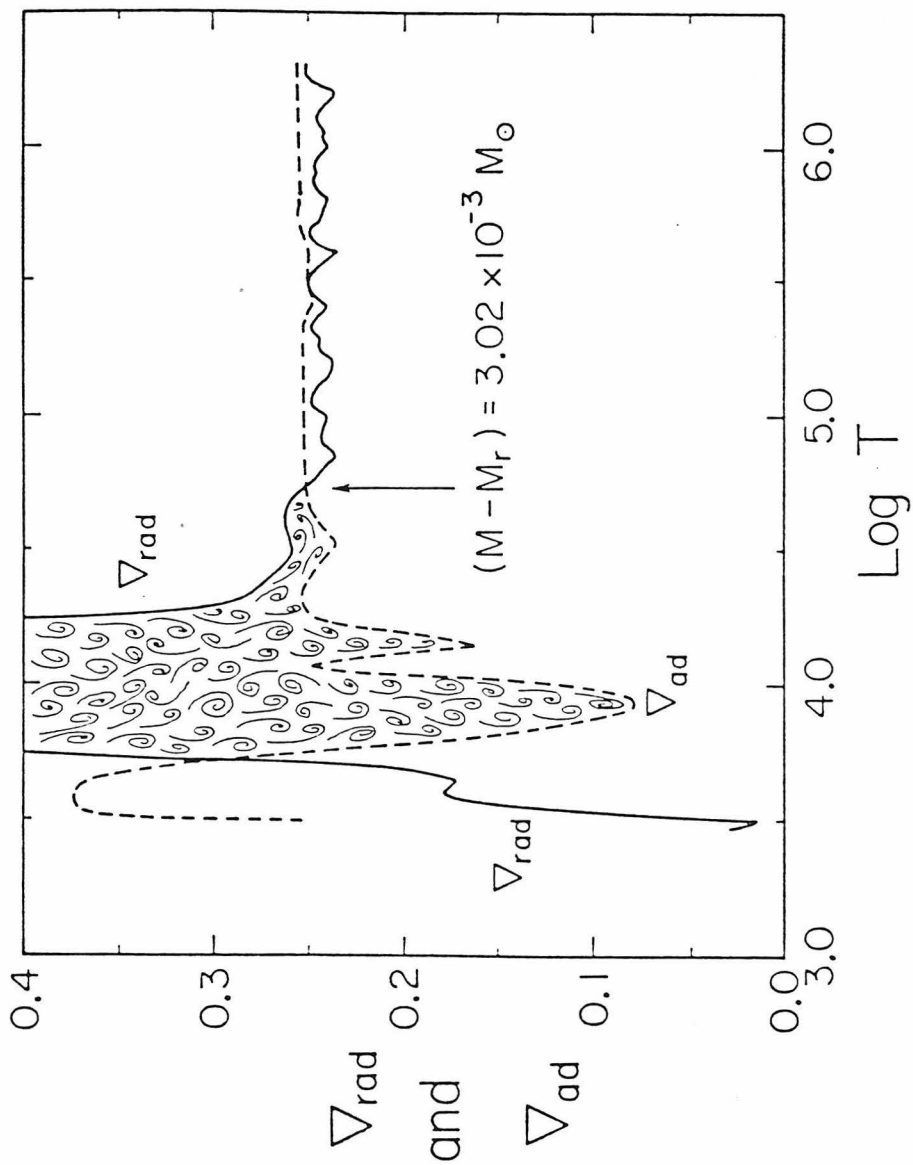


FIG. 3c

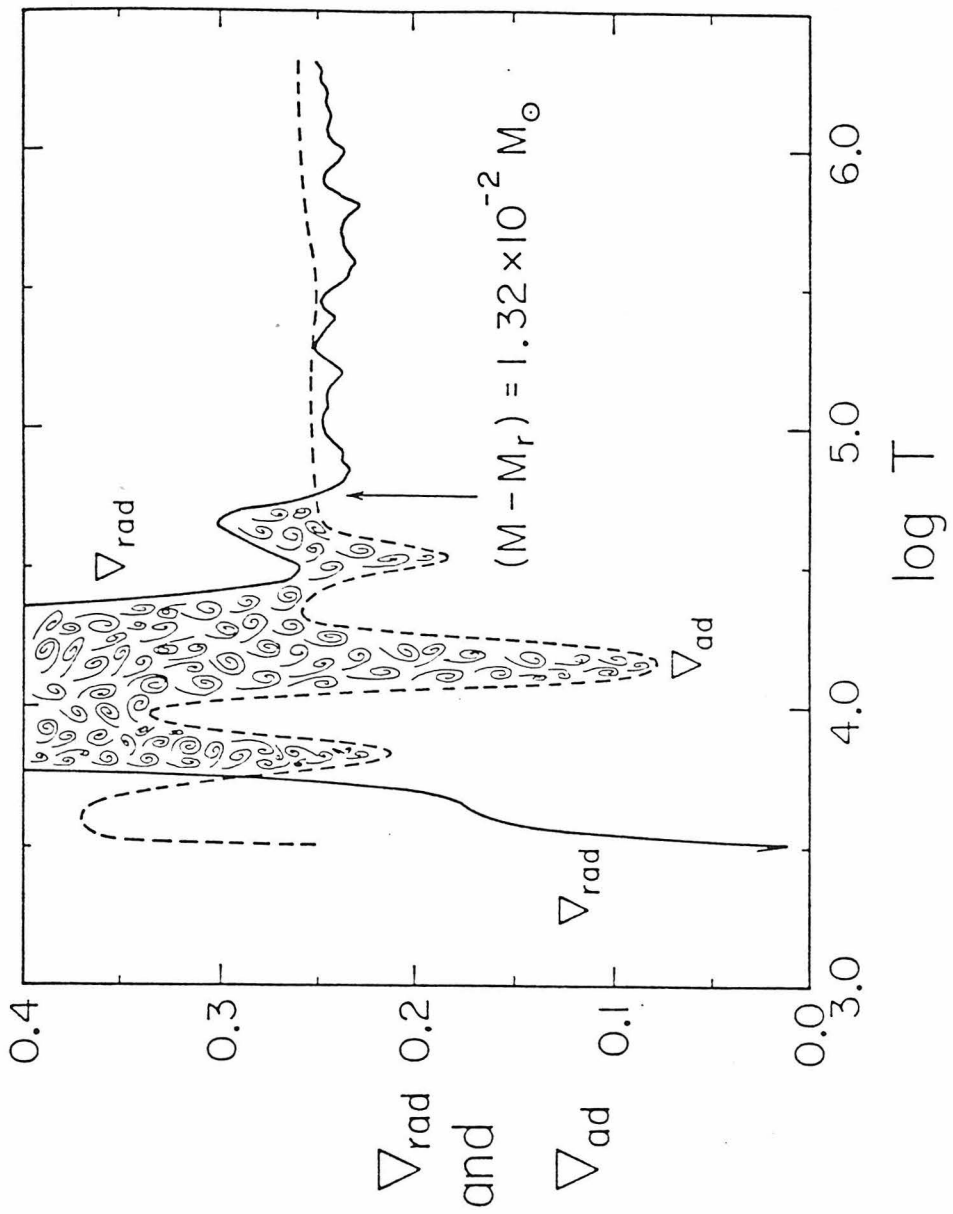


FIG. 3d

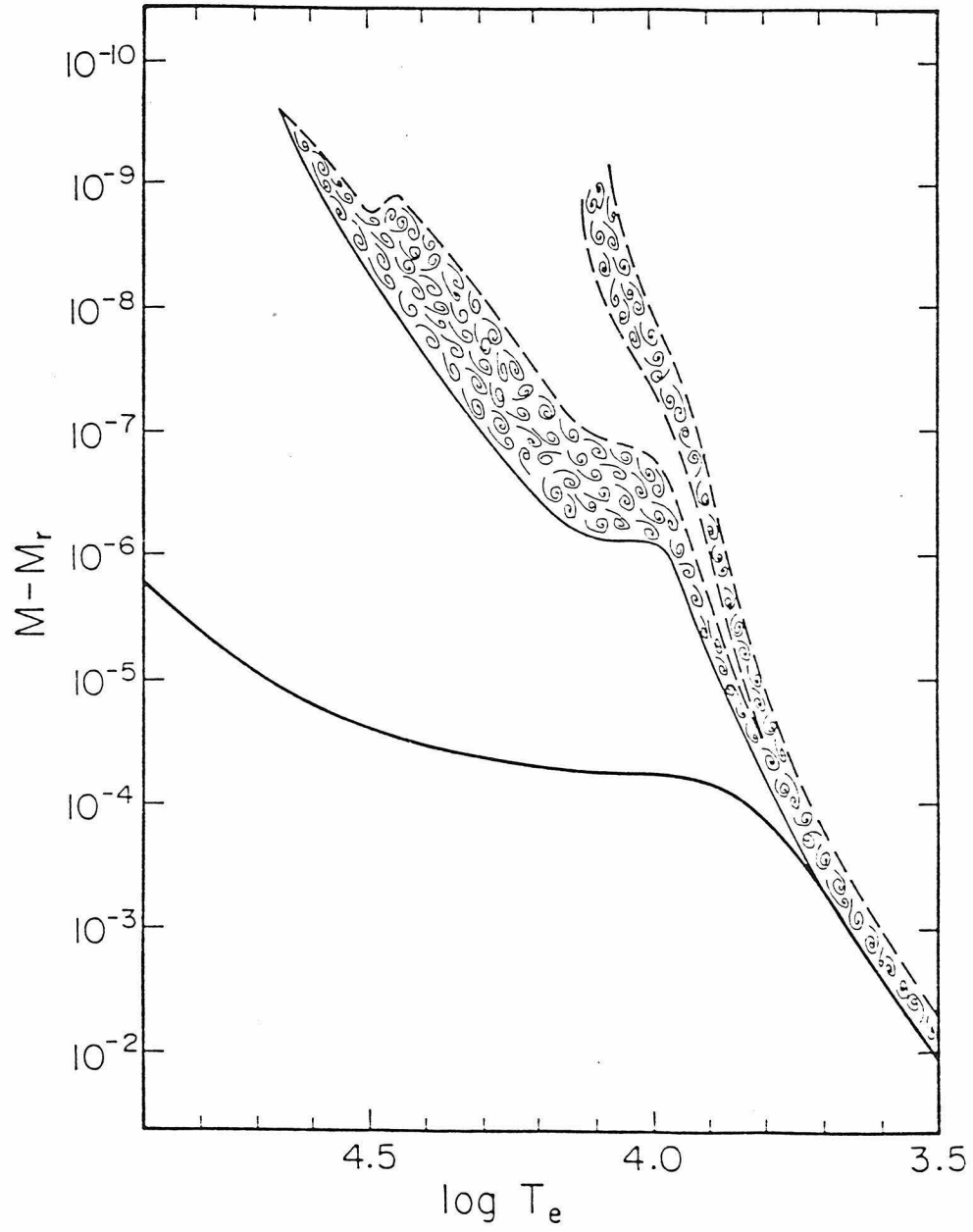


FIG. 4a

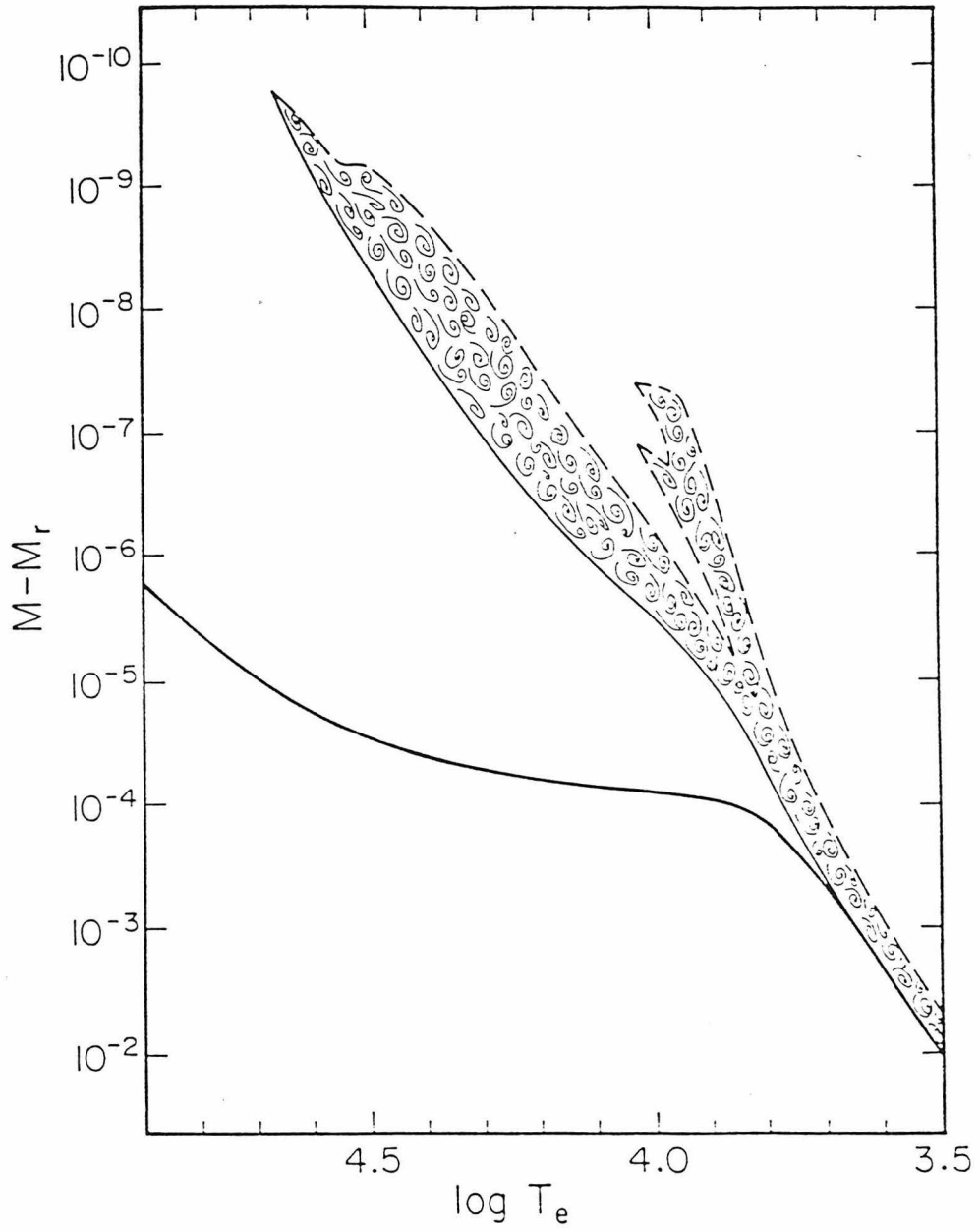


FIG. 4b

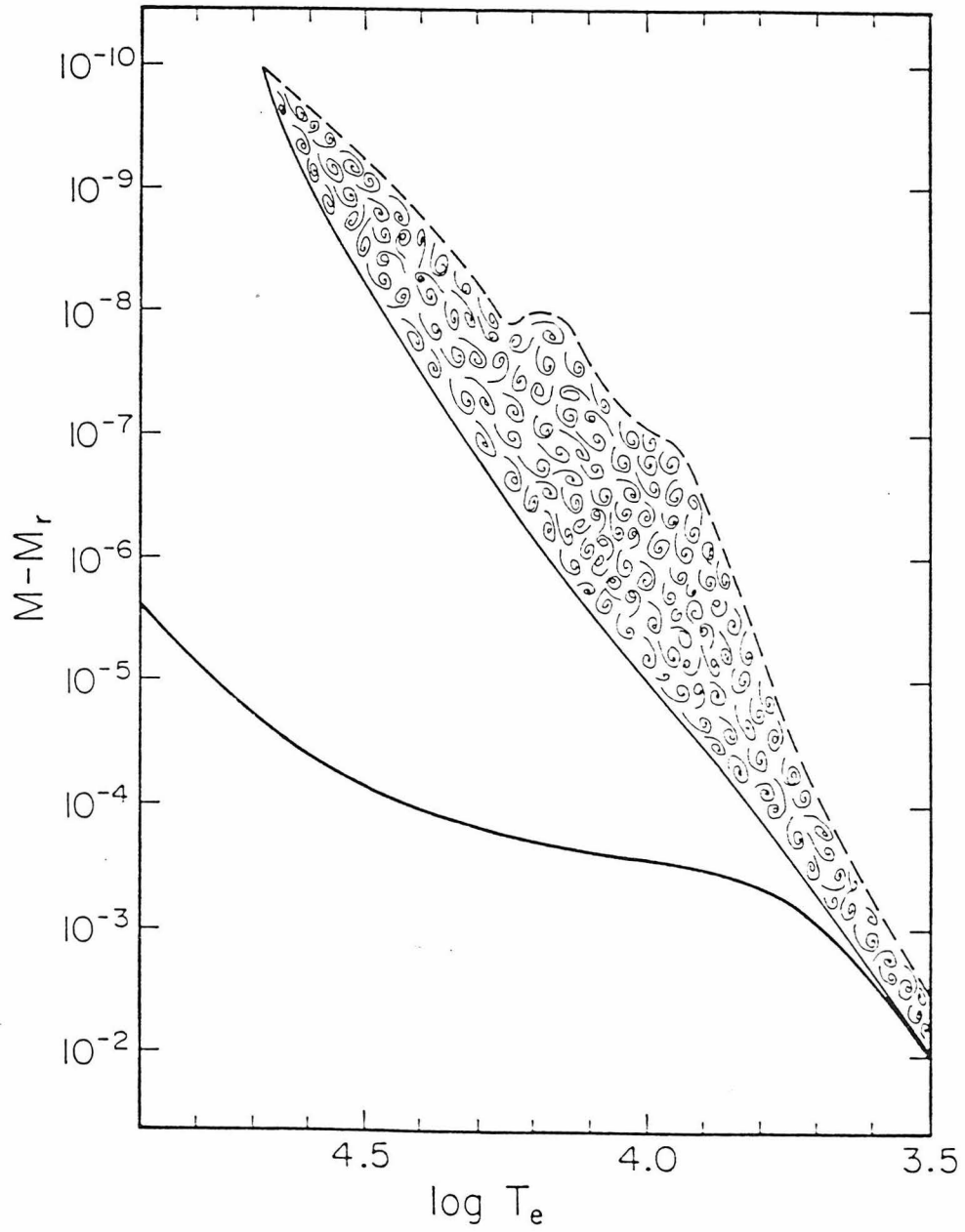


FIG. 4c

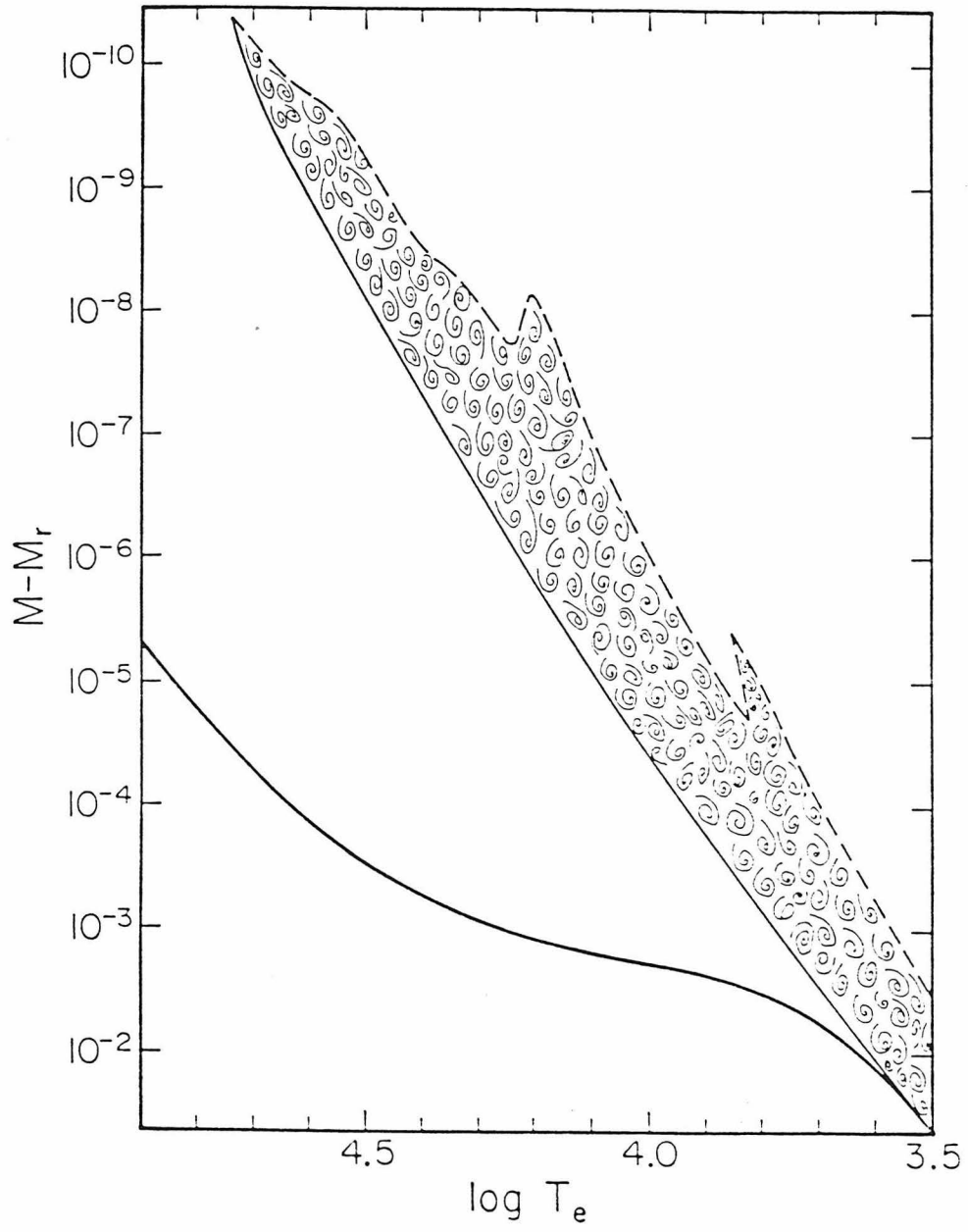


FIG. 4d

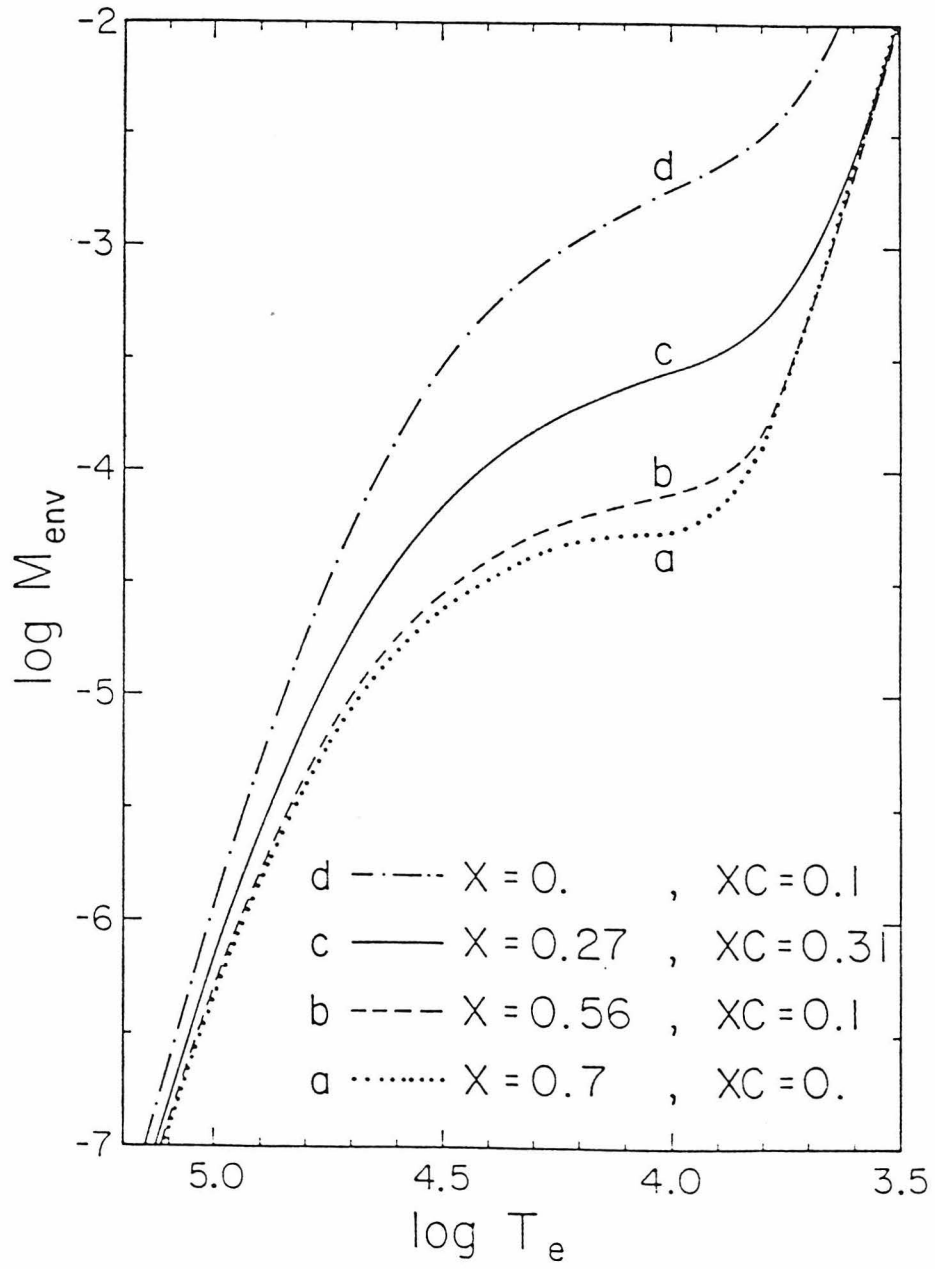


FIG. 5

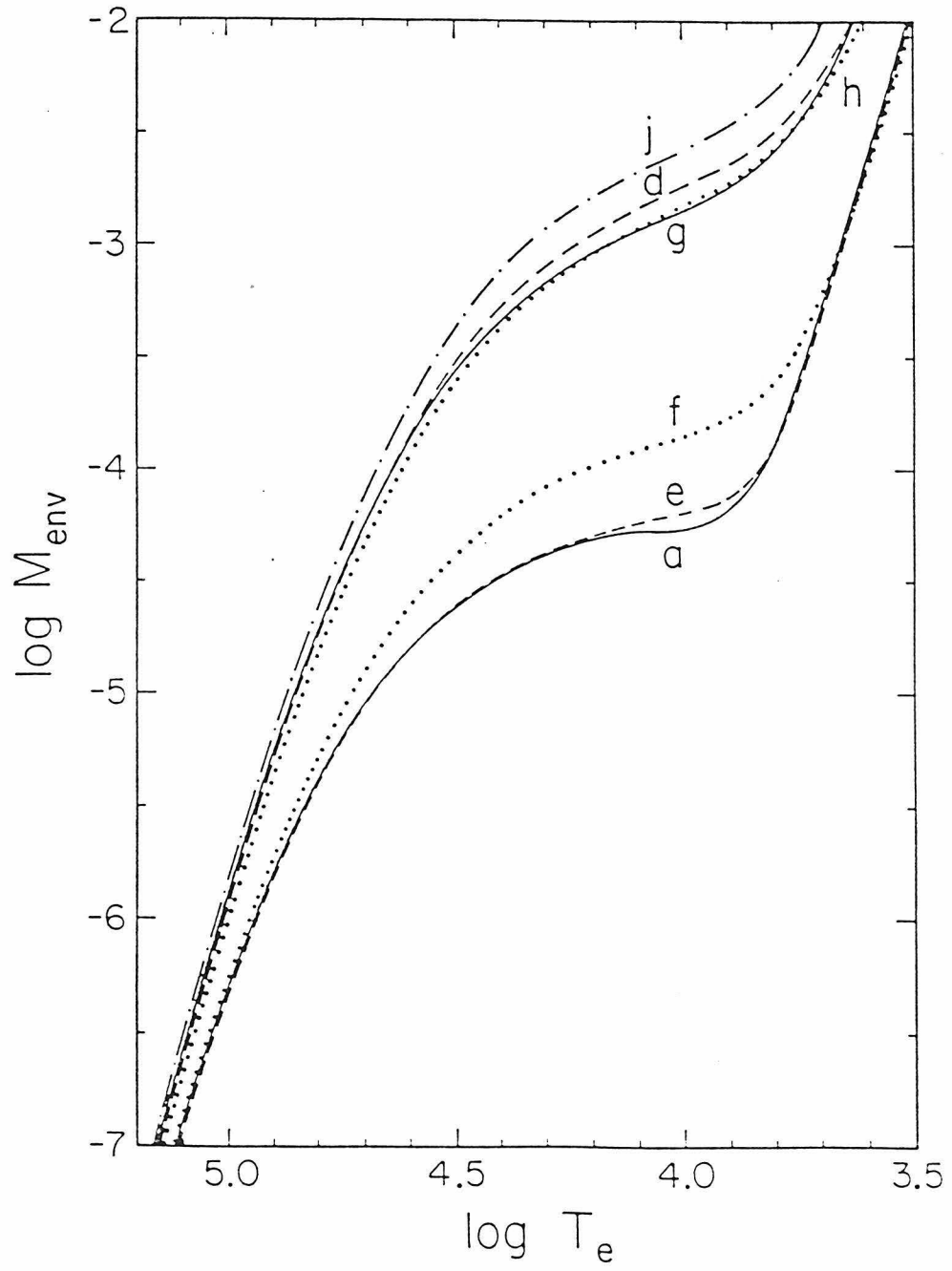


FIG. 6

CHAPTER 2.

I. Flash-Driven Luminosity and Radius Variations for Low Mass Stars

Arnold I. Boothroyd and I.-Juliana Sackmann

W. K. Kellogg Radiation Laboratory 106-38

California Institute of Technology, Pasadena, CA 91125

ABSTRACT

The observable and potentially observable consequences of helium shell flashes were investigated for a number of low mass stars. Stars of low metallicity ($Z = 0.001$) with initial masses of $1.0 M_{\odot}$, $1.2 M_{\odot}$, and $2.0 M_{\odot}$ were considered, as well as stars of solar metallicity ($Z = 0.02$) with initial masses of $1.2 M_{\odot}$ and $3.0 M_{\odot}$. For flashes whose strength was at or near maximum amplitude, light curves and radius curves were obtained over the full flash cycle. These are of interest to investigations of envelope instability and mass ejection. Potentially observable luminosity variations are confined to a few decades immediately following the helium shell flash, as compared to interflash periods of tens of thousands of years, and so would be exhibited by less than one AGB star in a thousand; radius variations would be even harder to observe directly. The slower variations, however, cause stars of initial mass near $1.0 M_{\odot}$ to spend as much as 20% to 30% of the interflash period at a luminosity a factor of

two lower than the interflash luminosity indicated by the $M_c - L$ relation. Higher mass stars stay closer to the $M_c - L$ line. Particularly for the low-metallicity cases, the post-flash luminosity maximum causes the star to spend a few centuries at a luminosity as much as twice that indicated by the $M_c - L$ relation. This could cause the star to encounter dynamic envelope instability and rapid mass loss at a core mass lower by of order $\Delta M_c \approx 0.1 M_\odot$ than would otherwise be the case.

I. INTRODUCTION

It is well known that regular luminosity and radius variations occur in RR Lyrae stars, Cepheids, and Miras. These pulsations, driven by ionization effects in the stellar envelope, take place on a timescale of hours to years. However, in addition to Mira-type pulsation, asymptotic giant branch stars have a more extensive (though much slower) form of luminosity and radius variations, driven by the repetitive thermonuclear runaway reactions in their interior known as helium shell flashes, or thermal pulses. The luminosity variations may in some cases be fast enough to be directly observable. The radial variations are quite as large as the luminosity variations, but a good deal harder to observe. Perhaps more important are the potential effects of the luminosity and radius variations on mass loss. As pointed out by Tuchman, Sack, and Barkat (1978, 1979), the flash-driven radius and luminosity increase could drive the star's envelope into a dynamically unstable regime, leading to rapid mass loss and potentially to ejection of practically the entire envelope of the star. This would cause the star to leave the asymptotic

giant branch for the planetary nebula stage at an earlier point in time than would otherwise be the case. This could, for example, solve discrepancies between observations and theoretical predictions of the relative number of low-period Mira variables (Tuchman, Sack, and Barkat 1979). There are also implications for interpretation of the core mass–luminosity relation, since the star spends part of the flash cycle at a luminosity rather different from that specified by the $M_c - L$ relation (see also Boothroyd and Sackmann 1987*a*, hereafter Paper II).

The existence of these flash-driven luminosity and radial variations is well established (but seldom reported in any detail) by theoretical investigations of shell flashes. Occasionally the surface variations during the shell flash cycle are diagrammed (see, e.g., Iben 1975, Härm and Schwarzschild 1975, Schönberner 1978, Sackmann 1980, Wood and Zarro 1981, and Iben 1982), but no previous systematic and self-consistent investigation has been made. It is the purpose of this paper to present the results of such an investigation for low mass stars (from $1 M_\odot$ to $3 M_\odot$) of both low metallicity ($Z = 0.001$) and solar metallicity ($Z = 0.02$).

II. COMPUTATIONAL DETAILS

Stars of relatively low mass, from one to a few solar masses, present certain difficulties to a theoretician interested in the later stages of their lifetimes. The main sequence and red giant branch stages are straightforward, but a star of less than about two and a half solar masses terminates the red giant branch with an exceedingly violent helium core flash in its degenerate helium core. This is sufficiently difficult to handle computationally that many investigators prefer to begin

with the subsequent horizontal branch stage, at the cost of a certain arbitrariness of initial conditions, and continue on from there to the asymptotic giant branch stage with its helium shell flashes. We have chosen instead to evolve our stars from initial zero age main sequence models, following them through their entire lifetime *including* the core flash, and thus preserving information on initial mass and total age of the stars. It is true that the core flash can only be approximated by any non-hydrodynamic, one-dimensional code (see, e.g., Deupree 1984), but an approximation is better than ignoring the event completely, and the effect of inaccuracies in the core flash is likely to be small. By the time the star reaches the asymptotic giant branch, the core regions affected by the core flash have in any case been reprocessed by later helium core and shell burning into the degenerate carbon-oxygen core of the double-shell burning stage.

For the low-metallicity case ($Z = 0.001$, with initial hydrogen and helium content $X = 0.759$, $Y = 0.24$), stars of initial mass $1.0 M_{\odot}$, $1.2 M_{\odot}$, and $2.0 M_{\odot}$ were considered; for the case of solar metallicity ($Z = 0.02$, with initial $X = 0.71$, $Y = 0.27$), stars of initial mass $1.2 M_{\odot}$ and $3.0 M_{\odot}$ were considered. The effect of a Reimers (1975) type wind mass loss $\dot{M} = -\eta(4 \times 10^{-13} M_{\odot}/\text{yr})L/(gR)$ (L , g , and R in solar units: Kudritzki and Reimers 1978) was included whenever a star's effective temperature fell below $5000 K$, i.e., for $\log T_e < 3.7$. As recommended in Kudritzki and Reimers (1978), the value of η was chosen to be $\eta = 0.4$ except for the $3.0 M_{\odot}$ case, where $\eta = 1.4$ was chosen. Every effort was made to include the latest nuclear reaction rates, neutrino losses, and opacities (including molecular opacities at low temperatures); the *dynamical* effects of carbon and oxygen ionizations were

also included. For a more complete discussion of the computational details, see Boothroyd and Sackmann (1987*b*, hereafter Paper III).

It should be noted that a mixing length to pressure scale height ratio of $\alpha \equiv l/H_p = 1.0$ was used when considering envelope convection; choice of a larger value of α would reduce somewhat the stellar radii found in this paper. Stellar radius R is approximately inversely proportional to α , and it seems probable that the appropriate value of α is somewhere around 1.5 to 2 (see Paper III), so the radius values quoted in this paper are probably overestimates by this same factor of 1.5 to 2.

III. RESULTS AND DISCUSSION

For each of the stars under consideration, a number of helium shell flashes were computed. It should be noted that for the lower mass stars, $1.2 M_{\odot}$ and below, the Reimers wind mass loss caused the asymptotic branch stage to terminate after only about half a dozen flashes had occurred. For these stars, the flashes did not quite reach the full amplitude appropriate to the stars' core masses. They do not fall far short, however (see Paper III), and as may be seen from Figure 1, the surface radial and luminosity variations driven by the flashes settle down to a regular form after only four or five flashes. Thus the variations encountered for the lowest mass stars in this work can be considered to be typical of such stars, even if a slightly lower mass loss rate were really appropriate (so that a couple of further flashes could occur).

Another point worthy of mention is that two stars of the same initial mass but different metallicities result in rather different asymptotic branch stars: a star of metallicity $Z = 0.02$ encounters helium shell flashes at a much smaller core mass than a star of metallicity $Z = 0.001$. (In this paper we follow the usual double-shell burning convention of considering the core mass M_c to be the mass M_H interior to the hydrogen-burning shell.) This is important because most parameters of a helium shell flash, including its effects on the surface of the star, are a strong function of the star's core mass but depend only very weakly if at all on the star's total mass or initial mass. Thus in comparing the behavior of different stars, one should attempt to look at the surface behavior as a function of core mass and metallicity: the star's total mass and its initial mass are nearly irrelevant to its behavior on the asymptotic giant branch, with the caveat that when the envelope mass grows very small the star leaves the asymptotic giant branch for the planetary nebula stage.

Figures 2 through 6 trace the variation of luminosity and radius with time over a flash cycle for each of the stars under consideration. The general shape of the light curves is very similar: from the pre-flash luminosity maximum (point *A*), a sharp decline takes place to a minimum (point *B*), followed by an even steeper return to approximately the pre-flash luminosity. From there, the luminosity continues to increase more slowly to a maximum (point *C*); stars of lower core mass have a smaller secondary peak following this maximum. The luminosity then declines on a *much* longer timescale to its interflash minimum (point *D*) before slowly back up to the next pre-flash maximum value (point *E*). The variations in radius track the variations in luminosity very closely, except when the envelope mass (exterior to

the hydrogen-burning shell) grows very small; for the $1.0 M_{\odot}$, $Z = 0.001$ star and the $1.2 M_{\odot}$, $Z = 0.02$ star, the last flash digrammed takes place when mass loss has reduced the envelope mass sufficiently that the star is already moving off to the left of the asymptotic giant branch in the H-R diagram, toward higher effective temperatures and lower radii. The luminosity and radius values for each of the stars at points *A* through *E* are given in Table 1.

The shape of the light curves and radius curves is easily explained in terms of the interior events of the star. Prior to the helium shell flash, almost all the star's luminosity is produced by the hydrogen-burning shell. When the shell flash occurs, a huge amount of energy is produced in the helium-burning shell, but at first this affects only the intershell zone directly. The intershell zone expands, pushing the hydrogen-burning shell out and causing it to cool; hydrogen burning stops entirely, and the stellar surface contracts and grows dimmer, since it is no longer supported by the luminosity from hydrogen burning. Eventually the increased luminosity of the helium-burning shell makes itself felt, and the surface expands and brightens (by the time this happens, the helium-burning rate is declining again, but is still quite large). From the peak until the interflash minimum, the surface luminosity (and radius) drop in concert with the declining helium burning. As helium burning declines, the intershell zone contracts and the hydrogen-burning shell heats up again and reignites. The interflash luminosity and radius minimum occurs as the growing hydrogen-burning luminosity becomes comparable to the declining helium-burning luminosity; thereafter, the surface luminosity tracks the hydrogen-burning luminosity, until the next flash.

All the stars have a small secondary peak in the *helium-burning rate*, subsequent to the main flash. In stars of low core mass this secondary helium-burning peak gives rise to the secondary surface luminosity and radius peak, as the surface by this time has settled down to track the helium-burning luminosity (see Figs. 2*a*, 3*a*, and 5*a*). In stars of higher core mass, however, the nuclear timescales are much shorter. Thus in such stars the secondary helium-burning peak occurs too soon after the main flash for the envelope to respond to it separately, and the secondary peak is absorbed into the primary surface luminosity and radius peak. Thus only stars of lower core mass, where the nuclear timescales of the helium-burning shell are much longer, have secondary maxima in their luminosity and radius curves.

As may be seen from Figures 2 through 6 and Table 1, the luminosity and radius variations are considerable: they vary in some cases by more than a factor of two from their quiescent pre-flash values. The question arises whether they may in some cases be fast enough to be observable. Table 2 was compiled in an attempt to answer this question. For those portions of the flash cycle where the surface change is most rapid, namely for the initial fast decline (between points *A* and *B*) and the subsequent even faster increase in luminosity and radius (between points *B* and *C*), the maximum rate of change of both luminosity and radius are given in Table 2, along with the percent of the total flash cycle during which these rapid motions are sustained (as well as their duration in years).

There are several obstacles to direct observation of these changes. Even the most rapid changes take place on a timescale of decades, so that observations must

cover a long interval (years at least) in order for any changes to be evident. Also, many of these stars may be expected to be Mira-type pulsators: these pulsations are fairly substantial, and have periods of the order of hundreds of days (Tuchman, Sack, and Barkat 1979), so that it would be necessary to follow the light curve of the star in fair detail over the observation interval in hopes of averaging these pulsations out. Worse yet, for these relatively low mass stars, the period during which rapid surface variations take place comprises less than one part in a thousand of the total flash cycle (see Table 2). At any point in time, less than one asymptotic giant branch star in a thousand can be expected to be changing rapidly due to a helium shell flash. Thus the luminosity variations might be detectable, but are unlikely to be found except by a lucky accident.

If anything, the prospect for direct observation of the radial motions are worse. The flash-driven radial contraction and expansion velocities do not exceed a kilometer per second (see Table 2), and might be only half as big (due to the fact that a larger value of the mixing length parameter α is appropriate, reducing the stellar radius: see Section II). Thus detection via the Doppler effect would be exceedingly difficult: larger radial velocities arise from the Mira-type pulsations, from the atmospheric turbulence, and from the mass flow of the stellar wind. Direct radius observations are not very promising either. Ground-based speckle interferometry (see, e.g., McCarthy 1982, Mariotti *et al.* 1983) has yielded radius measurements of about a dozen stars, and the space telescope could yield some direct radius measurements since its resolution is limited only by diffraction (Burke 1984), but such measurements are limited to relatively nearby objects. Future prospects are a bit

more encouraging: multiple mirror telescopes with a reasonably long baseline between mirrors might achieve exceptional resolutions (Weigelt 1983). One would have to be rather lucky, however, to find a star close enough to observe which happened to be in a stage of rapid flash-driven motion, and one would still have to average out any pulsational motion.

The flash-driven luminosity variations have an important effect on the interpretation of the $M_c - L$ relation. Discovered by Paczyński (1970) and confirmed by others (Iben 1977; Havazelet and Barkat 1979; Wood and Zarro 1981; see also Paper II), this relation relates the interflash luminosity L of an asymptotic giant branch star to its core mass $M_c \equiv M_H$ (although composition and total stellar mass also have some effect). It has proved to be extremely useful in modelling events on the asymptotic giant branch, providing simple analytic approximations for the description of the star's evolution there. It has also been used to infer a core mass from an observed asymptotic giant branch tip luminosity (Weidemann 1984; Aaronson and Mould 1985), thereby obtaining a final mass M_f for use in determining the Weidemann and Koester (1983) $M_i - M_f$ relation. These uses of the $M_c - L$ relation do not, however, take into account the variability of the luminosity during the flash cycle. Table 3 presents our results concerning the fraction of the time the star spends at a luminosity significantly different from what would be expected from use of the $M_c - L$ relation. The lowest mass stars especially spend as much as 20% to 30% at a luminosity less than half that given by the $M_c - L$ relation. This would lead to an underestimate of the core mass by as much as $\Delta M_c \approx 0.1 M_\odot$ for as many as 30% of the low mass stars whose luminosity was observed. Alternatively, one can

say that the asymptotic giant branch tip luminosity could be underestimated by as much as a factor of 2 in sparsely populated clusters. There is also a small chance of an overestimate. (This is discussed in more detail in Paper II.)

The effect on mass loss could be equally dramatic. The post-flash luminosity and radius maximum in effect drives the star up the asymptotic giant branch to a position which it would not reach until much later if quiescent burning was all that took place. The effect is especially pronounced in the low-metallicity stars ($Z = 0.001$), where the luminosity maximum is a factor of 2 greater than the quiescent value; in the high-metallicity stars ($Z = 0.02$) this factor is around 1.7. Actual investigations of envelope stability are beyond the scope of this paper. However, if the asymptotic giant branch for the star passes through a region of the $L - T_e$ plane where envelopes do become dynamically unstable, this envelope instability will be encountered at a core mass lower by as much as $\Delta M_c \approx 0.1$ than would be predicted from the $M_c - L$ relation. This could lead to major amounts of mass loss (Tuchman, Sack, and Barkat 1978, 1979), causing the star to terminate the asymptotic giant branch phase much earlier than would otherwise be the case.

This work was carried out at the W. K. Kellogg Radiation Laboratory. We wish to express our gratitude to Professors R. D. Blandford, C. A. Barnes, S. E. Koonin, and S. C. Frautschi for their encouragement and support; we have also benefitted from valuable discussions with Professors W. A. Fowler and J. R. Mould.

REFERENCES

- Aaronson, M., and Mould, J. 1985, *Ap. J.*, **288**, 551.
- Boothroyd, A. I., and Sackmann, I.-J. 1987*a* (Paper II).
- . 1987*b* (Paper III).
- Burke, B. 1984, private communication.
- Deupree, R. G. 1984, *Ap. J.*, **287**, 268.
- Härm, R., and Schwarzschild, M. 1975, *Ap. J.*, **200**, 324.
- Havazelet, D., and Barkat, Z. 1979, *Ap. J.*, **233**, 589.
- Iben, I., Jr. 1975, *Ap. J.*, **196**, 525.
- . 1977, *Ap. J.*, **217**, 788.
- . 1982, *Ap. J.*, **260**, 821.
- Kudritzki, R. P., and Reimers, D. 1978, *Astron. Astrophys.*, **70**, 227.
- Mariotti, J. M., Chelli, A., Foy, R., Léna, P., Sibille, F., and Tchountonov, G. 1983, *Astron. Astrophys.*, **120**, 237.
- McCarthy, D. W. 1982, *Ap. J. (Letters)*, **257**, L93.
- Paczynski, B. 1970, *Acta Astr.*, **20**, 47.
- Reimers, D. 1975, in *Problems in Stellar Atmospheres and Envelopes*, ed. B. Baschek, W. H. Kegel, and G. Traving (New York: Springer-Verlag), p. 229.
- Sackmann, I.-J. 1980, *Ap. J.*, **235**, 554.
- Schönberner, D. 1979, *Astron. Astrophys.*, **79**, 108.
- Tuchman, Y., Sack, N., and Barkat, Z. 1978, *Ap. J.*, **219**, 183.
- . 1979, *Ap. J.*, **234**, 217.
- Weidemann, V. 1984, *Astron. Astrophys. (Letters)*, **134**, L1.

Weidemann, V., and Koester, D. 1983, *Astron. Astrophys*, **121**, 77.

Weigelt, G. 1983, **Workshop on ESO's Very Large Telescope, Cargèse, 16–19 May 1983**, ed. J.-P. Swings and K. Kjær, p. 121.

Wood, P. R., and Zarro, D. M. 1981, *Ap. J.*, **247**, 247.

Table 1

Amplitudes of Luminosity and Radius Variations

Initial mass (M_{\odot}):	1.0	1.2	2.0	1.2	3.0
Metallicity Z :	0.001	0.001	0.001	0.02	0.02
Flash number:	4 – 5	4 – 5	5 – 6	6 – 7	21 – 22
Total mass (M_{\odot}):	~ 0.58	~ 0.88	~ 1.86	~ 0.62	~ 1.4
Core mass M_{H} (M_{\odot}):	~ 0.535	~ 0.553	~ 0.628	~ 0.524	~ 0.653
$\log(L_A/L_{\odot})$:	3.465	3.54	3.80	3.47	4.00
$\log(L_B/L_{\odot})$:	2.91	3.125	3.58	2.80	3.68
$\log(L_C/L_{\odot})$:	3.815	3.89	4.12	3.64	4.20
$\log(L_D/L_{\odot})$:	3.075	3.18	3.56	3.12	3.76
$\log(L_E/L_{\odot})$:	3.525	3.59	3.83	3.55	4.015
$\Delta M_{\text{bol},C-A}$ (mag):	-0.88	-0.88	-0.80	-0.43	-0.50
$\Delta M_{\text{bol},D-A}$ (mag):	0.98	0.90	0.60	0.88	0.60
R_A/R_{\odot} :	310	390	440	470	1000
R_B/R_{\odot} :	100	150	270	130	570
R_C/R_{\odot} :	480	690	840	570	1270
R_D/R_{\odot} :	140	170	260	250	670
R_E/R_{\odot} :	200	410	470	450	1020
R_B/R_A :	0.32	0.38	0.61	0.28	0.57
R_C/R_A :	1.55	1.77	1.91	1.21	1.27

Table 2

Greatest Rates of Change of Luminosity and Radius

Initial mass (M_{\odot}):	1.0	1.2	2.0	1.2	3.0
Metallicity Z :	0.001	0.001	0.001	0.02	0.02
Flash number:	4 – 5	4 – 5	5 – 6	6 – 7	21 – 22
Total mass (M_{\odot}):	~ 0.58	~ 0.88	~ 1.86	~ 0.62	~ 1.4
Core mass M_{H} (M_{\odot}):	~ 0.535	~ 0.553	~ 0.628	~ 0.524	~ 0.653
$\max_{A-B} \left \frac{d \log L}{dt} \right $ (/yr):	0.0034	0.0037	0.0052	0.0023	0.018
$\max_{A-B} \left \frac{dM_{\text{bol}}}{dt} \right $ (mag/yr):	0.0085	0.0093	0.013	0.0058	0.045
$\max_{A-B} \left \frac{dR}{dt} \right $ (R_{\odot} /yr):	1.4 ^a	2.0 ^a	5.1 ^a	1.1 ^a	22. ^a
$\max_{A-B} \left \frac{dR}{dt} \right $ (km/sec):	0.03 ^a	0.04 ^a	0.11 ^a	0.02 ^a	0.49 ^a
Duration (years):	150	100	40	250	16
Percent of flash cycle:	0.05%	0.04%	0.04%	0.17%	0.035%
$\max_{B-C} \left \frac{d \log L}{dt} \right $ (/yr):	0.016	0.0096	0.011	0.013	0.025
$\max_{B-C} \left \frac{dM_{\text{bol}}}{dt} \right $ (mag/yr):	0.040	0.024	0.028	0.033	0.063
$\max_{B-C} \left \frac{dR}{dt} \right $ (R_{\odot} /yr):	6.2 ^a	6.2 ^a	9.3 ^a	7.9 ^a	35. ^a
$\max_{B-C} \left \frac{dR}{dt} \right $ (km/sec):	0.14 ^a	0.14 ^a	0.21 ^a	0.17 ^a	0.77 ^a
Duration (years):	30	45	30	40	11
Percent of flash cycle:	0.010%	0.018%	0.032%	0.025%	0.024%

^a Note that these radial rates of change would be halved if the mixing length parameter α were doubled (i.e., if $\alpha \rightarrow 2$).

Table 3

Percent of Time Spent Off the $M_c - L$ Line

Initial mass (M_\odot):	1.0	1.2	2.0	1.2	3.0
Metallicity Z :	0.001	0.001	0.001	0.02	0.02
Flash number:	4 – 5	4 – 5	5 – 6	6 – 7	21 – 22
Total mass (M_\odot):	~0.58	~0.88	~1.86	~0.62	~1.4
Core mass M_H (M_\odot):	~0.535	~0.553	~0.628	~0.524	~0.653
Below $\log L(M_c) - 0.05$:	57%	48%	30%	57%	24%
Below $\log L(M_c) - 0.10$:	41%	32%	15%	44%	15%
Below $\log L(M_c) - 0.20$:	27%	20%	6%	27%	7%
Below $\log L(M_c) - 0.30$:	18%	12%	—	17%	—
Below $\log L(M_c) - 0.40$:	10%	2%	—	7%	—
Above $\log L(M_c)$:	1.9%	2.2%	4.3%	0.7%	3.0%

Note.—For the purposes of this table, the luminosities at points A and E of the flash cycle were assumed to lie on the $M_c - L$ relation that defines the value of $\log L(M_c)$.

FIGURE CAPTIONS

Fig. 1.—Variation of the stellar radius as a function of time over many flashes for a star of initial mass $3.0 M_{\odot}$, showing the regularity and the buildup to the final shape. Note that this diagram was obtained from a *prior run*, with no mass loss, coarser mass zoning and timestep, and *no* molecular opacities: if molecular opacities had been included, the radius would have been roughly doubled.

Fig. 2.—Surface variations of the star with initial mass $1.0 M_{\odot}$ and metallicity $Z = 0.001$: 4th to 5th flashes (core mass $M_{\text{H}} \approx 0.535$). (a) Variation of stellar luminosity and radius as a function of time: note the expanded timescale between the dashed lines. Time is measured relative to the time of the peak flash. (b) Histogram of the probability (per *unit* interval in $\log L$) of finding the star at a given value of $\log(L/L_{\odot})$. Note the low-probability tails at low and high luminosities (scaled by factors of 100 and 10 respectively) arising from the *fast* post-flash variation.

Fig. 3.—Surface variations of the star with initial mass $1.2 M_{\odot}$ and metallicity $Z = 0.001$: 4th to 5th flashes (core mass $M_{\text{H}} \approx 0.553$). Similar to Figure 2.

Fig. 4.—Surface variations of the star with initial mass $2.0 M_{\odot}$ and metallicity $Z = 0.001$: 5th to 6th flashes (core mass $M_{\text{H}} \approx 0.628$). Similar to Figure 2.

Fig. 5.—Surface variations of the star with initial mass $1.2 M_{\odot}$ and metallicity $Z = 0.02$: 6th to 7th flashes (core mass $M_{\text{H}} \approx 0.524$). Similar to Figure 2.

Fig. 6.—Surface variations of the star with initial mass $3.0 M_{\odot}$ and metallicity

$Z = 0.02$: 20th to 21st flashes (core mass $M_{\text{H}} \approx 0.648$). Similar to Figure 2.

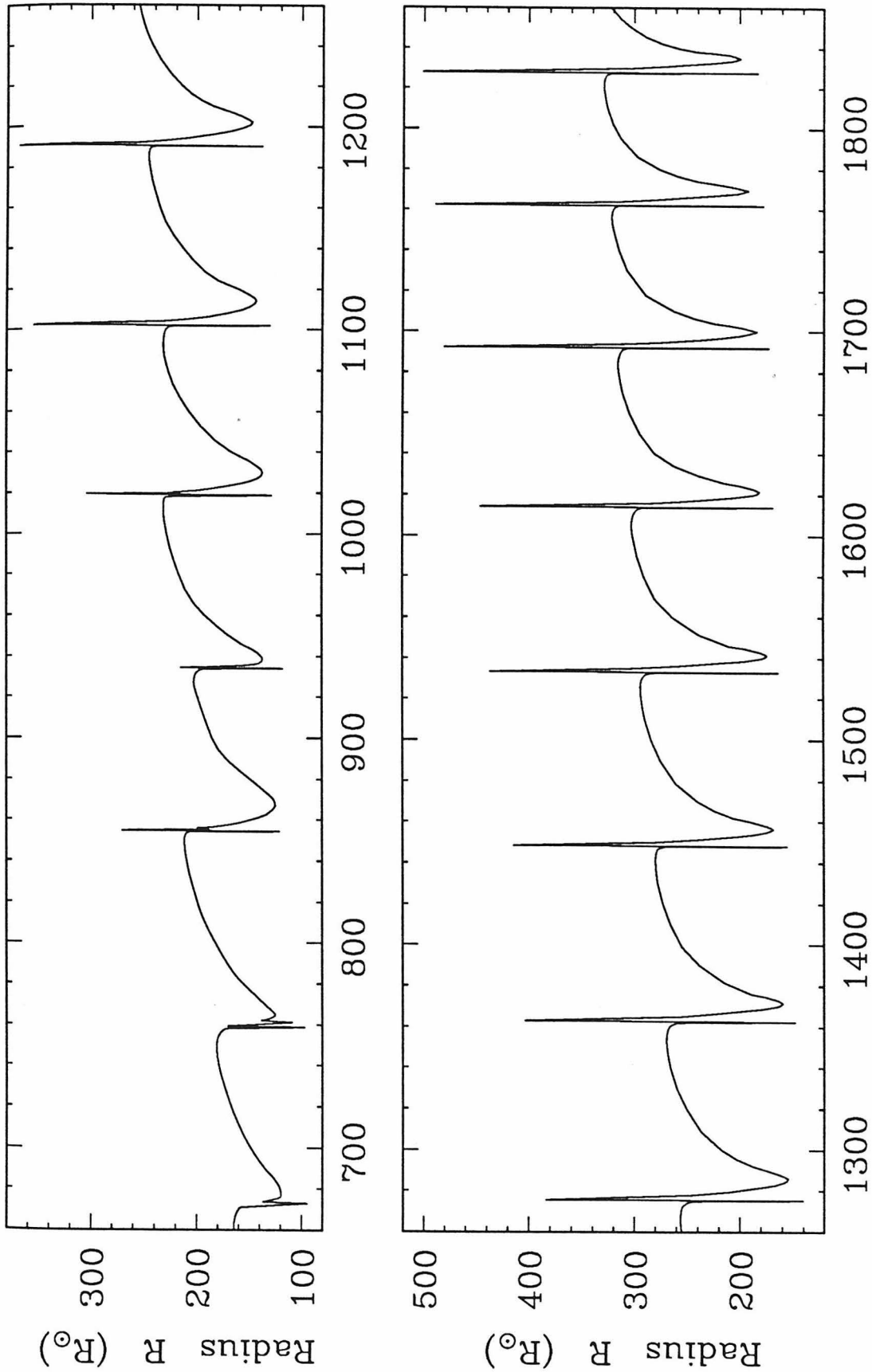


Fig. 1

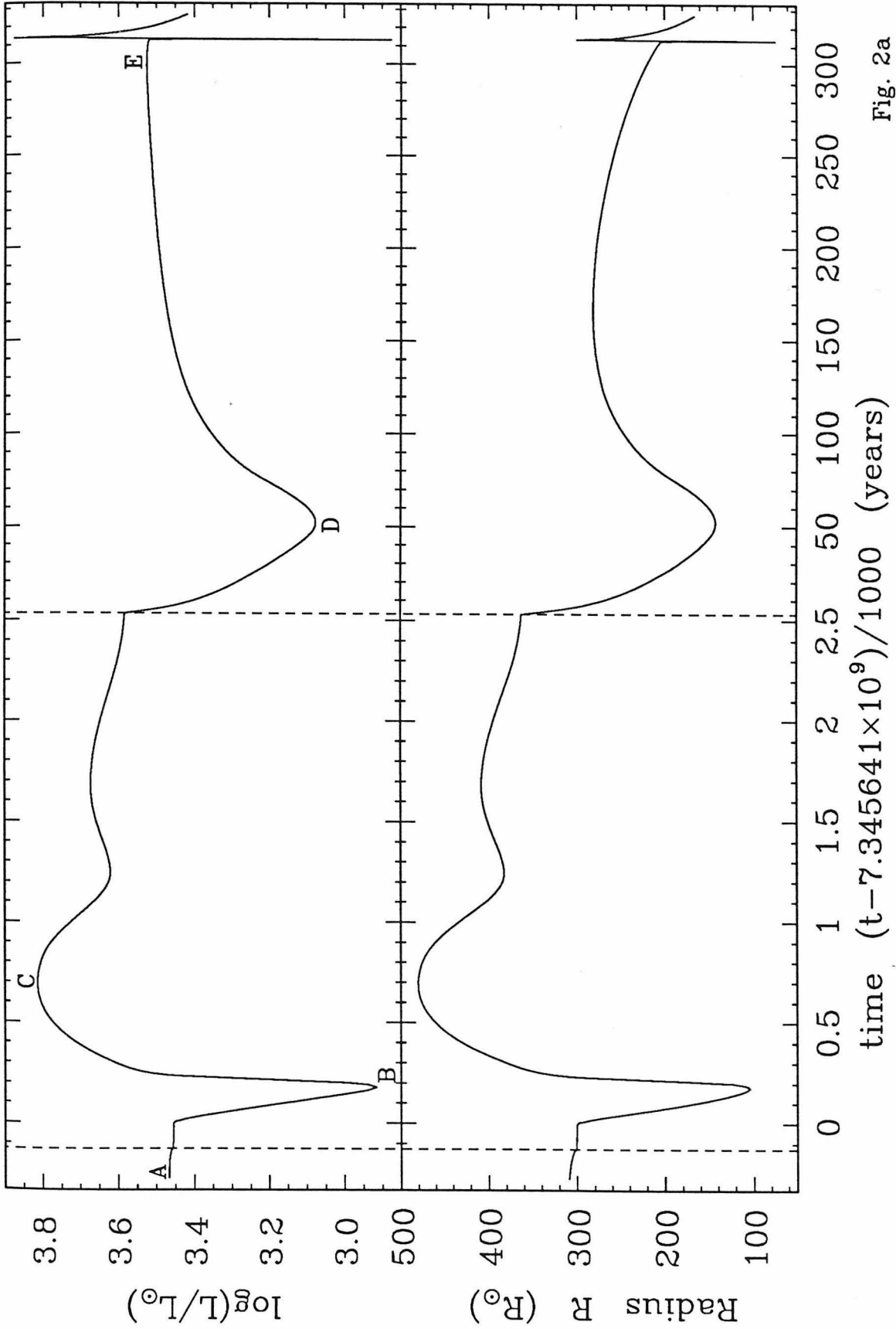


Fig. 2a

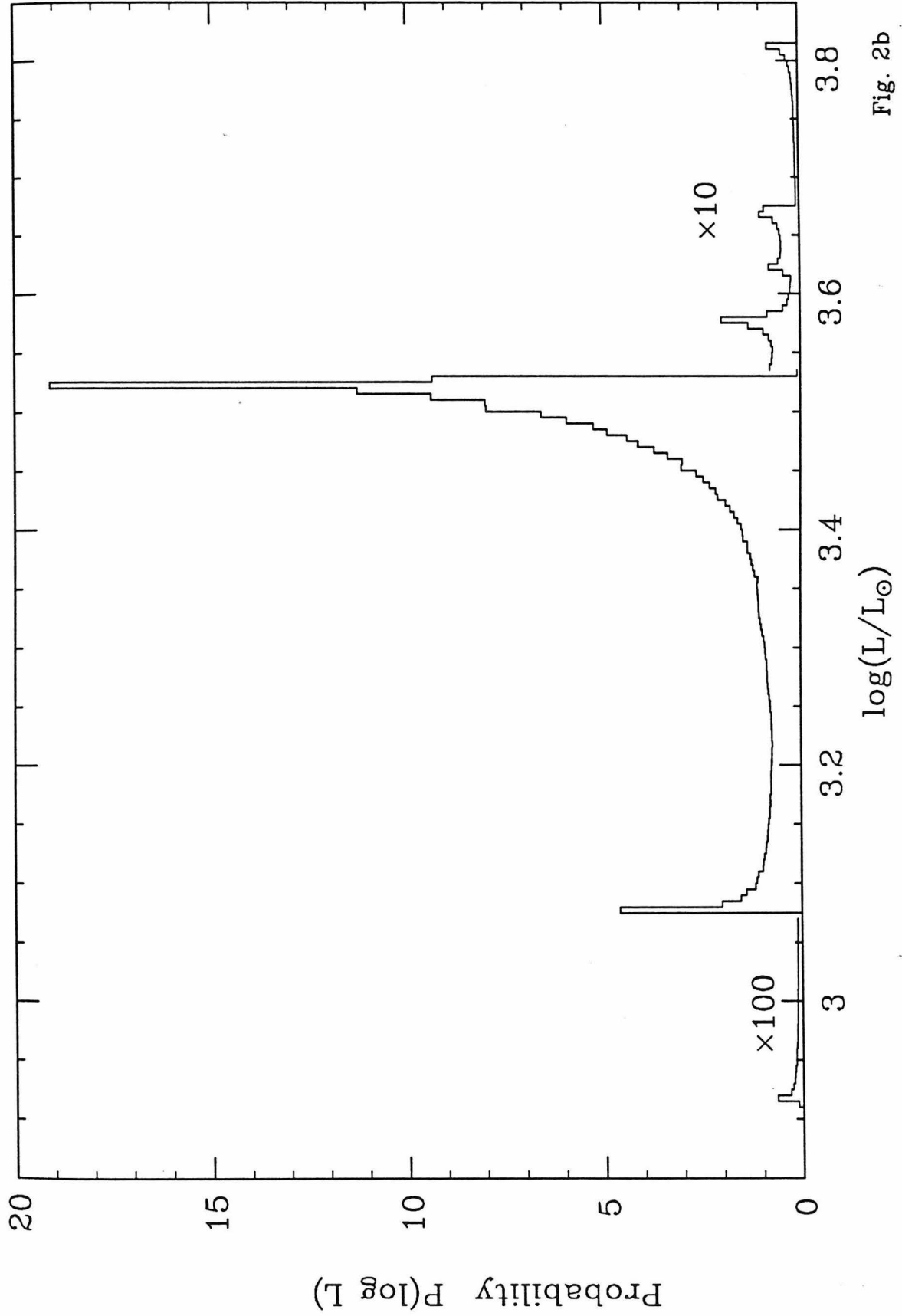


Fig. 2b

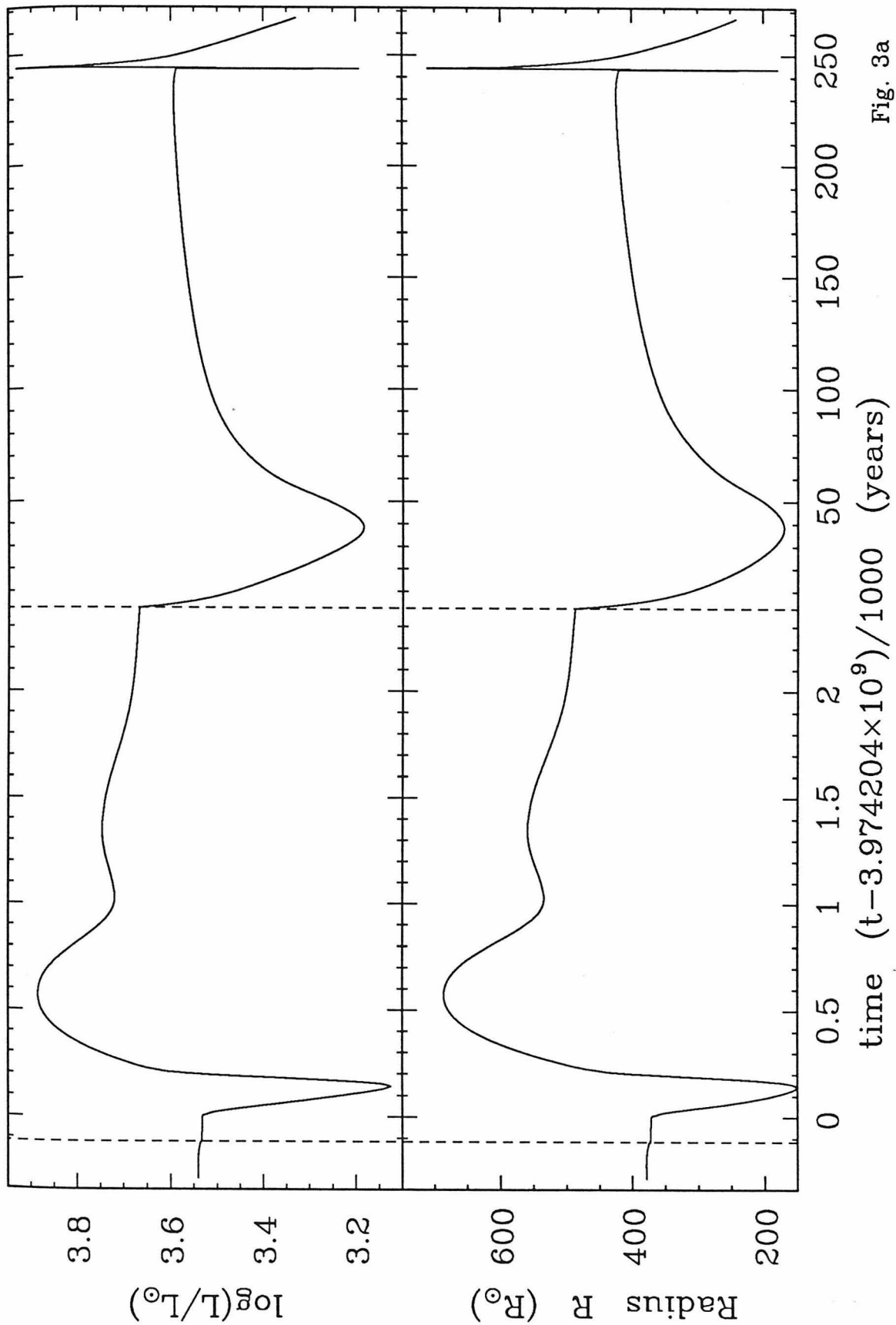


Fig. 3a

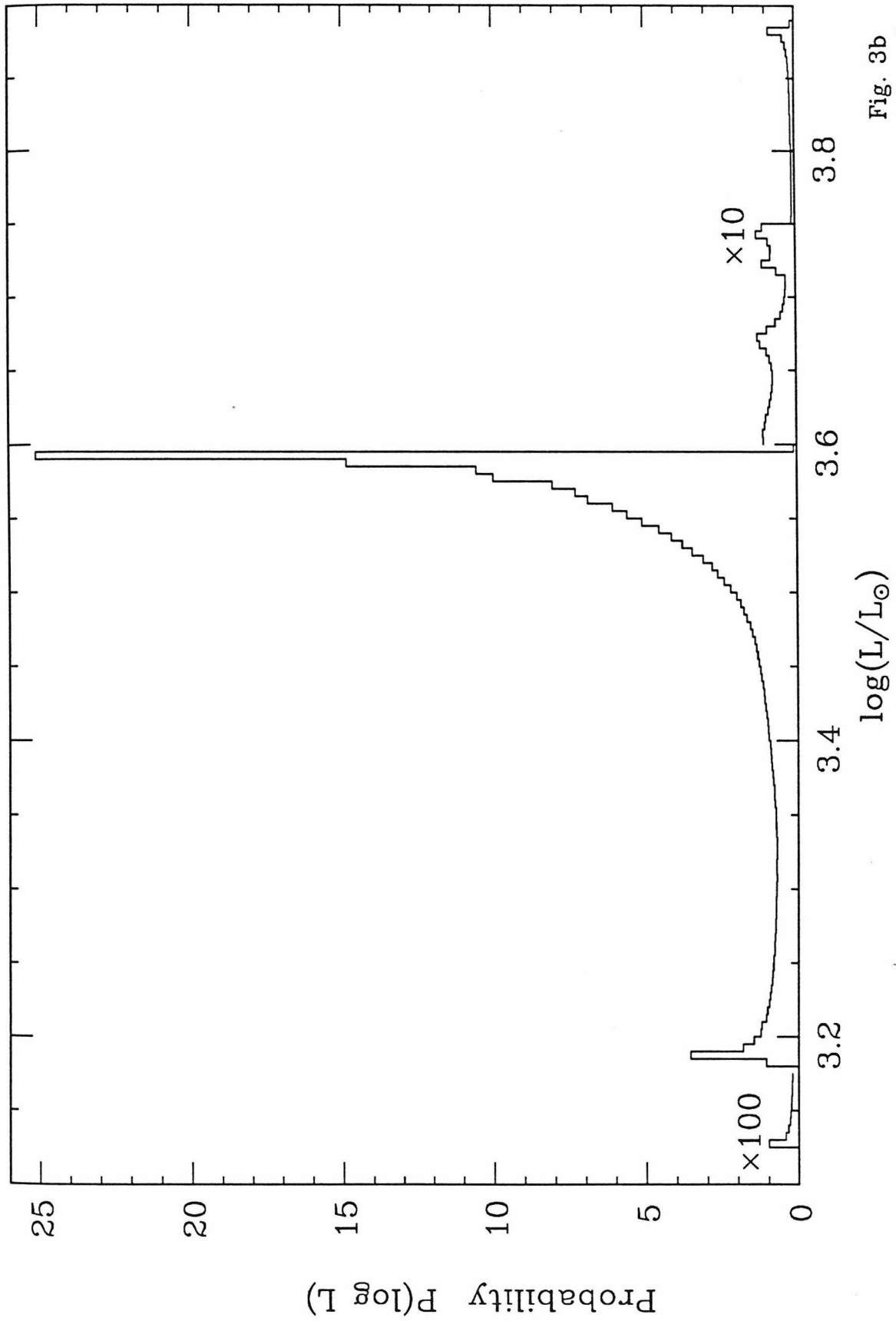


Fig. 3b

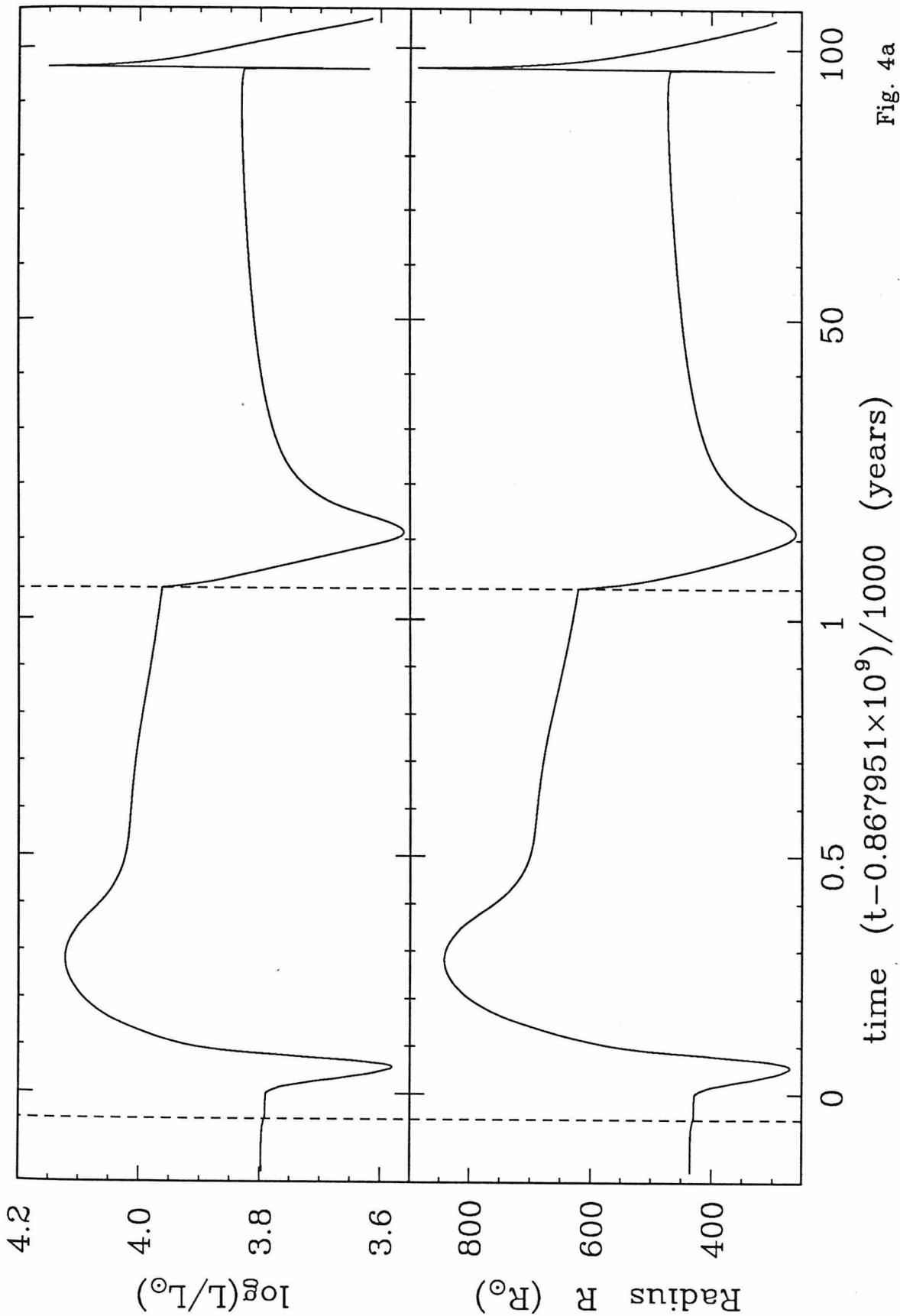


Fig. 4a

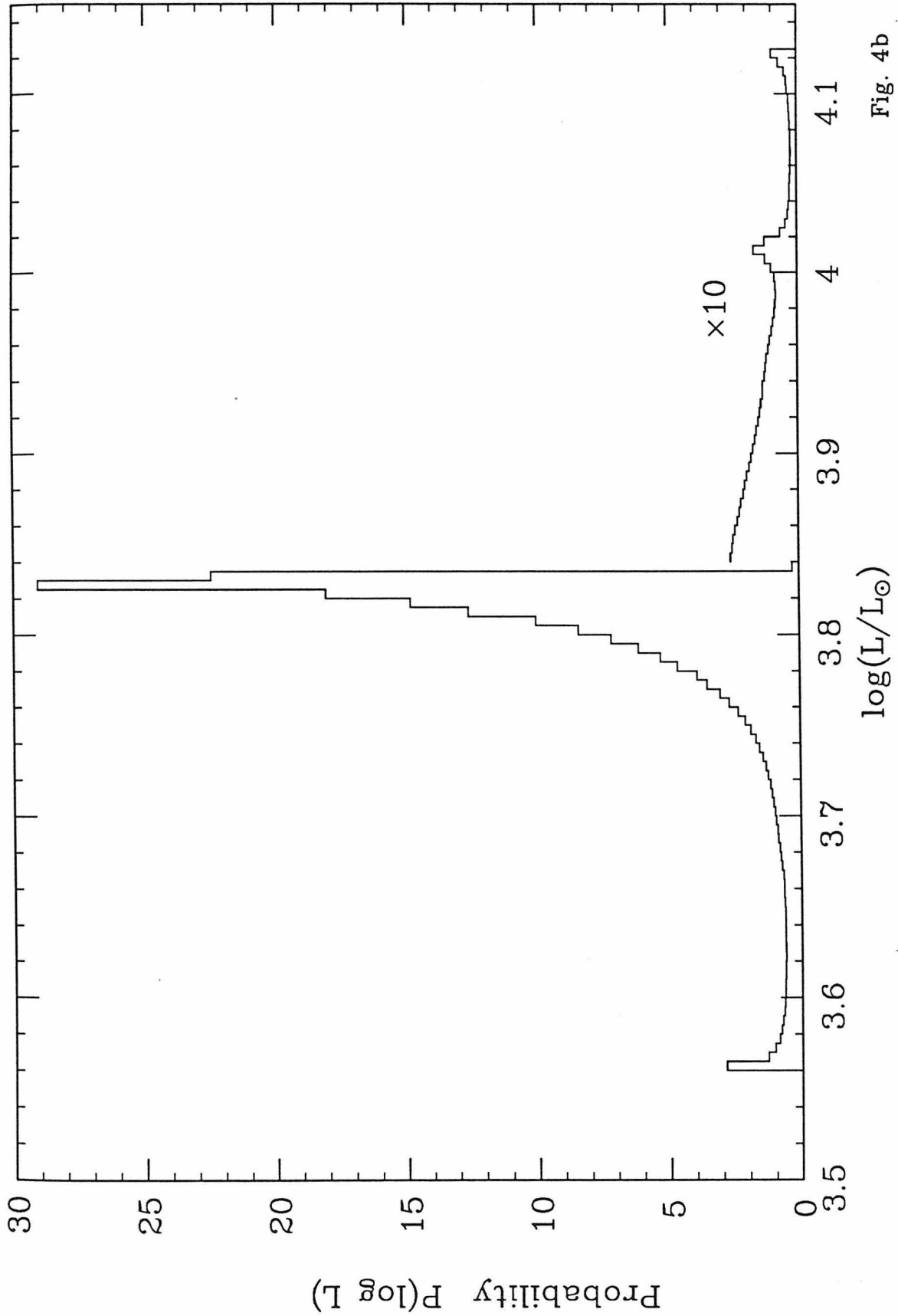


Fig. 4b

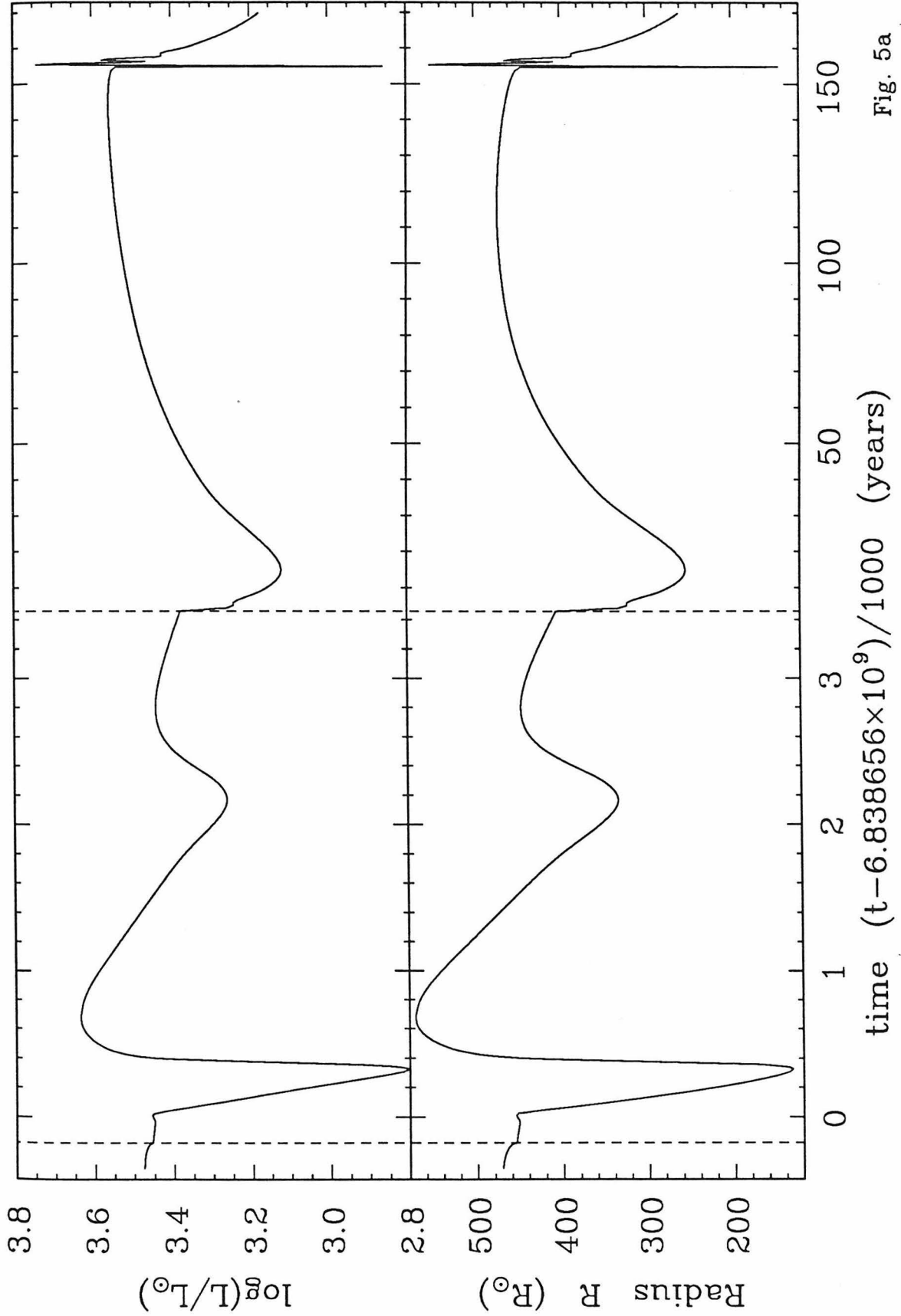


Fig. 5a

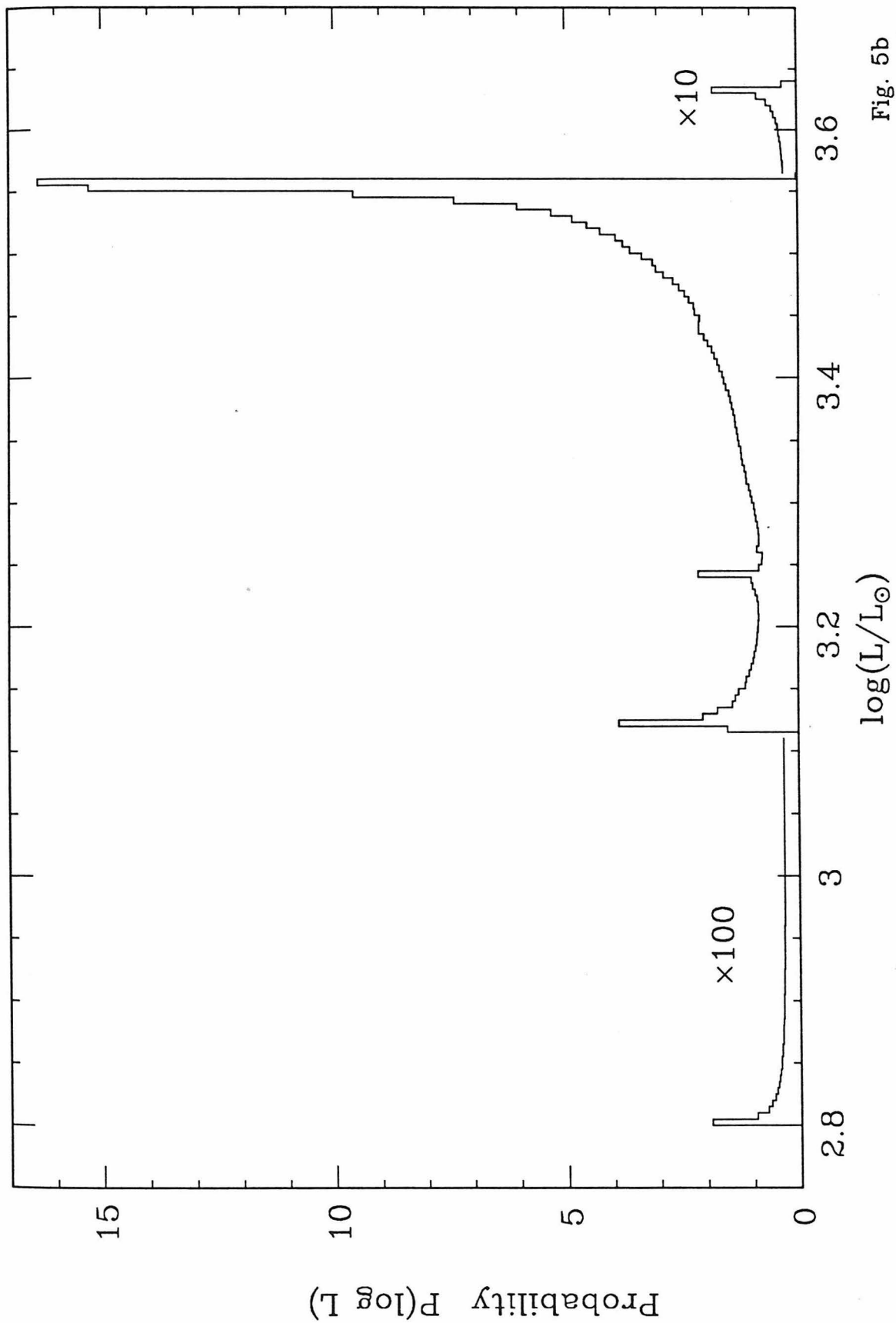


Fig. 5b

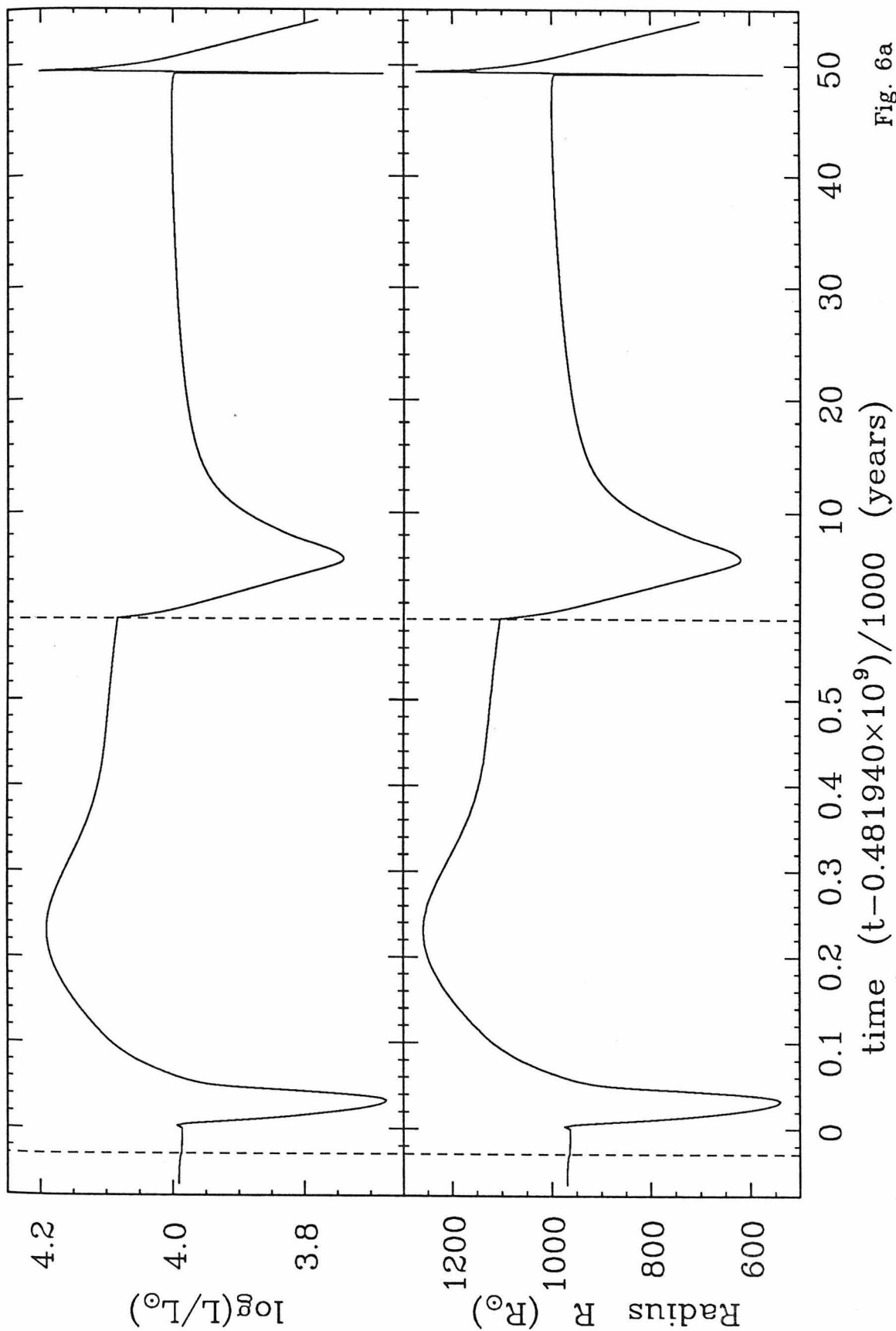


Fig. 6a

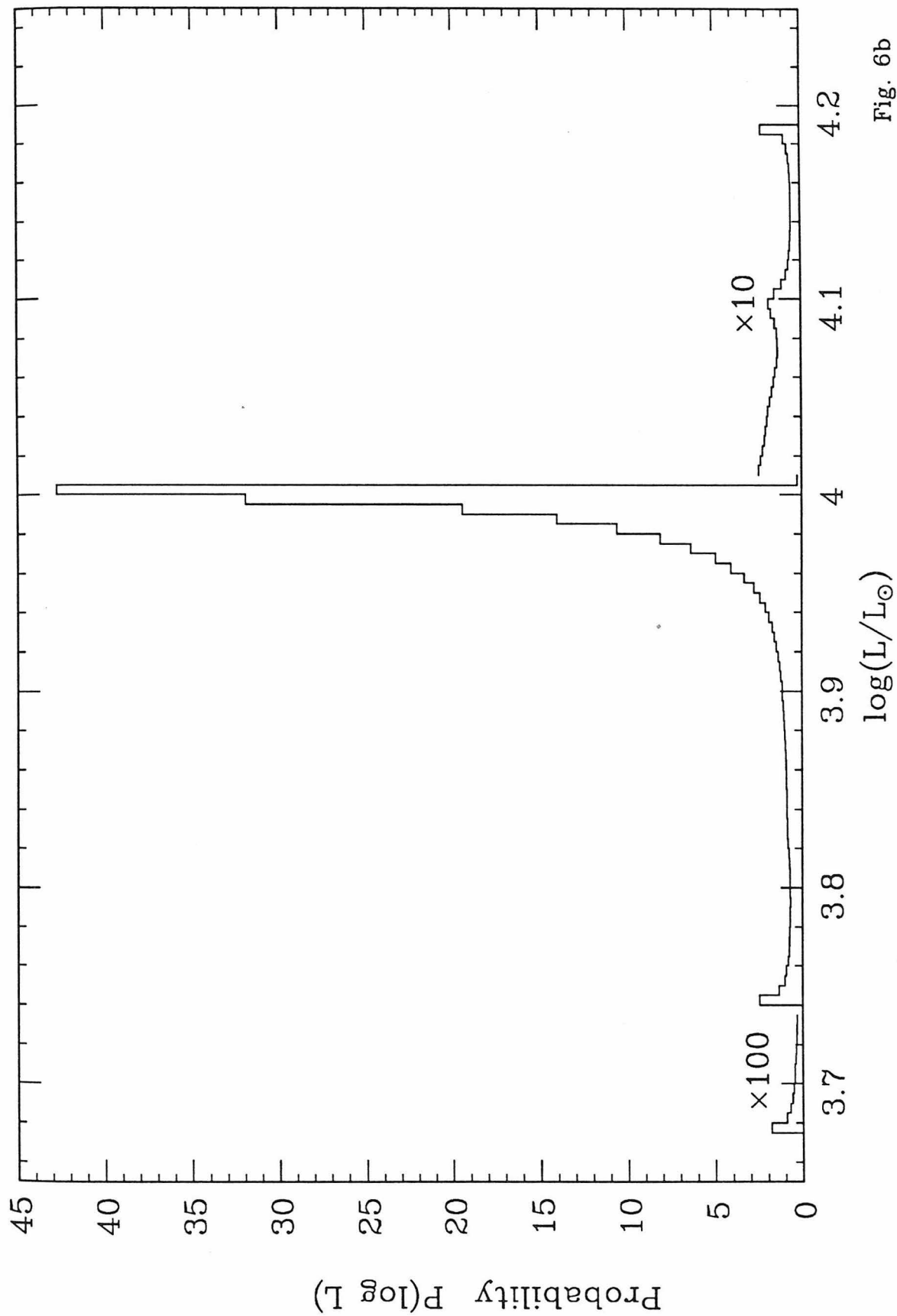


Fig. 6b

CHAPTER 3.

II. The Core Mass–Luminosity Relation for Low Mass Stars

Arnold I. Boothroyd and I.-Juliana Sackmann

W. K. Kellogg Radiation Laboratory 106-38

California Institute of Technology, Pasadena, CA 91125

ABSTRACT

It was investigated whether the core mass–luminosity ($M_c - L$) relation that had been established in the literature for intermediate mass stars ($3 M_\odot \lesssim M \lesssim 9 M_\odot$) can be extended to low mass stars ($0.8 M_\odot \lesssim M \lesssim 3 M_\odot$), where many of the observations take place. Stars were evolved from the main sequence up the red giant branch, through the helium core flash and the horizontal branch phase, up to the asymptotic giant branch where helium shell flashes were followed. *Two types of $M_c - L$ relations were obtained, one for the red giant branch (when a single hydrogen-burning shell surrounds a degenerate helium core), and another one for the asymptotic giant branch (when two burning shells, of helium and hydrogen respectively, surround a degenerate carbon-oxygen core).* Detailed calculations were carried out for a *metal-poor* case ($Z = 0.001$) for stars of initial masses $1.0 M_\odot$, $1.2 M_\odot$, $2.0 M_\odot$, and $3.0 M_\odot$, and for a *metal-rich* case ($Z = 0.02$) for stars of initial masses $1.2 M_\odot$ and $3.0 M_\odot$. The latest nuclear reaction rates were used, as well as

the latest opacities (including some molecular opacities), and mass loss via a Reimers-type wind. The dependence of the $M_c - L$ relation on chemical composition was investigated. For the *red giant branch*, the $M_c - L$ relation for the *metal-rich* case ($Z = 0.02$, $\mu \simeq 0.624$) was $L = (6.86M_H)^7$ for $0.3 M_\odot \lesssim M_H \lesssim 0.45 M_\odot$, where all units are in solar units; the composition dependence was $L \propto \mu^7(Z_{\text{CNO}})^{1/12}$ (μ is the envelope mean molecular weight, including free electrons). For the *asymptotic giant branch*, the $M_c - L$ relation for the *metal-rich* case ($Z = 0.02$, $\mu \simeq 0.618$) was $L = 52000(M_H - 0.456)$ for $0.52 M_\odot \lesssim M_H \lesssim 0.7 M_\odot$; the composition dependence was $L \propto \mu^3(Z_{\text{CNO}})^{1/25}$. The $M_c - L$ relation obtained for the low mass asymptotic giant branch stars drops less steeply than would be expected from the previous higher- M_c work; the difference is large at low core masses. Due to luminosity variations over the flash cycle, observers will see stars that do not lie on the $M_c - L$ relation; the probability and extent of these deviations was described. The fortunate circumstance was established that, for the $M_c - L$ relation of *low mass stars*, (i) changes in the hydrogen-burning reaction rate have only a very minor effect; (ii) uncertainties in the convective mixing length have negligible effect; and (iii) there is no evidence that the star's total mass has any effect.

I. INTRODUCTION

A star on the asymptotic giant branch (AGB) is in a double-shell burning phase. A central degenerate carbon-oxygen core is surrounded by a helium-burning

shell, a small intershell zone containing mostly helium, a hydrogen-burning shell, and an envelope whose composition is not much different from the star's initial main sequence composition. Such a star undergoes periodic nuclear runaway reactions in the helium-burning shell, known as helium shell flashes or thermal pulses. The core mass–luminosity ($M_c - L$) relation relates the interflash luminosity L of such an AGB star to its core mass M_c (although composition and perhaps total stellar mass also have a slight effect), where the core mass M_c is traditionally considered to be the mass M_H interior to the hydrogen-burning shell. The interflash luminosity is generated mostly by the hydrogen-burning shell, via the CNO cycle; it rises from a post-flash minimum to an interflash maximum which is sustained over roughly half the interflash period (for more details on the luminosity profile over a flash cycle, see Boothroyd and Sackmann 1987*a*, hereafter Paper I, and references therein). Theoretically, the $M_c - L$ relation has been used widely in semi-analytical models of asymptotic giant branch behavior. Observationally, it is also a powerful tool. For example, it has been used to infer a core mass from an observed AGB tip luminosity (Weidemann 1984; Aaronson and Mould 1985), thereby obtaining a final mass M_f for use in determining the Weidemann $M_i - M_f$ relation (an observationally determined relation giving the mass of the white dwarf produced at the end of a star's life, as a function of the star's initial mass).

Traditionally, the $M_c - L$ relation has been derived for the AGB. This stage of evolution has been computed most frequently for the intermediate mass stars ($3 M_\odot \lesssim M \lesssim 9 M_\odot$), since these are easier to compute than low mass stars ($M \lesssim 2 M_\odot$). Observationally, however, it is the low mass stars that are most

frequently encountered. An $M_c - L$ relation has not been derived for these low mass stars with direct, self-consistent computations. Semi-analytical theory predicts that deviations from linearity of the $M_c - L$ relation are to be expected at low enough core masses (Tuchman, Glasner, and Barkat 1983; see Section II below). Therefore, it was the aim of this paper to attack the low mass stars, following the full evolution, and to check whether previously-derived versions of the $M_c - L$ relation were adequate for the commonly observed, low mass stars.

Stars of relatively low mass, from one to a few solar masses, present certain difficulties to a theoretician interested in the later stages of their lifetimes. The main sequence and red giant branch (RGB) stages are straightforward, but a star of less than about two and a half solar masses terminates the RGB with an exceedingly violent helium core flash in its degenerate helium core. This is sufficiently difficult to handle computationally that many investigators prefer to begin with the subsequent horizontal branch stage, at the cost of a certain arbitrariness of initial conditions, and continue on from there to the AGB stage with its helium shell flashes. We have chosen instead to evolve our stars from initial zero age main sequence models, following them through their entire lifetime *including* the core flash, and thus preserving information on initial mass and total age of the stars. It is true that the core flash can only be approximated by any non-hydrodynamic, one-dimensional code (see, e.g., Deupree 1984), but an approximation is better than ignoring the event completely, and the effect of inaccuracies in the core flash is likely to be small. By the time the star reaches the asymptotic giant branch (AGB), the core regions affected by the core flash have in any case been reprocessed by later helium core and

shell burning into the degenerate carbon-oxygen core of the double-shell burning stage.

II. PREVIOUS WORK

The $M_c - L$ relation for the AGB was discovered by Paczyński (1970). He considered stars of mass $3 M_\odot$, $5 M_\odot$, and $7 M_\odot$, having metallicity $Z = 0.03$ (slightly greater than solar) and $Z_{\text{CNO}} = 0.015$, with initial hydrogen and helium content $X = 0.70$, $Y = 0.27$, giving $\mu \simeq 0.618$: μ is the mean molecular weight of the envelope, defined as

$$\mu = \left[\sum_i \frac{X_i(1 + Z_i)}{A_i} \right]^{-1} \simeq \frac{1}{2X + \frac{3}{4}Y + \frac{1}{2}Z} = \frac{4}{5X + 3 - Z}, \quad (1)$$

where X_i is the abundance by mass of the i^{th} type of atom, which has Z_i electrons and atomic mass A_i ; and as usual X , Y , and Z stand for the hydrogen, helium, and metal abundances. Paczyński used a convective mixing length to pressure scale height ratio of $\alpha \equiv l/H_p = 1$. He followed these stars from the main sequence through the AGB, suppressing flashes by artificially holding the separation between the hydrogen- and helium-burning shells to a constant value. He obtained the relation

$$L = 59250M_{\text{H}} - 30950 = 59250(M_{\text{H}} - 0.522) \quad (2)$$

(everything in solar units) for core masses in the range $0.57 M_\odot < M_{\text{H}} < 1.39 M_\odot$.

Iben (1977) considered a star of $7 M_\odot$. Tracking his references backwards, one finds that he evolved a star of $7 M_\odot$ of solar metallicity ($Z = 0.02$) with initial

$X = 0.70$, $Y = 0.28$, $\mu \simeq 0.617$ (Iben 1972) from the main sequence through eighteen flashes on the AGB (Iben 1975, 1976), at which point the star had a core mass of $M_{\text{H}} = 0.96 M_{\odot}$. At this point, Iben (1977) took this core with an envelope composition of $X = 0.6378$, $Y = 0.35$, $Z_{\text{CNO}} = 0.0122$ (giving $\mu \simeq 0.648$: presumably the envelope composition change was due to first and second dredge-up, though this is not stated explicitly), while keeping $Z = 0.02$ for the purpose of opacity calculations. One should note that Iben's definition of the mixing length ratio $\alpha \equiv l/H_p$ differs by nearly a factor of two from that of most other workers, so his quoted values of $\alpha = 1.0$ and $\alpha = 0.7$ should be read as $\alpha \approx 1.8$ and $\alpha \approx 1.3$ for comparison purposes (see Boothroyd and Sackmann 1987*b*, hereafter Paper III). Using artificial flash suppression (similar to Paczyński 1970), he evolved the star to a core mass of $M_{\text{H}} = 1.16 M_{\odot}$, and then $M_{\text{H}} = 1.36 M_{\odot}$. At these two points he turned off the flash suppression and followed the interpulse evolution through a fraction of a flash cycle. He quotes an $M_c - L$ relation of

$$L = 59000(M_{\text{H}} - 0.38), \quad (3)$$

but states that a better fit is obtained from the relation

$$L = 63400(M_{\text{H}} - 0.44)(M/7)^{0.4}, \quad (4)$$

where M is the star's total mass; this relation holds for core masses in the range $0.96 M_{\odot} \lesssim M_{\text{H}} \lesssim 1.36 M_{\odot}$. The dependence on total mass M was apparently obtained by removing $2 M_{\odot}$ from the envelope (when the core mass was $M_{\text{H}} = 0.96 M_{\odot}$) and following the star through one interflash period; he later revised this

mass dependence (Iben and Truran 1978: see below). Iben (1977), as well as being the only one to find a total mass dependence, is the only one to find a dependence on the mixing length parameter α ; this is likely due to the fact that he used the largest total mass as well as the largest (true) mixing length ratios. As pointed out by Tuchman, Glasner, and Barkat (1983), large total masses M and large mixing length parameters α can cause the convective envelope to reach down close to the burning shells, which can have an effect on the $M_c - L$ relation (see below). One might thus expect a mass dependence and mixing length dependence for the $M_c - L$ relation at higher masses such as considered by Iben (1977), but not at the lower masses and mixing lengths considered by other investigators.

Havazelet and Barkat (1979) followed a number of stars, of masses $2M_\odot$, $3M_\odot$, $3.7M_\odot$, $4M_\odot$, $5M_\odot$, and $6M_\odot$. From Table 1 of their paper, the $2M_\odot$ through $5M_\odot$ stars would encounter the first helium shell flash at core masses of $0.58M_\odot$, $0.82M_\odot$, $1.05M_\odot$, $1.07M_\odot$, and $1.36M_\odot$ respectively. These stars had metallicity $Z = 0.01$ (half of solar), with initial $X = 0.70$, $Y = 0.29$ (giving $\mu \simeq 0.616$), and $Z_{\text{CNO}} = 0.0014$ (rather small); they do not specify their mixing length parameter α , but probably used a value of 1.0, or perhaps 1.5. One or more of these stars was followed through a number of helium shell flashes (the details are not specified), resulting in an $M_c - L$ relation of

$$L = 65000(M_{\text{H}} - 0.525), \quad (5)$$

presumably valid for $M_{\text{H}} \gtrsim 0.6M_\odot$.

Becker and Iben (1980), in their Figure 8, plotted the interflash luminosity as a function of core mass for a number of stars from various sources, but did not attempt to reconcile the differences or expand on the relations of equations (2) and (4) above.

Wood and Zarro (1981) considered stars of masses $0.8 M_{\odot}$, $1.0 M_{\odot}$, $2.0 M_{\odot}$, and $3.0 M_{\odot}$, of solar metallicity ($Z = 0.02$), with initial $X = 0.68$, $Y = 0.30$ (giving $\mu \simeq 0.627$); although it is not specified, they probably used $Z_{\text{CNO}} \approx 0.01$, or slightly more. They used a mixing length parameter of $\alpha = 1$. They created a number of artificial starting models, whose structure approximated that of a star slightly before the shell flashing stage, and having initial core masses of $0.53 M_{\odot}$, $0.7 M_{\odot}$, and $0.8 M_{\odot}$; after some spurious transient effects due to this artificial starting point (often including a single strong shell flash), these stars settled down and entered the shell flashing stage on the AGB. Many flashes were followed, and the resulting $M_c - L$ relation was

$$L = 59250(M_{\text{H}} - .495) \quad (6)$$

for core masses $0.6 M_{\odot} \lesssim M_{\text{H}} < 0.9 M_{\odot}$, with *no* dependence on the total stellar mass.

The review article of Iben and Renzini (1983) quotes a number of $M_c - L$ relations. The Wood and Zarro (1981) relation of equation (6) above is quoted for low-mass stars (though the attribution is “as discovered by Paczyński 1970 and Uus 1970”). The relation for intermediate mass stars

$$L = 63400(M_{\text{H}} - 0.44)(M/7)^{0.19} \quad (7)$$

is taken from Iben and Truran (1978), where the power of the total mass dependence was cut in half from the relation of Iben (1977) as “a compromise with the results of Paczyński (1970) and Uus (1970) who argue the mass independence of the relationships.” Finally, a relation is quoted as

$$L = (59250 + 4150x)(M_H - 0.495 - 0.0505x), \quad x \equiv [(M - M_H)/6.04]^{1.83}. \quad (8)$$

This comes from Iben (1981), as an $M_c - L$ relation “that joins together the Paczyński (1970)–Uus (1970) relationship, which is valid for small stellar masses, and the Iben (1977) relationship, which is valid for large stellar masses ... The number 0.495 is taken from Wood and Zarro (1981).”

After the present work had been completed, the paper of Lattanzio (1986) appeared. He considered stars of mass $1.5 M_\odot$ and compositions having $Y = 0.20$ and 0.30 with $Z = 0.001, 0.01,$ and 0.02 , using $Z_{\text{CNO}} = 0.6Z$; the mixing length parameter was $\alpha = 1$. Starting from the zero age horizontal branch, these stars were evolved to the AGB and through 5 to 10 shell flashes. For Population I abundances the resulting $M_c - L$ relation was

$$L = 55320[2.3(Y - 0.20) + 1.0](M_H - a), \quad (9)$$

$$a \equiv 0.489 + 0.23(Y - 0.20) - 0.70(Z - 0.02),$$

presumably obtained from core masses $0.55 M_\odot \lesssim M_H \lesssim 0.6 M_\odot$. For the low-metallicity ($Z = 0.001$) case, the $M_c - L$ relation was

$$L = 51800[1.0 + 4.7(Y - 0.20)]M_H - 26260[1.0 + 6.2(Y - 0.20)], \quad (10)$$

presumably obtained from core masses $0.6 M_\odot \lesssim M_H \lesssim 0.65 M_\odot$. It should be noted that the slopes of these relations must be rather uncertain, due to the small range

of core masses over which they were obtained, with only the last flashes attaining (or perhaps not quite attaining) full amplitude.

Others have shown that the origin of the $M_c - L$ relationship can be understood in terms of the structure of a star with burning shells surrounding a degenerate core, using semi-analytical approximations. Refsdal and Weigert (1970) considered the case of a single hydrogen-burning shell surrounding a degenerate helium core of core mass $M_H \lesssim 0.45 M_\odot$, using homology relations. They found an $M_c - L$ relation $L \propto M_H^8$. Kippenhahn (1981) extended this theory to higher core masses by allowing for variation in the radiation pressure, but still considered only a hydrogen-burning shell. He claimed that the luminosity was a strong function of composition for small core masses, namely $L \propto \mu^7$, where μ is the mean molecular weight in the envelope as defined in equation (1); but that for higher core masses such as are typical of AGB stars the composition dependence would be rather weaker (due to the increased radiation pressure in the region just outside the burning shell). Some dependence on Z_{CNO} through the hydrogen-burning rate was implied but not given explicitly.

Tuchman, Glasner, and Barkat (1983) attempted to provide a more transparent theoretical derivation of the existence and form of the $M_c - L$ relation, for a more general case. They assume that

the star has the following characteristics:

- a) It has a core of mass M_c which resembles a classical white dwarf.
- b) It has a thin burning shell (or a double shell) which surrounds the core. The extension of the shell(s) in mass ΔM_s is very small compared to M_c .

c) Just above the burning shell(s) there exists a thin ‘transition zone’ (whose mass $\Delta M \ll M_c$) within which the drop of pressure P , density ρ , and temperature T , as well as the increase of radius r , are very sharp.

d) The luminosity in the transition zone is constant and equal to the local radiative luminosity l .

e) The composition within the transition zone is homogeneous and as usual is described by X , Y , and Z .

f) Within the transition zone we can safely approximate the opacity κ by the Thompson scattering expression $\kappa = 0.2(1 + X)$.

These conditions are generally satisfied for stars on the AGB, although Tuchman, Glasner, and Barkat (1983) point out that assumption (d) could be violated in some cases, if envelope convection reaches down too close to the burning shells (which could happen for high enough core masses and total stellar masses, and/or large enough values of the mixing length to pressure scale height parameter α). The results of their manipulations are a pair of equations relating the luminosity at the top of the hydrogen-burning shell to the temperature at that point, the core mass of the star, and the envelope composition; in principle, if not in practice, this pair of equations could be solved to give the luminosity in terms of the core mass and composition. Even without such a solution, however, they provide strong indications as to the expected dependence of the luminosity on composition. Composition enters the equations in three ways: through factors of $(1 + X)$ from the electron scattering opacity, through factors of approximately $(5X + 3 - Z)$ from the molecular weight μ , and through factors of $(X Z_{\text{CNO}})$ from the hydrogen-burning rate. From the way in which these factors enter the equations, the composition dependence of the $M_c - L$ could probably be approximated by a fairly strong μ -dependence

(likely stronger than linear) and a rather weak dependence on Z_{CNO} , likely between $(Z_{\text{CNO}})^{1/20}$ and $(Z_{\text{CNO}})^{1/3}$; considering that Z_{CNO} is generally proportional to the metallicity Z , the Z_{CNO} -dependence could be converted to a Z -dependence (with the same power). Any dependence on total mass or on mixing length would come from violation of their assumption (d), as discussed above. It should be noted that the $M_c - L$ relation, as they derive it, would be expected to be approximately linear only for a certain range of core masses M_c ; fairly small deviations from linearity are expected at large core masses ($M_c \gtrsim 1.2 M_\odot$), and large deviations at low core masses ($M_c \lesssim 0.5 M_\odot$).

III. COMPUTATIONAL DETAILS OF THE PRESENT WORK

For the low-metallicity case ($Z = 0.001$, with initial hydrogen and helium content $X = 0.759$, $Y = 0.24$, giving $\mu \simeq 0.589$, and $Z_{\text{CNO}} = 0.00075$), stars of initial mass $1.0 M_\odot$, $1.2 M_\odot$, $2.0 M_\odot$, and $3.0 M_\odot$ were considered; for the case of solar metallicity ($Z = 0.02$, with initial $X = 0.71$, $Y = 0.27$, giving $\mu \simeq 0.613$, and $Z_{\text{CNO}} = 0.015$), stars of initial mass $1.2 M_\odot$ and $3.0 M_\odot$ were considered. (Note that $Z_{\text{CNO}} = 0.75Z$ for both cases, obtained from composition values of Ross and Aller [1976], which are quite similar to those of Grevesse [1984].) The initial stellar composition was obtained via Steigman (1985), by considering a primordial helium abundance of $Y_p = 0.24$ in the interstellar medium, which grows due to nucleosynthesis in stars according to $\Delta Y \approx 1.5\Delta Z$; these values are consistent with the values given by Steigman (1985) of $Y_p = 0.24 \pm 0.01$ and of $\Delta Y/\Delta Z = 1.7 \pm 0.9$, $\Delta Y/\Delta Z \leq 1.3 \pm 3.6$, and $\Delta Y/\Delta Z \approx 2 \pm 1$. It should be noted that first dredge-up

changed the surface composition slightly, so that on the AGB the molecular weight of the envelope had become $\mu \simeq 0.598$ for the $Z = 0.001$ cases and $\mu \simeq 0.618$ for the $3 M_{\odot}$, $Z = 0.02$ case, $\mu \simeq 0.624$ for the $1.2 M_{\odot}$, $Z = 0.02$ case.

The effect of a Reimers (1975) type wind mass loss

$$\dot{M} = -\eta(4 \times 10^{-13} M_{\odot}/\text{yr}) \frac{L}{g \cdot R} = -\eta(1.34 \times 10^{-5} M_{\odot}/\text{yr}) \frac{L^{3/2}}{M \cdot T_e^2} \quad (11)$$

(M , L , g , and R in solar units, T_e in Kelvins: Kudritzki and Reimers 1978) was included whenever a star's effective temperature T_e fell below 5000 K, i.e., for $\log T_e < 3.7$. As recommended in Kudritzki and Reimers (1978), the value of η was chosen to be $\eta = 0.4$ except for the $3.0 M_{\odot}$ case, where $\eta = 1.4$ was chosen. (It should be noted that the Reimers mass loss rate is close to being inversely proportional to the mixing length parameter α , through the effect of the latter on the radius and effective temperature.)

Every effort was made to include the latest nuclear reaction rates and neutrino losses, including neutrino-pair bremsstrahlung. The latest Los Alamos opacities were used (Keady 1985): these include opacities due to a number of molecules at low temperatures. The *dynamical* effects of carbon and oxygen ionizations were also included.

The $^{14}\text{N}(p, \gamma)^{15}\text{O}$ reaction rate determines the rate of CNO-cycle burning. A recent measurement of this rate has been made (Schröder *et al.* 1986, 1987). Preliminary analysis (Rolfs 1986) indicated that at the astrophysical energies relevant to the present work the rate (dominated by the direct capture process) should be

only about $\frac{1}{2}$ the value given in Fowler, Caughlan, and Zimmerman (1975, hereafter FCZ II). This reduced rate was used in the work presented in this paper. Later, more complete analysis (Schröder *et al.* 1986) indicated that a resonance far below threshold, which had never been considered in previous analyses, contributed significantly. At the relevant astrophysical energies, the resulting total $^{14}\text{N}(p, \gamma)^{15}\text{O}$ rate was 3 to 4 times that indicated by the preliminary analysis, i.e., $1\frac{1}{2}$ to 2 times the rate given in FCZ II. To test what effect this increased rate would have, a $3.0 M_{\odot}$ star was evolved with this new, higher CNO-burning rate from the main sequence, through several helium shell flashes on the AGB. Differences from the case of low CNO-burning rate were small in all stages of the star's lifetime, including the AGB, where the interflash luminosity was increased by only about 4% (see Figure 1; see also Paper III). Final analysis (Schröder *et al.* 1987), obtained after this paper was completed, indicated a smaller contribution from the subthreshold resonance, giving a rate very similar to that of FCZ II.

It should be noted that in this work a mixing length to pressure scale height ratio of $\alpha \equiv l/H_p = 1.0$ was used. The appropriate value for α is rather uncertain, values up to $\alpha = 2.0$ or more being not unreasonable, but the effect of this ratio on the star's *luminosity* is negligible for low mass stars. Certain runs comprising a number of flashes on the AGB were repeated with increased values of α , but even increasing α by a factor of two caused only a 1% increase in the star's luminosity (though it had of course a large effect on the radius and effective temperature of the star). For a more complete discussion of this, and other computational details, see Paper III.

IV. RESULTS AND DISCUSSION

a) The $M_c - L$ Relation on the Red Giant Branch

It was first pointed out by Refsdal and Weigert (1970) and Kippenhahn (1981) that an $M_c - L$ relation exists for the pre-core flash red giant branch (RGB) phase for low mass stars, when a single hydrogen-burning shell surrounds a degenerate helium core. Their semi-empirically derived relation was of the form

$$L \propto \mu^\zeta M_{\text{H}}^\phi (Z_{\text{CNO}})^\xi, \quad (12)$$

with $\zeta \approx 7$, $\phi \approx 8$, and (from Tuchman, Glasner, and Barkat 1983) probably $0 < \xi \ll 1$. The above is in agreement with the results of our direct computations. A low mass star climbing the RGB suffers a small luminosity dip as it settles down into the form to which the above work applies (moving a little way back down the RGB before continuing upward), and subsequently follows the $M_c - L$ relation of equation (12) until the helium core flash occurs. Surprisingly, one can define an $M_c - L$ relation even for the lower part of the RGB, before the luminosity dip, although the relation is followed less accurately there. In Figure 2, low-metallicity RGB stars of initial mass $0.8 M_\odot$, $1.0 M_\odot$, $1.2 M_\odot$, and $2.0 M_\odot$ having $Z = 0.001$, $Z_{\text{CNO}} = 0.00075$, and $\mu \simeq 0.598$ are fitted by the relation

$$L = \begin{cases} 42200 M_{\text{H}}^5 = (8.41 M_{\text{H}})^5, & 0.18 \lesssim M_{\text{H}} \lesssim 0.32 \quad (10 \lesssim L \lesssim 150) \\ 412000 M_{\text{H}}^7 = (6.34 M_{\text{H}})^7, & 0.32 \lesssim M_{\text{H}} \lesssim 0.48 \quad (150 \lesssim L \lesssim 2000) \end{cases} \quad (13)$$

(everything in solar units, as usual). In Figure 3, a solar composition RGB star of initial mass $1.2 M_\odot$ having $Z = 0.02$, $Z_{\text{CNO}} = 0.015$, and $\mu \simeq 0.624$ is fitted by the

relation

$$L = \begin{cases} 44600M_{\text{H}}^5 = (8.51M_{\text{H}})^5, & 0.16 \lesssim M_{\text{H}} \lesssim 0.25 \quad (5 \lesssim L \lesssim 50) \\ 714000M_{\text{H}}^7 = (6.86M_{\text{H}})^7, & 0.25 \lesssim M_{\text{H}} \lesssim 0.45 \quad (50 \lesssim L \lesssim 2000). \end{cases} \quad (14)$$

For both of these cases, the M_{H} -dependence in the region $0.3 M_{\odot} < M_{\text{H}} < 0.4 M_{\odot}$ is consistent with the prediction of equation (12): this region can be as well fitted by M_{H}^8 as by M_{H}^7 . A dependence of M_{H}^7 has been chosen in equations (13) and (14) in order to fit the region $M_{\text{H}} \gtrsim 0.4 M_{\odot}$ as well.

Equations (13) and (14) characterize stars of two different compositions. The high-core mass portions of these relations are identical except for the normalization constants in front, of 412000 and 714000 respectively; the difference in these “constants” must be due to the difference in composition. If one assumes that the composition dependence is of the form given by equation (12), and that $\phi = 7$ (i.e., that $L \propto \mu^7$, as claimed by Kippenhahn 1981), then one obtains a constraint on the Z_{CNO} -dependence from the difference between equations (13) and (14):

$$\left(\frac{0.598}{0.624}\right)^7 \left(\frac{0.00075}{0.015}\right)^{\xi} \approx \frac{412000}{714000}, \quad \text{giving} \quad \xi \approx 0.084 \approx \frac{1}{12}. \quad (15)$$

One can then combine equations (13) and (14) into a single equation giving the luminosity of a low mass star on the upper RGB as a function of its core mass and envelope composition:

$$L = (2.91 \times 10^7)(Z_{\text{CNO}})^{1/12} \mu^7 M_{\text{H}}^7 = (11.6\mu M_{\text{H}})^7 (Z_{\text{CNO}})^{1/12}, \quad (16)$$

valid for $0.3 M_{\odot} \lesssim M_{\text{H}} \lesssim 0.45$, where μ is as given in equation (1) and the overall normalization has been shifted by $2^{1/12}$ to account for the difference between the

true CNO-burning rate and the rate used in this work (see Section III). This RGB $M_c - L$ relation could be useful, for example, in determining quickly and easily the core mass at the helium core flash from observations of the luminosity of the tip of the RGB, giving the core mass for the subsequent horizontal branch phase, or in semi-analytical models of stellar behavior on the upper part of the RGB.

b) The $M_c - L$ Relation on the Asymptotic Giant Branch

For the purposes of defining the $M_c - L$ relation on the asymptotic giant branch (AGB), the luminosity and core mass were taken at the pre-flash luminosity maximum, when the helium burning is approximately at its minimum; this is consistent with the previous work quoted in Section II above. For each of the stars described in Section III above, the interflash luminosity values L (over a number of flash cycles) are plotted against core mass M_H in Figure 4; the previous $M_c - L$ relations of Section II are also shown. (The Iben and Truran 1978 relation is really applicable only to much higher core masses, but has been included because it is occasionally applied to lower core masses by unaware users.) The Lattanzio (1986) relations plotted in Figure 4 were obtained from equations (9) and (10) for the *same* compositions as for the stars of the present work; that they are both *steeper* and *lower* than anybody else's results (including our own) is likely due (at least in part) to the fact that Lattanzio's (1986) flashes had not quite reached full amplitude.

For any particular star, the first flash occurs at a low interflash luminosity; but the interflash luminosity grows steeply as the flash strength approaches its asymptotic value, until after about half a dozen flashes the interflash luminosity

approaches closely the value appropriate to the star's core mass and composition as defined by the $M_c - L$ relation. The $3 M_\odot$, $Z = 0.001$ star is an exception to this: after seven flashes, it still is far from its asymptotic value. This is expected, since its core mass of $M_H \approx 0.79$ is far larger than the core masses of the other stars of this work, and stars of higher core mass require more flashes before reaching their asymptotic values. As expected, different $M_c - L$ relations are followed by the stars of different composition: at a given core mass, stars of solar metallicity ($Z = 0.02$, $\mu \approx 0.62$) are about 25% more luminous than metal-poor stars ($Z = 0.001$, $\mu \approx 0.598$). Again as expected, the $M_c - L$ relation is less steep at low core masses than it is at higher core masses: deviations from linearity of the $M_c - L$ relation are showing up. Note that a star of solar metallicity encounters its first helium shell flash at a much lower core mass (and thus lower luminosity) than a metal-poor star of the same initial mass; this is discussed in more detail in Paper III.

For the metal-poor stars ($Z = 0.001$, $\mu \simeq 0.598$), the $M_c - L$ relation for low core masses ($0.5 M_\odot \lesssim M_H \lesssim 0.7 M_\odot$) is well approximated (see Figure 5) by a pair of straight line segments:

$$L = \begin{cases} 38000(M_H - 0.447), & 0.52 \lesssim M_H < 0.60 & (3000 \lesssim L < 6000) \\ 50000(M_H - 0.484), & 0.60 < M_H \lesssim 0.7 & (6000 < L \lesssim 10000) \end{cases} \quad (17)$$

where L and M_H are in solar units as usual. A slightly better fit can be obtained by using a quadratic in M_H : see equation (19) below.

For the stars of solar metallicity ($Z = 0.02$, $\mu \simeq 0.618$), the $M_c - L$ relation is fairly well fitted for low core masses ($0.5 M_\odot \lesssim M_H \lesssim 0.7 M_\odot$) by multiplying the

luminosity obtained via equation (17) by a factor of 1.25; but a single straight line works at least as well (see Figure 6):

$$L = 52000(M_{\text{H}} - 0.456), \quad 0.52 \lesssim M_{\text{H}} \lesssim 0.7 \quad (3000 \lesssim L \lesssim 12000). \quad (18)$$

Again, the quadratic of equation (19) below yields a slightly better fit.

For both metallicities, one might expect the $M_c - L$ relation to have a somewhat steeper dependence on the core mass M_{H} for *higher* core masses (i.e., for $M_{\text{H}} > 0.7 M_{\odot}$), but that is beyond the scope of this work on low mass stars. The effect of the CNO-burning rate correction discussed in Section III above would be to increase the luminosities given by equations (17) and (18) by about 3%.

It is not easy to estimate a composition dependence for the $M_c - L$ relation on the AGB given in equations (17) and (18). Kippenhahn (1981) points out that the μ -dependence grows weaker for increasing core mass, due to the increasing importance of radiation pressure; the Z_{CNO} -dependence might also differ for different core masses. However, a rough approximation can perhaps be made in the limited range of core masses covered by the present work, namely $0.5 M_{\odot} \lesssim M_{\text{H}} \lesssim 0.7 M_{\odot}$. The cases $Z = 0.001$, $\mu \simeq 0.598$ and $Z = 0.02$, $\mu \simeq 0.618$ of Figures 5 and 6 respectively yield $M_c - L$ relations that differ by a factor of about 1.25 over most of this range, though there is some indication that the difference is smaller for the higher core masses. To extract the dependence on Z_{CNO} , one may consider the comparison between the old and the new CNO-burning rates discussed in Section III. The difference of a factor of 3 to 4 in this rate is equivalent to a difference of the same

magnitude in Z_{CNO} ; but as seen in Figure 1, the effect of this difference leads to a change of only about 4% in the interflash luminosity. This implies a very weak Z_{CNO} -dependence of the $M_c - L$ relation, not stronger than $(Z_{\text{CNO}})^{1/25}$. This leads to a μ -dependence of the order of μ^3 or a little more, in order to obtain a factor of 1.25 difference between the metal-poor ($Z = 0.001$, $\mu \simeq 0.598$) and the metal-rich ($Z = 0.02$, $\mu \simeq 0.618$) case. The μ -dependence will be even weaker for higher core masses. Given this composition dependence, both cases are fairly well fit by the quadratic

$$L = 238000\mu^3(Z_{\text{CNO}})^{1/25}(M_{\text{H}}^2 - 0.0305M_{\text{H}} - 0.1802), \quad 0.5 < M_{\text{H}} < 0.66, \quad (19)$$

which may be inverted to give

$$M_{\text{H}} = \left[\frac{L}{238000\mu^3(Z_{\text{CNO}})^{1/25}} + 0.1804 \right]^{1/2} + 0.015, \quad 2000 \lesssim L \lesssim 10000. \quad (20)$$

(The effect of the correction for the new vs. old CNO-burning rate has been included in these two equations.) Note that these equations cannot be expected to give accurate results outside the given ranges of validity.

Figure 7 illustrates the fit of equation (19) to the data, where the data for the metal-rich case ($Z = 0.02$, $\mu \simeq 0.618$) has been multiplied by 0.8 to bring it into coincidence with the data for the metal-poor case ($Z = 0.001$, $\mu \simeq 0.598$). The prediction of Kippenhahn (1981) that the composition dependence grows weaker with increasing core mass is consistent with the fact that the highest- M_{H} points of the $Z = 0.02$ case lie slightly below the line of equation (19): these points have

been shifted down too far, due to our approximation of a uniform composition dependence. Also shown in Figure 7 are portions of the $M_c - L$ relations of previous investigators, again shifted according to the composition dependence given in equation (19). (There is little point in using the composition dependence to attempt to bring the Iben [1977] relation into coincidence with the others: it applies only to much higher core masses where the composition dependence is different. If one did make the attempt, the extrapolated Iben [1977] relation would still lie at higher luminosity than the results of the present work.)

As seen in Figure 7, the shifted versions of equations (2), (5), and (6) all lie at lower luminosities than the results of the present work. This is partially accounted for by the fact that the previous investigators fit their $M_c - L$ relations over a range of core masses that extend to much higher values of M_H ; thus the given portions of their relations lie in the region where the $M_c - L$ relation is becoming non-linear, and are therefore expected to underestimate the luminosity somewhat. In addition, the Paczyński (1970) relation gives the average (rather than maximum) interflash luminosity, a difference of a factor of roughly 1.2 for a core mass $M_H \approx 0.65$ (see Paper I). It seems probable, however, that some of the discrepancy remains unaccounted for, at least in the case of the Wood and Zarro (1981) relation. This remaining discrepancy is rather small, of the order of 10%; contributing causes likely include differences in the helium-burning reaction rates, which might have a larger effect on the $M_c - L$ relation than differences in the CNO-burning rate. It is also possible that different opacities could have some effect.

One point remains to be stressed: the luminosity of a typical star at any given core mass has a significant probability of lying *below* the $M_c - L$ relation, due to the variation of the luminosity over the flash cycle; there is also a small probability (a couple of percent) that the luminosity lies above the $M_c - L$ relation (see Paper I). These luminosity variations are quite large: the minimum and maximum luminosities over the flash cycle differ by about a factor of $\frac{1}{2}$ and a factor of 2 respectively from the interflash luminosity given by the $M_c - L$ relation. If the star's position in its flash cycle is unknown, then the $M_c - L$ relation should really be replaced by a probability distribution giving the probability of finding a given luminosity at a given core mass. Figures 8 and 9 represent an attempt to do this for the cases $Z = 0.001$ and $Z = 0.02$ of the present work, using the information presented in Paper I. Contours of constant *integrated* probability are given: these contours follow the points where the integral of the probability density, integrated inward from the extremes of the distribution at a given core mass, reaches a given (constant) value. Thus the top line marked "0" gives the maximum luminosity over the flash cycle for a given core mass, the bottom line marked "0" gives the minimum luminosity over the flash cycle for a given core mass, and, for example, above the $M_c - L$ relation the line marked "2" gives the luminosity above which the star spends 2% of its time during the flash cycle, while below the $M_c - L$ relation the line marked "10" gives the luminosity below which the star spends 10% of its time during the flash cycle. Thus in Figure 8, for example, a star which has a core mass $M_H = 0.6 M_\odot$ has an interflash luminosity of $L = 6000 L_\odot$, but rises as high as $L = 12700 L_\odot$ and drops as low as $L = 3100 L_\odot$ during the course of its flash cycle. It spends 1% of the flash

cycle above a luminosity of $8600 L_{\odot}$, 2% of the flash cycle above $7300 L_{\odot}$, and 3% of the flash cycle above $6400 L_{\odot}$; it spends 10% of the flash cycle below $4200 L_{\odot}$, 20% of the flash cycle below $5000 L_{\odot}$, and 30% of the flash cycle below $5500 L_{\odot}$.

This luminosity variation over the flash cycle has a significant effect for observers who wish to use the $M_c - L$ relation to infer a star's core mass from its observed luminosity, as do Weidemann (1984) and Aaronson and Mould (1985). Let us take the same example of a star of composition appropriate to Figure 8 whose true core mass is $M_H = 0.6 M_{\odot}$. There is a 10% chance that this star's luminosity lies in the range $3100 L_{\odot} < L < 4200 L_{\odot}$, which means that there is a 10% chance that this star would be assigned a core mass in the range $0.53 M_{\odot} < M_H < 0.557 M_{\odot}$, using the $M_c - L$ relation on which it must be assumed the star lies. Similarly, since there is a 1% chance that the star's luminosity lies in the range $8600 L_{\odot} < L < 12700 L_{\odot}$, there is a 1% chance that this star would be assigned a core mass in the range $0.657 M_{\odot} < M_H < 0.74 M_{\odot}$. There is only a 67% chance that this star would be assigned a core mass in the range $0.589 M_{\odot} < M_H < 0.609 M_{\odot}$. Thus most stars, having luminosities close to the $M_c - L$ line, would be assigned core masses quite close to the correct values; but the core masses would be badly underestimated for a significant fraction of the stars, whose luminosities lie below the $M_c - L$ line, while the core masses would be overestimated for that couple of a percent of the stars whose luminosities lie above the $M_c - L$ line.

Note that the situation is more favorable if one is interested in the core mass at the *tip of the AGB* in some particular cluster of stars (as are Weidemann 1984

and Aaronson and Mould 1985), rather than the core mass of one particular star. If there are two or more stars near the tip of the AGB, the probability is still small that any star will have a higher luminosity than that given by the $M_c - L$ relation, but the probability is large that at least one star will lie very near the luminosity given by the $M_c - L$ relation; in such a case it is this latter star that will define the tip of the AGB, and the correct core mass will be assigned to it. Of course, a sparse cluster may not have any stars near the tip of the AGB, causing the tip luminosity and core mass to be badly underestimated. This is probably the cause for some of the lowest-luminosity points in Figure 4 of Aaronson and Mould (1985), which gives the tip luminosity as a function of the age of the star cluster: the lowest-luminosity points there lie at a luminosity a fair bit *lower* than half the luminosity of the majority of the points for similar cluster ages. Thus only part of the scatter in the points is due to the deviations from the $M_c - L$ relation.

In this connection, it should be noted that the $M_c - L$ relation of Iben and Renzini (1983) was used by Aaronson and Mould (1985) to convert their Figure 4 (described above) to their Figure 5, which gave a star's final mass (determined from the AGB tip core mass) as a function of the star's initial main sequence mass (obtained from the cluster age). Use of the $M_c - L$ relation of equation (20) above instead does indeed shift the points in this diagram slightly, but by rather less than the scatter in the points. The largest difference is for stars of initial mass M_i near $2M_\odot$; the final masses of such stars are shifted upward, but only by $\Delta M_f \approx 0.03M_\odot$, compared to a scatter of the order of $0.1M_\odot$. Thus there is no real need to revise Figure 5 of Aaronson and Mould (1985).

V. CONCLUSIONS

The $M_c - L$ relations of Section IV *a*, for the *upper red giant branch*, are consistent with the theoretical predictions of Refsdal and Weigert (1970) and Kippenhahn (1981). The fact that $L \propto M_H^7$ in the present work, rather than M_H^8 , is probably due to the fact that the present work was fit to the relation at relatively high core masses ($M_H \approx 0.4 M_\odot$). The composition dependence is less certain than the M_H -dependence, but probably adequate since μ does not vary very much and the dependence on Z_{CNO} is weak, so that errors in the composition dependence have only a small effect on the luminosity.

The $M_c - L$ relations of Section IV *b*, for the *asymptotic giant branch*, are consistent with what one would expect from Tuchman, Glasner, and Barkat (1983): the $M_c - L$ relation flattens out at lower core masses, and the composition dependence is weaker than for the RGB case. (Again, possible errors in the derived composition dependence have only a small effect, for the same reason.) Even taking into account composition dependence and the non-linearity of the $M_c - L$ relation at low core masses, there seems to be a discrepancy of perhaps 10% between the results of the present work and those of Wood and Zarro (1981), whose relation should be valid for some little distance below $M_H = 0.65 M_\odot$; this is probably attributable to changes in the helium-burning reaction rates (both the triple-alpha and the $^{12}\text{C}(\alpha, \gamma)^{16}\text{O}$ reactions have been updated, the latter changing by a factor of 3: see Paper III), updated opacities, etc.

It should be emphasized that while equations (6) and (7) above (contained in Iben and Renzini 1983) apply to intermediate and high core masses, the $M_c - L$ relation for low core masses ($M_H \lesssim 0.65 M_\odot$) is that of equations (19) and (20) of the present work. At low core masses ($M_H \lesssim 0.55 M_\odot$) and low luminosities ($L \lesssim 4000 L_\odot$), the differences can be quite large, as much as $\Delta M_H \sim 0.05$ at a given luminosity. Linear $M_c - L$ relations fitted at higher core masses all pass through zero close to $M_H = 0.5 M_\odot$, where in fact a luminosity value of about $L = 2500 L_\odot$ is appropriate: the $M_c - L$ relation “flattens out” at low core masses. The situation for observers is complicated by the fact that variations in the luminosity over the flash cycle cause a star to deviate from the $M_c - L$ relation; the deviations can be as much as a factor of 2 in luminosity, and there is a substantial probability that the star will lie below the $M_c - L$ relation (see Figures 8 and 9).

The present work agrees with that of Paczyński (1970) and Wood and Zarro (1981) in that, for the *low core masses* under consideration, *no* evidence was found for any dependence of the $M_c - L$ relation on the total stellar mass. Nor does the $M_c - L$ relation for low core masses depend significantly on the choice of the mixing length parameter α .

This work was carried out at the W. K. Kellogg Radiation Laboratory. We wish to express our gratitude to Professors R. D. Blandford, C. A. Barnes, S. E. Koonin, and S. C. Frautschi for their encouragement and support; we have also benefitted from valuable discussions with Professors W. A. Fowler and J. R. Mould.

REFERENCES

- Aaronson, M., and Mould, J. 1985, *Ap. J.*, **288**, 551.
- Boothroyd, A. I., and Sackmann, I.-J. 1987*a* (Paper I).
- . 1987*b* (Paper III).
- Deupree, R. G. 1984, *Ap. J.*, **287**, 268.
- Fowler, W. A., Caughlan, G. R., and Zimmerman, B. A. 1975, *Ann. Rev. Astron. Astrophys.*, **13**, 69.
- Grevesse, N. 1984, *Physica Scripta*, **T8**, 49.
- Havazelet, D., and Barkat, Z. 1979, *Ap. J.*, **233**, 589.
- Iben, I., Jr. 1972, *Ap. J.*, **178**, 433.
- . 1975, *Ap. J.*, **196**, 525.
- . 1976, *Ap. J.*, **208**, 165.
- . 1977, *Ap. J.*, **217**, 788.
- . 1981, *Ap. J.*, **246**, 278.
- Iben, I., Jr., and Renzini, A. 1983, *Ann. Rev. Astron. Astrophys.*, **21**, 271.
- Iben, I., Jr., and Truran, J. W. 1978, *Ap. J.*, **220**, 980.
- Keady, J. 1985, private communication.
- Kippenhahn, R. 1981, *Astron. Astrophys.*, **102**, 293.
- Kudritzki, R. P., and Reimers, D. 1978, *Astron. Astrophys.*, **70**, 227.
- Lattanzio, J. C. 1986, *Ap. J.*, **311**, 708.
- Paczyński, B. 1970, *Acta Astr.*, **20**, 47.
- Refsdal, S., and Weigert, A. 1970, *Astron. Astrophys.*, **6**, 426.

- Reimers, D. 1975, in *Problems in Stellar Atmospheres and Envelopes*, ed. B. Baschek, W. H. Kegel, and G. Traving (New York: Springer-Verlag), p. 229.
- Rolfs, C. 1986, private communication.
- Ross, J. E., and Aller, L. H. 1976, *Science*, **191**, 1223.
- Schröder, U., Becker, H. W., Bogaert, G., Görres, J., Rolfs, C., Trautvetter, H. P., Azuma, R. E., and King, J. D. 1986, draft manuscript.
- . 1987, submitted to *Nucl. Phys.*
- Steigman, G. 1985, in *Nucleosynthesis: Challenges and New Developments*, ed. W. D. Arnett and J. W. Truran (Chicago: University of Chicago Press), p. 48.
- Tuchman, Y., Glasner, A., and Barkat, Z. 1983, *Ap. J.*, **268**, 356.
- Uus, U. 1970, *Nauch. Inform. Acad. Nauk.*, **17**, 3.
- Weidemann, V. 1984, *Astron. Astrophys. (Letters)*, **134**, L1.
- Wood, P. R., and Zarro, D. M. 1981, *Ap. J.*, **247**, 247.

FIGURE CAPTIONS

Fig. 1.—The effect on the asymptotic giant branch $M_c - L$ relation of the CNO-burning rate. The new CNO-burning rate is between three and four times the old rate, but the interflash luminosity is increased by only about 4%.

Fig. 2.—The $M_c - L$ relation for the case $Z = 0.001$, $\mu \simeq 0.598$ of the present work, for *red giant branch* (single hydrogen-shell burning) stars: see equation (13).

Fig. 3.—The $M_c - L$ relation for the case $Z = 0.02$, $\mu \simeq 0.618$ of the present work, for *red giant branch* (single hydrogen-shell burning) stars: see equation (14).

Fig. 4.—Previous $M_c - L$ relations superimposed on the interflash luminosity values obtained in the current work. (Note that the $3 M_\odot$, $Z = 0.001$ star of the current work is far from reaching its full amplitude.) The dotted curves are the general fit of eq. (19). P: Paczyński (1970) relation, eq. (2); HB: Havazelet and Barkat (1979) relation, eq. (5); WZ: Wood and Zarro (1981) relation, eq. (6); I_7 , I_1 : Iben (1977) relation, as modified in Iben and Truran (1978) and quoted in Iben and Renzini (1983), eq. (7), for total masses $7 M_\odot$ and $1 M_\odot$ respectively (dashed to indicate extrapolation below its region of validity); L_1 : Lattanzio (1986) Pop. I relation of eq. (9), for $Y = 0.28$, $Z = 0.02$; L_2 : Lattanzio (1986) Pop. II relation of eq. (10), for $Y = 0.26$, $Z = 0.001$.

Fig. 5.—The $M_c - L$ relation for the case $Z = 0.001$, $\mu \simeq 0.598$ of the present work: solid curve from eq (17), dotted curve from eq. (19).

Fig. 6.—The $M_c - L$ relation for the case $Z = 0.02$, $\mu \simeq 0.618$ of the present work: solid curve from eq (18), dotted curve from eq. (19).

Fig. 7.—The asymptotic giant branch relation of eq. (19) fitted to all the data, where the data for $Z = 0.02$ has been multiplied by 0.8 to bring it into (approximate) coincidence with the data for $Z = 0.001$. Dashed lines: “P:” Paczyński (1970) relation of eq. (2), shifted by 0.782; “HB:” Havazelet and Barkat (1979) relation of eq. (5), shifted by 0.868; “WZ:” Wood and Zarro (1981) relation of eq. (6), shifted by 0.761.

Fig. 8.—The $M_c - L$ probability distribution (over all points in the flash cycle) for the case $Z = 0.001$, $\mu \simeq 0.598$ (giving the range of luminosities to be expected at a given core mass: the probabilities are obtained by considering the relative amount of time spent at a given luminosity, during the flash cycle). The central solid line is the $M_c - L$ relation of eq. (19); lines above this are marked by the percent probability that the star’s luminosity lies above them, while lines below are marked by the percent probability that the star’s luminosity lies below them. Thus the two lines marked “0” give the limits of the luminosity range encountered by a star over its flash cycle.

Fig. 9.—The $M_c - L$ probability distribution (over all points in the flash cycle) for the case $Z = 0.02$, $\mu \simeq 0.618$; notation as in Fig. 8.

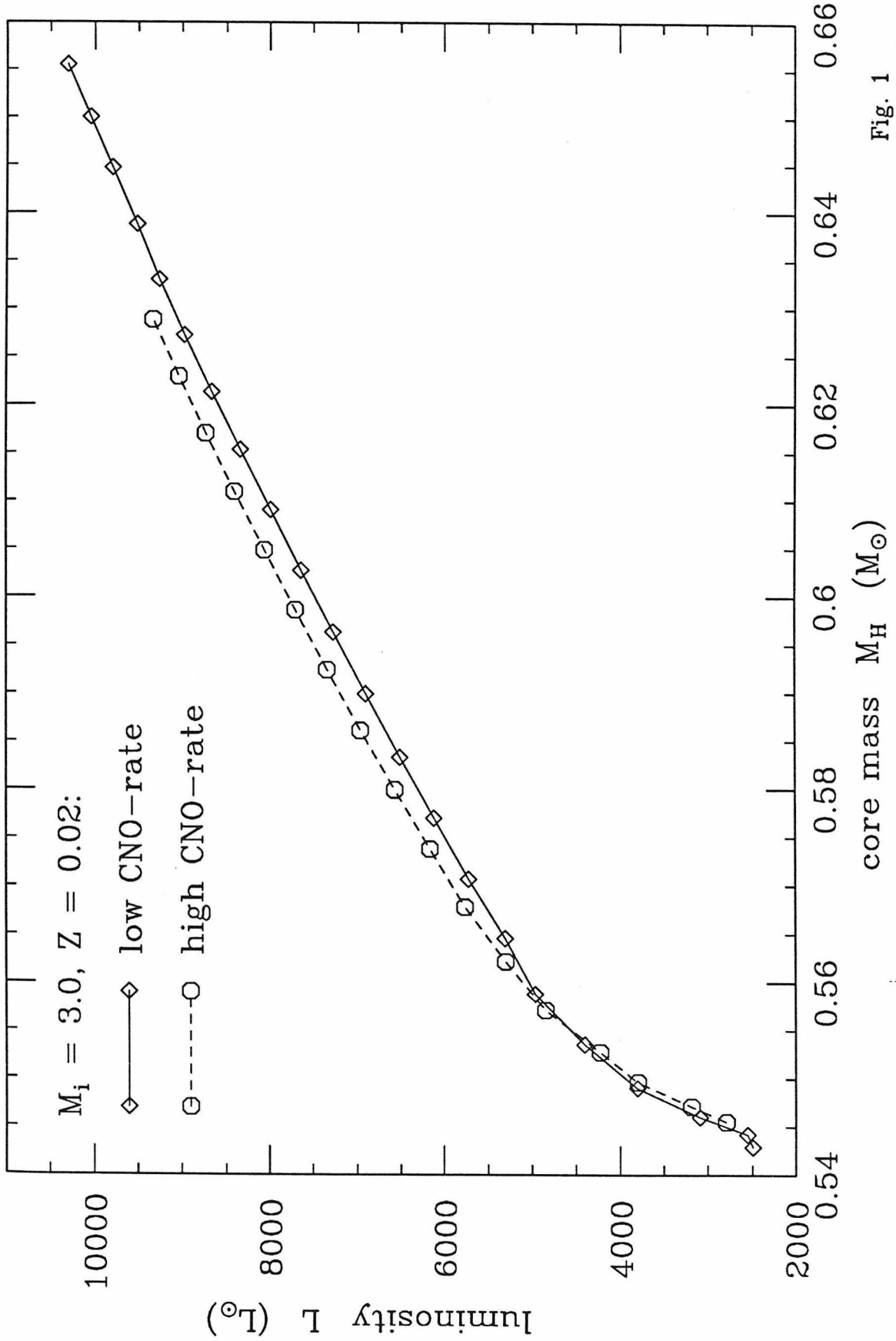


Fig. 1

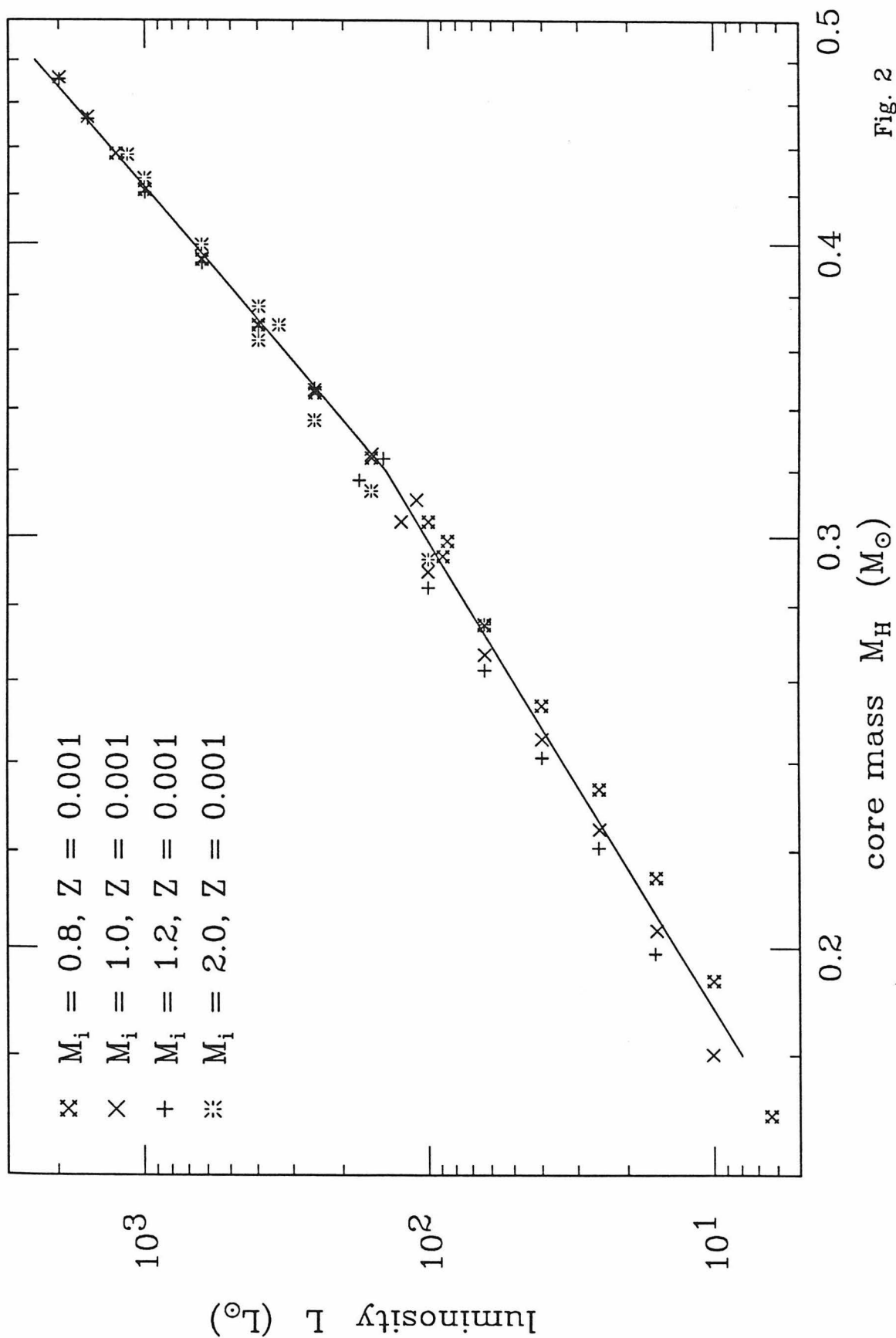


Fig. 2

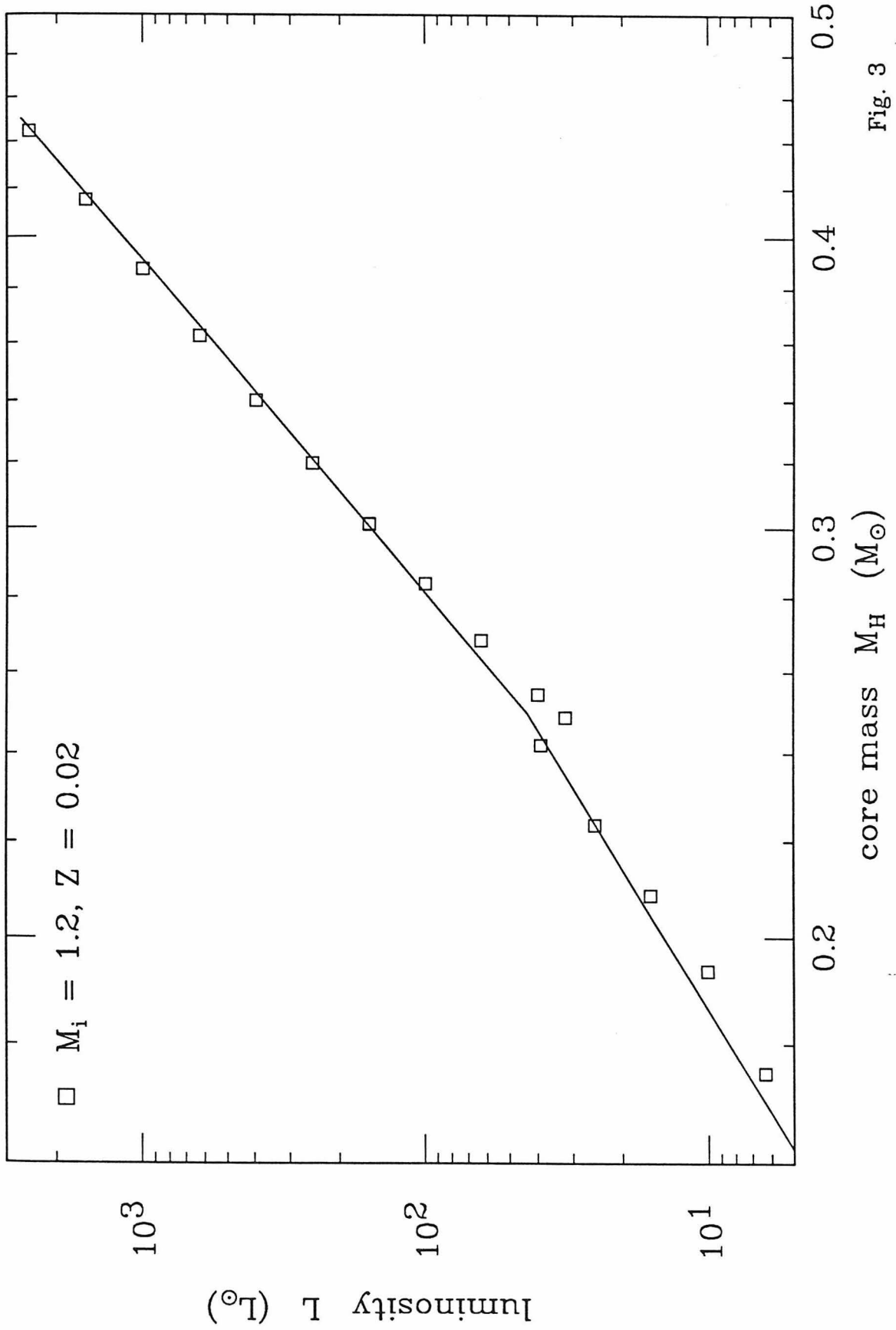


Fig. 3

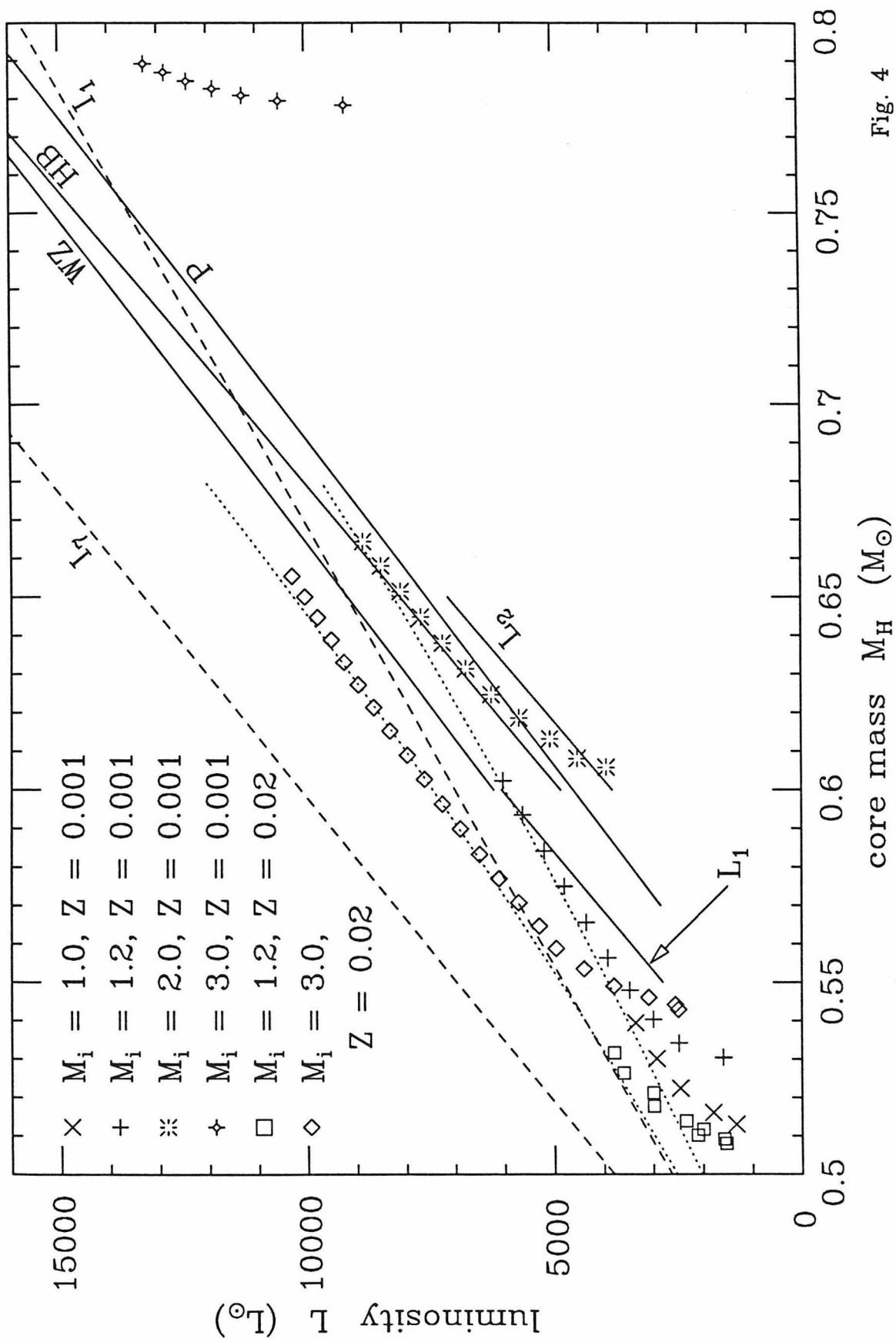


Fig. 4

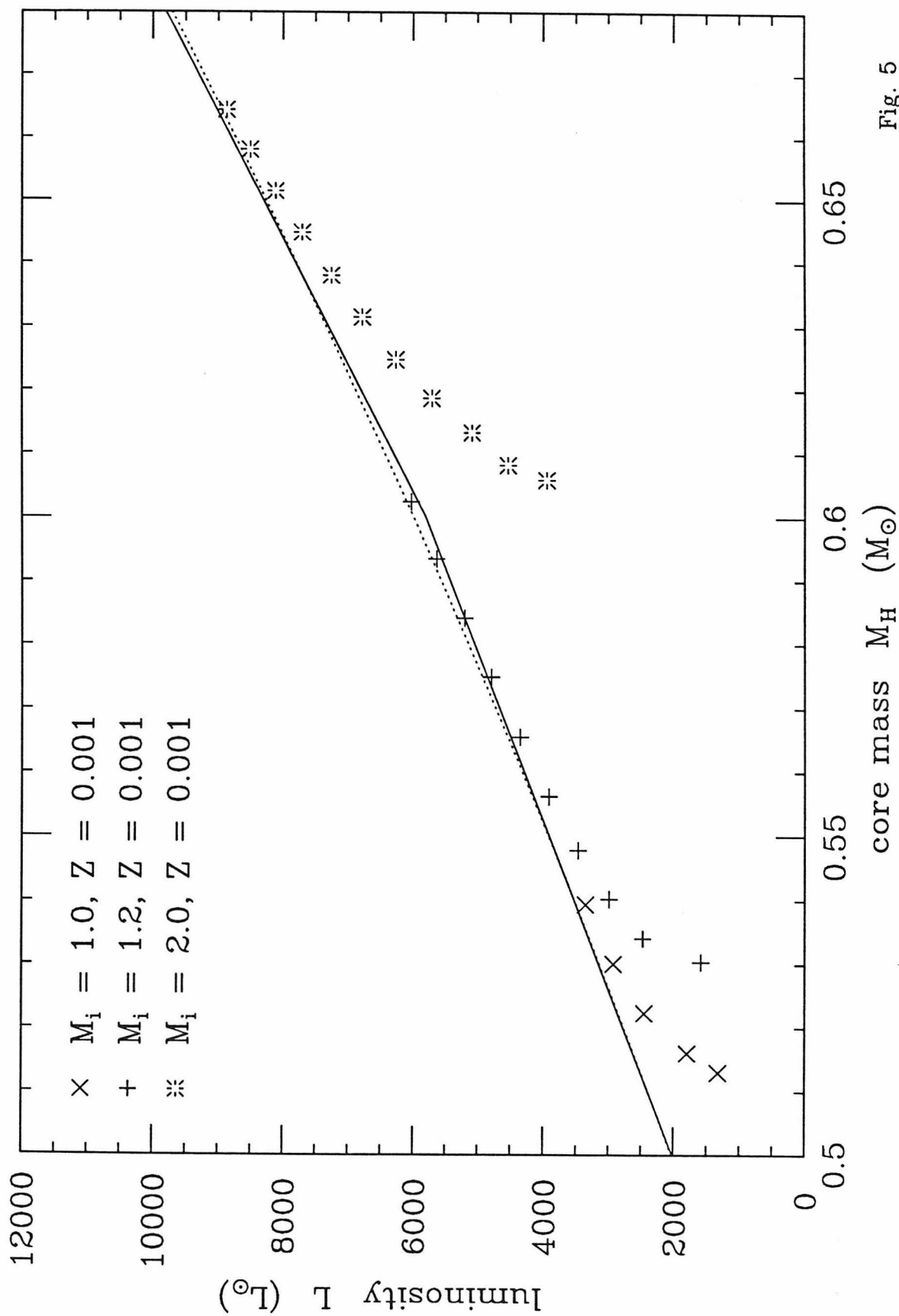


Fig. 5

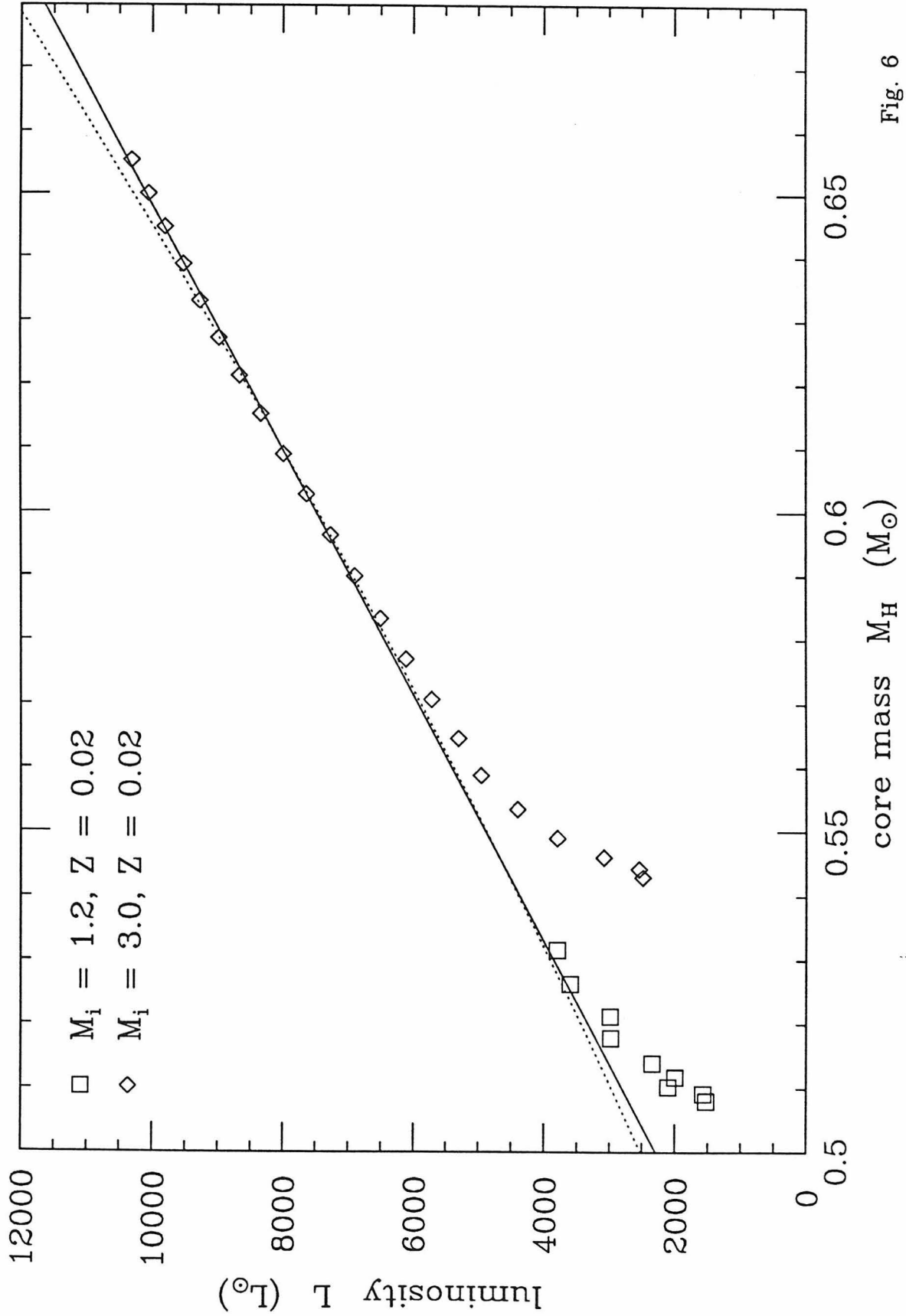


Fig. 6

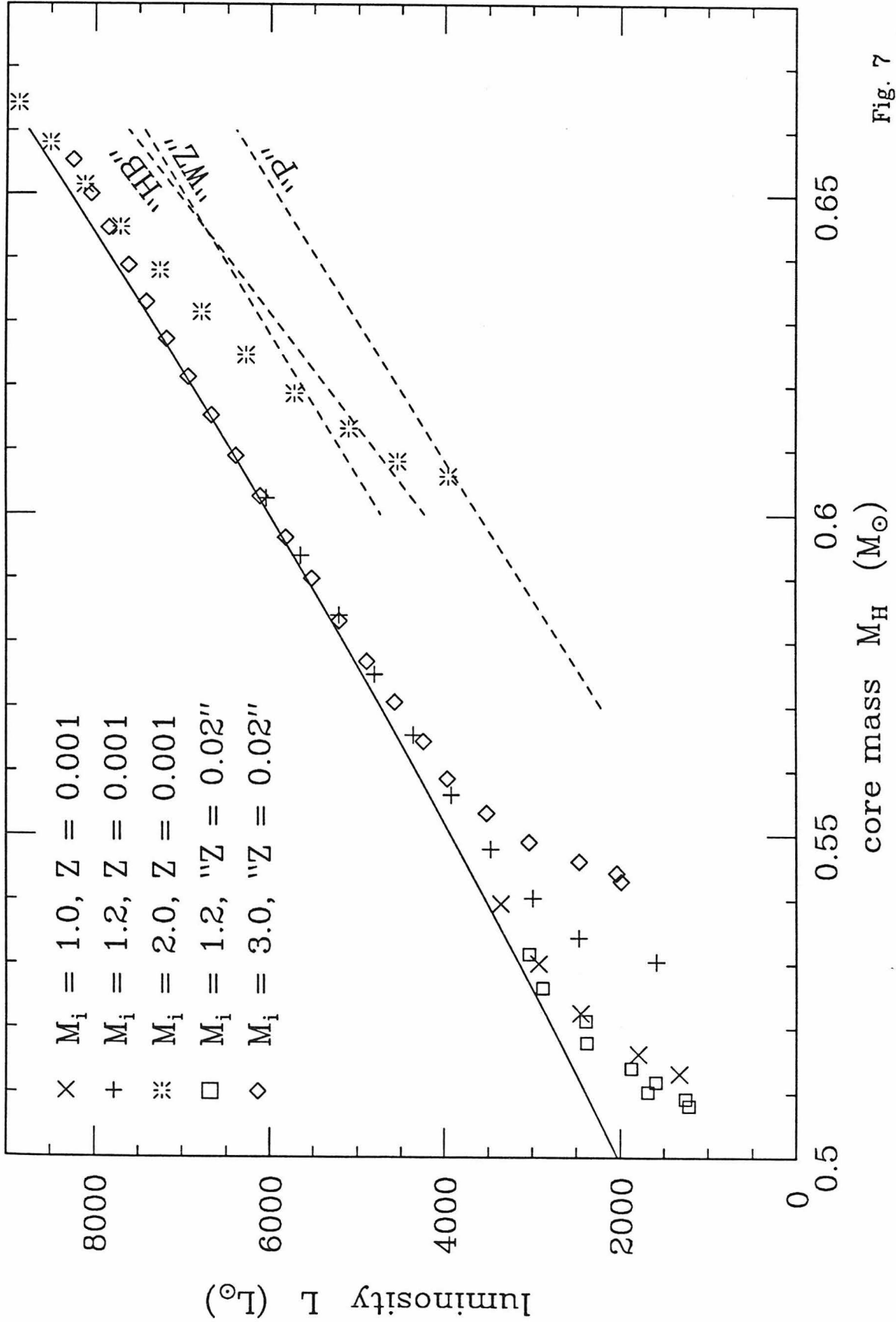


Fig. 7

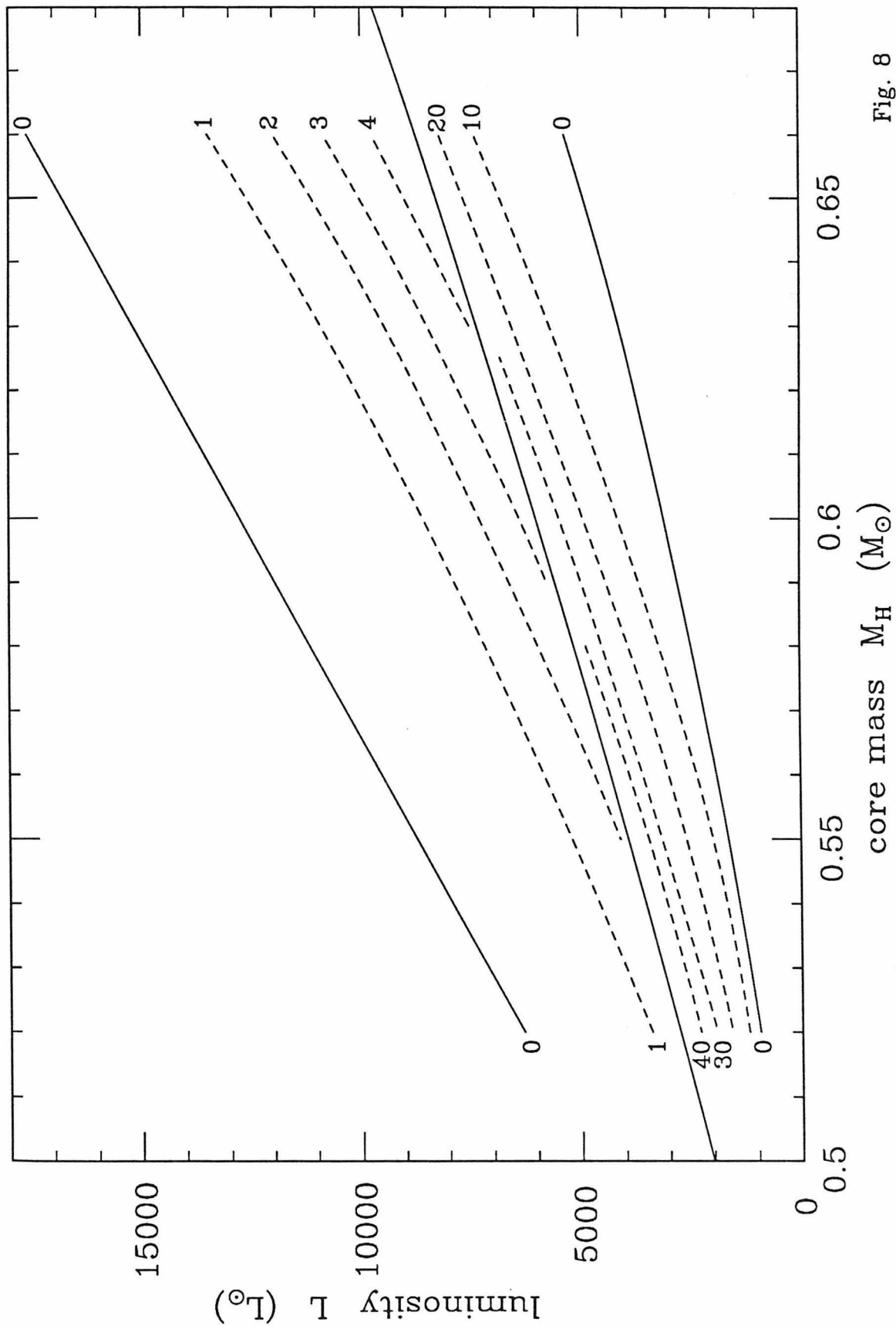


Fig. 8

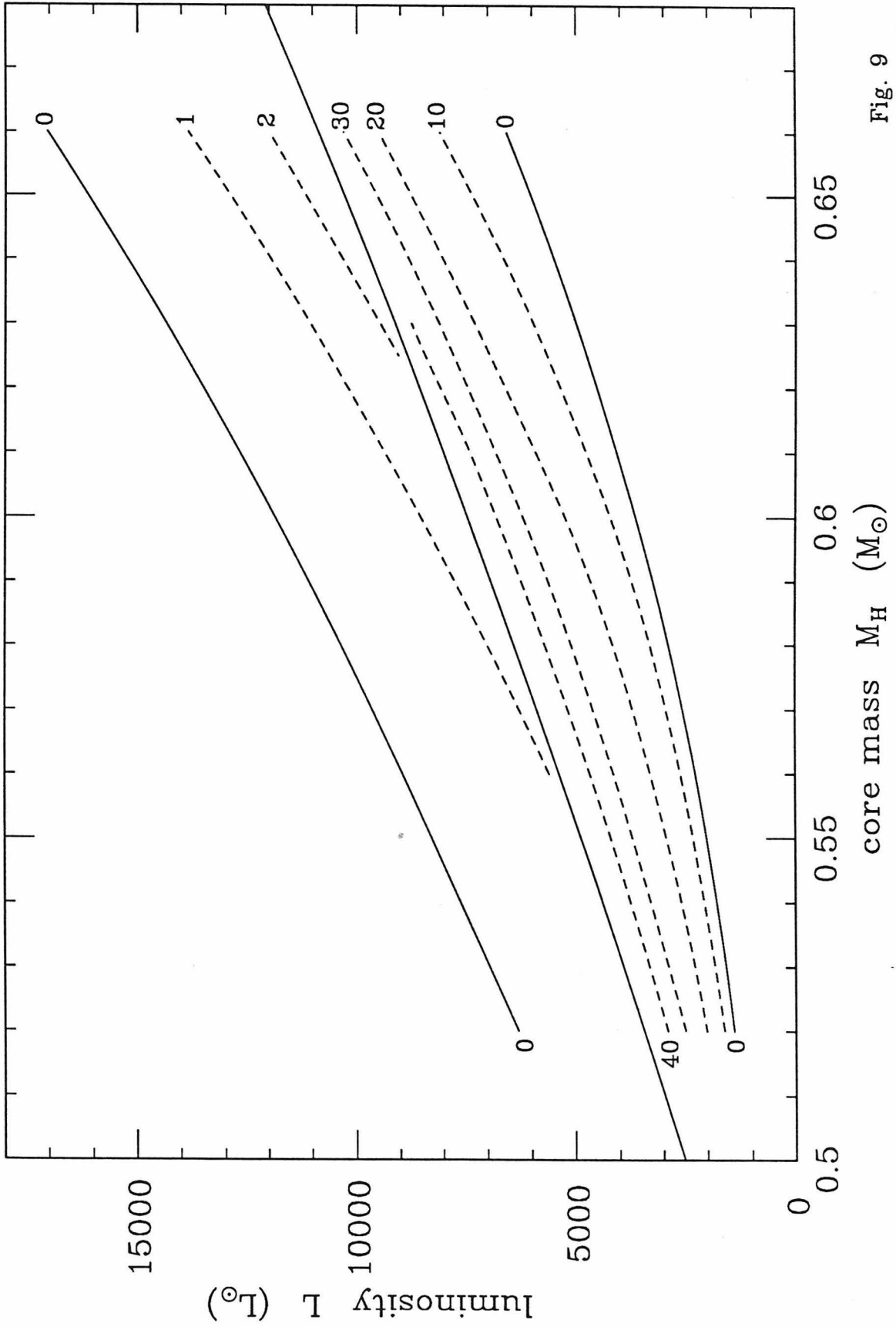


Fig. 9

CHAPTER 4.

III. The Production of Low Mass Carbon Stars

Arnold I. Boothroyd and I.-Juliana Sackmann

W. K. Kellogg Radiation Laboratory 106-38

California Institute of Technology, Pasadena, CA 91125

ABSTRACT

Detailed stellar evolutionary calculations were carried out for a *metal-poor* case ($Z = 0.001$) for stars of initial masses $1.0 M_{\odot}$, $1.2 M_{\odot}$, $2.0 M_{\odot}$, and $3.0 M_{\odot}$, and for a *metal-rich* case ($Z = 0.02$) for stars of initial masses $1.2 M_{\odot}$ and $3.0 M_{\odot}$. The latest nuclear reaction rates were used, as well as the latest Los Alamos opacities, including low-temperature carbon opacities and some molecular opacities, and mass loss via a Reimers-type wind. The stars were evolved from the main sequence through the red giant branch (RGB), including the helium core flash that occurs in stars of $M_i \lesssim 2 M_{\odot}$, through core helium burning on the horizontal branch, and finally through a number of helium shell flashes (thermal pulses) asymptotic giant branch. The new, increased $^{12}\text{C}(\alpha, \gamma)^{16}\text{O}$ reaction rate resulted in carbon-poor, oxygen-rich cores ($C \sim 20\%$, $O \sim 80\%$), but had little effect on flash-produced “carbon pocket” abundances ($C \sim 20\%$, $^{16}\text{O} \sim 2\%$), nor did any significant ^{20}Ne -production via $^{16}\text{O}(\alpha, \gamma)^{20}\text{Ne}$ result from the increased ^{16}O -production.

One run ($M_i = 3.0 M_\odot$, $Z = 0.02$) was performed with a new, increased $^{14}\text{N}(p, \gamma)^{15}\text{O}$ reaction rate; this proved to have little effect.

The flash strength $L_{\text{He}}^{\text{max}}$ was *not* found to level out for the later flashes, but to grow *linearly*, growing faster (and reaching considerably greater strengths) for low- Z stars than for high- Z stars. *No* evidence was found for the existence of any universal curve giving $L_{\text{He}}^{\text{max}}$ as a function of core mass $M_c \equiv M_{\text{H}}$. This implies that *misleading results* may be obtained from the commonly used computational short-cut of arbitrarily manipulating envelope mass or core mass in the hopes of simulating the behavior of a star of different initial mass. The general relations that do exist, namely the $M_c - T_b$ and $M_c - \tau_{if}$ relations, turn out to depend appreciably on the composition.

The onset of shell flashes was found to occur considerably earlier in luminosity than indicated by the Iben-Renzini relation, allowing flashes to build up in strength before reaching the luminosity domain where carbon stars are observed to exist. This onset turned out to occur much earlier for high- Z stars than for low- Z stars; it depended much less on the initial mass for the high- Z case than the low- Z case.

Classical “third dredge-up” and carbon star production were obtained in two cases, both having metallicity $Z = 0.001$. A $1.72 M_\odot$ star (of *initial* mass $2.0 M_\odot$) whose mixing length parameter had been increased to $\alpha = 1.5$ became a carbon star on its 11th flash, with

peak flash strength $\log(L_{\text{He}}^{\text{max}}/L_{\odot}) = 7.86$ and a core mass of $M_{\text{H}} = 0.665 M_{\odot}$; the post-flash luminosity dip brought the star’s luminosity down to $\log(L/L_{\odot}) = 3.78$ (i.e., $M_{\text{bol}} = -4.68$). A $0.81 M_{\odot}$ star (of *initial* mass $1.2 M_{\odot}$) became a carbon star immediately after its mixing length parameter was increased to $\alpha = 3.0$, on its 6th flash, with peak flash strength $\log(L_{\text{He}}^{\text{max}}/L_{\odot}) = 7.53$ and a core mass of $M_{\text{H}} = 0.566 M_{\odot}$; the post-flash luminosity dip brought this star’s luminosity down to $\log(L/L_{\odot}) = 3.34$ (i.e., $M_{\text{bol}} = -3.59$). No runs having $\alpha = 1.0$ had any “third dredge-up” episodes on the AGB: a value of $\alpha \gtrsim 1.5$ appears to be a *necessary* condition for dredge-up in low mass stars, and an increase in the value of α leads to conditions more favorable to dredge-up (by increasing the depth in temperature reached by the convective envelope). Other conditions tending to favor dredge-up are high flash strength (to expand the “carbon pocket” out to lower temperatures), relatively large envelope mass (which increases the depth of envelope convection), and low metallicity (which has the same effect, besides leading to higher flash strengths). It should be noted that a reasonable wind mass loss rate *severely* limits the total number of flashes experienced on the AGB, particularly for stars of initial masses $M_i \lesssim 1.2 M_{\odot}$. Also, it was found that for stars of $Z = 0.001$, only stars of $M_i \lesssim 2 M_{\odot}$ experience flashes at a low enough core mass to become carbon stars while still satisfying the observational initial–final mass relation discovered by Weidemann and Koester; we found that a Reimers wind mass loss is sufficient to

account for the total mass loss required by the Weidemann-Koester relation in stars of $M_i \lesssim 1.5 M_\odot$, but that additional mass loss is required for higher initial masses. It should be noted that the correct choice of Reimers wind parameter η depends sensitively on the choice of mixing length (i.e., $\eta \propto 1/\alpha$), composition, and opacities; for low mass stars of $Z = 0.001$, a value of $\eta = 0.4$ is appropriate only for $\alpha \approx 2$.

I. INTRODUCTION

For some years there was a large discrepancy between the theory of carbon star production and observations of carbon stars: this discrepancy was commonly referred to as the “Carbon Star Mystery” (Iben 1981). Carbon stars are produced when helium shell flashes (thermal pulses) during the asymptotic giant branch (AGB) stage of evolution cause carbon to be produced and dredged up to the surface. Early theoretical work found dredge-up to occur in stars of masses greater than about $5 M_\odot$, but failed to find dredge-up in stars of lower masses, resulting in only relatively high-mass and high-luminosity carbon stars (see, e.g., Iben 1976; Sackmann 1976, 1980*a*; Paczyński 1977; Wood and Cahn 1977; Iben and Truran 1978; Iben 1981; Renzini and Voli 1981). On the other hand, observers found most carbon stars to be of lower mass and luminosity (see, e.g., Mould and Aaronson 1979, 1982; Blanco, McCarthy, and Blanco 1980; Frogel, Persson, and Cohen 1980; Richer 1981; Aaronson and Mould 1982, 1985). Part of the discrepancy was removed when several factors were proposed that would tend to *block* the production

of *high-mass carbon stars*. The results of Weidemann and Koester (1983), Weidemann (1984), and Aaronson and Mould (1985) on observational constraints on the initial–final mass relation indicated that stars of initial mass greater than some critical value $M_i \approx 5 M_\odot$ might lose all their envelopes (and leave the AGB to become white dwarfs) before they could begin to experience helium shell flashes. Castellani *et al.* (1985*a*) point out that for high mass stars, semiconvective “core breathing pulses” during core helium burning substantially increase the star’s subsequent core mass. A star with large enough core mass ignites carbon quiescently in its core, never experiencing shell flashes and thus having no chance to become a carbon star: the work of Castellani *et al.* (1985*a*) implies that a smaller stellar mass suffices to avoid shell flashes than was previously supposed. A similar end result is reported by Bertelli, Bressan, and Chiosi (1985) *if* substantial overshooting occurs in the convective core of the star. At the same time, other workers began to obtain indications as to how low-mass carbon stars might be produced. Sackmann (1980*b*) produced the first low-mass carbon star: a very strong flash, occurring in a star with a very small envelope mass, caused sufficient post-flash expansion that even the shallow hydrogen and helium ionization envelope convective zone typical of such a small envelope mass could dredge carbon up to the surface, producing a carbon star in a single dredge-up episode. Sackmann (1980*b*) also pointed out for the first time the importance of the increased opacity due to large amounts of carbon at cool temperatures. Iben and Renzini (1982*a, b*) followed up this suggestion that carbon opacities should be included, and discovered a new semiconvective region that mixes carbon upward from the tip of the flash-produced carbon pocket. Iben and Renzini

(1982*b*) and Iben (1983) produced low-mass, low-luminosity carbon stars via classical dredge-up. Wood (1981*b*) found dredge-up in a star of only $2 M_{\odot}$ total mass. However, all of these stellar models were based on rather artificial starting models; it was exploratory work rather than a systematic investigation. In addition, none of these investigations included continuing mass loss, which turns out to be of major importance.

We started by investigating the effects of detailed carbon opacities on static stellar envelopes (Sackmann and Boothroyd 1985); the effects turned out to be large, but we found that time-dependent evolutionary sequences were necessary in order to make conclusive statements about the effect of carbon on envelope convection.

The purpose of the present work was to evolve systematically a *self-consistent* grid of low mass stars, starting from well-understood main sequence models and using the latest and most up-to-date input physics (nuclear reaction rates, opacities, mass loss rates), in order to search for the production of carbon stars at low masses. We concentrated on stars of low metallicity, where the least theoretical work on helium shell flashes had been carried out, but which were of most relevance observationally.

Stars of relatively low mass, from one to a few solar masses, present certain difficulties to a theoretician interested in the later stages of their lifetimes. The main sequence and red giant branch (RGB) stages are straightforward, but a star of less than about $2.5 M_{\odot}$ terminates the RGB with an exceedingly violent helium core flash in its degenerate helium core. This is sufficiently difficult to handle computationally

that many investigators prefer to begin with the subsequent horizontal branch stage, at the cost of a certain arbitrariness of initial conditions, and continue on from there to the AGB stage with its helium shell flashes. We have chosen instead to evolve our stars from initial zero age main sequence (ZAMS) models, following them through their entire lifetime *including* the core flash, and thus preserving information on initial mass and total age of the stars. It is true that the core flash can only be approximated by any non-hydrodynamic, one-dimensional code (see, e.g., Deupree 1984), but an approximation is better than ignoring the event completely, and the effect of inaccuracies in the core flash is likely to be small. By the time the star reaches the AGB, the core regions affected by the core flash have in any case been reprocessed by later helium core and shell burning into the degenerate carbon-oxygen core of the double-shell burning stage.

After the calculations of the present work had been completed, we became aware of dredge-up results obtained by Hollowell (1986, 1987) and by Lattanzio (1987), for somewhat different types of stars than those considered in the present work; their results and ours are thus complementary, filling in more points in parameter space. Certain of our results are presented elsewhere: flash light curves and flash-driven radius variations are presented in Boothroyd and Sackmann (1987*a*: hereafter Paper I), and the core mass–luminosity relation resulting from our work is discussed in Boothroyd and Sackmann (1987*b*: hereafter Paper II).

II. METHODS AND COMPUTATIONAL DETAILS

Stars of two different metallicities were considered: low metallicity ($Z = 0.001$,

appropriate to the Magellanic Cloud carbon star observational data) and solar metallicity ($Z = 0.02$). For the low-metallicity case ($Z = 0.001$), stars of initial mass $0.8 M_{\odot}$, $1.0 M_{\odot}$, $1.2 M_{\odot}$, $2.0 M_{\odot}$, and $3.0 M_{\odot}$ were considered; these had initial hydrogen and helium content $X = 0.759$, $Y = 0.24$ (giving a mean molecular weight of $\mu \simeq 0.589$), and $Z_{\text{CNO}} = 0.00075$. (Unfortunately, for the mass loss rate used in the present work, the $0.8 M_{\odot}$ star became a white dwarf without ever experiencing helium burning, and thus never reached the AGB stage.) For the case of solar metallicity ($Z = 0.02$), stars of initial mass $1.2 M_{\odot}$ and $3.0 M_{\odot}$ were considered; these had initial $X = 0.71$, $Y = 0.27$ (giving $\mu \simeq 0.613$), and $Z_{\text{CNO}} = 0.015$. (Note that $Z_{\text{CNO}} = 0.75Z$ for both cases; this is obtained from use of the composition values of Ross and Aller 1976, which are quite similar to those of Grevesse 1984.) The choice of initial stellar helium abundance was obtained via Steigman (1985), by considering a primordial helium abundance of $Y_p = 0.24$ in the interstellar medium, which grows (due to nucleosynthesis in stars) according to $\Delta Y \approx 1.5\Delta Z$; these values are consistent with the values given by Steigman (1985) of $Y_p = 0.24 \pm 0.01$ and of $\Delta Y/\Delta Z = 1.7 \pm 0.9$, $\Delta Y/\Delta Z \leq 1.3 \pm 3.6$, and $\Delta Y/\Delta Z \approx 2 \pm 1$. It should be noted that first dredge-up (while on the RGB) changed the surface composition slightly, mainly increasing the helium abundance at the expense of hydrogen; thus during later stages, most importantly the AGB stage, the molecular weight of the envelope had become $\mu \simeq 0.598$ (due to $Y_{\text{env}} \simeq 0.26$) for the $Z = 0.001$ cases, $\mu \simeq 0.618$ (due to $Y_{\text{env}} \simeq 0.28$) for the $3 M_{\odot}$, $Z = 0.02$ case, and $\mu \simeq 0.624$ (due to $Y_{\text{env}} \simeq 0.29$) for the $1.2 M_{\odot}$, $Z = 0.02$ case.

The present work was carried out with an *extensively* modified version of Paczyński's stellar evolution program. Some details of the old (unmodified) version are given in Paczyński (1969, 1970*a, b*, 1974). However, the present version is comprised of about 85% modifications and additions to that program, so a somewhat detailed description is in order.

a) General Program Organization

The original program came in two separate parts. A Henyey-type code followed the evolution of the interior, with outer boundary conditions interpolated from a pre-computed grid (in $\log L$ and $\log T_e$) of static envelopes. The original static envelope computation program is described in Paczyński (1969); modifications for the present work are described in Sackmann and Boothroyd (1985), the most important changes being the inclusion of carbon ionizations and new opacities. (Some further modifications in the opacity handling are described below.) Inclusion of mass loss (see Section II*d* below) required a three-dimensional grid of pre-computed envelopes, to allow for interpolation in total stellar mass M_{tot} as well as in luminosity and temperature. This turned out to be excessively clumsy. At high luminosities L and low effective temperatures T_e , the necessary grid spacing in T_e became extremely fine (to 0.001 in $\log T_e$). This is because the fitting point between envelope and interior is taken at $10^5 K$, where *all* quantities change extremely steeply as a function of M_r , the mass coordinate. (If the fitting had been done further out in the star, at a lower temperature such as 2 or $3 \times 10^4 K$, the gradients with respect to M_r would have been smaller and the fitting less difficult, but it

would then have been necessary to include superadiabatic convection and the large effects of hydrogen and helium partial ionizations.) The need for larger numbers of envelopes negated the savings in computer time that otherwise would be associated with a reusable grid of envelopes. Thus, part way through the computations of the present work, the envelope computation program was combined with the Henyey interior evolution program, allowing automatic computation of the required static envelopes. Envelope composition changes in Y and Z (due to dredge-up) were also much easier to handle correctly by this method. The boundary point between the static envelope and the interior was generally taken to be at a temperature of about $10^5 K$, although higher-temperature boundary points, up to $3 \times 10^6 K$, were chosen (automatically) as necessary to keep the envelope mass from dropping below 0.5% of the star's total mass. (Note however that for a star on the AGB the greater part of the mass exterior to the hydrogen-burning shell lies below a temperature of $10^5 K$.)

The Henyey part of the program handles the interior, which is divided into as many as 400 mass layers. These mass layers are redistributed automatically as necessary to keep good track of the variations of temperature, density, radius, luminosity, and chemical composition throughout the interior. To minimize errors introduced by this redistribution, the rezoning algorithm makes use of quadratic interpolation, with restrictions to prevent the possibility of unphysical interpolation values. Also, during helium shell flashes on the AGB, the helium-burning shell is rezoned only once per flash cycle, at the interflash helium-burning minimum. It

should be noted that during the helium shell flash stage, about 150 layers were devoted to the helium-burning shell, and about 70 to the intershell zone above it.

The original Paczyński program made use of tables of pre-computed values to speed up computations, as described in Paczyński (1970*b*); our program retains this approach, but with modifications to improve accuracy. The equations of stellar structure may be written

$$\begin{aligned} \frac{\partial \ln P}{\partial M_r} &= -\frac{GM_r}{4\pi r^4 P}, & \frac{\partial L_r}{\partial M_r} &= \varepsilon_n - \varepsilon_\nu - Q_T \frac{\partial \ln T}{\partial t} + Q_R \frac{\partial \ln \rho}{\partial t}, \\ \frac{\partial \ln r}{\partial M_r} &= \frac{1}{4\pi r^3 \rho}, & \frac{\partial \ln T}{\partial M_r} &= \frac{\partial \ln P}{\partial M_r} \min(\nabla_{\text{rad}}, \nabla_{\text{ad}}), \end{aligned} \quad (1)$$

where symbols have their usual meaning: temperature T , density ρ , radius r , mass M_r interior to that radius, luminosity (integrated flux) L_r at that radius, pressure P , time t , nuclear energy generation rate ε_n and neutrino energy loss rate ε_ν (per unit mass), gravitational constant G , temperature gradient ∇ , and internal energy derivatives

$$Q_T \equiv \left(\frac{\partial U}{\partial \ln T} \right)_\rho, \quad Q_R \equiv - \left(\frac{\partial U}{\partial \ln \rho} \right)_T, \quad (2)$$

where U is the internal energy per unit mass. Note that the adiabatic and radiative temperature gradients are defined respectively as

$$\begin{aligned} \nabla_{\text{ad}} &\equiv \left(\frac{\partial \ln T}{\partial \ln P} \right)_{\text{ad}} = \frac{P}{\rho T C_P} \delta, \\ \nabla_{\text{rad}} &\equiv \left(\frac{\partial \ln T}{\partial \ln P} \right)_{\text{rad}} = \left(\frac{3\kappa}{16\pi acG} \frac{P}{T^4} \right) \frac{L_r}{M_r}, \end{aligned} \quad (3)$$

where κ is the opacity, c is of course the speed of light, $a \equiv 4\sigma/c$ (where σ is the Stefan-Boltzmann black-body radiation constant), and

$$\delta \equiv - \left(\frac{\partial \ln \rho}{\partial \ln T} \right)_P = \frac{T}{\rho} \left(\frac{\partial P}{\partial T} \right)_\rho / \left(\frac{\partial P}{\partial \rho} \right)_T, \quad (4)$$

$$C_P \equiv \left(\frac{\partial U}{\partial T} \right)_P = \left(\frac{\partial U}{\partial T} \right)_\rho + \frac{\delta}{\rho} \left(\frac{\partial P}{\partial T} \right)_\rho.$$

There are a total of nine different thermodynamic quantities tabulated for the use of the Henyey program, as described below.

The *ions* in the interior of a star form an ideal gas in general, but at high densities (where the electrons become degenerate) there are some corrections to the ideal gas behavior. Fortunately, these corrections can all be expressed in terms of a fractional correction $\overline{u_{\text{ex}}}$ to the ion internal energy:

$$\overline{u_{\text{ex}}} \simeq \mu_A \sum_i \frac{X_i}{A_i} u_{\text{ex}}(\Gamma_i), \quad (5)$$

where

$$\Gamma_i = \mathcal{Z}_i^{5/3} \Gamma_e, \quad \frac{1}{\mu_A} = \sum_i \frac{X_i}{A_i}, \quad \frac{1}{\mu_e} = \sum_i \frac{X_i \mathcal{Z}_i}{A_i}, \quad (6)$$

$$\Gamma_e \equiv \frac{e^2}{k_B T} \left(\frac{4\pi}{3} \sum_i \mathcal{Z}_i n_i \right)^{1/3} = \frac{2.275 \times 10^5}{T} \left(\frac{\rho}{\mu_e} \right)^{1/3},$$

and X_i is the mass fraction of atoms of type i , which have atomic number \mathcal{Z}_i and atomic mass A_i , with number density n_i . Note u_{ex} is a function only of the degeneracy parameter Γ (which is easily calculated from temperature, density, and composition); thus u_{ex} and its Γ -derivative were tabulated as a function of $\log \Gamma$. The value of this correction was obtained from Cohen and Murphy (1969) for slight degeneracy (small Γ), and from the review article of Ichimaru (1982) for strong

degeneracy (large Γ), the formula itself being attributed to Slattery, Doolan, and DeWitt (1980).

In the stellar interior as defined by our program, i.e., at temperatures above $10^5 K$, it is a fairly good approximation to assume everything is completely ionized. For hydrogen and helium, this approximation is very good, but the heavier elements (“metals”) can hold onto a few of their inner electrons until temperatures significantly above $10^5 K$ are reached. This generally has little effect, since only a small fraction of the electrons of elements that comprise a small fraction of the star’s substance are involved. However, during helium shell flashes on the AGB, the carbon-rich (and somewhat oxygen-rich) intershell zone could possibly expand and cool sufficiently for carbon to recombine with its innermost electron. This might then have a small but significant effect on the pressure, and the released ionization energy would give an extra “push” to the expansion. It was thus decided to include the effects of carbon and oxygen ionizations, *including* their dynamic effects (i.e., their effects on the internal energy). The prescription of Chapter 15 of Cox and Giuli (1968) was followed, using the non-degenerate version of the Saha ionization equation and including the effects of depression of the continuum, Debye-shielding, and limited ion size as recommended therein. For each ionization state of carbon and oxygen, a large number of excited states were included (probably more than necessary); data for the ionizations and excited states of carbon were obtained from Moore (1970), and of oxygen from Moore (1971). The mean number of free electrons contributed by each carbon atom and each oxygen atom was computed and tabulated as a function of $\log T$ and $\log(\rho/\mu_e)$, where $1/\mu_e$ is the

(total) number of electrons per unit mass (note that μ_e is a function of composition and of ionization states). The mean internal energy per carbon atom and per oxygen atom due to ionizations and excited states was also computed for use in those quantities (next paragraph) requiring the internal energy. It should be noted that for the relevant stellar temperatures and densities, namely $5 \lesssim \log T < 7$ and $-10 \lesssim [\log(\rho/\mu_e) - 3(\log T - 5)] \lesssim -4$, these carbon and oxygen ionization results are essentially independent of composition. This was tested by performing the computations for four different compositions: (1) hydrogen mass fraction $X = 0$, helium $Y = 0.5$, carbon $C = 0.4$, oxygen $O = 0.1$; (2) $X = 0$, $Y = 0.75$, $C = 0.2$, $O = 0.05$; (3) $X = 0$, $Y = 0.95$, $C = 0.04$, $O = 0.01$; and (4) $X = 0.7$, $Y = 0.25$, $C = 0.04$, $O = 0.01$. The results differed by less than 1%, usually *much* less.

The contribution P_e of free electrons to the pressure differs from that of an ideal gas at high densities, where electron degeneracy occurs. Thus $\log P_e$ was tabulated as a function of $\log T$ and $\log(\rho/\mu_e)$. The remaining four tabulated quantities were $\log Q_T$, $\log Q_R$, ∇_{ad} , and $\log(\nabla_{\text{rad}} \cdot M_r/L_r)$; as may be seen from their defining equations above, these involve such non-trivial quantities as the internal energy and the total pressure, as well as the stellar opacity κ . The tabulation was in terms of $\log T$, $\log \rho$, and *composition* for these last four quantities: for each temperature and density, the values were tabulated for five different compositions. Interpolation in hydrogen abundance X , helium abundance Y , and (effective) carbon abundance C' could thus be carried out in the Henyey program among these five mixes: (1) $X = X_0$, $Y = Y_0 = 1 - X_0 - Z$, $C' = C'_0$, $O' = O'_0$; (2) $X = \frac{1}{2}X_0$, $Y = 1 - \frac{1}{2}X_0 - Z$, $C' = C'_0$, $O' = O'_0$; (3) $X = 0$, $Y = 1 - Z$, $C' = C'_0$, $O' = O'_0$; (4) $X = 0$, $Y = 0$,

$C' = 0.2$, $O' = 0.8$; (5) $X = 0$, $Y = 0$, $C' = 0.8$, $O' = 0.2$. (The values X_0 , Y_0 , C'_0 , and O'_0 are those chosen for the initial stellar composition. The effective carbon abundance C' includes half of the nitrogen abundance, and the effective oxygen abundance O' includes the other half, since in some of the calculated quantities nitrogen is assumed intermediate in its effects between carbon and oxygen.)

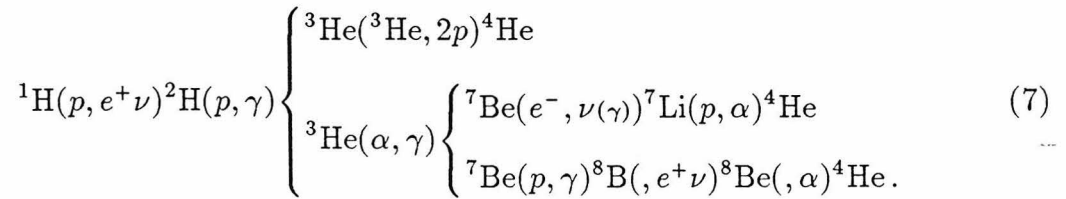
The latest Los Alamos stellar opacities were used. The opacity tables described in Sackmann and Boothroyd (1985) were included: these applied to mixtures having metallicity $Z \geq 0.03$, allowing for arbitrary amounts of added carbon in a mixture whose initial metallicity was $Z = 0.03$. In addition to these, six tables of low-metallicity Los Alamos opacities were kindly provided by Keady (1985): these comprised opacities for hydrogen-poor ($X = 0$) and hydrogen-rich ($X = 0.7$) mixtures, with metallicities $Z = 0.02$, $Z = 0.001$, and $Z = 0.0001$. (It should be noted that the Los Alamos tables include opacities due to a number of molecules at low temperatures.) The combined set of opacity tables did not contain any tables for “low metallicity with added carbon;” thus the opacity κ for any given composition was interpolated linearly in the hydrogen content X and the total metallicity Z , where the latter comprised everything except hydrogen and helium.

b) Nuclear Reaction Handling and Reaction Rates

The Henyey program keeps track of the abundances of hydrogen X (the isotope ^1H only), helium Y (^4He), carbon C (^{12}C), nitrogen N (^{14}N), and two isotopes of oxygen (^{16}O and ^{18}O). Hydrogen burns via the proton-proton chain and the CNO-cycle; the latter affects the abundances of carbon, nitrogen, and oxygen

as well as those of hydrogen and helium. The weak screening corrections to the hydrogen-burning reactions are included, as given in Salpeter (1954). Helium burning takes place via a number of individual reactions, producing carbon, oxygen, and neon (which last is kept track of only indirectly, as “one minus everything else”). After helium is exhausted, no further burning takes place in intermediate mass stars, so carbon burning via the C + C reaction is included only roughly, as a check. In helium- and carbon-burning reactions, both the weak screening corrections according to Salpeter (1954) and the strong screening corrections as given by Itoh *et al.* (1979, 1980) and Ichimaru and Utsumi (1983) are included. Every effort was made to include the most up-to-date reaction rates.

The proton-proton chain is straightforward at low temperatures, with a rate determined by the first reaction in the chain. At higher temperatures, a branch at ${}^3\text{He}$ can become significant, and at still higher temperatures, a branch at ${}^7\text{Be}$ can become significant: the full chain, including branches, is given by



The rate is still determined by the ${}^1\text{H}(p, e^+\nu){}^2\text{H}$ reaction, but the number of hydrogen atoms burned (and the energy deposited) *per* ${}^1\text{H}(p, e^+\nu){}^2\text{H}$ reaction will be affected. Let ϑ be the fraction following the high-temperature branch at ${}^3\text{He}$, and ξ the fraction of these following the higher-temperature branch at ${}^7\text{Be}$. Then, *for each* ${}^1\text{H}(p, e^+\nu){}^2\text{H}$ reaction, $2(1 + \vartheta)$ atoms of ${}^1\text{H}$ are burned to produce $\frac{1}{2}(1 + \vartheta)$

atoms of ${}^4\text{He}$, yielding $[1 + \vartheta(0.9572 - 0.4163\xi)](13.116 \text{ MeV})$ of deposited energy; and

$$\begin{aligned} \frac{\vartheta}{1 - \vartheta} &= \frac{2}{\sqrt{1 + (X/Y)^2\varphi} - 1}, & \varphi &\equiv 32 \frac{\langle {}^3\text{He}({}^3\text{He}, 2p){}^4\text{He} \rangle \langle {}^1\text{H}(p, e^+\nu){}^2\text{H} \rangle}{\langle {}^3\text{He}(\alpha, \gamma){}^7\text{Be} \rangle^2}, \\ \frac{\xi}{1 - \xi} &= \frac{X}{1 + X} \psi, & \psi &\equiv 2 \frac{\langle {}^7\text{Be}(p, \gamma){}^8\text{B} \rangle}{\langle {}^7\text{Be}(e^-, \nu(\gamma)){}^7\text{Li} \rangle}. \end{aligned} \quad (8)$$

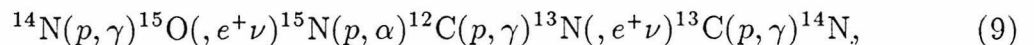
(These formulas follow from consideration of the rates of the equations at each branch, and of the rates that determine the relative abundances of the reactants; differing neutrino losses in different branches account for the difference in the energy deposited from a “ $1 + \vartheta$ ” dependence.) Thus the proton-proton chain was specified by tabulating the ${}^1\text{H}(p, e^+\nu){}^2\text{H}$ rate and the quantities φ and ψ , as a function of $\log T$. The ${}^3\text{He}({}^3\text{He}, 2p){}^4\text{He}$ rate was obtained from Fowler, Caughlan, and Zimmerman (1975: hereafter FCZ II); the ${}^1\text{H}(p, e^+\nu){}^2\text{H}$ and ${}^3\text{He}(\alpha, \gamma){}^7\text{Be}$ rates were obtained from Harris, Fowler, Caughlan, and Zimmerman (1983: hereafter HFCZ III); the ${}^7\text{Be}(p, \gamma){}^8\text{B}$ and ${}^7\text{Be}(e^-, \nu(\gamma)){}^7\text{Li}$ rates were obtained from Caughlan, Fowler, Harris, and Zimmermann (1985: hereafter CFHZ IV).

The ${}^{14}\text{N}(p, \gamma){}^{15}\text{O}$ reaction determines the basic rate of the CNO-cycle. The rate given in FCZ II is based largely on the results of Bailey and Hebbard (1963*a, b*), which was taken to imply that direct capture to two excited states dominated the reaction rate at astrophysical energies. A recent remeasurement of this rate has been made (Schröder *et al.* 1986, 1987). Preliminary analysis (Rolfs 1986) indicated that one of the two excited states in fact contributed very little to the rate: the sign of an interference term had been wrongly determined from the earlier work of Bailey and Hebbard (1963*a, b*). The preliminary results from Rolfs (1986) were

used to estimate $S(0)$, $S'(0)$, and $S''(0)$, resulting (via the formulas given in Fowler, Caughlan, and Zimmerman 1967: hereafter FCZ I) in a reaction rate *reduced* by a factor of about 2 from that given in FCZ II. It is this *revised* rate that was used for all the calculations of the present work, with one exception (as described below). Later, more complete analysis (Schröder *et al.* 1986) indicated that a resonance far below threshold, which had never been considered in previous analyses, contributed significantly. At the relevant astrophysical energies, the resulting total $^{14}\text{N}(p, \gamma)^{15}\text{O}$ rate was 3 to 4 times that indicated by the preliminary analysis, i.e., $1\frac{1}{2}$ to 2 times the rate given in FCZ II. (To test what effect this increased rate would have, a $3.0M_{\odot}$ star was evolved with this new, *higher* CNO-burning rate from the main sequence, through several helium shell flashes on the AGB. Differences from the case of low CNO-burning rate were small, though significant, in all stages of the star's lifetime, as described below in the section on results.) Final analysis (Schröder *et al.* 1987), recieved after this paper was essentially complete, indicates that the subthreshold resonance contributes less than previously thought, yielding a rate quite similar to that of FCZ II.

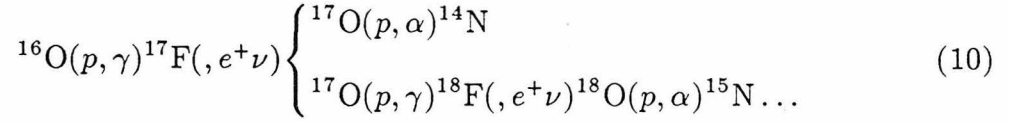
The CNO-cycle is somewhat more complicated than the proton-proton chain.

The main cycle follows



with the overall rate determined by the slowest reaction, the $^{14}\text{N}(p, \gamma)^{15}\text{O}$ reaction discussed in the preceeding paragraph. There is, however, a branch of about 0.1%

at ^{15}N : the $^{15}\text{N}(p, \gamma)^{16}\text{O}$ reaction. The ^{16}O in its turn slowly burns to ^{14}N , directly or indirectly (there being a branch at ^{17}O):



(The less direct branch re-enters the main CNO-cycle at ^{15}N , thus ending up indirectly as ^{14}N again.) Note that while the $^{17}\text{O}(p, \gamma)^{18}\text{F}$ rate is fairly well known, being somewhat faster than $^{16}\text{O}(p, \gamma)^{17}\text{F}$, the rate of the $^{17}\text{O}(p, \alpha)^{14}\text{N}$ branch is uncertain to within one or two orders of magnitude. Since the difference to the CNO-cycle is not major, the two branches were simply assumed to be equally probable.

In *equilibrium* CNO-burning, only small quantities of the CNO-isotopes are present aside from ^{14}N , and the equilibrium CNO-burning rate *and energy production rate* depend only on temperature, density, and the abundances of ^1H and ^{14}N . The small but non-zero CNO-equilibrium abundances of ^{12}C , ^{16}O , and ^{18}O are given by ratios of the relevant rates and masses: namely

$$\begin{aligned} \frac{^{12}\text{C}_{\text{eq}}}{^{14}\text{N}} &= \frac{6 \langle ^{14}\text{N}(p, \gamma)^{15}\text{O} \rangle}{7 \langle ^{12}\text{C}(p, \gamma)^{13}\text{N} \rangle}, \\ \frac{^{16}\text{O}_{\text{eq}}}{^{14}\text{N}} &= \frac{8 \langle ^{14}\text{N}(p, \gamma)^{15}\text{O} \rangle \langle ^{15}\text{N}(p, \gamma)^{16}\text{O} \rangle}{7 \langle ^{16}\text{O}(p, \gamma)^{17}\text{F} \rangle \langle ^{15}\text{N}(p, \alpha)^{12}\text{C} \rangle}, \\ \frac{^{18}\text{O}_{\text{eq}}}{^{16}\text{O}} &= \frac{9 \langle ^{17}\text{O}(p, \gamma)^{18}\text{F} \rangle \langle ^{16}\text{O}(p, \gamma)^{17}\text{F} \rangle}{8 \langle ^{17}\text{O}(p, \alpha)^{14}\text{N} \rangle \langle ^{18}\text{O}(p, \alpha)^{15}\text{N} \rangle} \approx \frac{9}{8} \cdot \frac{1}{2} \frac{\langle ^{16}\text{O}(p, \gamma)^{17}\text{F} \rangle}{\langle ^{18}\text{O}(p, \alpha)^{15}\text{N} \rangle}. \end{aligned} \quad (11)$$

(It should be noted that ^{18}O is only kept track of because of its importance in helium-burning; it has little importance in the CNO-cycle.)

In general, however, these isotopes are *not* in their CNO-equilibrium abundances. In the specified (Ross and Aller 1976) initial composition, both ^{12}C and ^{16}O

start out well above their equilibrium values; nor do their surface abundances ever approach the CNO-equilibrium values. ^{12}C burns quickly, reaching its equilibrium value before the main CNO-cycle has really begun (as does ^{18}O , though this is of little importance). ^{16}O burns slowly, reaching equilibrium on a timescale comparable to the CNO-burning timescale; in fact, under some circumstances the ^{16}O abundance may never reach its CNO-equilibrium value, hydrogen being exhausted first. If an isotope's abundance is greater (or smaller) than its equilibrium abundance, it will burn faster (or slower) than would be the case for equilibrium CNO-burning, by an amount proportional to the difference from equilibrium. Thus, in order to handle CNO-burning, the CNO-equilibrium factors of equation (11) were tabulated as a function of temperature, along with the burning rates of $^{14}\text{N}(p, \gamma)^{15}\text{O}$, $^{12}\text{C}(p, \gamma)^{13}\text{N}$, $^{16}\text{O}(p, \gamma)^{17}\text{F}$, and $^{18}\text{O}(p, \alpha)^{15}\text{N}$. For the latter three of these reactions, the *deviations* from the CNO-equilibrium behavior were computed in the program, their equilibrium rates being considered part of the basic CNO-cycle (whose rate is determined by the $^{14}\text{N}(p, \gamma)^{15}\text{O}$ reaction). In this way it was possible to take into account essentially the full behavior of the CNO-cycle, without requiring the full network and without needing small timesteps. The $^{15}\text{N}(p, \gamma)^{16}\text{O}$, $^{16}\text{O}(p, \gamma)^{17}\text{F}$, and $^{12}\text{C}(p, \gamma)^{13}\text{N}$ rates were taken from FCZ II. The $^{15}\text{N}(p, \alpha)^{12}\text{C}$ and $^{18}\text{O}(p, \alpha)^{15}\text{N}$ rates were taken from HFCZ III, with the “(0 - 1) term” in the latter taken to be zero as recommended by Harris (1986) and by Fowler (1986).

The helium-burning reactions are a good deal more straightforward than the hydrogen-burning reactions. The $^{14}\text{N}(\alpha, \gamma)^{18}\text{F}$ rate was taken from FCZ II, and the $^{18}\text{O}(\alpha, \gamma)^{22}\text{Ne}$ rate from HFCZ III. The $^4\text{He}(2\alpha, \gamma)^{12}\text{C}$ (“triple-alpha”) rate was

taken from a looseleaf revision insert for CFHZ IV; this revised rate was not much different from the CFHZ IV rate. The $^{12}\text{C}(\alpha, \gamma)^{16}\text{O}$ rate was taken from CFHZ IV; note that this rate is about a factor of three higher than that given in FCZ II. These rates were tabulated, including screening corrections, as a function of $\log \rho$ and $\log T$. Note that in some early runs the $^{16}\text{O}(\alpha, \gamma)^{20}\text{Ne}$ reaction (from CFHZ IV) was considered instead of the $^{18}\text{O}(\alpha, \gamma)^{22}\text{Ne}$ reaction, keeping track of ^{20}Ne instead of ^{18}O .

As well as actual nuclear reactions, one must consider the energy losses from several neutrino processes. Rates for the pair neutrino, photoneutrino, and plasma neutrino processes were taken from Munkata, Kohyama, and Itoh (1985). Some early runs used the rates of Baudet, Petrosian, and Salpeter (1967), modified by factors (of order unity) as recommended by Dicus (1972); as one might expect, these modified rates were generally in agreement with the rates of Munkata, Kohyama, and Itoh (1985), though differences of up to 15% did occur in one portion of the temperature-density plane. Rates for neutrino-pair bremsstrahlung were taken from Itoh and Kohyama (1983), for an assumed composition of equal amounts (by weight) of carbon and oxygen: the rates for carbon and for oxygen are fairly similar, so variations in composition have little effect on the neutrino-pair bremsstrahlung rate.

c) Convection and Semiconvection Handling

In the static envelope computation routine, convection is handled by the mixing length theory as described in Paczyński (1969). This algorithm allows for superadiabatic convection, where the actual temperature gradient ∇ is intermediate

between the adiabatic gradient ∇_{ad} and the radiative gradient ∇_{rad} (rather than being essentially equal to ∇_{ad} , as is the case in the interior of the star). The choice of mixing length used in the computations can make quite a large difference to the envelope structure, and thus to the structure of the star as a whole. In general, a mixing length to pressure scale height ratio of $\alpha \equiv l/H_p = 1.0$ was used in the present work. The appropriate value for α is rather uncertain, values up to $\alpha = 2.0$ or more being not unreasonable. After a major portion of the work had been completed, several circumstances were noted indicating that this latter value was more appropriate: a value of $\alpha = 1.0$ leads to excessively cool stellar effective temperatures on the RGB and AGB, and a value of as much as $\alpha \approx 2$ is necessary if one desires to match the observed solar effective temperature with a standard solar model, using the code of the present work. Certain runs comprising a number of flashes on the AGB were repeated with increased values of α . It should be noted that even increasing α by a factor of 2 caused only a 1% increase in the star's luminosity; but the value of α had of course a large effect on the radius, effective temperature, and depth of envelope convection in the star, with concomittant effects on Reimers (1975) mass loss and on dredge-up as described in Section III below. It should be noted that the definition of the mixing length parameter α is not universal to all computer codes: while most codes yield results similar to that of the present work, the code designed and used by Iben (and recently used by Becker and by Hollowell) appears to contain a factor of about two relative to other codes. An envelope model supplied by Becker (1986) with $\alpha_{\text{Iben}} = 2.5$ could only be replicated using $\alpha = 4.37$ with the code of the present work; while we used an

identical composition, our opacities were similar to those used by Becker (1986) but not quite identical, so the difference of a factor of 1.75 is not exact, but this is in line with other comparisons between the Iben code and other codes. Thus quoted values of α_{Iben} used in the Iben code correspond to values of α perhaps twice as large used in other codes.

It was brought to our attention, after the present work was in progress, that the mixing length theory of convection can be significantly improved if one adopts a scheme whereby α varies over the depth of the convective envelope (Deupree 1979; Deupree and Varner 1980; Chan, Wolff, and Sofia 1981). *No such modification was included* in the present work, however, for the sake of consistency within the present work and with other investigators, and to avoid the necessity for program modifications which would increase the computer time required for envelope computations. The variable- α schemes have most of their effect near the star's surface, which is a region of relatively little interest to the present work. For a variable- α scheme with a mixing length scale parameter α_1 , the conditions at the base of the envelope could presumably be matched by the usual fixed- α mixing length algorithm with some particular value of α , though the surface conditions (particularly the radius and effective temperature) might not agree. Thus, for the purposes of the present work, a variable- α scheme would presumably not be much of an improvement.

In the interior of the star, convection is not superadiabatic: in a convective region, the actual temperature gradient ∇ is essentially equal to the adiabatic temperature gradient ∇_{ad} . This simplification is more than outweighed, however, by

the complicating effects of a non-uniform composition. One must allow for the possibility of semiconvection, and perhaps of convective overshoot. In addition, Wood (1981*a*) has pointed out that while there is *no* energy cost (only a change in entropy) associated with mixing together regions of different composition, there *is* an energy cost associated with dredging higher-mass atoms up into a region of lower-mass atoms, due to the work that must be done against gravity; few if any stellar evolution codes treat these matters correctly. While the algorithm designed by the authors for the present work avoids spurious energy costs associated with the mixing itself, the work done against gravity was not included: the method necessary to include this latter in the program looked to be excessively complicated for the scope of this project.

The convection algorithm of the present work is designed to handle the possibility of convection and/or semiconvection in any region of the star (except the carbon-oxygen degenerate core). The extent of convection and semiconvection is computed once per time step (after the Henyey iterations have converged to the structure for that point in time); this is somewhat less accurate than computing convection for each Henyey iteration, as is done in some other codes, but it is much more economical of computer time.

A convective region may grow by overshoot into the adjacent radiative layers, the radiative layers becoming convective due to the change in composition when they are mixed with the convective region. Due to the discrete time steps necessarily used by a stellar evolution code, the convective region may grow by several mass

layers from one time step to the next. In general, C/O-rich (i.e., carbon- and/or oxygen-rich) and hydrogen-rich compositions are more conducive to convection than helium-rich compositions, due to the (generally) higher opacities of carbon, oxygen, and hydrogen as compared to helium. This makes possible a fairly straightforward “single-sweep” algorithm, since one does not need to worry about a convective region overshooting into more hydrogen-rich or more C/O-rich radiative regions (although up to one mass layer’s worth of overshoot in this “improbable” direction was allowed, to maintain complete generality of the convection algorithm). Starting at the bottom of that stellar region where hydrogen has been exhausted but helium has not, and moving outward, each mass layer is considered in turn until a formally convective layer is found (i.e., a layer where $\nabla_{\text{rad}} > \nabla_{\text{ad}}$). If mixing this layer with the next layer outward would cause the latter to become (or remain) convective, this mixing is performed. Layer after layer may thus be added to this region, one at a time, until a layer is found which would not be convective when mixed; this layer is then the first radiative layer outside the convective region which has just been found. Since the “carbon plus oxygen” abundance decreases as one looks at layers further out in the star, this method correctly handles the possibility of a C/O-rich convective region overshooting into a helium-rich radiative region. Note that some investigators (see, e.g., Bertelli, Bressan, and Chiosi 1985) recommend continuing this overshoot for some distance *beyond* the point where the layers become non-convective (i.e., have $\nabla_{\text{rad}} < \nabla_{\text{ad}}$): this was *not* done in the present work, for the sake of simplicity and because it would introduce another uncertain parameter to determine *how much* farther overshoot should continue.

This is by no means the whole story; several other possibilities are considered, in order to take semiconvection into account. A semiconvective region is a region with non-uniform composition which is everywhere “just on the verge of being convective” ($\nabla_{\text{rad}} = \nabla_{\text{ad}}$ everywhere): if changes in stellar conditions would cause part of this region to become convective, it would mix in adjacent material until it became “just on the verge” again, with a slightly modified chemical profile. Suppose that the algorithm has found a formally convective layer, but mixing this layer with the next layer outward would cause this first layer to become *non-convective*. In this case, just enough mixing is performed to cause the first layer to have $\nabla_{\text{rad}} = \nabla_{\text{ad}}$ (a semiconvective layer), and the next layer is considered. Due to the finite size of the time step, several layers may be mixed together (as if they were the lower part of a convective region) before the bottommost of them becomes non-convective; in this case, it is as if one swept a small, fictitious convective zone upward through the semiconvective region (layers at the bottom becoming semiconvective in turn as material is mixed in at the top) in order to adjust the composition profile back into agreement with the semiconvective condition (i.e., a profile yielding $\nabla_{\text{rad}} = \nabla_{\text{ad}}$ everywhere in the region). It is also possible for a semiconvective region to adjoin a convective region; in this case, as the program mixes layers into the convective region, a point in the *middle* of the mixed region may become non-convective; this point is the outer boundary of the convective region, and the program continues on with the upper part of the “convective” region, which now sweeps through and readjusts the semiconvective region as described above. (Note that this convection

and semiconvection algorithm is quite similar to one developed independently by Castellani *et al.* [1985b] for use in core helium burning.)

The above description of convection and semiconvection in the helium zone applies also to the outer, hydrogen-containing region of the star, except that in the latter region the “sweep” moves *inward* (since the abundance of hydrogen decreases as one goes *inward* in the star). Note that it is possible for a hydrogen-rich convective region to overshoot inward below the hydrogen-helium (H-He) discontinuity (e.g., in “third dredge-up”). A special routine (seldom if ever needed) handles the possibility of “collisions” where the sweeps meet at the H-He discontinuity (e.g., if dredge-up reached down into a helium semiconvective region). Due to the fact that convection is computed only once per model, it is sometimes necessary to limit the amount by which convective boundaries are allowed to change from one model to the next, in order to avoid spurious effects. The program applies such limits as necessary; an attempt to exceed these limits causes the program to reduce the size of the time step between successive models.

d) Mass Loss

The effect of a Reimers (1975) type wind mass loss

$$\begin{aligned} \dot{M} &= -\eta(4 \times 10^{-13}) \frac{L}{g \cdot R} = -\eta(4 \times 10^{-13}) \frac{L \cdot R}{M} \\ &= -\eta(1.34 \times 10^{-5}) \frac{L^{3/2}}{M \cdot T_e^2} \end{aligned} \tag{12}$$

(M , L , g , and R in solar units, \dot{M} in M_{\odot}/year , and T_e in Kelvins: Kudritzki and Reimers 1978) was included whenever a star’s effective temperature T_e fell

below about 5000 K , i.e., when $\log T_e < 3.7$. As recommended in Kudritzki and Reimers (1978), the value of the normalization factor η was chosen to be $\eta = 0.4$ except for the $3.0 M_\odot$ case, where $\eta = 1.4$ was chosen. It should be noted that the Reimers mass loss rate is close to being inversely proportional to the mixing length parameter α , as described in Section III below, through the effect of α on the radius and effective temperature. It turned out (as discussed in Section IIIa below) that the present work probably overestimates the mass loss rate.

III. RESULTS AND DISCUSSION

a) Pre-Asymptotic Giant Branch Evolution

Stars of several initial masses M_i of both low metallicity ($Z = 0.001$, initial $Y = 0.24$) and solar metallicity ($Z = 0.02$, initial $Y = 0.27$), all with a mixing length parameter $\alpha = 1.0$, were considered in this work. Their evolutionary tracks in the H-R diagram are presented in Figure 1a ($Z = 0.001$, $M_i = 3.0 M_\odot$, $1.0 M_\odot$, and $0.8 M_\odot$), Figure 1b ($Z = 0.001$, $M_i = 2.0 M_\odot$, $1.2 M_\odot$, and $0.8 M_\odot$ again to allow comparisons of giant branch positions: trying to put all low-metallicity stars in the same figure results in confusing overlap of tracks), and Figure 2 ($Z = 0.02$, $M_i = 3.0 M_\odot$ and $1.2 M_\odot$). The starting models for all of the stellar evolutionary runs were pre-main sequence uniform-composition models, assumed to be in hydrostatic equilibrium with no gravitational energy generation (points P of Figures 1 and 2); for all but the lowest mass stars, a fast and perhaps not very meaningful phase occurred in which the $^{12}\text{C}(p, \gamma)^{13}\text{N}(e^+\nu)^{13}\text{C}(p, \gamma)^{14}\text{N}$ reaction brought the core carbon abundance down to its CNO-equilibrium value. For a real star, this phase

would presumably start while the star was still contracting, so the positions of the points P would be different. However, the endpoints of this phase, the zero age main sequence (ZAMS) points (points A of Figures 1 and 2), are essentially independent of the details of the pre-main sequence evolution. Note also that in the $Z = 0.001$ stars of $M_i \leq 1.0 M_\odot$, the proton-proton chain reaction is fast enough that the non-equilibrium $^{12}\text{C}(p, \gamma)^{13}\text{N}$ reaction has negligible effect, and the pre-main sequence stage does not appear.

A number of significant evolutionary points are marked in Figures 1 and 2. Points P (starting point) and A (beginning of the main sequence) were discussed above. For the higher mass stars, whose main-sequence hydrogen burning takes place via the CNO-cycle in a convective core, point B marks the red edge (lowest stellar effective temperature T_e) of the main sequence, where hydrogen is not far from exhaustion in the core; lower mass stars, whose hydrogen burning takes place via the proton-proton chain in a radiative core, have no really equivalent point. Point C marks the core hydrogen exhaustion, when the hydrogen-burning shell surrounding the helium core takes over; as the core contracts, the star's surface expands and cools until the base of the red giant branch (RGB) is reached (marked by point D). As the helium core inside the hydrogen-burning shell grows more massive, the star climbs the RGB; at this point "first dredge-up" occurs, as the star's convective envelope reaches down into the outer parts of regions that core hydrogen burning had processed. A core mass–luminosity relation exists for the upper RGB, as discussed in Paper I; and Reimers (1975) type wind mass loss occurs, causing significant amounts of mass loss as discussed below. The tip of the RGB is

marked by point E: at this point, the start of core helium burning (by the triple-alpha reaction) causes the star to quickly move back down the RGB. (In higher mass stars, this core helium burning starts quietly; however in stars of $M_i \lesssim 2.5 M_\odot$, the helium ignition takes place under degenerate conditions, causing a violent helium core flash. The core flash is discussed in more detail below.) After moving back down the RGB, the star (now on the horizontal branch) burns helium in a convective core, while hydrogen still burns in a surrounding shell. The star moves toward hotter effective temperatures: the blue edge (maximum T_e) of this loop is marked as point F. As core helium approaches exhaustion, the star moves back to cooler T_e until, at point G, core helium is exhausted. The hydrogen-burning shell goes dead, and a helium-burning shell begins to burn its way outward (in mass) through the star toward the hydrogen-helium discontinuity; as this happens, the star moves up what is sometimes called the early asymptotic giant branch (E-AGB) or pre-flash AGB. In *high mass* stars a “second dredge-up” phase occurs here, envelope convection reaching down below the H-He discontinuity; but none of the stars considered in the present work are massive enough for this to occur. When the helium-burning shell surrounding the degenerate carbon-oxygen core is very close (in terms of mass) to the H-He discontinuity, the hydrogen-burning shell re-ignites; shortly thereafter, the first helium shell flash (thermal pulse) occurs, marked by point H. We will refer to the following stage simply as the asymptotic giant branch (AGB); it is also referred to as the TP-AGB (thermally pulsing AGB) by some authors. The flashes continue regularly until mass loss and growth of the core cause the envelope mass to become very small, at which point the star leaves the AGB: it moves rapidly

to hotter effective temperatures to become the nucleus of a planetary nebula (the nebula comprises part of the star's lost envelope), and eventually cools down to become a white dwarf. It may be seen from Figures 1 and 2 that our RGB and AGB stellar models have rather cool effective temperatures (as low as $T_e \sim 2000 K$ for the case of solar metallicity), due partly to the large low-temperature molecular opacities; this implies that our choice of mixing length parameter $\alpha = 1.0$ was too small (note that $T_e \propto \alpha^{1/2}$, as discussed in Section IIIb below).

The times t (in units of 10^9 years) at which each of the stars reaches the points A through H are given in Table 1. The times are measured from the first model (point P) rather than from the ZAMS (point A), but as may be seen from the small values of $t(A)$ in Table 1, this makes no real difference. The timescales for all subsequent stages of evolution contain no surprises. High mass stars evolve faster than low mass stars; for stars of the same initial mass, stars with low metallicity evolve faster than stars with solar metallicity. The main sequence (core hydrogen burning) lifetime $\Delta t(A \rightarrow C)$ comprises the major portion of the total pre-flash lifetime; the horizontal branch (core helium burning) lifetime $\Delta t(E \rightarrow G)$ comprises a significant fraction of the total pre-flash lifetime only for the higher masses, $M_i \gtrsim 2 M_\odot$. Note that the time spent going back down the RGB is very short, so the horizontal branch starts at a time essentially equal to $t(E)$, the age at the tip of the RGB.

The effects of the Reimers (1975) wind mass loss rate of Equation (12) are presented in Table 2. As recommended in Kudritzki and Reimers (1978), a normalization value of $\eta = 1.4$ was used for the (relatively) high-mass, high-luminosity,

solar metallicity cases with $M_i = 3.0 M_\odot$ (and also for the $Z = 0.001, 3.0 M_\odot$ case), while a value of $\eta = 0.4$ was used for the low-mass, low-metallicity stars (and also for the $Z = 0.02, 1.2 M_\odot$ case): thus the stars of initial mass $3.0 M_\odot$ all had $\eta = 1.4$, while all stars with $M_i \leq 2.0 M_\odot$ had $\eta = 0.4$. The constraint that $\eta \approx 0.4$ for low mass stars is obtained from work such as that of Renzini (1977, 1981), by comparing the morphology of globular clusters with that predicted by theoretical evolutionary calculations: the requirement that a $0.85 M_\odot$ star of low metallicity lose about $0.2 M_\odot$ of its mass while on the RGB is used to obtain the required value of η . Unfortunately, the Reimers (1975) mass loss rate of Equation (12) is also proportional to the star's radius, which is affected by opacities and by the choice of the mixing length parameter α . The added molecular opacities at low temperatures cause a larger stellar radius to be obtained on the RGB; and as discussed in Section IIIb below, the radius (and thus the mass loss rate) is essentially inversely proportional to α . All other things being equal, stellar models of the present work have larger radii than those of Renzini (1977, 1981); thus it turns out that $\eta = 0.4$ *overestimates* the mass loss rate for our low mass stars. Thus our $Z = 0.001, M_i = 0.8 M_\odot$ star loses $0.33 M_\odot$ and never reaches the tip of the RGB where the helium core flash would take place. From the fact that our $Z = 0.001, M_i = 1.0 M_\odot$ and $1.2 M_\odot$ respectively lose $0.24 M_\odot$ and $0.17 M_\odot$ on the RGB, one can see that requiring a $0.85 M_\odot$ star to lose only $0.2 M_\odot$ would require a mass loss rate between 1.5 and 2 times smaller than the value actually used, whether from a smaller η or a larger α . Thus the mass loss results of the present work are probably overestimates, by a factor of 1.5 to 2.

As may be seen from Table 2, the smaller the star's initial mass, the greater is the amount of mass loss, even in absolute terms; major mass loss $\Delta M(D \rightarrow E)$ takes place on the RGB only for $M_i \lesssim 1.2 M_\odot$, higher mass stars suffering relatively little pre-flash mass loss. This is as expected: not only is the mass loss rate inversely proportional to the total stellar mass, but lower mass stars spend longer on the RGB, and lie at cooler effective temperatures (i.e., larger radii) as may be seen from Figures 1 and 2. The effect of increasing Z is to increase lifetimes and to reduce effective temperatures, so it is not surprising that the $Z = 0.02$, $M_i = 1.2 M_\odot$ star loses twice as much mass as the $Z = 0.001$, $M_i = 1.2 M_\odot$ star. This variation with Z is not inconsistent with observations, as interpreted by Renzini (1981). For $M_i \lesssim 2 M_\odot$, most of the pre-flash mass loss takes place on the RGB; for stars of higher mass, which do not experience a helium core flash, the RGB tip lies at lower luminosity than for lower mass stars, but flashes begin at a higher luminosity on the AGB (see Figures 1 and 2). Thus the pre-flash mass loss of higher mass stars takes place mostly on the pre-flash AGB, but is in any case not very large in amount even with a large value of η .

We were pleased (and somewhat surprised) to find that the stellar evolutionary code of the present work was capable of handling the extremely violent helium core flash of low mass stars. While a non-hydrodynamic, one-dimensional code such as ours can at best produce only an approximation to the true core flash behavior (see, e.g., Deupree 1984), this is better than nothing. Table 3 presents our core flash results. They are fairly typical of core flash results obtained using non-hydrodynamic codes (see, e.g., Rood 1972; Renzini 1977; Despain 1981), with

reasonable RGB tip luminosities of $\log(L/L_{\odot}) \sim 3.3$ ($M_{\text{bol}} \sim -3.5$) and core masses of $M_c \equiv M_{\text{H}} \sim 0.45 M_{\odot}$, and resulting in nucleosynthesis of relatively little carbon ($C_c \sim 0.03$). This is in spite of the fact that, unlike Despain (1981), we find core flash ignition to take place centrally (rather than off-center): the increased triple-alpha rate due to screening corrections at high density offsets the effect of the slight temperature inversion caused in the core by neutrino losses. Note that the timescale is only $\sim 10^5$ years from peak helium-burning luminosity $L_{\text{He}}^{\text{max}}$ of the core flash (which takes place at the tip of the RGB) to the subsequent helium-burning minimum $L_{\text{He}}^{\text{min}}$ (which takes place after the star has moved back down the RGB, just prior to the beginning of the horizontal branch stage of core helium burning); thus the time for the beginning of the horizontal branch stage is essentially the same as the time $t(\text{E})$ at the tip of the RGB.

During the later stages of core helium burning (on the horizontal branch), the convective core is surrounded by a semiconvective region that mixes helium down into the core from regions outside the formal boundary of convection. As discussed in Renzini (1977), when the core helium abundance grows small ($Y_c \lesssim 0.1$), a convective instability occurs, causing large amounts of helium to be suddenly mixed into the core, and generally causing numerical non-convergence in stellar evolution codes; the standard “fix” for this is to suppress the possibility of growth of the helium convective core (and detach it from surrounding semiconvection) when $Y_c \lesssim 0.1$. Recently, Castellani *et al.* (1985) used an improved semiconvection algorithm (plus a reduction in timestep size) to follow the convective instability in detail. They found that a series of three “breathing pulses” occurred before the end

of core helium burning, extending the horizontal branch lifetime by roughly 40% and resulting in cores containing more oxygen and less carbon than would otherwise be the case. In these pulses, the rapid ingestion of helium into the core caused a rapid blueward loop in the H-R diagram, followed by a slower redward motion. Lattanzio (1986) confirms their results, reports similar breathing pulses with a somewhat different semiconvective algorithm. The present work also confirms the existence of these breathing pulses; however, they involve large and very rapid changes in semiconvective (and convective) boundaries, which can cause inaccuracies and convergence problems in the program of the present work, so our breathing pulse results cannot be considered particularly accurate, even in the cases when they did not have to be suppressed to avoid convergence problems. Table 4 presents the number n_{bp} of breathing pulses obtained for each star, and the final core carbon and oxygen abundances. The very small final carbon abundance $C_c \lesssim 0.2$ is due mainly to our use of the increased $^{12}\text{C}(\alpha, \gamma)^{16}\text{O}$ reaction rate from CFHZ IV, although the values of C_c are indeed smaller by roughly 30% in cases when breathing pulses did not have to be suppressed. Note that for low mass stars these breathing pulses have a relatively small effect on the size of the core mass M_H (which grows larger due to the increased horizontal branch lifetime), although there can be a large effect for high mass stars as discussed in the Introduction (Castellani *et al.* 1985, Lattanzio 1986).

As discussed in Section II*b*, after the present work was largely completed it was found that the preliminary revised CNO-rate (Rolfs 1986) was too low by a factor of 3 to 4 compared to the analysis of Schröder *et al.* (1986), and a run with

$Z = 0.02$, $M_i = 3.0 M_\odot$ was made using this new, high CNO-rate for purposes of comparison with the earlier run having these same values of Z and M_i but using the low CNO-rate. As may be seen from the figures and from Tables 1, 2, 4, and 5, this change makes surprisingly little difference to any stellar quantity; the difference is generally a few percent or less, whether in the pre-flash evolution discussed up to now or in the helium shell flash regime discussed below. Note that the *correct* CNO-rate appears to lie *between* the two rates used in this work (Schröder *et al.* 1987).

b) Helium Shell Flashes on the Asymptotic Giant Branch

For each of the stars which reached the AGB, a number of helium shell flashes were computed; as discussed in Section iii) below, for the lowest mass stars it was generally the wind mass loss that caused the runs to be terminated as they left the AGB (having lost their entire envelopes). For the case of $Z = 0.02$, the star of $M_i = 1.2 M_\odot$ went through 9 flashes, while 22 flashes were computed for the star of $M_i = 3.0 M_\odot$, and 17 flashes for the comparison run with $M_i = 3.0 M_\odot$ using the high CNO-rate. (As may be seen from the diagrams discussed below, the effect of the higher CNO-rate was very small here, just as in the previous evolution.) For the case $Z = 0.001$, the star of $M_i = 1.0 M_\odot$ went through 5 flashes. For the star of $Z = 0.001$ and $M_i = 1.2 M_\odot$, 7 flashes were computed with $\alpha = 1.0$, then the 6th through 8th recomputed with $\alpha = 1.5$, the 6th through 10th with $\alpha = 2.0$, and the 6th and 7th with $\alpha = 3.0$ (as discussed in Section IIIc below). For the star of $Z = 0.001$ and $M_i = 2.0 M_\odot$, 11 flashes were computed with $\alpha = 1.0$, and the 10th

through 17th recomputed with $\alpha = 1.5$ (as discussed in Section IIIc). For the star of $Z = 0.001$ and $M_i = 3.0 M_\odot$, 7 flashes were computed.

As discussed in detail in Papers I and II, a helium shell flash has a fairly dramatic effect on the surface luminosity (although the changes are still on timescales of decades to centuries at their fastest, and so would be *extremely* difficult to follow observationally). The flash causes a very fast dip in luminosity and radius, followed by a somewhat slower increase to as much as a factor of 2 above the pre-flash luminosity (this is of relevance to possible envelope ejection, as discussed in Paper I); this rise is followed by a slow dip to as much as a factor of 2 below the pre-flash luminosity, lasting for a significant fraction of the interflash period, and having important effects for interpretation of observed luminosities (as discussed in Papers I and II and in Section IIIc below).

i) The First Flash

The helium shell flashes (also called thermal pulses) on the AGB start as small oscillations in the helium-burning luminosity L_{He} , growing *very* rapidly in strength as the helium-burning shell approaches the re-ignited hydrogen-burning shell. The first significant helium shell flash is generally defined either as the first in which $L_{\text{He}}^{\text{max}} > L$ (where as usual L is the star's surface luminosity), or else as the first in which flash-driven intershell convection appears (reaching upward from the helium-burning shell into the intershell region); for all the stars of the present work, these two definitions are equivalent. For each stellar run, the star's position in the H-R diagram at the time of the first flash is marked as the point H in Figures 1 and 2.

Table 5 presents the stellar parameters at the time of the first flash. Note that “first dredge-up” (on the RGB) has changed the envelope abundances: Y_{env} has been increased from its initial main sequence value by between 0.01 (for stars of $M_i \sim 3M_\odot$) and 0.02 (for stars of $M_i \lesssim 2M_\odot$), while the envelope carbon abundance has been reduced to $\sim 2/3$ of its initial value of $C_{\text{env}} \simeq 0.22Z$; oxygen retains its initial abundance. Figures 1 and 2 illustrate that stars of initial masses $M_i \lesssim 1.2M_\odot$ encounter their first flash at a lower luminosity than the tip of their RGB, causing an overlap in the H-R diagram between their RGB and their AGB. However, in all cases of the present work, the AGB extends to higher luminosities than the RGB even with the over-estimated mass loss rate used here; they would extend to even higher luminosities if a lower mass loss rate were used, as discussed in Section iii) below. Thus only in the very lowest mass stars, such as the $M_i = 0.85 M_\odot$ case discussed by Renzini (1981), does the tip of the RGB come very close to coinciding with the tip of the AGB, although the overlap can still be troublesome to observers.

An important point to note from Table 5 is that the first flash takes place at significantly *lower* stellar luminosity $L \equiv L_{\text{TP}}$ (by as much as $\Delta \log L \sim 0.6$, i.e., $\Delta M_{\text{bol}} \sim 1.5$) than that indicated by the L_{TP} -relation given by Iben and Renzini (1983) for stars of $Z = 0.02$, $Y = 0.28$. (Their relation was apparently obtained by interpolation between high-mass and very low-mass stars; unfortunately, it turns out that L_{TP} is not smoothly varying in this regime). Flashes start at lower luminosity L_{TP} in our $Z = 0.02$ stars than in our $Z = 0.001$ stars, but even in the latter the L_{TP} value is significantly below the Iben and Renzini (1983) L_{TP} -relation. Our results agree very well, however, with those presented by Lattanzio

(1987) in his Figure 1, both for high- Z and low- Z cases; note that Lattanzio (1987) also finds a fairly strong Y -dependence, increased Y causing increased L_{TP} . We concur with Lattanzio's (1987) findings that for stars of relatively low initial mass (i.e., $M_i \lesssim 3 M_\odot$), L_{TP} varies much less steeply as a function of M_i for high- Z stars than for low- Z stars: L_{TP} differs by only $\Delta \log L_{\text{TP}} \simeq 0.2$ between the $M_i = 1.2 M_\odot$ and the $M_i = 3.0 M_\odot$ cases for $Z = 0.02$, as compared to $\Delta \log L_{\text{TP}} \simeq 0.8$ between the same values of M_i for $Z = 0.001$.

This reduction in the luminosity L_{TP} at which flashes begin in low mass stars is of major importance to the theory of carbon star production. A lower L_{TP} value allows for a larger number of flashes to occur in a star before it reaches the luminosity where carbon stars are found observationally. This allows the flashes to build up to a strength that can be expected to cause dredge-up, rather than requiring dredge-up practically on the first flash as would otherwise be necessary (as indicated by the analyses of, e.g., Richer 1981; Scalo and Miller 1981; Miller and Scalo 1982). Incidentally, it should be noted that for the first few flashes the star's luminosity lies significantly *below* the core mass–luminosity ($M_c - L$) relation (discovered by Paczyński [1970a]; discussed in detail in Paper II).

ii) The Growth of the Flash Strength

The flash strength, i.e., the peak flash helium-burning luminosity $L_{\text{He}}^{\text{max}}$, grows rapidly at first from one flash to the next. Normally, it is $\log L_{\text{He}}^{\text{max}}$ which is plotted or tabulated (see, e.g., Paczyński 1974; Sackmann 1980a; Iben 1983). One then finds that the growth of $\log L_{\text{He}}^{\text{max}}$ flattens out after of the order of ten flashes. This

flattening, however, is largely an artifact of the use of a logarithmic scale: it means only that the flash strength $L_{\text{He}}^{\text{max}}$ grows slower than exponentially. Figure 3 is a *linear* plot of $L_{\text{He}}^{\text{max}}$ as a function of core mass for each of the stars of the present work; after the first few flashes, $L_{\text{He}}^{\text{max}}$ grows essentially linearly with core mass (or with flash number), and in the absence of dredge-up there is little or no evidence of any flattening out of this growth. (A plot of these same flashes on a logarithmic scale would show *strong* flattening.)

Another important point to note from Figure 3 is that the flash strength grows much more quickly for low- Z stars than for high- Z stars. After 10 flashes, the $Z = 0.001$ stars of $M_i = 1.2 M_{\odot}$ and $2.0 M_{\odot}$ had flash strengths of $L_{\text{He}}^{\text{max}} \sim 7 \times 10^7 L_{\odot}$ (and the growth rate of the $M_i = 1.0 M_{\odot}$ star was similar), while the $Z = 0.02$ stars of $M_i = 3.0 M_{\odot}$ and $M_i = 1.2 M_{\odot}$ had flash strengths respectively of only $L_{\text{He}}^{\text{max}} \sim 1 \times 10^7 L_{\odot}$ and $L_{\text{He}}^{\text{max}} \sim 2 \times 10^6 L_{\odot}$ after the same number of flashes. The flash strength of the $Z = 0.001$, $M_i = 3.0 M_{\odot}$ star (which had a much higher core mass than the other stars of the present work) grew rather more slowly in terms of flash number than the other low- Z stars, but since the core mass increased relatively little between successive flashes the growth of $L_{\text{He}}^{\text{max}}$ as a function of core mass M_{H} looks to have much the same slope as for the other low- Z stars (see Fig. 3). In comparison, Hollowell (1987) found $L_{\text{He}}^{\text{max}} \simeq 1.5 \times 10^8 L_{\odot}$ for the 16th flash of a $Z = 0.001$, $M_{\text{tot}} = 0.7 M_{\odot}$ star (computed without mass loss), while Lattanzio (1987) found $L_{\text{He}}^{\text{max}} \sim 10^7 L_{\odot}$ for flashes in stars of $Z = 0.003$ and 0.006 ($M_{\text{tot}} = 1.5 M_{\odot}$, no mass loss). As discussed in Section IIIc, a stronger flash strength is more favorable to dredge-up, which is thus easier to obtain in low- Z stars. Also, the reduction in

the growth rate of $L_{\text{He}}^{\text{max}}$ after dredge-up increases the star's metallicity is thus not surprising (see Section IIIc).

It is important to note that Figure 3 shows *no* signs of the existence of any universal curve giving $L_{\text{He}}^{\text{max}}$ as a function of core mass $M_c \equiv M_H$ (even for fixed metallicity), although growth rates are similar. Thus misleading results can be obtained if one *arbitrarily* adds or subtracts mass to the envelope of a given stellar model on the AGB in the hopes of simulating the evolution of a star with a *different initial mass*, a short-cut which has frequently been employed, by many investigators. It is unfortunate that this short-cut is invalid.

iii) Mass Loss During the Shell Flash Phase

Figure 4 shows the average mass loss rates, averaged over a flash cycle from one flash to the next: they are generally of order a few times $10^{-7} M_{\odot}/\text{year}$, except for the stars with the higher η value. (Note that, due to the relatively long-lived post-flash luminosity and radius dip, this rate is slightly smaller than would be found if the star were simply assumed to follow the $M_c - L$ relation of Paper II, without flashes; however, a computation suppressing flashes by assuming steady double-shell burning averages out the luminosity and radius variations caused by flashes, and thus might be expected to give a result quite close to that found when flashes are included.) Recall that stars of lower mass or of higher metallicity sit at cooler effective temperatures on the AGB than higher mass stars of the same luminosity (as may be seen in Figs. 1 and 2); this effect, plus the inverse dependence of the mass loss rate of Equation (12) on the star's total mass, means that there is no

general relation giving the mass loss rate as a function of core mass. As discussed in Paper II, after the first few flashes the star's surface luminosity L follows the $M_c - L$ relation, growing approximately linearly as a function of core mass $M_c \equiv M_H$; since the radius R grows also, and the mass loss rate of Equation (12) is proportional to the product of L and R , one should expect to find the mass loss rate growing faster than linearly with M_H after the first few flashes. This is visibly the case in Figure 4 for the $Z = 0.02$, $M_i = 3.0 M_\odot$ case and the $Z = 0.001$, $M_i = 1.2 M_\odot$ and $2.0 M_\odot$ cases with $\alpha = 1.0$. Also, the growth of the mass loss rate should be expected to slow down or reverse for the *last* couple of flashes, as the star moves off the AGB toward higher effective temperatures T_e and smaller radii, and this is indeed visible for the $Z = 0.02$, $M_i = 1.2 M_\odot$ case, the $Z = 0.001$, $M_i = 1.0 M_\odot$ case, and the $Z = 0.001$, $M_i = 1.2 M_\odot$ case for $\alpha = 2.0$ (these being the only stars that were followed through to the very last flash on the AGB). Note the effect on the mass loss rate (at fixed η) of changing the value of α : for the $Z = 0.001$, $M_i = 1.2 M_\odot$ case at a core mass $M_H \simeq 0.57 M_\odot$ and total mass $M_{\text{tot}} \sim 0.78 M_\odot$, values of $\alpha = 1.0$, 1.5, and 2.0 result respectively in average mass loss rates of $3.9 \times 10^{-7} M_\odot/\text{year}$, $2.9 \times 10^{-7} M_\odot/\text{year}$, and $2.2 \times 10^{-7} M_\odot/\text{year}$; while increasing α from 1.0 to 1.5 reduces the mass loss rate from $4.8 \times 10^{-7} M_\odot/\text{year}$ to $3.4 \times 10^{-7} M_\odot/\text{year}$ in the case of $M_i = 2.0 M_\odot$, $Z = 0.001$ when at $M_H \simeq 0.66 M_\odot$ and $M_{\text{tot}} \sim 1.73 M_\odot$. This is due to the fact that the mass loss rate of Equation (12) is proportional to the stellar radius R , which is close to being inversely proportional to the value of α . The sharp increase in the mass loss rate of the $M_i = 2.0 M_\odot$, $\alpha = 1.5$ case subsequent to

dredge-up is due to the larger stellar radius R caused by the increased metallicity Z resulting from dredge-up.

As discussed in Section IIIa above the Reimers (1975) wind of Equation (12) can cause extensive mass loss on the RGB for low mass stars: see $\Delta M(\text{D} \rightarrow \text{E})$ in Table 2. As shown in Figure 5, this mass loss formula has even more dramatic effects during shell flashes on the AGB, where higher stellar luminosities and larger stellar radii cause even higher mass loss rates. Note that the stars of $M_i = 3.0 M_\odot$ have mass loss normalization parameter $\eta = 1.4$ in Equation (12), a factor of 3.5 larger than the value of $\eta = 0.4$ used for the lower mass stars of $M_i \leq 2.0 M_\odot$. In all cases, the mass loss *severely limited* the maximum number of flashes that could occur on the AGB. For the mass loss rate of the present work, the $Z = 0.001$, $M_i = 1.0 M_\odot$ star was limited to 5 flashes, and the $Z = 0.001$, $M_i = 1.2 M_\odot$ star to 8 flashes (note that the increase of α to 2.0 before the 6th flash was what allowed computation up to the 10th flash for that star: see dashed curve of Fig. 5). By extrapolation of the curves of Figure 5 to the point where $M_{\text{tot}} \approx M_{\text{H}}$, one can estimate that the $Z = 0.001$, $M_i = 2.0 M_\odot$ star would be limited to about 30 flashes, by which time it would have reached a core mass of $M_{\text{H}} \sim 0.77 M_\odot$; the $Z = 0.001$, $M_i = 3.0 M_\odot$ star (with higher η value) might be limited to of the order of 30 flashes, reaching a core mass of $M_{\text{H}} \sim 0.85 M_\odot$. The $Z = 0.02$, $M_i = 1.2 M_\odot$ star was limited to 9 flashes, and the $Z = 0.02$, $M_i = 3.0 M_\odot$ star to 25 flashes (though more would have been possible for this star if its η -value had been the same as that of the lower mass stars).

As discussed in Section IIIa above, the mass loss rate used to obtain these results is likely an overestimate by as much as a factor of 2. A mass loss rate reduced by this factor would allow a larger number of flashes to take place. However, the mass loss rate increases as the star ascends the AGB; thus, even considering that pre-flash mass loss would be halved, one cannot simply assume that the allowed number of flashes would be doubled. If one were to redraw the curves of Figure 5, assuming only half as much mass loss had taken place at any given core mass, and then extrapolate the curves forward, one would find that the stars of $M_i = 1.0 M_\odot$ and $1.2 M_\odot$ could gain only about half a dozen additional flashes, while stars of $M_i = 2.0 M_\odot$ and $3.0 M_\odot$ could gain only about a dozen.

These results on the limited number of flashes allowed by wind mass loss are essentially in agreement with the results of more restricted investigations performed by Schönberner (1979) and by Harpaz and Kovetz (1981), for solar metallicity and using $\eta = 1.0$ in the Reimers (1975) mass loss formula given in Equation (12). Schönberner (1979) considered stars of $Y_{\text{env}} = 0.24$, $Z = 0.021$, and masses *on the horizontal branch* of $M_{\text{tot}} = 1.0 M_\odot$ and $1.45 M_\odot$ (which would correspond to somewhat larger initial masses M_i on the main sequence); these experienced 10 flashes and 23 flashes respectively, ending up with $M_f = 0.598 M_\odot$ and $0.644 M_\odot$. Harpaz and Kovetz (1981) considered a star of $Y_{\text{env}} = 0.28$, $Z = 0.02$, with a mass *on the horizontal branch* of $M_{\text{tot}} = 1.2 M_\odot$; this star experienced only 5 flashes, ending up with $M_f = 0.593 M_\odot$. These agree with each other and with the present work as closely as can be expected, considering the differences in initial composition, low-temperature opacities, and choice of η values.

The point $M_{\text{tot}} \approx M_{\text{H}}$ mentioned above gives the star's final mass M_f , which it will retain (to a good approximation) through its subsequent evolution as the nucleus of a planetary nebula (NPN) and then as a white dwarf. For each of the stars considered here, Table 6 gives the final mass M_f implied by the computations using the mass loss rate of Equation (12), and estimates (as described above) of the value of M_f that would result if the mass loss rate had been halved. Also presented in Table 6 are the expected values of M_f resulting from the *observationally determined* initial–final mass ($M_i - M_f$) relation discovered by Weidemann and Koester (1983): it should be noted that observational uncertainties, and uncertainties in the theoretical derivation of the derived M_i and M_f values, lead to an uncertainty in the $M_i - M_f$ relation which is greater for stars of higher initial mass (where there is less data, and larger scatter) than for lower mass stars. This uncertainty should not exceed $\Delta M_f \simeq 0.10 M_{\odot}$ for $M_i \lesssim 3 M_{\odot}$ and may be somewhat smaller, particularly for $M_i \sim 1 M_{\odot}$, where the spread in the data is less. (As discussed in Weidemann (1984), there is likely also a spread in M_f of order $\Delta M_f \lesssim 0.10 M_{\odot}$ due to different amounts of mass loss taking place in stars of the same initial mass M_i .) The M_f values given in Table 6 for stars of $Z = 0.001$ were taken from the observations of Aaronson and Mould (1985); they observed the luminosity of the tip of the AGB for clusters in the Large and Small Magellanic Clouds (LMC and SMC), which in general have lower metallicity than our galaxy, obtaining M_f from the $M_c - L$ relation and M_i from the cluster age as discussed in Paper II. The M_f values in Table 6 for stars of $Z = 0.02$ were taken from Weidemann (1984), from a relation (referenced as provided in a private communication by Schönberner) obtained from

observations of the nuclei of planetary nebulae (NPN) in the local *galactic* neighborhood (which would thus generally have higher metallicities): this relation also agreed better with the (less accurate) results of observations of white dwarfs in the local galactic neighborhood from which Weidemann and Koester (1983) derived the observational $M_i - M_f$ relation in its initial form. It may be noted from Table 6 that for low initial masses ($M_i = 1.0 M_\odot$ and $1.2 M_\odot$) the results of a Reimers wind are in reasonable agreement with the observed $M_i - M_f$ relation, particularly if one considers the (more probable) reduced-wind estimates. However, the higher initial masses ($M_i = 2.0 M_\odot$ and $3.0 M_\odot$) generally lead to larger values of M_f than indicated by the observed $M_i - M_f$ relation, sometimes *much* larger. It thus appears that for stars with initial mass M_i below some limit M_{WK} a Reimers wind is sufficient to satisfy the observed $M_i - M_f$ relation, but that for stars of $M_i > M_{WK}$ additional mass loss must be invoked, such as a “superwind” that results in envelope ejection. The results presented in Table 6 imply a value of $M_{WK} \sim 1.5 M_\odot$ for $Z = 0.001$; for $Z = 0.02$, about all that can be said is that probably $1.2 M_\odot < M_{WK} < 3 M_\odot$.

It should be noted that there are additional reasons (both theoretical and observational) to expect that relatively fast envelope ejection takes place, at least in some stars. A number of theoretical studies of dynamic envelope pulsation have indicated that for a given stellar mass, a high enough luminosity leads to dynamic instability, resulting in violent pulsations that eject significant amounts of mass repeatedly on a relatively short timescale (see, e.g., Sparks and Kutter 1972; Smith and Rose 1972; Wood 1974; Kutter and Sparks 1974; Tuchman, Sack, and Barkat 1978, 1979; Fedayev 1982; Tuchman 1984). In addition, observations of OH/IR stars

indicate mass loss rates of as much as 10^{-5} to $10^{-4} M_{\odot}/\text{year}$ in some cases, one or two orders of magnitude higher than expected from the Reimers (1975) relation (see, e.g., Werner *et al.* 1980; Baud and Habing 1983).

One final point can be obtained from Table 6. The final mass M_f given by the $M_i - M_f$ relation is essentially equal to the core mass M_H at the time when the envelope mass approaches zero (whether from wind mass loss alone or from wind mass loss plus envelope ejection); but for the $Z = 0.001$, $M_i = 3.0 M_{\odot}$ case flashes did not begin until the core mass M_H was slightly *larger* than the expected final mass M_f from the observed $M_i - M_f$ relation. On the other hand, the $Z = 0.001$, $M_i = 2.0 M_{\odot}$ star went through roughly 20 flashes (and for $\alpha = 1.5$ encountered dredge-up and carbon star production, as discussed in Section IIIc below) before reaching its expected final mass. It may thus be concluded that, for $Z = 0.001$, stars of low initial mass ($M_i \lesssim 2 M_{\odot}$) will encounter a sufficient number of flashes to become carbon stars, while stars of higher initial mass ($M_i \gtrsim 3 M_{\odot}$) will not: this is in agreement with Weidemann (1984) and Aaronson and Mould (1985). In addition, the effect of wind mass loss in constantly reducing the envelope mass can act to inhibit dredge-up (as discussed in Section IIIc below), whether reducing the number of dredge-up episodes or possibly preventing dredge-up entirely in some cases. Thus mass loss has a *major* impact on AGB evolution and carbon star production.

iv) The Core Mass–Base Temperature Relation for Flash-Driven Convection

As shown in Figure 6, there does indeed appear to be a general relation for low mass stars (of a given composition) between their core mass $M_c \equiv M_H$ and the

maximum temperature T_b (strictly, T_b^{\max}) reached at the base of the (temporary) flash-driven intershell convective region which reaches up from the helium-burning shell toward the hydrogen-burning shell. However, the $M_c - T_b$ relation given by Iben and Truran (1978) for *high mass* stars *cannot* be extrapolated down to these low core masses: their relation

$$T_b = 310 + 285(M_H - 0.96), \quad (13)$$

where T_b is in units of $10^6 K$ and M_H in solar units, is represented in Figure 6 by the dashed line marked “IT,” lying at much lower values of T_b than the current work. As presented in Malaney and Boothroyd (1986), for these low core masses other investigators have found both slightly higher T_b values (Iben and Renzini 1982*a, b*) and somewhat lower T_b values (Becker 1986: by 10 or $20 \times 10^6 K$). Combined with the results shown in Figure 6, it appears that the $M_c - T_b$ relation has considerable composition dependence, probably with *some* dependence on other stellar parameters. It is possible that part of the discrepancies between different investigators may be due to sensitivity of the computed value of T_b to the size of the mass zoning in the intershell region: Sackmann (1976) showed that the flash strength (and thus presumably T_b) was reduced if the number of mass layers was too small (i.e., zoning not fine enough); the discrepancy (but not its direction) was reported in Sackmann (1980*a*). (The models of the present work included up to 400 mass layers, of which ~ 150 comprised the helium-burning shell and ~ 70 the rest of the intershell region.) Thus *any* $M_c - T_b$ relation, including the low core mass $M_c - T_b$ relation given in

Malaney and Boothroyd (1986), namely

$$\begin{aligned} T_b &= 250 + 305(M_H - 0.53), & M_H < 0.65 \\ T_b &= 290 + 67(M_H - 0.65), & 0.65 < M_H < 1.0 \end{aligned} \tag{14}$$

(dashed line marked “MB” in Fig. 6), should be used with a certain amount of caution.

v) Composition of the Flash-Produced Carbon Pocket

The helium shell flash drives a intershell convective region upward from the helium-burning shell nearly to the hydrogen-burning shell; when this convection dies away after the flash, it leaves behind a “carbon pocket”: a strongly carbon-enriched region of nearly uniform composition in the intershell region. (It is from this carbon pocket that dredge-up can mix carbon to the surface to form a carbon star.) As indicated in the literature (e.g., Christy-Sackmann and Paczyński 1975; Iben 1975, 1976; Sugimoto and Nomoto 1975; Sackmann 1980a), the triple-alpha reaction burns helium to carbon at the base of the flash-driven convection, but the $^{12}\text{C}(\alpha, \gamma)^{16}\text{O}$ reaction does not have time to convert more than a small fraction of this carbon to oxygen: due to the short timescale of the flash, burning does not go to completion. As may be seen from Figure 7, this remains true *even after the* $^{12}\text{C}(\alpha, \gamma)^{16}\text{O}$ *reaction rate was increased by a factor of 3* (the difference between the CFHZ IV rate and the FCZ II rate). As discussed in Section IIIa, the increase in the $^{12}\text{C}(\alpha, \gamma)^{16}\text{O}$ rate makes a big difference to the composition of the carbon-oxygen degenerate core; but the flash-produced carbon pocket composition remains essentially the same. After the first few flashes, the composition of the carbon

pocket settles down as shown in Figure 7 to a nearly constant mixture, with carbon comprising 20 – 25% (by mass), ^{16}O comprising about 2%, and helium comprising essentially all the rest. Nor is there much difference between stars of different metallicities, as may be seen by comparing parts *a* and *b* of Figure 7. (It should be noted that Fig. 7 applies to the *tip* of the carbon pocket; but the composition of the carbon pocket is quite uniform, varying by only a few percent.)

Figure 8 shows the amount of ^{18}O left behind at the tip of the carbon pocket, relative to the star's metallicity. Most of the envelope CNO-abundance (comprising about 75% of the metallicity Z , as discussed in Section II) has been converted to ^{14}N in the region left behind by the hydrogen-burning shell; during the flash this ^{14}N burns to ^{18}O via the $^{14}\text{N}(\alpha, \gamma)^{18}\text{F}(e^+\nu)^{18}\text{O}$ reaction, but as shown in Figure 8 this ^{18}O is almost completely converted to ^{22}Ne by the $^{18}\text{O}(\alpha, \gamma)^{22}\text{Ne}$ reaction (except in the first few flashes). Note that the decline in the ^{18}O abundance is steeper for the stars of low metallicity, presumably due to their steeper increase in flash strength. It should also be mentioned that the amount of ^{18}O is quite significantly smaller in lower regions of the carbon pocket, which remain convective longer and thus have more time to process the ^{14}N that was mixed in previously (when the flash-driven convection was growing). The absence of ^{18}O is important for the possibility of *s*-processing during flashes from the $^{13}\text{C}(\alpha, n)$ neutron source. If the semiconvective “dredge-down” of hydrogen discussed in Section IIIc below occurs, mixing small amounts of hydrogen into the carbon pocket, then ^{13}C can be produced via the $^{12}\text{C}(p, \gamma)^{13}\text{N}(e^+\nu)^{13}\text{C}$ reaction; since relatively small amounts of hydrogen would be burned in the presence of relatively large amounts of ^{12}C , much of this ^{13}C would

not be burned to ^{14}N . (Note that the CNO-equilibrium $^{13}\text{C}/^{12}\text{C}$ ratio is roughly $\frac{1}{4}$, but if much hydrogen were present almost all the carbon would be converted to nitrogen.) The rate of proton capture on ^{18}O is two orders of magnitude faster than on ^{12}C , so that the presence of substantial amounts of ^{18}O in the carbon pocket would have blocked this ^{13}C production mechanism.

vi) The Core Mass–Interflash Period Relationship

Paczynski (1970*a*) discovered the exceedingly useful core mass–luminosity relation, discussed in detail in Paper II; but he also discovered another useful relation, namely the core mass–interflash period ($M_c - \tau_{if}$) relation (Paczynski 1975), which he gave as

$$\log \tau_{if} = 3.05 - 4.5(M_H - 1.0) = 4.5(1.678 - M_H), \quad 0.5 \lesssim M_H \lesssim 1.4 \quad (15)$$

(interflash period τ_{if} in years, M_H in solar masses) for stars of $Y = 0.27$, $Z = 0.03$. Wood and Zarro (1981) obtained a similar relation for $Y_{\text{env}} = 0.30$, $Z = 0.02$:

$$\log \tau_{if} = 3.68(1.914 - M_H), \quad 0.6 \lesssim M_H \lesssim 0.9. \quad (16)$$

Figure 9 illustrates that these relations are consistent with the relation implied by the current work for initial $Y = 0.27$, $Z = 0.02$, namely

$$Z = 0.02 : \quad \log \tau_{if} = 4.5(1.689 - M_H), \quad 0.5 \lesssim M_H \lesssim 0.7. \quad (17)$$

However, Figure 9 indicates that the $M_c - \tau_{if}$ relation has quite a *strong* composition dependence: for initial $Y = 0.24$, $Z = 0.001$, the relation becomes

$$Z = 0.001 : \quad \log \tau_{if} = 4.95(1.644 - M_H), \quad 0.5 \lesssim M_H \lesssim 0.8, \quad (18)$$

or if one assumes, as *may* be indicated by the lesser slope of the Wood and Zarro (1981) relation, that the relation is less steep at higher core masses than at lower core masses, one obtains the *slightly* steeper relation

$$Z = 0.001 : \quad \log \tau_{if} = 5.5(1.54 - M_H), \quad 0.5 \lesssim M_H \lesssim 0.7. \quad (15)$$

In either case, the interflash period for the low- Z case is nearly twice that in the high- Z case at the same core mass. One should note that Lattanzio (1986) obtained a similar composition dependence, finding also a dependence on Y for the low- Z case. The magnitudes of his interflash periods agree with ours (as shown in Fig. 9), but his relations have a flatter slope; most likely, this means that his stars had not *quite* reached full amplitude flashes, since his relations were obtained from consideration of only 5 to 10 flashes for stars of only a single mass.

c) Carbon Star Production: Conditions for Dredge-up

For the stars of low metallicity ($Z = 0.001$) and initial masses $1.0 M_\odot$, $1.2 M_\odot$, and $2.0 M_\odot$, Figure 10 illustrates the approach toward dredge-up. After the first few flashes, the outermost extent M_{Cis}^{\max} of flash-driven intershell convection consistently reaches up to within a few times $10^{-5} M_\odot$ of the hydrogen-helium (H-He) discontinuity M_H ($\equiv M_c$). The innermost extent M_{CE}^{\min} of envelope convection occurs at the post-flash maximum in the surface luminosity, not long after the flash has ended (see Paper I for flash light curves); in general, M_{CE}^{\min} reaches down to within a few times $10^{-5} M_\odot$ of M_H , as may also be seen from Figure 10. Stars of solar metallicity ($Z = 0.02$; initial masses $1.2 M_\odot$ and $3.0 M_\odot$) behave similarly, as

shown in Figure 11, but do not experience any semiconvection at the tip of the “carbon pocket” left behind by the flash-driven intershell convection. For the stars of low metallicity ($Z = 0.001$), after the first few flashes a semiconvective region *does* appear at the tip of the carbon pocket during the post-flash luminosity maximum (see Figure 10c). The semiconvection is driven by the increased opacity of carbon as the carbon pocket is pushed out to lower temperatures by the post-flash expansion; the bottom M_{sc}^{\min} of the semiconvective region thus lies some distance below the previous tip M_{Cis}^{\max} of the carbon pocket, and carbon is mixed (in diminishing quantities) all the way to the top M_{sc}^{\max} of the region, somewhat above M_{Cis}^{\max} . Thus this temporary semiconvective region spreads out the tip of the carbon pocket, mixing some carbon all the way up to the H-He discontinuity and *perhaps* mixing some hydrogen downward (resolution is limited by the finite size of the mass layers in the model). However, unless semiconvection is significantly more extensive than indicated by our models, such hydrogen “dredge-down” would mix downward no more than about $10^{-9} M_{\odot}$ of hydrogen, producing only about $10^{-8} M_{\odot}$ of ^{13}C when the region later heats up. Thus this “dredge-down,” while similar to that found by Hollowell (1986) in his models (of the same metallicity) that did not include convective overshoot, produces an order of magnitude less ^{13}C ; when the intershell convection from the next flash engulfs this region, the $^{13}\text{C}(\alpha, n)^{16}\text{O}$ reaction could not produce more than a few neutrons per Fe-seed, resulting in very little *s*-processing.

As shown in Figure 10*b, c* and 11*b, c*, for both metallicities $Z = 0.001$ and $Z = 0.02$ the innermost extent M_{CE}^{\min} of envelope convection (occurring at the post-flash luminosity maximum) *does not* approach the H-He discontinuity M_H

closer than several times $10^{-5} M_{\odot}$ for runs having a value of the mixing length parameter $\alpha = 1.0$: *no* dredge-up was found for this value of α . Thus the value of α was increased for two of the runs (metallicity $Z = 0.001$, initial masses $1.2 M_{\odot}$ and $2.0 M_{\odot}$) in the expectation that this would result in deeper convective envelopes. (As mentioned in Sections IIc and IIIb, there are several reasons to believe higher values of α are appropriate, in addition to the question of the existence of dredge-up.)

For the star of initial mass $2.0 M_{\odot}$ (metallicity $Z = 0.001$, initial $Y = 0.24$, post-RGB $Y_{\text{env}} = 0.257$ due to “first dredge-up”), the value of α was incremented gradually from 1.0 to 1.5 in the interval between the 9th and 10th flashes (when the star’s total mass was about $1.75 M_{\odot}$). As may be seen from Figure 10, with $\alpha = 1.5$ the star came very close to dredge-up on the 10th flash, which had $M_{CE}^{\text{min}} \approx M_{\text{H}}$; and dredge-up actually occurred on the 11th flash. At this time the total stellar mass was $M_{\text{tot}} = 1.72 M_{\odot}$, and the core mass was $M_{\text{H}} = 0.665 M_{\odot}$; the peak flash strength was $\log(L_{\text{He}}^{\text{max}}/L_{\odot}) = 7.86$. Due to this single dredge-up episode, the star *became a carbon star* with $n(\text{C})/n(\text{O}) = 2.1$, as compared to 0.3 prior to dredge-up; the envelope metallicity increased from $Z = 0.0010$ to $Z = 0.0017$ due to the added carbon. The pre-flash luminosity of this star was $\log(L/L_{\odot}) = 3.954$ (i.e., $M_{\text{bol}} = -5.11$), but during the post-flash luminosity dip the star’s luminosity dropped to $\log(L/L_{\odot}) = 3.782$ (i.e., $M_{\text{bol}} = -4.68$). From Papers I and II, we note that a star of this metallicity and core mass spends about 20% of its time in this luminosity dip, although only half of that is spent below a luminosity of $\log(L/L_{\odot}) \approx 3.9$ (i.e., $M_{\text{bol}} \approx -5.0$).

Figure 12 illustrates the behavior of convection as a function of time during and shortly after the 11th flash, showing the dredge-up as envelope convection dips below the H-He discontinuity. The depth of dredge-up was $\Delta M_{\text{dredge}} \equiv M_{\text{H}} - M_{\text{CE}}^{\text{min}} = 0.00283 M_{\odot}$, of which all but $2 \times 10^{-5} M_{\odot}$ comprised “carbon pocket” material having $C \simeq 0.24$ (by mass). Between the 10th and 11th flashes, the hydrogen-burning shell advances by $\Delta M_{\text{H}} = 0.00643$, giving $\lambda \equiv \Delta M_{\text{dredge}} / \Delta M_{\text{H}} = 0.446 M_{\odot}$; but use of this value of λ in a “dredge-up law” would *not* be appropriate. Not only did the other star with dredge-up yield a much smaller value of λ (as described below), but dredge-up was *by no means* a regularly recurring phenomenon: the large increase in metallicity Z due to dredge-up, aided perhaps by the (relatively slight) reduction in envelope mass due to mass loss, was sufficient to *prevent the star from experiencing dredge-up on subsequent flashes*. This was at least partly due to the effect on the peak helium flash strength $L_{\text{He}}^{\text{max}}$: as may be seen from Figure 3, the peak flash strength grows at a slower rate subsequent to dredge-up, as might be expected from the increased metallicity. Finally, it should be noted that *no* semiconvection was observed to take place on the 11th flash, when dredge-up occurred, although semiconvection was present in previous and subsequent flashes.

For the star of initial mass $1.2 M_{\odot}$ (metallicity $Z = 0.001$, initial $Y = 0.24$, post-RGB $Y_{\text{env}} = 0.264$ due to “first dredge-up”), the value of α was incremented gradually from 1.0 to 1.5 in the interval between the 5th and 6th flashes (when the star’s total mass was about $0.83 M_{\odot}$). Three further flashes were computed with $\alpha = 1.5$, but no dredge-up was found. Returning to the interval after the 5th flash, the value of α was incremented to 2.0; with this value of α , five further

flashes were computed (by which point mass loss had stripped away the entire envelope and no further flashes could occur); no dredge-up was found for $\alpha = 2.0$ either. It should be noted that for the last (10th) flash, the star had a total mass of only $M_{\text{tot}} = 0.6064 M_{\odot}$ and a core mass $M_{\text{H}} = 0.6030$ (giving an envelope mass of only $M_{\text{env}} = 0.0034 M_{\odot}$), but the *peak flash strength* of $\log(L_{\text{He}}^{\text{max}}/L_{\odot}) = 7.86$ was apparently *insufficient* to cause dredge-up of the type described in Sackmann (1980*b*), who had $\log(L_{\text{He}}^{\text{max}}/L_{\odot}) \sim 8.2$: although the envelope structure was similar, the carbon pocket failed by a margin of $\sim 10^{-4} M_{\odot}$ to be pushed out into the low-temperature part of the envelope. Returning again to the interval after the 5th flash, the value of α was incremented to 3.0; this proved sufficient to cause dredge-up on the very next flash, namely the 6th flash. At this time the total stellar mass was $M_{\text{tot}} = 0.81 M_{\odot}$, and the core mass was $M_{\text{H}} = 0.566 M_{\odot}$; the peak flash strength was $\log(L_{\text{He}}^{\text{max}}/L_{\odot}) = 7.53$. Due to this single dredge-up episode, the star *became a carbon star* with $n(\text{C})/n(\text{O}) = 3.1$, as compared to 0.4 prior to dredge-up; the envelope metallicity increased from $Z = 0.0010$ to $Z = 0.0022$ due to the added carbon. The pre-flash luminosity of this star was $\log(L/L_{\odot}) = 3.647$ (i.e., $M_{\text{bol}} = -4.35$), but during the post-flash luminosity dip the star's luminosity dropped to $\log(L/L_{\odot}) = 3.345$ (i.e., $M_{\text{bol}} = -3.59$). From Papers I and II, we note that a star of this metallicity and core mass spends nearly 40% of its time in this luminosity dip; 20% is spent below a luminosity of $\log(L/L_{\odot}) \approx 3.5$ (i.e., $M_{\text{bol}} \approx -4.0$), and 10% below $\log(L/L_{\odot}) \approx 3.43$ (i.e., $M_{\text{bol}} \approx -3.8$).

Figure 13 illustrates the behavior of convection as a function of time during and shortly after the 6th flash, showing the dredge-up. The depth of dredge-up

was $\Delta M_{\text{dredge}} = 0.00113 M_{\odot}$, of which all but $6 \times 10^{-5} M_{\odot}$ comprised “carbon pocket” material having $C \simeq 0.26$ (by mass). Between the 5th and 6th flashes, the hydrogen-burning shell advances by $\Delta M_{\text{H}} = 0.00924$, giving $\lambda = 0.122$; again, this value of λ is essentially irrelevant. On the subsequent (7th) flash, only helium was dredged up; for this flash, the star had $M_{\text{tot}} = 0.78 M_{\odot}$, $M_{\text{H}} = 0.574 M_{\odot}$, and $\log(L_{\text{He}}^{\text{max}}/L_{\odot}) = 7.53$. The value of $\Delta M_{\text{dredge}} = 6 \times 10^{-5} M_{\odot}$ failed by $1.5 \times 10^{-5} M_{\odot}$ to reach the tip of the carbon pocket, which had been smeared upward by $1.5 \times 10^{-5} M_{\odot}$ due to a small semiconvective region (on the 6th flash, when dredge-up took place, *no* semiconvection was found, although semiconvection had been present in previous flashes). It appears that repeated dredge-up was again inhibited by the large increase in metallicity, aided by the decrease in envelope mass.

It should be noted that the mass loss rate obtained with $\eta = 0.4$, $\alpha = 1.0$ is likely to be an overestimate by a factor of about 2, as discussed in Section IIIa above. Thus, for example, a star of initial mass $1.2 M_{\odot}$ with $Z = 0.001$ should still have a mass of $M_{\text{tot}} \approx 1.0 M_{\odot}$ on its 6th flash (rather than $0.81 M_{\odot}$); such a star would have a larger envelope mass for a given flash strength than the case considered above (or alternatively, it would reach a much higher flash strength before the envelope mass dropped to a given value). This likely would allow dredge-up to occur in such a star for a more reasonable value of $\alpha \lesssim 2$, though perhaps at a higher core mass than the above lower mass, $\alpha = 3.0$ case.

Interpretation of the above results is aided by consideration of the dredge-up results obtained by others. The starting model of Sackmann (1980*b*) was created

from scratch on the AGB: it had $M_{\text{tot}} = 0.815 M_{\odot}$, $M_{\text{H}} = 0.800 M_{\odot}$, $Y_{\text{env}} = 0.27$, $Z = 0.03$, and $\alpha = 1.0$, and no possibility of mass loss was considered. Its 2nd flash, at a core mass of $M_{\text{H}} = 0.805$ and with $\log(L_{\text{He}}^{\text{max}}/L_{\odot}) \sim 8.2$, had sufficiently large post-flash expansion to bring the tip of the carbon pocket down to temperatures handled by the program's static envelope routines. The small size of the envelope ($M_{\text{env}} = 0.01$) meant that envelope convection did not reach below the hydrogen and helium ionization zones, the base of convection being at a temperature $\log T \approx 4.7$; below this point, the temperature rises to $\log T \approx 7$ in a zone whose thickness in terms of mass is only $\Delta M \sim 10^{-4} M_{\odot}$. Since the carbon pocket overlapped the static envelope by nearly $0.01 M_{\odot}$, dredge-up took place and produced a carbon star. Due to the high core mass, however, this carbon star had a relatively high luminosity of about $\log(L/L_{\odot}) \approx 4.26$ (i.e., $M_{\text{bol}} \approx -5.9$).

Wood and Zarro (1981) also created some stars from scratch, but with a large enough intershell mass that they would be expected to be in the pre-flash regime. These stars had $Z = 0.02$, $Y_{\text{env}} = 0.30$, $\alpha = 1.0$, initial core mass $M_{\text{H}} = 0.53 M_{\odot}$, and masses between $0.8 M_{\odot}$ and $3.0 M_{\odot}$ (with no mass loss); but extensive runs of flashes were carried out only for the $M_{\text{tot}} = 2.0 M_{\odot}$, where runs were also started from $M_{\text{H}} = 0.7 M_{\odot}$ and $M_{\text{H}} = 0.8 M_{\odot}$. No dredge-up was found for these cases. Wood (1981*b*) continued similar calculations for lower metallicities; all had $Y_{\text{env}} = 0.30$, $\alpha = 1.0$, and starting core mass $M_{\text{H}} \approx 0.55$. For $Z = 0.01$ with $M_{\text{tot}} = 2.0 M_{\odot}$ no dredge-up was found, over a wide range of core masses; the same was true for $Z = 0.001$ with $M_{\text{tot}} = 1.75 M_{\odot}$. However, for a star of $Z = 0.001$ with $M_{\text{tot}} = 2.0 M_{\odot}$, dredge-up occurred at $M_{\text{H}} = 0.674 M_{\odot}$ ($M_{\text{bol}} \sim$

–5.2), producing a carbon star after several more flashes (at $M_{\text{H}} = 0.698 M_{\odot}$); for a star of $Z = 0.001$ with $M_{\text{tot}} = 2.25 M_{\odot}$ dredge-up started even earlier, at $M_{\text{H}} = 0.663$. Further calculations involving envelope integrations only may be less accurate, depending on parameterized inner boundary conditions that were obtained from the full evolutionary runs; but at least qualitatively, they indicate that either a decrease in Z or an increase in α allows dredge-up to take place at smaller total stellar masses and smaller core masses.

The initial model of Iben (1982) was obtained from K. Despain, who had evolved (without mass loss) a star of mass $0.6 M_{\odot}$ and envelope composition $Z = 0.001$, $Y_{\text{env}} = 0.25$, having $\alpha = 1.5$, from a zero age horizontal branch model (supplied by J. Hawley) to core helium exhaustion; Iben (1982) continued the evolution (with $\alpha_{\text{Iben}} = 1.5$, no mass loss) through a number of flashes on the AGB. Between the 7th and 8th flashes, he gradually added $0.1 M_{\odot}$ to the envelope to get a star of mass $0.7 M_{\odot}$, following five more flashes; the last (12th) flash was at core mass $M_{\text{H}} = 0.612 M_{\odot}$. Iben and Renzini (1982*a, b*) evolved this star through the 13th flash, at $M_{\text{H}} = 0.624 M_{\odot}$, with an improved formula for low-temperature carbon opacities: this resulted in dredge-up and carbon star production on that flash, with $\Delta M_{\text{dredge}} \sim 2 \times 10^{-4} M_{\odot}$ and $n(\text{C})/n(\text{O}) = 5.6$. They then improved the carbon opacity formula further (Iben and Renzini 1982*b*), and repeated the evolution from the 12th flash through the 13th and 14th flashes, finding dredge-up for both the latter. The 13th flash had $M_{\text{H}} = 0.624 M_{\odot}$, $\log(L_{\text{He}}^{\text{max}}/L_{\odot}) = 8.003$, and resulted in $n(\text{C})/n(\text{O}) = 2.3$; the 14th flash had $M_{\text{H}} = 0.624 M_{\odot}$, $\log(L_{\text{He}}^{\text{max}}/L_{\odot}) = 8.142$, and $\Delta M_{\text{dredge}} \sim 4.2 \times 10^{-4} M_{\odot}$ ($\lambda \sim 0.04$), causing $n(\text{C})/n(\text{O})$ to increase to a

value of 5.2. In these models, there was semiconvection attached to the base of envelope convection during dredge-up, mixing hydrogen downward but having little effect on the “classical” dredge-up that mixed carbon upward. Iben (1983) continued this work, testing the effect (for $Y_{\text{env}} = 0.25$, core masses from $0.58 M_{\odot}$ to $0.65 M_{\odot}$) of changing the metallicity, the total mass, and the mixing length; it appears that this was done by manipulating the envelopes sitting on top of the core obtained from Iben (1982). In all cases the flash strength was $\log(L_{\text{He}}^{\text{max}}/L_{\odot}) \sim 8$ at $M_{\text{H}} \sim 0.63 M_{\odot}$, where dredge-up was strongest (flash strength then levelling off or declining and dredge-up soon terminating). With $M_{\text{tot}} = 0.7 M_{\odot}$, $Z = 0.001$, and $\alpha_{\text{Iben}} = 1.0$ and 1.5 , dredge-up and carbon star production took place with $\lambda \lesssim 0.05$; increasing M_{tot} to $1.0 M_{\odot}$ at $Z = 0.001$, $\alpha_{\text{Iben}} = 1.5$ yielded $\lambda \lesssim 0.3$, and dredge-up beginning earlier and lasting for more flashes. For a star with $M_{\text{tot}} = 1.0 M_{\odot}$, $Z = 0.02$, and $\alpha_{\text{Iben}} \leq 1.0$, dredge-up did not occur; with $\alpha_{\text{Iben}} = 1.5$ dredge-up *did* occur (with $\lambda \lesssim 0.1$), but due to the large Z the value of $n(\text{C})/n(\text{O})$ did not quite reach unity. (In interpreting these results, note from Section IIc that $\alpha_{\text{Iben}} = 1.5$ in the codes used by Iben, Becker, and Hollowell corresponds to $\alpha \approx 2.5$ to 3.0 in all other codes that we are aware of, $\alpha_{\text{Iben}} = 1.0$ corresponds to $\alpha \approx 1.7$ to 2.0 , and $\alpha_{\text{Iben}} = 0.7$ corresponds to $\alpha \approx 1.2$ to 1.4 .)

Similarly to Iben and Renzini (1982*a, b*), Hollowell (1986, 1987) took as his starting model the star of $M_{\text{tot}} = 0.7 M_{\odot}$, $Z = 0.001$, $Y_{\text{env}} = 0.25$, and $\alpha_{\text{Iben}} = 1.5$ produced by Iben (1982) and evolved it forward without mass loss, but he started from its 9th flash (rather than the 12th); also, his program included revised low-temperature carbon opacities, and used a *diffusion approximation to convection*

(still with $\alpha_{\text{Iben}} = 1.5$) in order to take account of the fact that the timescale for complete convective mixing of the envelope is rather longer than the time-steps needed when carbon is being dredged up (and thus the instantaneous approximation for convective mixing is not valid: the abundances in the envelope convective region are not uniform during dredge-up). He followed the star from the 9th through the 16th flashes, both with and without convective overshoot. Without convective overshoot, he found *no* dredge-up, although semiconvection did mix sufficient hydrogen downward to result in quite significant ^{13}C -production and thus in significant *s*-processing via the $^{13}\text{C}(\alpha, n)^{16}\text{O}$ neutron source. In a separate run, he considered the case of convective overshoot by assuming that overshoot “smeared” the boundary of convection over a region roughly of size $l < H_p$, where $l = \alpha_{\text{Iben}} H_p \sqrt{v_{\text{conv}} \Delta t / (\alpha_{\text{Iben}} H_p)}$ (Hollowell 1987: diffusion approximation), rather than being a sharp composition jump at the formal edge of convection. With this form of overshoot, he found dredge-up and carbon star formation to take place on the 14th flash, with $M_{\text{H}} = 0.639 M_{\odot}$ and $\log(L_{\text{He}}^{\text{max}}/L_{\odot}) \simeq 8.15$, and having $\lambda \simeq 0.01$; the 15th flash produced a similar amount of dredge-up, but there was much less dredge-up on the 16th flash.

Lattanzio (1986) considered stars of metallicities $Z = 0.001, 0.01, \text{ and } 0.02$, helium abundances $Y = 0.20 \text{ and } 0.30$ (where $Y \equiv Y_{\text{env}}$ for the stars of mass $M_{\text{tot}} \leq 2.0 M_{\odot}$), $\alpha = 1.0$, and several initial masses from $1.0 M_{\odot}$ to $3.0 M_{\odot}$; he followed their evolution (without mass loss) from the zero age main sequence or zero age horizontal branch up to the first helium shell flash. Each of the stars of mass $M_{\text{tot}} = 1.5 M_{\odot}$ was followed through 5 to 10 flashes on the AGB; no dredge-up was found. Lattanzio (1987) then considered stars of mass $M_{\text{tot}} = 1.5 M_{\odot}$, $Z = 0.003$

and 0.006, $Y = 0.20$ and 0.30 , and $\alpha = 1.5$. For each of the four combinations of Z and Y , the star was evolved from the zero age main sequence, “jumping over” the helium core flash, up through a number of flashes on the AGB. The $Z = 0.006$, $Y = 0.20$ model was followed through 13 flashes, without any dredge-up occurring. The $Z = 0.006$, $Y = 0.30$ model was followed through 23 flashes, slight carbon dredge-up occurring on the 23rd flash with $M_{\text{H}} = 0.7M_{\odot}$ and quiescent $M_{\text{bol}} = -5.5$, with $M_{\text{bol}} = -4.9$ at the post-flash luminosity dip. The $Z = 0.003$, $Y = 0.30$ model was followed through 26 flashes, with carbon dredge-up first occurring on the 19th flash with $M_{\text{H}} = 0.69 M_{\odot}$, quiescent $M_{\text{bol}} = -5.4$, and dip $M_{\text{bol}} = -4.9$ and $\log(L_{\text{He}}^{\text{max}}/L_{\odot}) \approx 7$; by the 26th flash, $n(\text{C})/n(\text{O})$ had increased from 0.293 to 0.6. The $Z = 0.003$, $Y = 0.20$ model was followed through 17 flashes, with carbon dredge-up first occurring on the 11th flash with $M_{\text{H}} = 0.62 M_{\odot}$ and quiescent $M_{\text{bol}} = -4.8$; it became a carbon star on the 17th flash, with $M_{\text{H}} = 0.65 M_{\odot}$, quiescent $M_{\text{bol}} = -5.2$, and dip $M_{\text{bol}} = -4.4$. On the 17th flash, it had $\Delta M_{\text{dredge}} = 0.00286 M_{\odot}$, giving $\lambda = 0.38$.

There seems little doubt that the theory of low mass (low luminosity) carbon star formation has been brought into much closer agreement with observations. A number of cases of “classical” dredge-up have been found in low mass stars, and really no “non-classical” forms of dredge-up have been encountered for low mass stars of low luminosity. The report of Iben and Renzini (1982*a*) that semiconvection was important in mixing carbon outward was contradicted by their improved results (Iben and Renzini 1982*b*) finding that semiconvection was of importance mainly to the “dredge-down” of hydrogen.

The basic requirement for dredge-up in low mass stars seems to be the use of a mixing length to pressure scale height ratio value of $\alpha \gtrsim 1.5$ (i.e., $\alpha_{\text{Iben}} \gtrsim 0.8$); only Wood (1981*b*) obtained dredge-up with $\alpha = 1.0$, and he required a rather large total mass, $M_{\text{tot}} \sim 2 M_{\odot}$. It should be noted that, while the value of α has relatively little effect on the depth in *mass* of AGB star convective envelopes, it has a *large* effect on the depth in *temperature* of the convective envelope: the near-constancy in mass is due to the fact that the base of the convective envelope sits in a zone just outside the core which is very thin in mass, but in which the temperature varies from $\log T \sim 7$ to $\log T \sim 4.5$ (and density and radius also vary by large factors). There were four cases in the present work when dredge-up either occurred or came very close to occurring (i.e., when $M_{CE}^{\text{min}} \lesssim M_{\text{H}}$ was attained), namely the 10th and 11th flashes with $\alpha = 1.5$ of the star of initial mass $2.0 M_{\odot}$ and total mass $\sim 1.7 M_{\odot}$ ($M_{\text{H}} \sim 0.67$, $Z = 0.001$), and the 6th and 7th flashes with $\alpha = 3.0$ of the star of initial mass $1.2 M_{\odot}$ and total mass $\sim 0.8 M_{\odot}$ ($M_{\text{H}} \sim 0.67$, $Z = 0.001$ and 0.0022). It is probably no coincidence that for all four cases the temperature T_{CE}^{max} at the base of the convective envelope always had a value of $\log T_{CE}^{\text{max}} \sim 6.5$ at the time of deepest envelope penetration (when $M_{CE} \equiv M_{CE}^{\text{min}}$), although very different values of α were needed to obtain this for the two different stellar masses. This suggests that the value of α necessary for dredge-up is just that value which is needed to cause the base of envelope convection to reach to some particular temperature T_{CE}^{max} ; but this is not necessarily very helpful to the theorist, since it seems unlikely that this necessary temperature value is invariant under changes in *all* stellar input parameters. Certainly there are other necessary

conditions for dredge-up. In addition, determining the value of α needed to obtain some particular value of T_{CE}^{\max} is far from trivial, since the temperature T_{CE} at the base of the envelope varies over the flash cycle and is a function of several stellar parameters besides α .

The effect of several other stellar parameters on dredge-up may be explainable at least partly in terms of their effect on the convective envelope base temperature T_{CE}^{\max} . A decrease in the envelope mass M_{env} causes a decrease in T_{CE} , and indeed it is clear from the present work and that of Wood (1981*b*) and Iben (1983) that a decreased envelope mass makes dredge-up more difficult: a smaller envelope must be compensated for by some other factor, such as a larger value of α , or by a larger flash strength (as in Sackmann 1980*b*). An increase in the metallicity Z also seems to inhibit dredge-up, as indicated by the present work and by Wood (1981*b*), Iben (1983) and Lattanzio (1987); and indeed the value of T_{CE} was smaller by a factor of 4 for our star of $Z = 0.02$, initial mass $3.0 M_{\odot}$, and $\alpha = 1.0$ on its 20th flash than T_{CE} for our star of $Z = 0.001$, initial mass $1.2 M_{\odot}$, and $\alpha = 1.0$ on its 11th flash (at which points these stars had similar envelope masses as well as *fairly* similar core masses and surface luminosities). There is, however, another way in which a higher value of Z acts to inhibit dredge-up: as may be seen from Figure 3, the peak flash strength L_{He}^{\max} grows *much* more quickly for low- Z stars than for high- Z stars. That the flash strength is crucial to dredge-up is indicated by Sackmann (1980*b*), Iben (1982), and Hollowell (1987) as well as by the present work: all other things being more-or-less equal, one must wait for the flash strength to grow sufficiently large before dredge-up can occur. (This is obvious from physical

principles: the stronger the flash, the more post-flash expansion it causes; and it is the post-flash expansion which allows/causes the envelope to reach inward in mass below the H-He discontinuity.)

Both Iben (1983) and Hollowell (1987) find that dredge-up only continues for a few consecutive flashes before “turning off” again, the turn-off being accompanied by a levelling off or even decrease in the flash strength $L_{\text{He}}^{\text{max}}$. This is confirmed by the present work: for both cases, dredge-up of carbon lasted for only one flash, and $L_{\text{He}}^{\text{max}}$ decreased in the next flash for the case $M_i = 1.2 M_{\odot}$, $M_{\text{tot}} \sim 0.8 M_{\odot}$, $\alpha = 3.0$; in the case $M_i = 2.0 M_{\odot}$, $M_{\text{tot}} \sim 1.7 M_{\odot}$, $\alpha = 1.5$, the behavior of $L_{\text{He}}^{\text{max}}$ in subsequent flashes was not smooth (see Fig. 3), but certainly it did not continue to grow as fast as before. It seems probable (though not completely certain) that the levelling off or decrease in $L_{\text{He}}^{\text{max}}$ is due to the increase in Z caused by dredge-up; but the turning off of dredge-up must be due at least in part to the effect of increased metallicity Z and decreased envelope mass M_{env} on T_{CE}^{max} , since $L_{\text{He}}^{\text{max}}$ sharply increased in the first of the subsequent flashes for the $M_i = 2.0 M_{\odot}$ case, but dredge-up nonetheless failed to recur (although it came closer than on the following flashes, when $L_{\text{He}}^{\text{max}}$ was smaller: see Fig. 10*b, c*). It should be noted that the decrease in M_{env} takes place even in the absence of mass loss (though rather more slowly) due to the growth of the core mass M_{H} ; and the effect of a decrease in M_{env} will be greatest if M_{env} is already small, i.e., if the total stellar mass is small. Considering these various factors, one can explain the differing number of dredge-up episodes found in different stellar models. The $0.7 M_{\odot}$ models of Iben (1983) and Hollowell (1987) have small M_{env} and relatively fast increase of Z , and so experience only

3 or 4 dredge-up episodes. The $1.0 M_{\odot}$ models of Iben (1983) have larger M_{env} and slower increase of Z , and so experience 6 to 10 dredge-up episodes. The stars of the present work have very sharp increase of Z , and fast decrease of M_{env} due to mass loss; they thus experience only one dredge-up episode. The $1.5 M_{\odot}$ models of Lattanzio (1987) have large M_{env} , and slow fractional increase in Z (due partly to their larger initial Z values of 0.003 and 0.006); in consequence, they experience at least 7 or 8 dredge-up episodes (and possibly more: computations were terminated at that point). Of course, the number of dredge-up episodes is also affected by the balance between the value of α and the other initial stellar parameters (such as M_i , Y , and Z) which determines how easy it is to get dredge-up in the first place, and thus how great a change is necessary in order to turn it off.

This work was carried out at the W. K. Kellogg Radiation Laboratory. We wish to express our gratitude to Professors R. D. Blandford, C. A. Barnes, S. E. Koonin, and S. C. Frautschi for their encouragement and support; we have also benefitted from valuable discussions with Professors W. A. Fowler J. R. Mould, R. Christy, A. Cox, Z. Barkat, and V. Weidemann.

REFERENCES

- Aaronson, M., and Mould, J. 1982, *Ap. J. Suppl.*, **48**, 161.
———. 1985, *Ap. J.*, **288**, 551.
Bailey, G. M., and Hebbard, D. F. 1963a, *Nucl. Phys.*, **46**, 529.

- . 1963*b*, *Nucl. Phys.*, **49**, 666.
- Baud, B., and Habing, H. J. 1983, *Astron. Astrophys.*, **127**, 73.
- Baudet, G., Petrosian, V., and Salpeter, E. E. 1967, *Ap. J.*, **150**, 979.
- Becker, S. A. 1986, private communication.
- Bertelli, G., Bressan, A. G., and Chiosi, C. 1985, *Astron. Astrophys.*, **150**, 33.
- Blanco, V. M., McCarthy, M., and Blanco, B. M. 1980, *Ap. J.*, **242**, 938.
- Boothroyd, A. I., and Sackmann, I.-J. 1987*a* (Paper I).
- . 1987*b* (Paper II).
- Castellani, V., Chieffi, A., Pulone, L., and Tornambè, A. 1985*a*, *Ap. J. (Letters)*, **294**, L31.
- . 1985*b*, *Ap. J.*, **296**, 204.
- Caughlan, G. R., Fowler, W. A., Harris, M. J., and Zimmerman, B. A. 1985, *Atomic Data and Nuclear Data Tables*, **32**, 197. (CFHZ IV)
- Chan, K. L., Wolff, C. L., and Sofia, S. 1981, *Ap. J.*, **244**, 582.
- Christy-Sackmann, I.-J., and Paczyński, B. 1975, in *Proc. 19th Internat. Colloquium on Stellar Hydrodynamics, Liège*, ed. M. Gabriel, p. 335.
- Cohen, E. G. D., and Murphy, T. J. 1969, *Phys. Fluids*, **12**, 1404.
- Cox, J. P., and Giuli, R. T. 1968, *Principles of Stellar Structure* (New York: Gordon & Breach).
- Despain, K. H. 1981, *Ap. J.*, **251**, 639.
- Deupree, R. G. 1979, *Ap. J.*, **234**, 228.
- . 1984, *Ap. J.*, **287**, 268.
- Deupree, R. G., and Varner, T. M. 1980, *Ap. J.*, **237**, 558.

- Dicus, D. A. 1972, *Phys. Rev.*, **D6**, 941.
- Fedeyev, Yu. A. 1982, *Astrophys. Space Sci.*, **86**, 143.
- Fowler, W. A. 1986, private communication.
- Fowler, W. A., Caughlan, G. R., and Zimmerman, B. A. 1967, *Ann. Rev. Astron. Astrophys.*, **5**, 525. (FCZ I)
- . 1975, *Ann. Rev. Astron. Astrophys.*, **13**, 69. (FCZ II)
- Frogel, J. A., Persson, S. E., and Cohen, J. G. 1980, *Ap. J.*, **239**, 495.
- Grevesse, N. 1984, *Physica Scripta*, **T8**, 49.
- Harpaz, A., and Kovetz, A. 1981, *Astron. Astrophys.*, **93**, 200.
- Harris, M. 1986, private communication.
- Harris, M. J., Fowler, W. A., Caughlan, G. R., and Zimmerman, B. A. 1983, *Ann. Rev. Astron. Astrophys.*, **21**, 165. (HFCZ IV)
- Hollowell, D. E. 1986, preprint.
- . 1987, private communication.
- Iben, I., Jr. 1975, *Ap. J.*, **196**, 525.
- . 1976, *Ap. J.*, **208**, 165.
- . 1981, *Ap. J.*, **246**, 278.
- . 1982, *Ap. J.*, **260**, 821.
- . 1983, *Ap. J. (Letters)*, **275**, L65.
- Iben, I., Jr., and Renzini, A. 1982a, *Ap. J. (Letters)*, **259**, L79.
- . 1982b, *Ap. J. (Letters)*, **263**, L23.
- . 1983, *Ann. Rev. Astron. Astrophys.*, **21**, 271.
- Iben, I., Jr., and Truran, J. W. 1978, *Ap. J.*, **220**, 980.

- Ichimaru, S. 1982, *Rev. Mod. Phys.*, **54**, 1017.
- Ichimaru, S., and Utsumi, K. 1983, *Ap. J. (Letters)*, **269**, L51.
- Itoh, N., and Kohyama, Y. 1983, *Ap. J.*, **275**, 858.
- Itoh, N., Totsuji, H., Ichimaru, S., and DeWitt, H. E. 1979, *Ap. J.*, **234**, 1079.
- . 1980, *Ap. J.*, **239**, 415.
- Keady, J. 1985, private communication.
- Kudritzki, R. P., and Reimers, D. 1978, *Astron. Astrophys.*, **70**, 227.
- Kutter, G. S., and Sparks, W. M. 1974, *Ap. J.*, **192**, 447.
- Lattanzio, J. C. 1986, *Ap. J.*, **311**, 708.
- . 1987, *Ap. J. (Letters)*, **313**, L15.
- Malaney, R. A., and Boothroyd, A. I. 1986, preprint OAP-667 (to be published in *Ap. J.*, Sept. 15, 1987).
- Miller, G. E., and Scalo, J. 1982, *Ap. J.*, **263**, 259.
- Moore, C. E. 1970, *Selected Tables of Atomic Spectra, Nat. Stand. Ref. Data Ser., Nat. Bur. Stand. (U.S.)*, **3**, Sec. 3 (Washington: U.S. Government Printing Office).
- . 1971, *Atomic Energy Levels, Nat. Stand. Ref. Data Ser., Nat. Bur. Stand. (U.S.)*, **35**, Vol. I (Washington: U.S. Government Printing Office). (Reprint of *NBS Circular*, **467**, Vol. I.)
- Mould, J., and Aaronson, M. 1979, *Ap. J.*, **232**, 427.
- . 1982, *Ap. J.*, **263**, 629.
- Munkata, H., Kohyama, Y., and Itoh, N. 1985, *Ap. J.*, **296**, 197.
- Paczynski, B. 1969, *Acta Astr.*, **19**, 1.

- . 1970a, *Acta Astr.*, **20**, 47.
- . 1970b, *Acta Astr.*, **20**, 195.
- . 1974, *Ap. J.*, **192**, 483.
- . 1975, *Ap. J.*, **202**, 558.
- . 1977, *Ap. J.*, **214**, 812.
- Reimers, D. 1975, in *Problems in Stellar Atmospheres and Envelopes*, ed. B. Baschek, W. H. Kegel, and G. Traving (New York: Springer-Verlag), p. 229.
- Renzini, A. 1977, in *Advanced Stages in Stellar Evolution*, ed. P. Bouvier and A. Maeder (Sauverny: Geneva Observatory), p. 149.
- . 1981, in *Effects of Mass Loss on Stellar Evolution*, ed. C. Chiosi and R. Stalio (Dordrecht: Reidel), p. 319.
- Renzini, A., and Voli, M. 1981, *Astron. Astrophys.*, **94**, 175.
- Richer, H. B. 1981, *Ap. J.*, **243**, 744.
- Rolfs, C. 1986, private communication.
- Rood, R. T. 1972, preprint OAP-279.
- Ross, J. E., and Aller, L. H. 1976, *Science*, **191**, 1223.
- Sackmann, I.-J. 1976, preprint OAP-463.
- . 1980a, *Ap. J.*, **235**, 554.
- . 1980b, *Ap. J. (Letters)*, **241**, L37.
- Sackmann, I.-J., and Boothroyd, A. I. 1985, *Ap. J.*, **293**, 154.
- Salpeter, E. E. 1954, *Australian J. Phys.*, **7**, 353.
- Scalo, J., and Miller, G. E. 1981, *Ap. J.*, **246**, 251.
- Schönberner, D. 1979, *Astron. Astrophys.*, **79**, 108.

- Schröder, U., Becker, H. W., Bogaert, G., Görres, J., Rolfs, C., Trautvetter, H. P., Azuma, R. E., and King, J. D. 1986, draft manuscript.
- . 1987, submitted to *Nucl. Phys.*
- Slattery, W. L., Doolan, G. D., and DeWitt, H. E. 1980, *Phys. Rev.*, **A21**, 2087.
- Smith, R. L., and Rose, W. K. 1972, *Ap. J.*, **176**, 395.
- Sparks, W. M., and Kutter, G.S. 1972, *Ap. J.*, **192**, 447.
- Steigman, G. 1985, in *Nucleosynthesis: Challenges and New Developments*, ed. W. D. Arnett and J. W. Truran (Chicago: University of Chicago Press), p. 48.
- Sugimoto, D., and Nomoto, K., 1975, *Pub. Astr. Soc. Japan*, **27**, 197.
- Tuchman, Y. 1984, *M. N. R. A. S.*, **208**, 215.
- Tuchman, Y., Sack, N., and Barkat, Z. 1978, *Ap. J.*, **219**, 183.
- . 1979, *Ap. J.*, **234**, 217.
- Weidemann, V. 1984, *Astron. Astrophys. (Letters)*, **134**, L1.
- Weidemann, V. and Koester, D. 1983, *Astron. Astrophys.*, **121**, 77.
- Werner, M. W., Beckwith, S., Gatley, I., Sellgren, K., and Berriman, G. 1980, *Ap. J.*, **239**, 540.
- Wood, P. R. 1974, *Ap. J.*, **190**, 609.
- . 1981a, *Ap. J.*, **248**, 311.
- . 1981b, in *Physical Processes in Red Giants*, ed. I. Iben Jr. and A. Renzini (Dordrecht: Reidel), p. 135.
- Wood, P. R., and Cahn, J. H. 1977, *Ap. J.*, **211**, 499.
- Wood, P. R., and Zarro, D. M. 1981, *Ap. J.*, **247**, 247.

Table 1

Pre-AGB Evolutionary Timescales, in Gigayears

M_i/M_\odot :	0.8	1.0	1.2	2.0	3.0	1.2	3.0	3.0n ^a
Z:	0.001	0.001	0.001	0.001	0.001	0.02	0.02	0.02
$t(A)$:	0.000	0.000	~0.010	~0.0028	~0.0008	~0.031	~0.0067	~0.0060
$t(B)$:	—	—	—	0.5790	0.2216	—	0.2847	0.2857
$t(C)$:	14.196	5.889	2.922	0.6007	0.2291	4.194	0.2992	0.3057
$t(D)$:	15.570	6.903	3.654	0.6899	0.2421	6.072	0.3140	0.3196
$t(E)$:	16.11 ^b	7.227	3.852	0.7495	0.2428	6.689	0.3177	0.3237
$t(F)$:	—	7.296	3.922	0.8272	0.2989	6.777	0.4311	0.4517
$t(G)$:	—	7.330	3.963	0.8619	0.3142	6.817	0.4683	0.4819
$t(H)$:	—	7.345	3.974	0.8676	0.3169	6.838	0.4803	0.4973

^a With the high CNO-rate.

^b Time of leaving RGB.

Table 2

Pre-Flash Mass Loss from Reimers Wind^a

M_i/M_\odot :	0.8	1.0	1.2	2.0	3.0	1.2	3.0	3.0n ^b
Z:	0.001	0.001	0.001	0.001	0.001	0.02	0.02	0.02
η :	0.4	0.4	0.4	0.4	1.4	0.4	1.4	1.4
$M_{\text{tot}}(E)/M_\odot$:	0.471 ^c	0.760	1.033	1.959	3.000	0.855	2.997	2.996
$M_{\text{tot}}(F)/M_\odot$:	—	0.753	1.025	1.959	2.998	0.844	2.964	2.962
$M_{\text{tot}}(G)/M_\odot$:	—	0.750	1.018	1.958	2.998	0.839	2.950	2.952
$M_{\text{tot}}(H)/M_\odot$:	—	0.708	0.986	1.927	2.735	0.752	2.893	2.873
$\Delta M(D \rightarrow E)$:	41% ^c	24%	14%	2.1%	0%	29%	0.1%	0.1%
$\Delta M(E \rightarrow F)$:	—	0.6%	0.7%	0%	0.06%	1.0%	1.1%	1.1%
$\Delta M(F \rightarrow G)$:	—	0.3%	0.5%	0.04%	0%	0.4%	0.5%	0.3%
$\Delta M(G \rightarrow H)$:	—	4.3%	2.7%	1.6%	8.8%	7.3%	1.9%	2.6%
$\Delta M(A \rightarrow H)$:	—	29%	18%	3.7%	8.8%	37%	3.6%	4.2%

^a Likely a factor of 2 overestimate for low mass stars: see Section IIIa.

^b With the high CNO-rate.

^c Final mass after leaving RGB.

Table 3

Helium Core Flash and Resulting Core Carbon Production

M_i/M_\odot :	1.0	1.2	2.0	1.2
Z :	0.001	0.001	0.001	0.02
$\log(L/L_\odot)$:	3.305	3.302	3.065	3.4232
M_{bol} :	-3.49	-3.48	-2.89	-3.81
M_{H}/M_\odot :	0.473	0.471	0.438	0.453
$\log(L_{\text{He}}^{\text{max}}/L_\odot)$:	10.52	10.46	9.24	9.91
$\log(L_{\text{He}}^{\text{min}}/L_\odot)$:	0.72	0.75	0.74	0.74
$\Delta t_{\text{max} \rightarrow \text{min}}$ (yr):	1.3×10^5	1.2×10^5	1.1×10^5	2.9×10^5
resulting Y_c :	0.968	0.970	0.976	0.952
resulting C_c :	0.031	0.029	0.023	0.028

Table 4

Breathing Pulses and Final Core Carbon and Oxygen Abundances

M_i/M_\odot :	1.0	1.2	2.0	3.0	1.2	3.0	3.0n ^a
Z :	0.001	0.001	0.001	0.001	0.02	0.02	0.02
n_{bp} :	0	2	1	0 ^b	0 ^b	0 ^b	0 ^b
C_c :	0.23	0.16	0.16	0.23	0.21	0.20	0.20
O_c :	0.77	0.84	0.84	0.77	0.76	0.78	0.77

^a With the high CNO-rate.

^b Breathing pulses suppressed (to obtain numerical convergence).

Table 5

Stellar Conditions at the First Helium Shell Flash

M_i/M_\odot :	1.0	1.2	2.0	3.0	1.2	3.0	3.0n ^a
Z :	0.001	0.001	0.001	0.001	0.02	0.02	0.02
initial Y :	0.24	0.24	0.24	0.24	0.27	0.27	0.27
η :	0.4	0.4	0.4	1.4	0.4	1.4	1.4
M_{tot}/M_\odot :	0.708	0.986	1.927	2.735	0.752	2.893	2.873
M_{H}/M_\odot :	0.513	0.530	0.606	0.778	0.508	0.543	0.546
M_{env}/M_\odot :	0.185	0.456	1.321	1.957	0.244	2.350	2.327
age t (Gyr):	7.345	3.974	0.868	0.317	6.838	0.480	0.497
$Y_{\text{env}}^{\text{b}}$:	0.262	0.264	0.257	0.246	0.293	0.280	0.281
$C_{\text{env}}/Z^{\text{b}}$:	0.14	0.14	0.11	0.12	0.17	0.13	0.14
$O_{\text{env}}/Z^{\text{b}}$:	0.47	0.48	0.47	0.47	0.48	0.46	0.47
$\log(L/L_\odot)$:	3.123	3.201	3.597	3.964	3.184	3.397	3.446
M_{bol} :	-3.04	-3.23	-4.22	-5.14	-3.19	-3.72	-3.84
$\log(L_{\text{He}}^{\text{max}}/L_\odot)$:	4.74	4.50	4.89	4.55	4.23	4.62	4.45

^a With the high CNO-rate.

^b Mass fractions: resulting from “first dredge-up” on the RGB.

Table 6

Final Masses M_f on the AGB: Reimers Wind and the $M_i - M_f$ Relation

initial mass M_i/M_\odot	Z	η	flashes begin at: M_H/M_\odot	Reimers wind: M_f/M_\odot	reduced wind ^a : M_f/M_\odot	$M_i - M_f$ relation ^b : M_f/M_\odot
1.0	0.001	0.4	0.513	0.54	~ 0.58	$\sim 0.57^c$
1.2	0.001	0.4	0.530	0.59	~ 0.63	$\sim 0.64^c$
2.0	0.001	0.4	0.606	~ 0.77	~ 0.85	$\sim 0.72^c$
3.0	0.001	1.4	0.778	~ 0.85	~ 0.9	$\sim 0.75^c$
1.2	0.02	0.4	0.508	0.53	~ 0.59	$\sim 0.57^d$
3.0	0.02	1.4	0.543	0.67	~ 0.73	$\sim 0.65^d$

^a Estimates from Figure 4, assuming mass loss rate reduced by a factor of 2.

^b Observationally determined; discovered by Weidemann and Koester (1983).

^c From SMC and LMC data of Aaronson and Mould (1985): see text.

^d From Schönberner's NPN relation, in Weidemann (1984): see text.

FIGURE CAPTIONS

Fig. 1.—Evolution in the H-R diagram for stars of metallicity $Z = 0.001$. The marked points are as follows: P: pre-main-sequence starting point for the run; A: zero age main sequence point (circled); B: red edge of main sequence; C: hydrogen core exhaustion; D: base of red giant branch; E: tip of red giant branch (circled); F: blue edge of loops during core helium burning; G: core helium exhaustion; H: first helium shell flash. Continuous lines follow pre-flash evolution; after helium shell flashes begin, only the (maximum) interflash luminosity maximum is plotted. (a): Stars of initial masses $0.8 M_{\odot}$, $1.0 M_{\odot}$, and $3.0 M_{\odot}$. (b): Stars of initial masses $0.8 M_{\odot}$, $1.2 M_{\odot}$, and $2.0 M_{\odot}$.

Fig. 2.—Evolution in the H-R diagram for stars of metallicity $Z = 0.02$, with initial masses $1.2 M_{\odot}$ and $3.0 M_{\odot}$. The dotted curve shows the pre-flash evolution of the $3.0 M_{\odot}$ star where the high CNO-burning rate was used; otherwise, as in Fig. 1.

Fig. 3.—The peak flash helium-burning energy generation rate $L_{\text{He}}^{\text{max}}$ for each flash; note the linear scale. Solid lines are used for stars having $Z = 0.001$, dotted lines for stars having $Z = 0.02$. The dot-dashed line follows the star of initial mass $2.0 M_{\odot}$ and initial $Z = 0.001$, with α increased to 1.5; note the effect of dredge-up.

Fig. 4.—The average mass loss rate over each flash cycle, between one flash and the next. Note that stars of $M_i = 3.0 M_\odot$ have $\eta = 1.4$, the rest having $\eta = 0.4$. Solid lines correspond to $\alpha = 1.0$, dotted lines to $\alpha = 1.5$ ($Z = 0.001$, $1.2 M_\odot$ and $2.0 M_\odot$ stars), and the dashed line to $\alpha = 2.0$ ($Z = 0.001$, $1.2 M_\odot$ only). Note the reduction in mass loss rate caused by increasing α , and the increase in mass loss rate caused by the increased metallicity due to dredge-up (in the $2.0 M_\odot$ case).

Fig. 5.—The mass loss during flashes: the star's total mass M_{tot} is plotted at each flash; solid, dotted, and dashed lines correspond to α values of 1.0, 1.5, and 2.0 as in Fig. 4. Note that changing the mixing length α changes the mass loss rate, as does the change in metallicity caused by dredge-up.

Fig. 6.—The core mass–base temperature ($M_c - T_b$) relation, where T_b is actually T_b^{max} , the maximum temperature at the base of the flash-driven intershell convective zone, and $M_c \equiv M_H$. The solid lines follow the evolution of stars of metallicity $Z = 0.001$, while the dotted lines follow the evolution of stars of metallicity $Z = 0.02$. The dashed lines are $M_c - T_b$ relations: IT: the Iben and Truran (1978) relation; MB: the Malaney and Boothroyd (1986) relation.

Fig. 7.—The flash-produced intershell abundances of He, C, and ^{16}O at the upper edge of the carbon pocket (the region mixed by the flash-driven intershell convection). (a): For stars of metallicity $Z = 0.001$. (b): For stars of metallicity $Z = 0.02$.

Fig. 8.—The flash-produced intershell ^{18}O abundances at the tip of the carbon pocket, relative to the stars' (initial) metallicities. Note the logarithmic scale: ^{18}O disappears very quickly as flash strength grows.

Fig. 9.—The core mass–interflash period ($M_c - \tau_{if}$) relations (note $M_c \equiv M_H$). The solid lines marked $Z = 0.001$ and $Z = 0.02$ are the fits (described in the text) to the data for stars of these metallicities, with the alternate $Z = 0.001$ (low core mass fit) being indicated by long dashes. P (dashed) marks the Paczyński (1975) $M_c - \tau_{if}$ relation, WZ (short dashes) the Wood and Zarro (1981) relation, L₁ (dotted) the Lattanzio (1986) Population I relation, and L₂ (dotted) the Lattanzio (1986) relation for $Y_{\text{env}} = 0.24$, $Z = 0.001$.

Fig. 10.—The behavior of flash-driven intershell convection and post-flash envelope convection in each flash (as a function of core mass) for the stars of metallicity $Z = 0.001$. The convective boundaries are given in terms of the difference in mass between their positions M_r and the position M_H of the H-He discontinuity (note that the core mass M_c is identified with M_H). The reference point $M_r - M_H = 0$ is marked with a dotted line. (a): The solid lines, from the bottom up, mark respectively the points M_{He} (the point where the helium abundance goes to zero), M_{Cb}^{min} (the innermost extent of the base of flash-driven intershell convection), and M_{Cis}^{max} (the outermost extent of flash-driven intershell convection); the dashed lines at the top mark M_{CE}^{min} (the innermost extent of envelope convection at the post-flash luminosity maximum). (b): An expanded view of M_{Cis}^{max} and M_{CE}^{min} ; note the

dredge-up point where the envelope convection (M_{CE}^{\min}) dips deeply into the carbon pocket left behind by flash-driven intershell convection (M_{Cis}^{\max}). (c): A further expanded view. The dotted lines indicate the innermost extent M_{sc}^{\min} and outermost extent M_{sc}^{\max} of the semiconvective region which comes into existence at the tip of the carbon pocket during the post-flash luminosity maximum (so that $M_{sc}^{\min} < M_{Cis}^{\max} < M_{sc}^{\max}$); note that this semiconvective region sometimes reaches into a region where hydrogen is present (in small amounts).

Fig. 11.—The same as Fig. 10, but for the stars of metallicity $Z = 0.02$. Note that there is *no* semiconvection at the tip of carbon pocket.

Fig. 12.—Dredge-up for the star of initial mass $2.0 M_{\odot}$ and metallicity $Z = 0.001$, occurring on the 11th flash after the mixing length was increased to $\alpha = 1.5$. The solid lines indicate the boundaries of the flash-driven intershell convective region and the base M_{CE} of the envelope convective region, plotted as a function of time. The dotted line indicates the H-He discontinuity M_H .

Fig. 13.—Dredge-up for the star of initial mass $1.2 M_{\odot}$ and metallicity $Z = 0.001$, occurring on the 6th flash when the mixing length was increased to $\alpha = 3.0$; otherwise the same as Fig. 12.

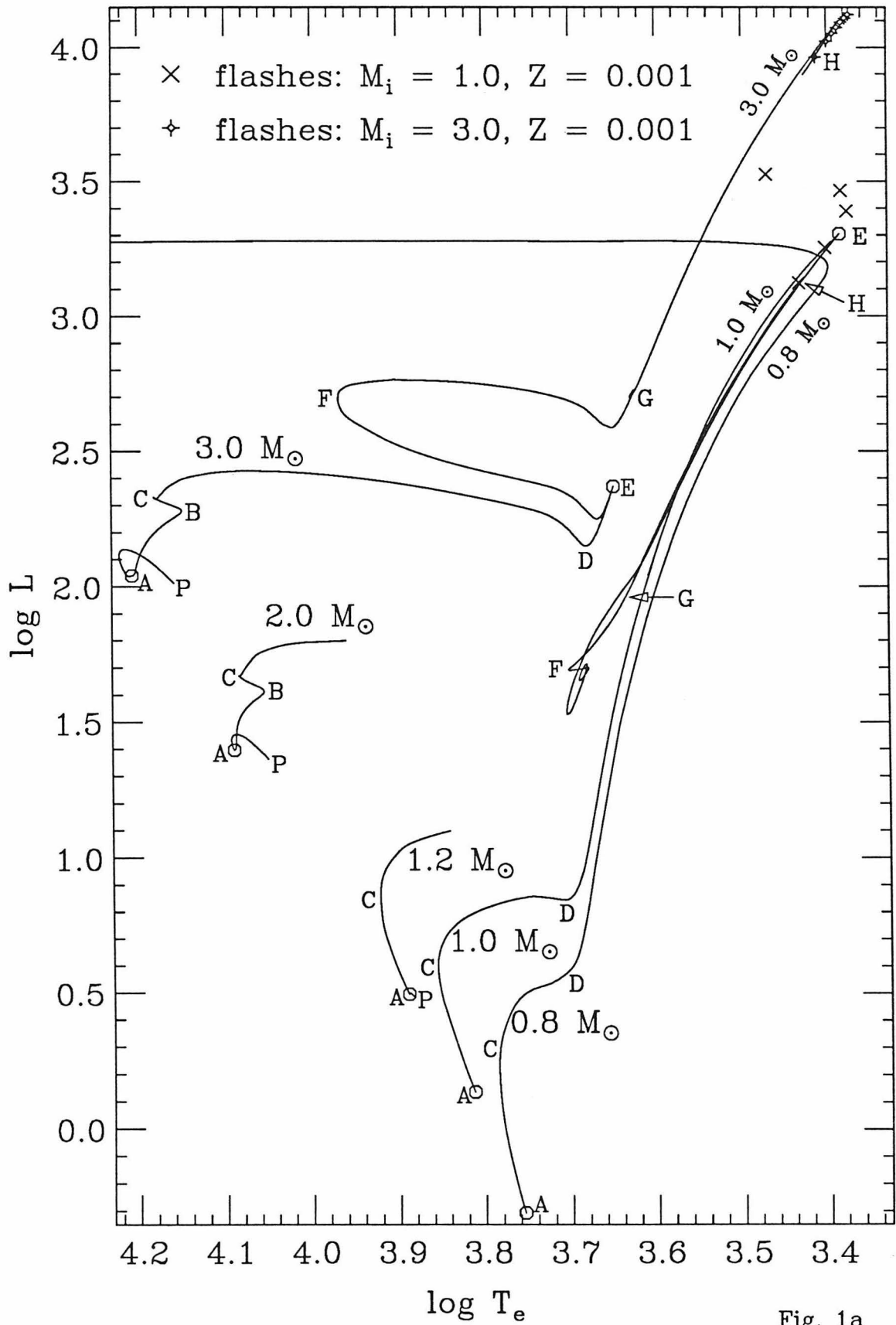


Fig. 1a

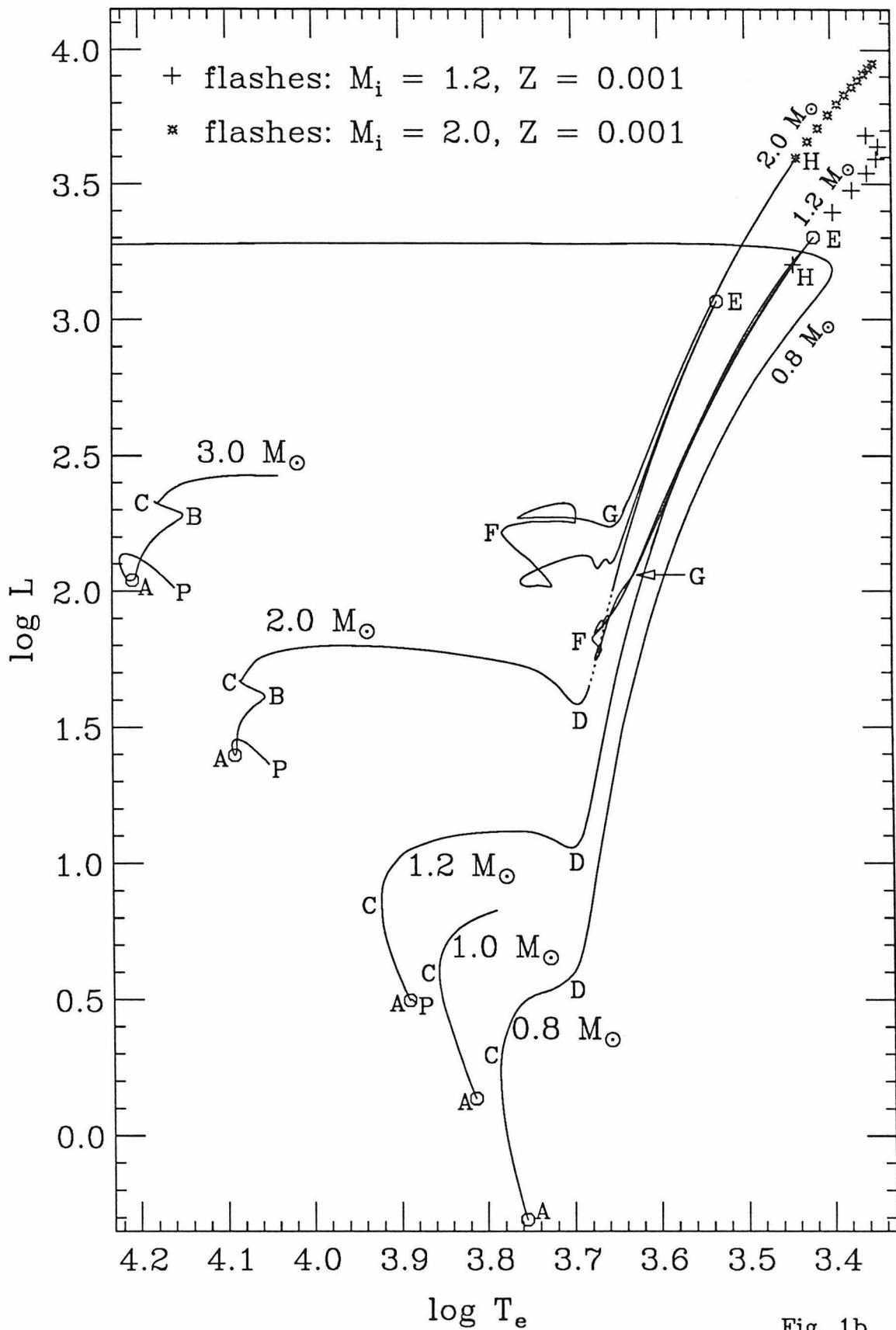


Fig. 1b

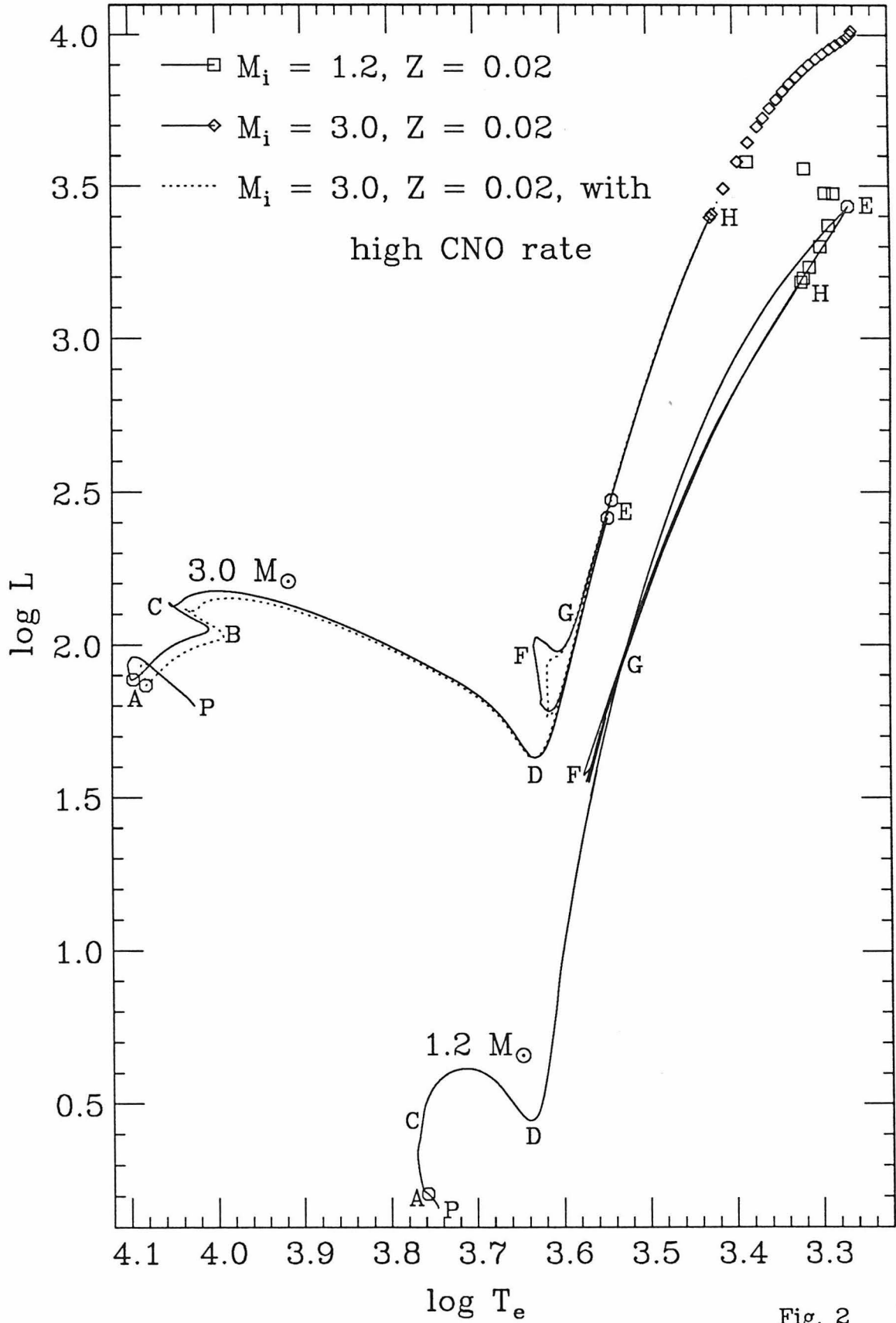


Fig. 2

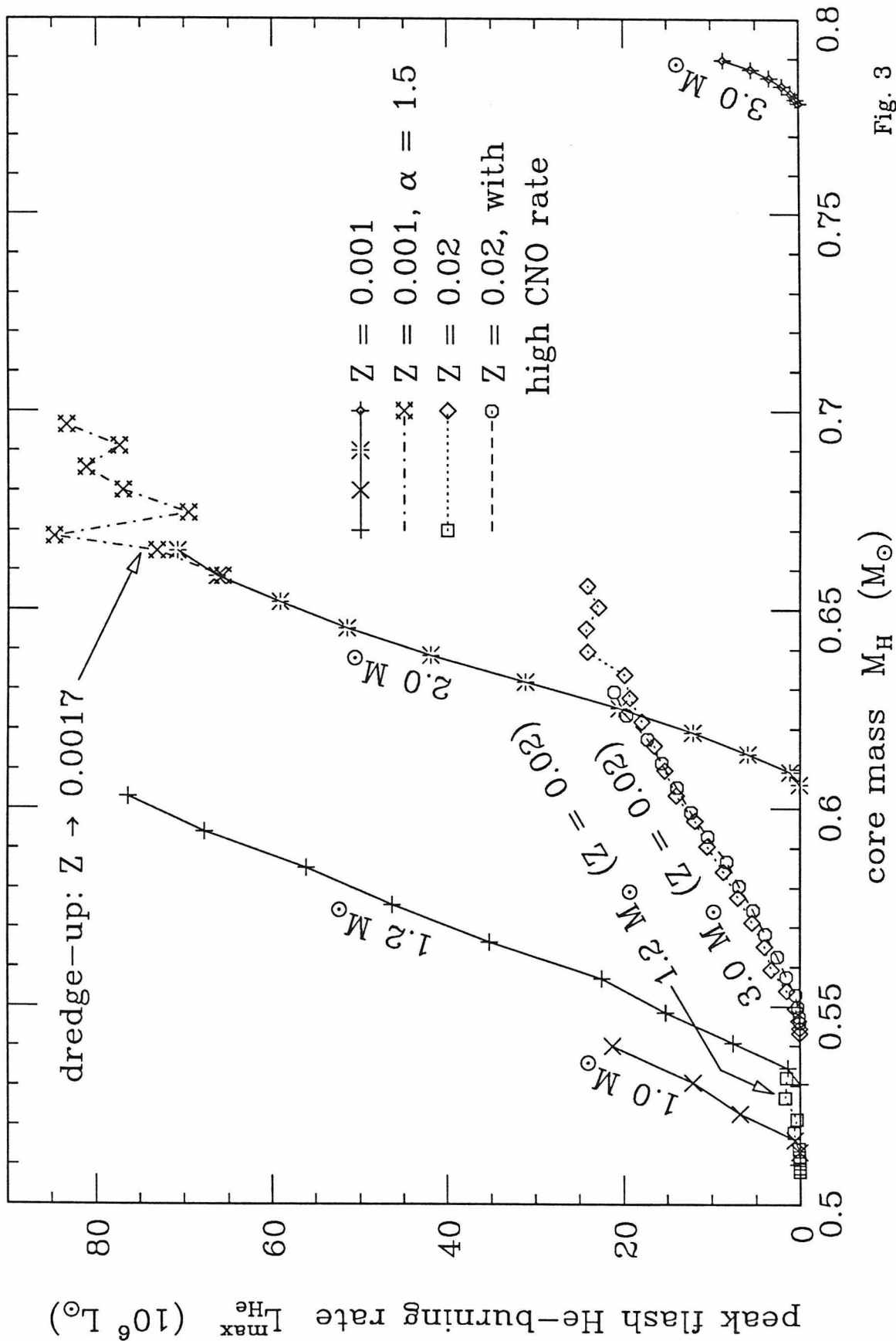


Fig. 3

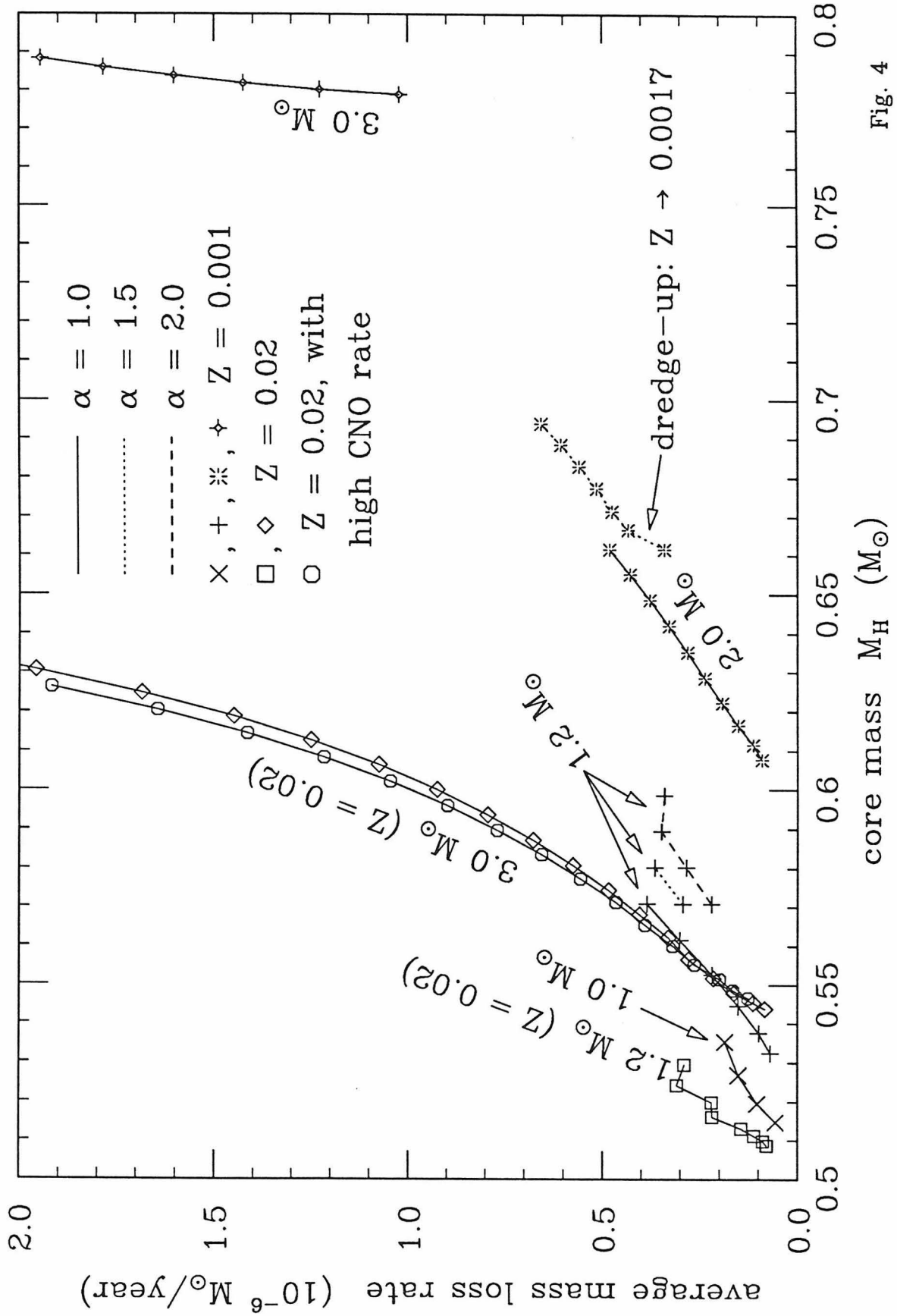


Fig. 4

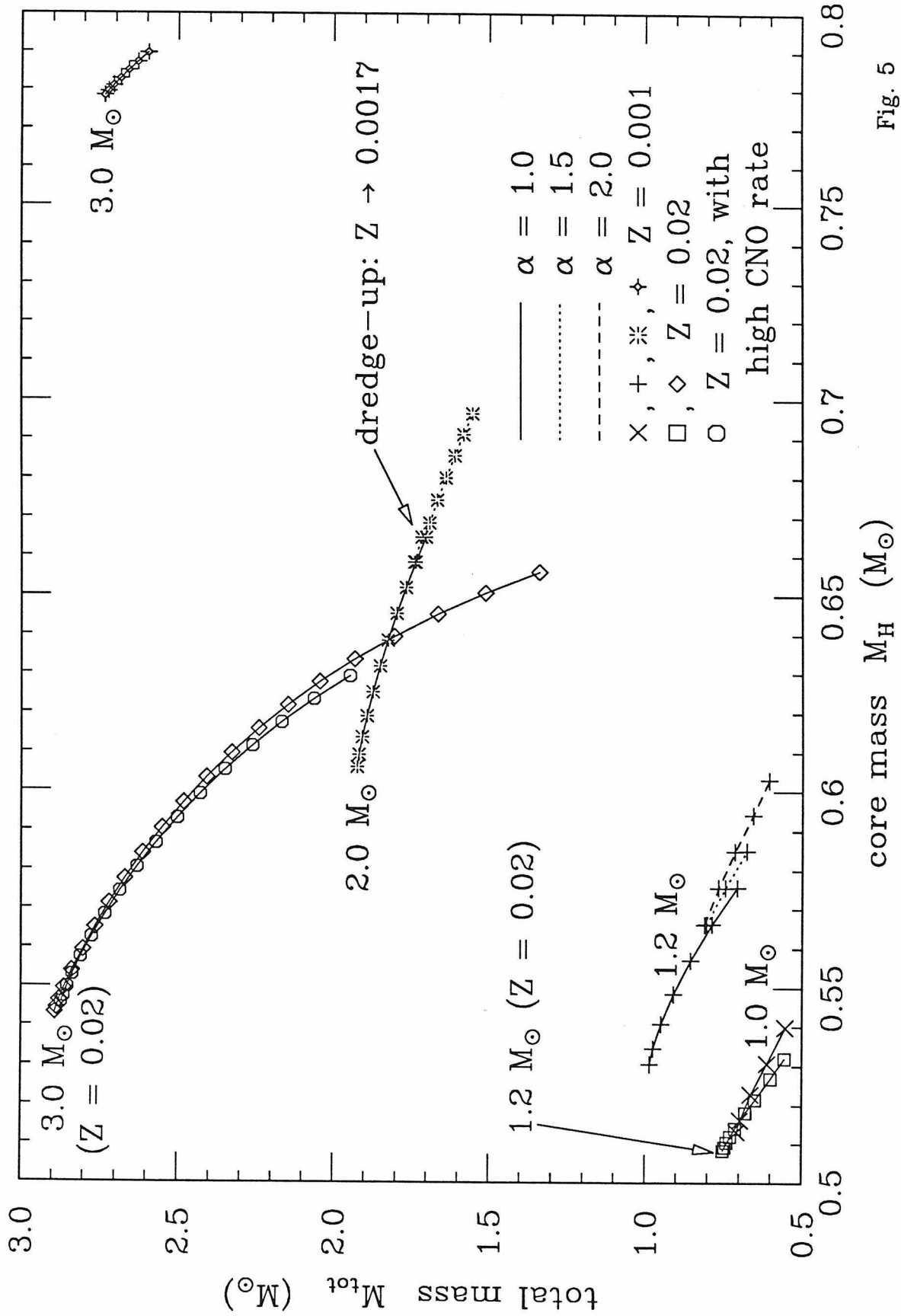


Fig. 5

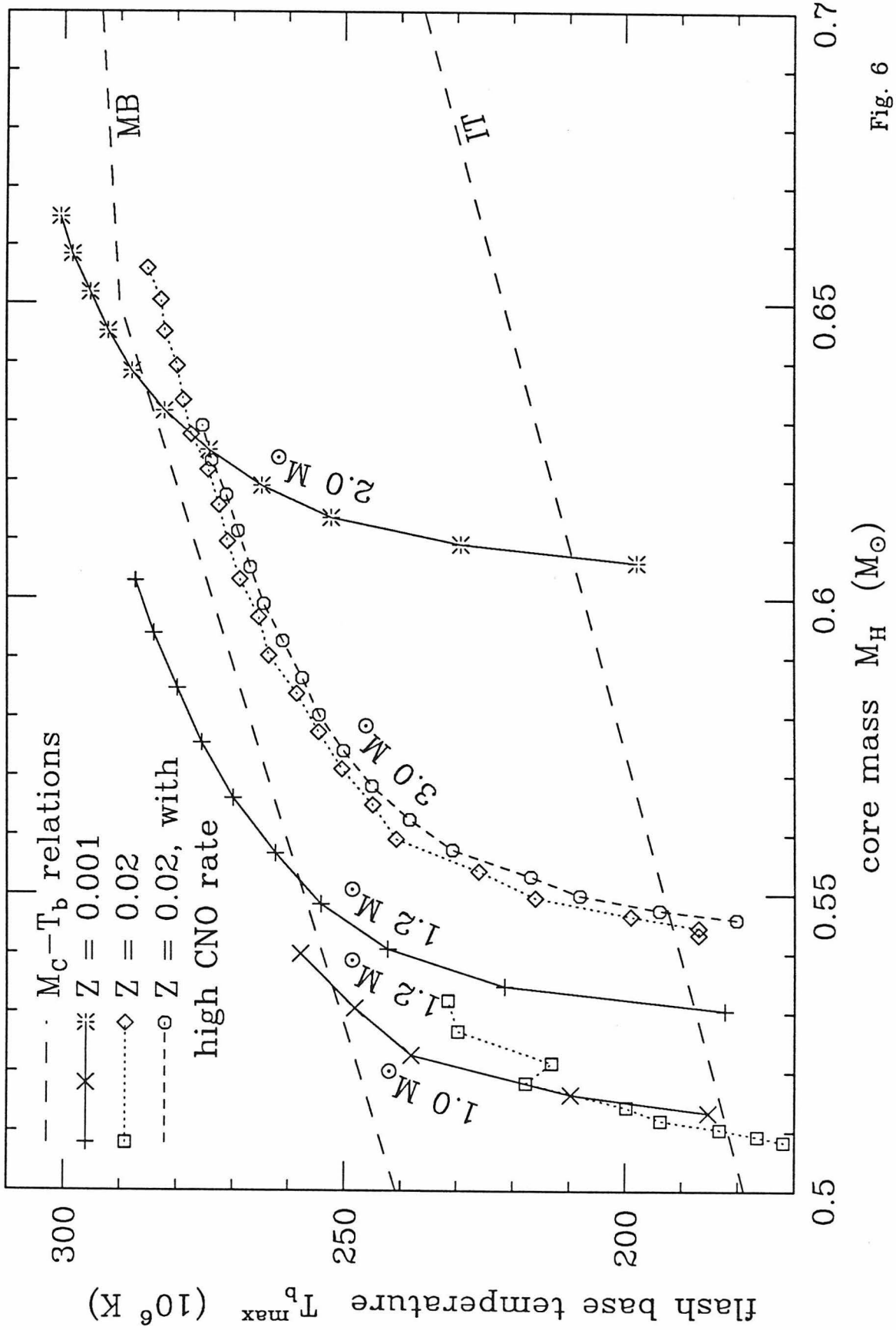


Fig. 6

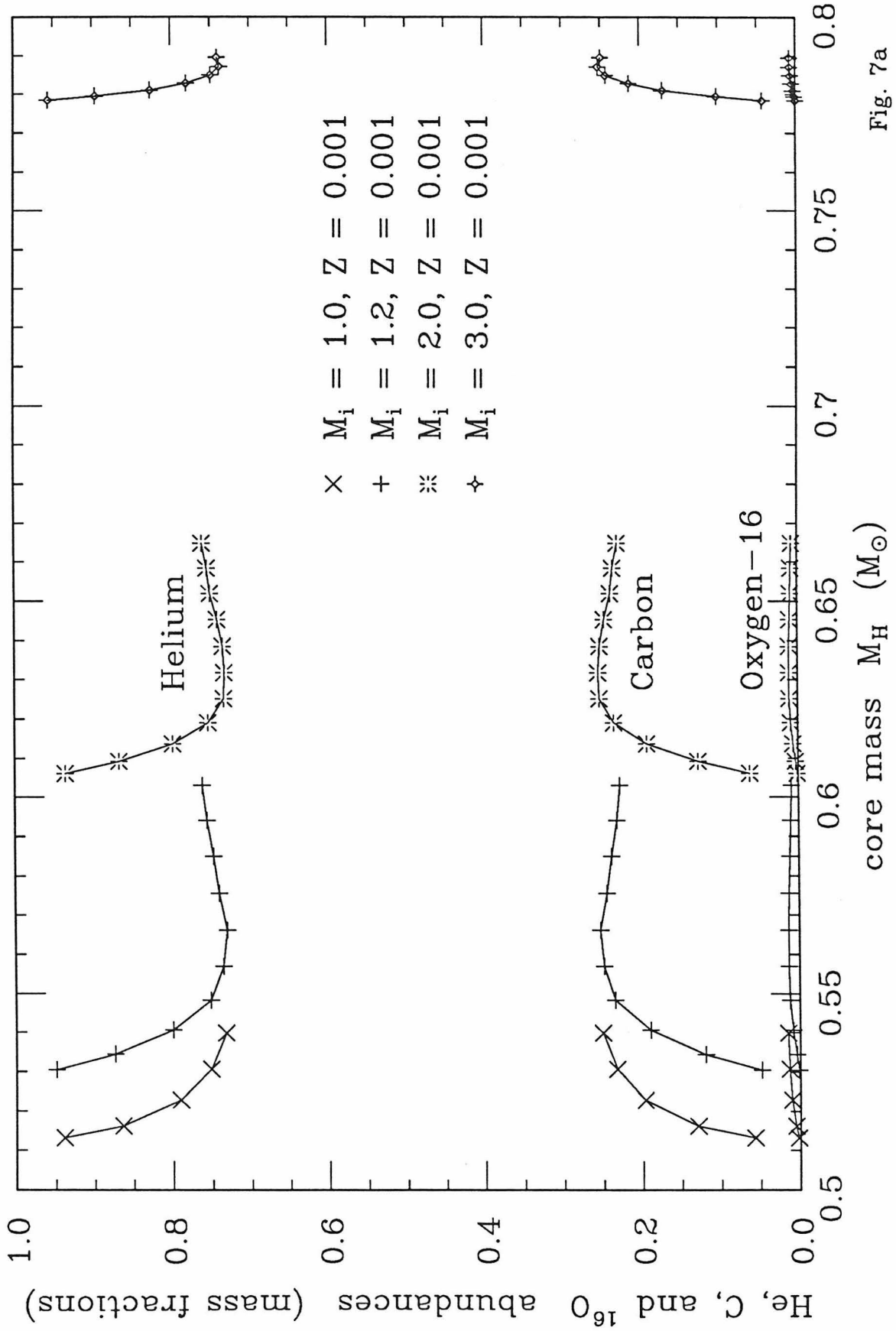


Fig. 7a

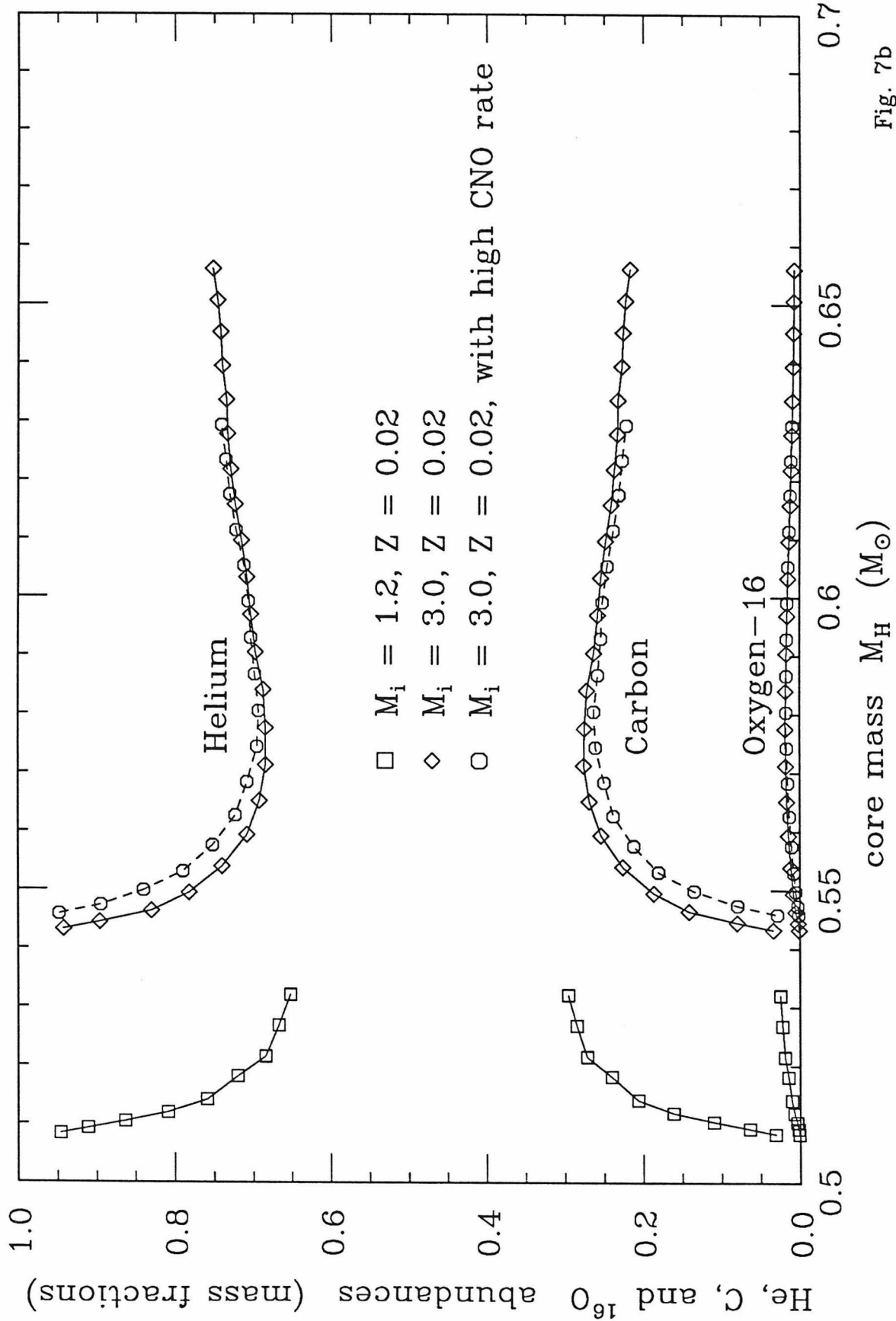


Fig. 7b

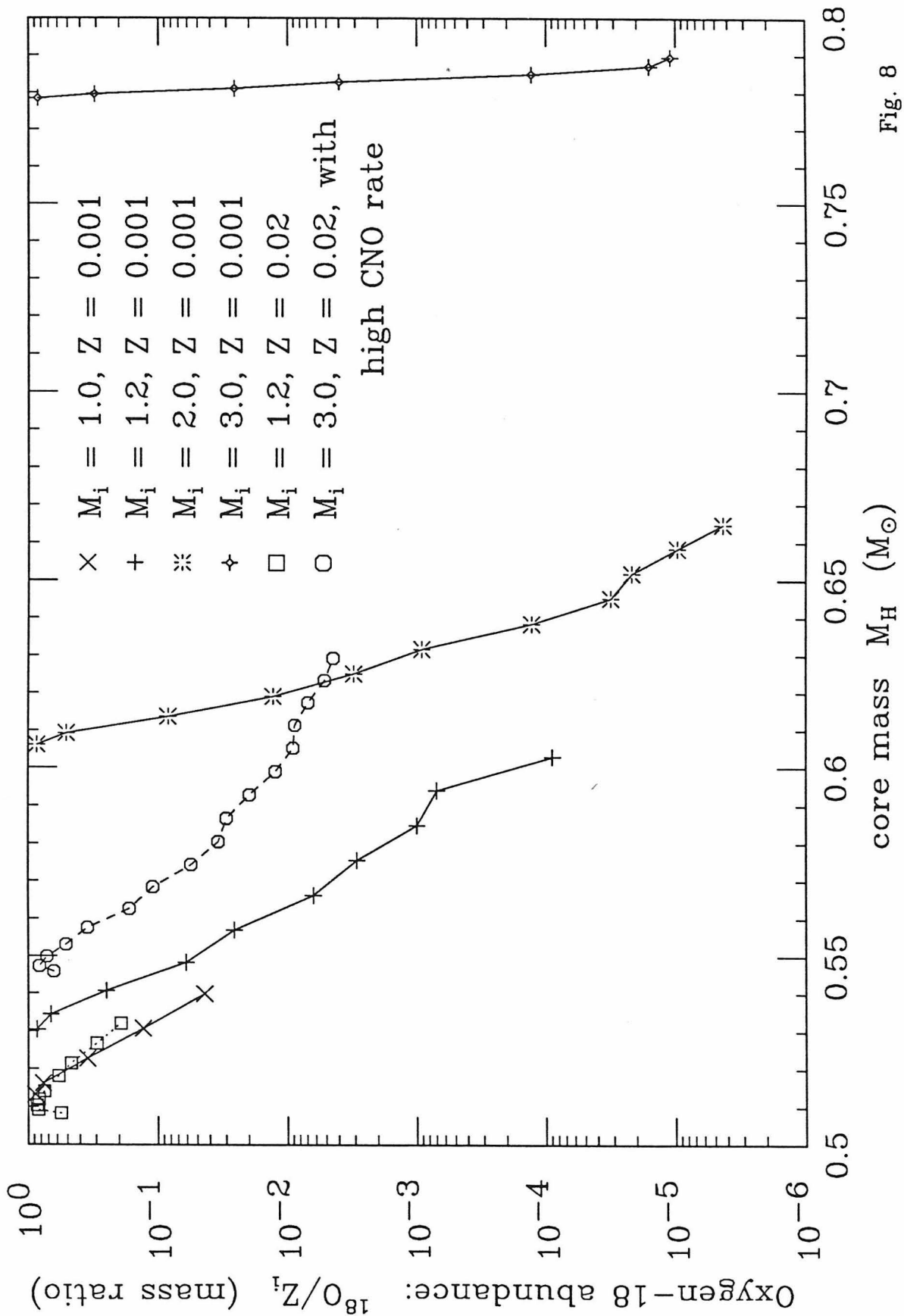


Fig. 8

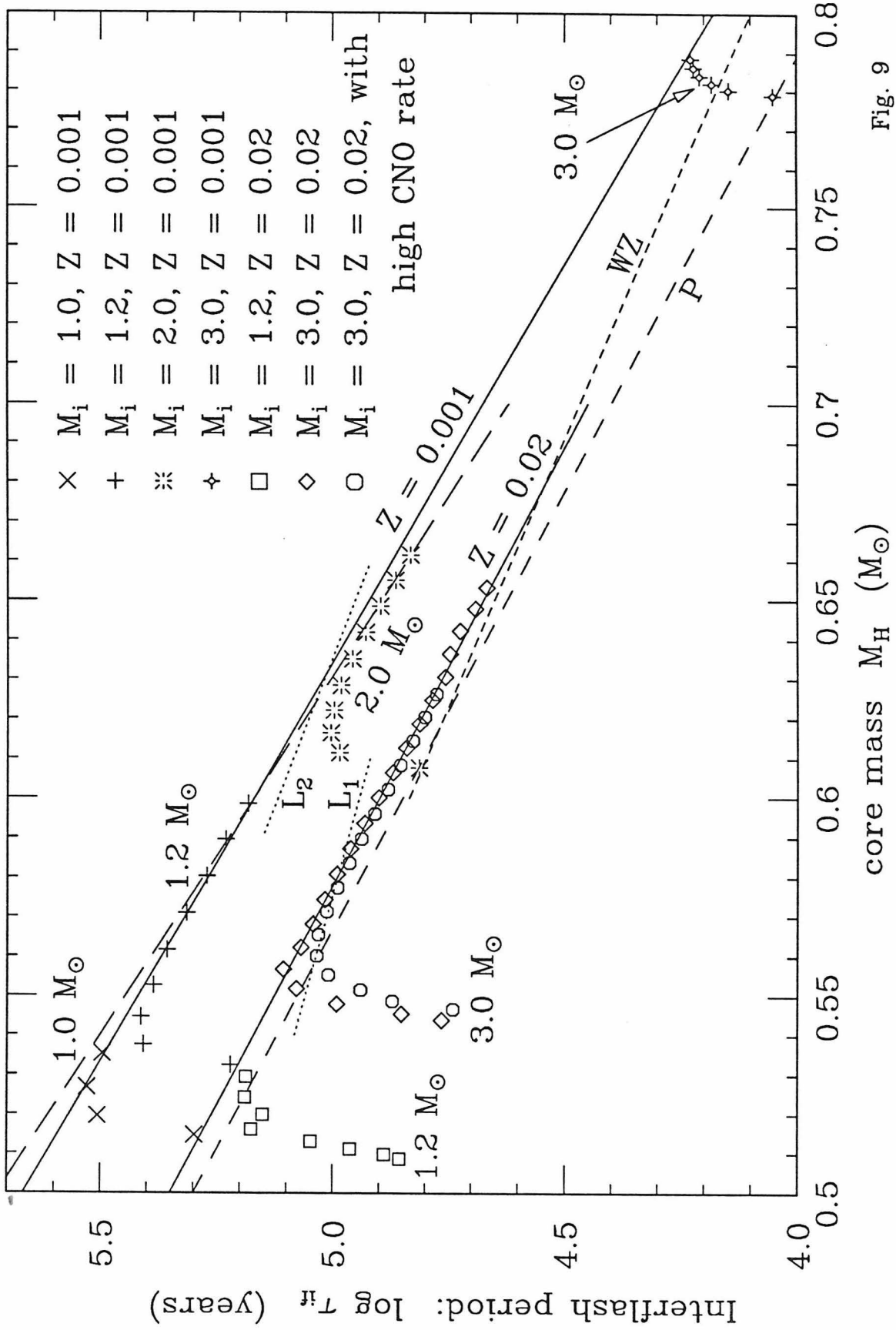


Fig. 9

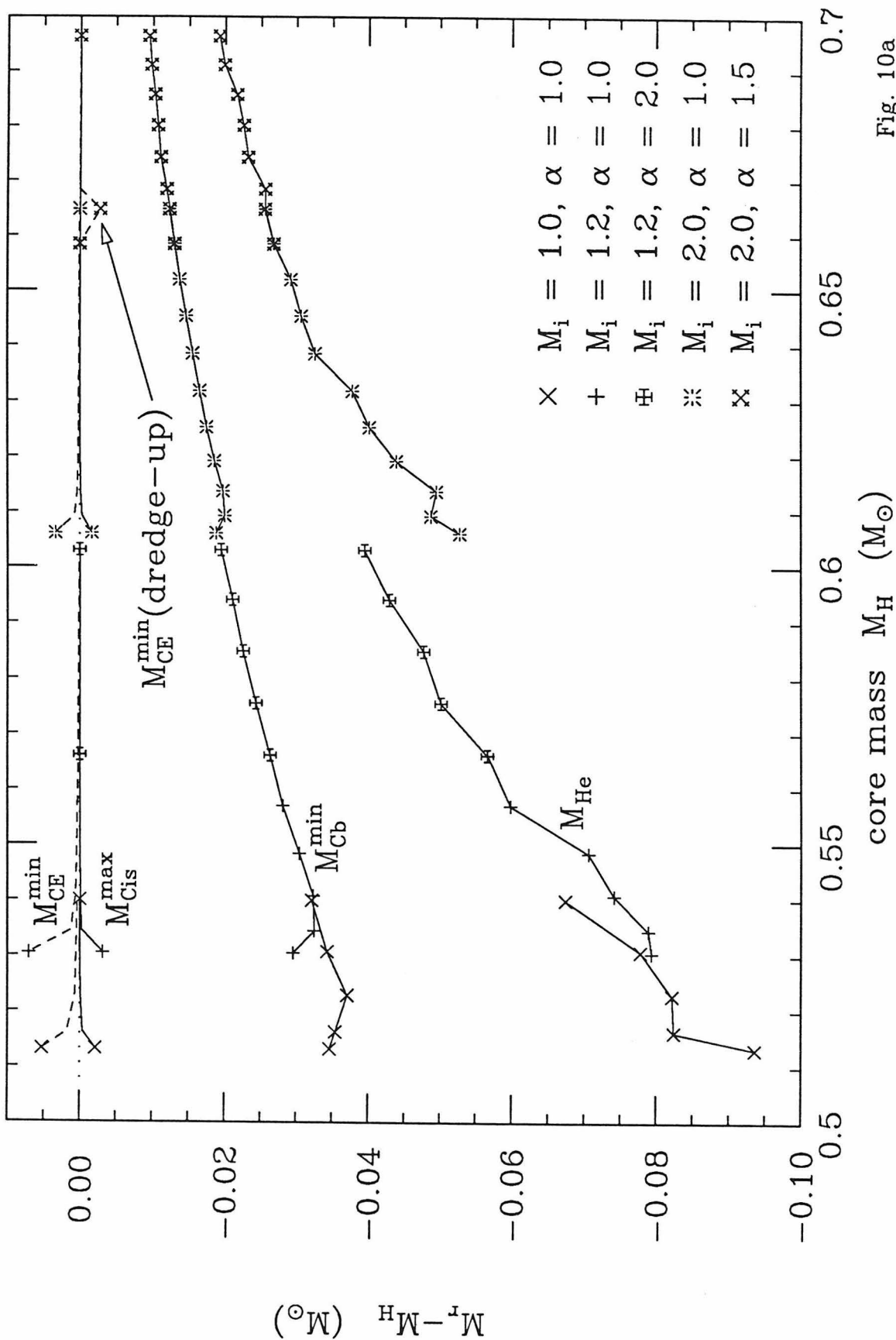


Fig. 10a

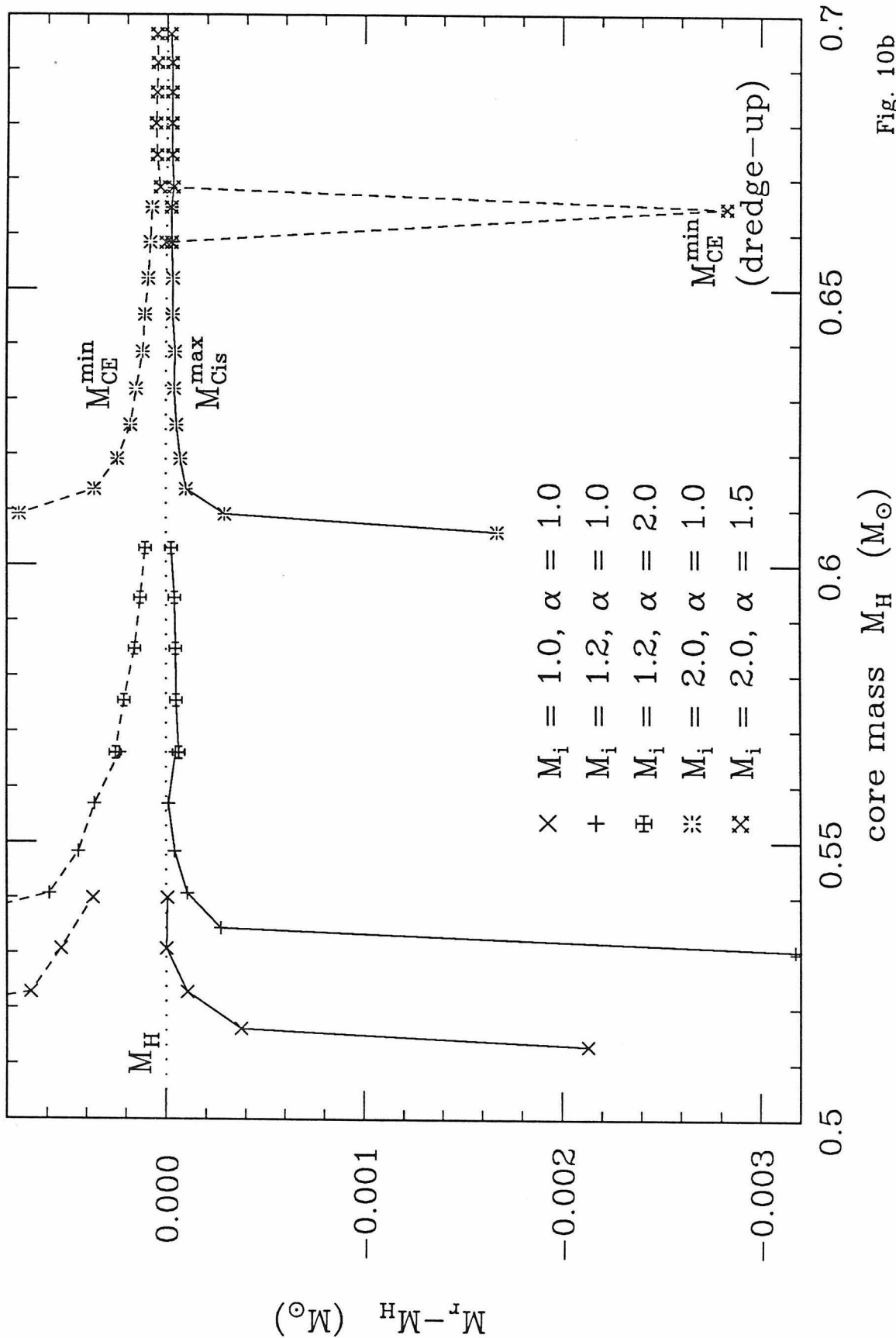


Fig. 10b

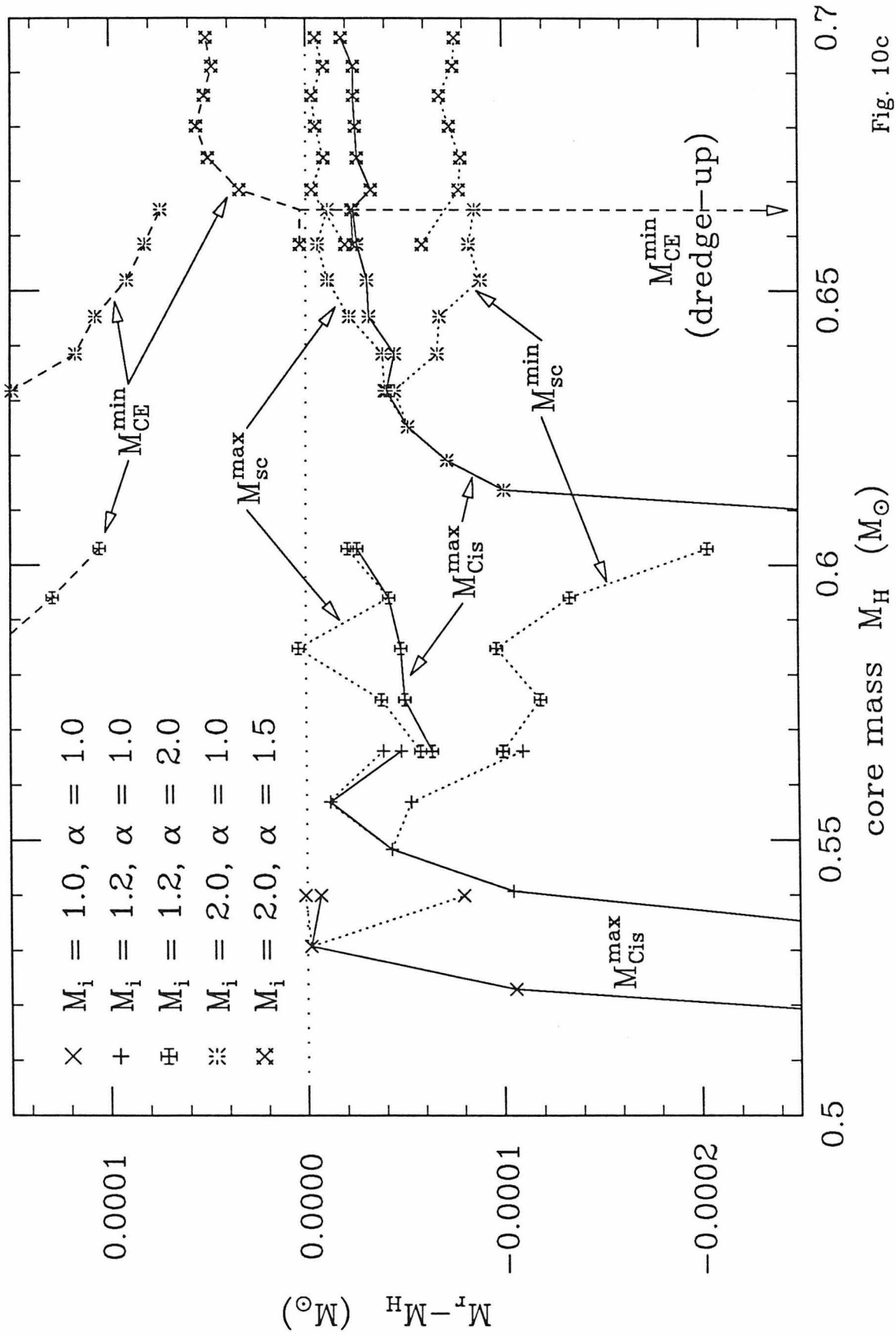
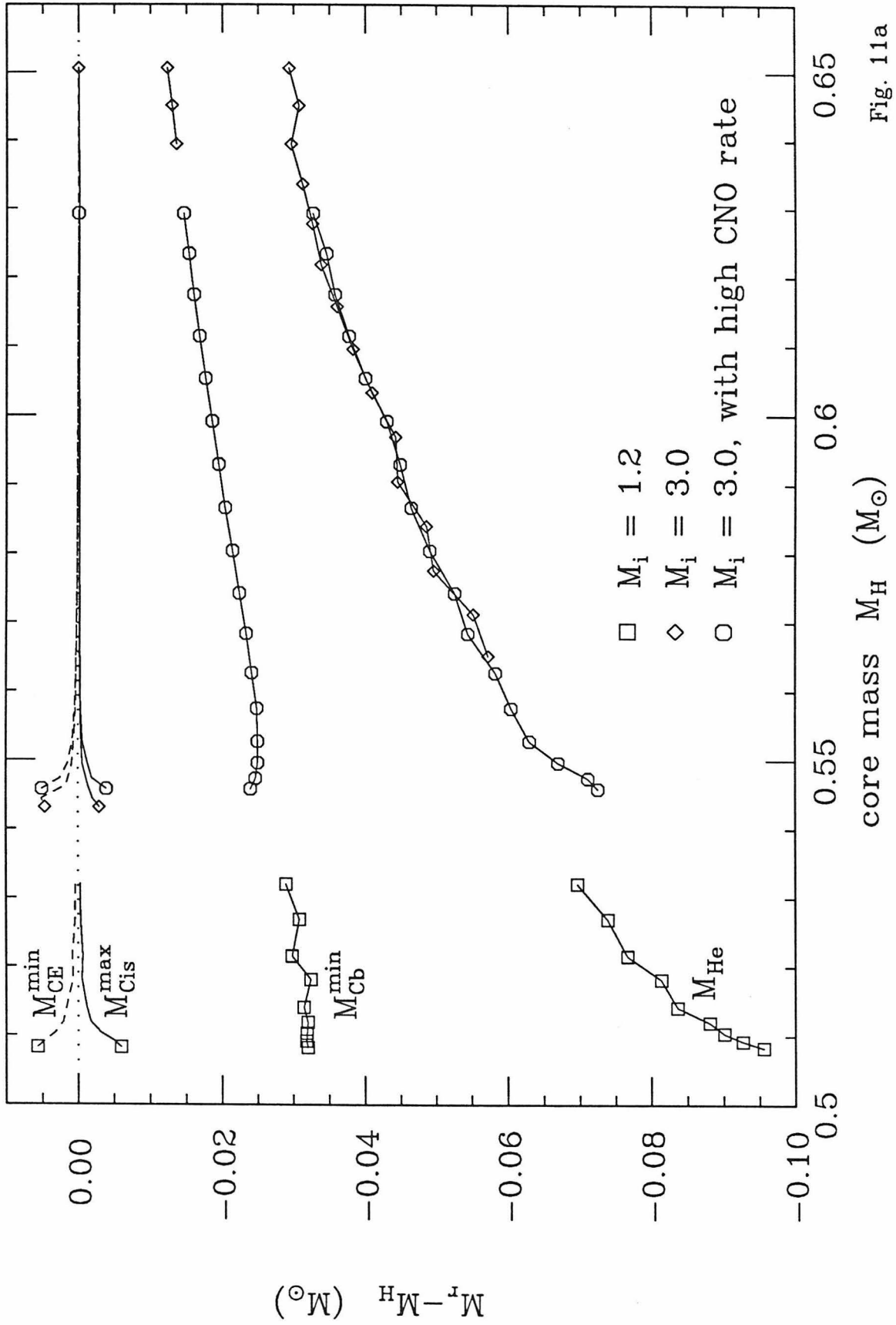


Fig. 10c



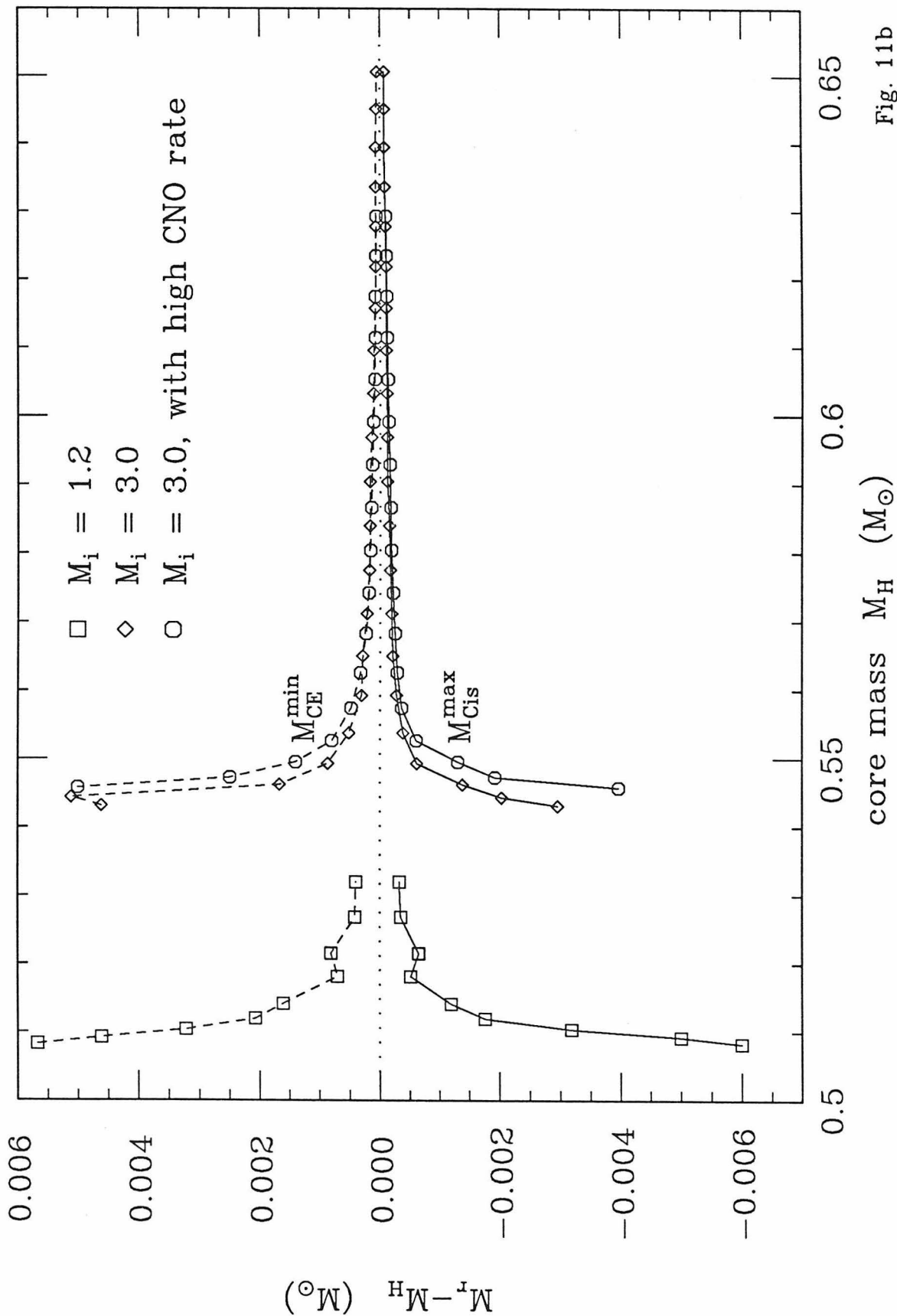


Fig. 11b

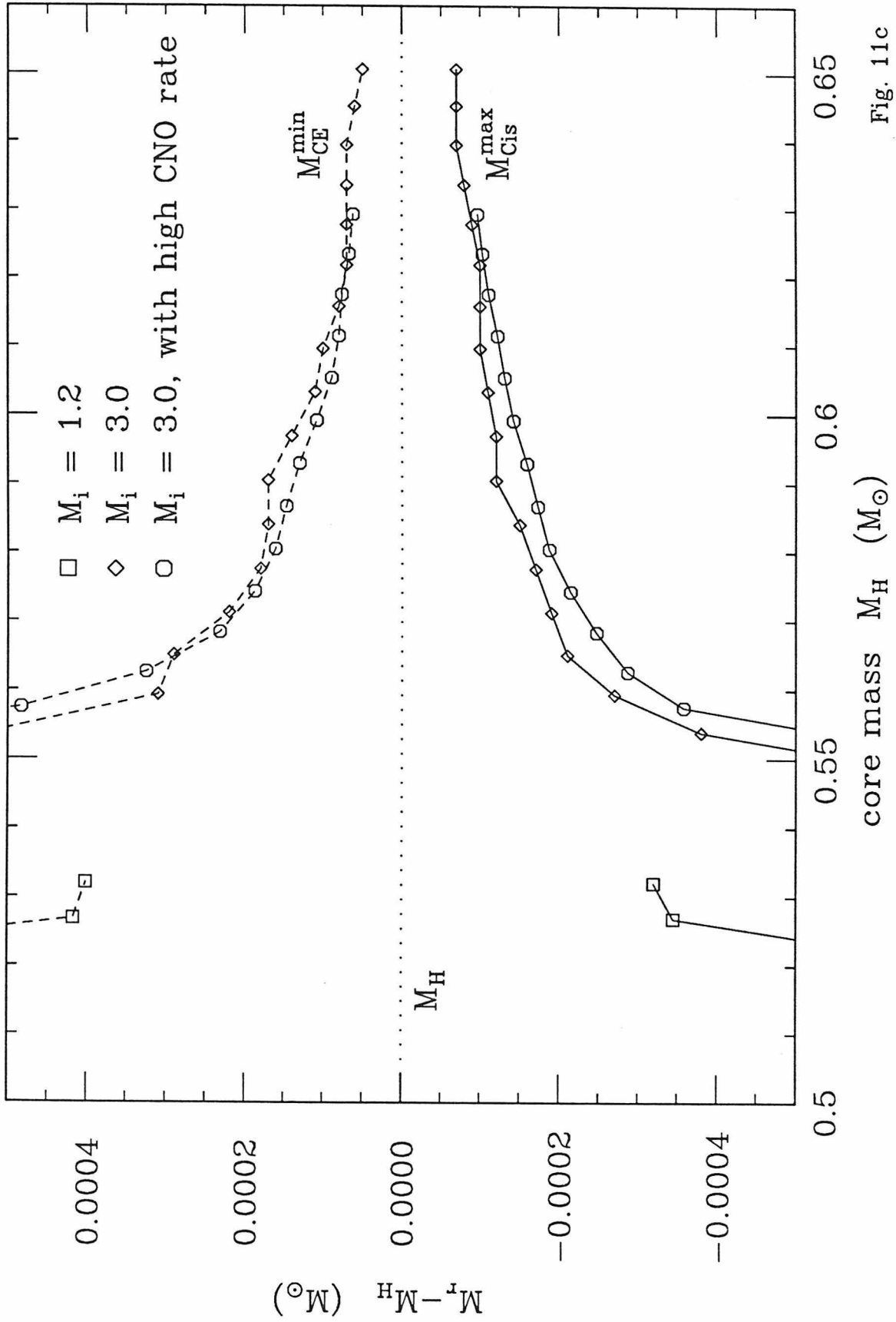


Fig. 11c

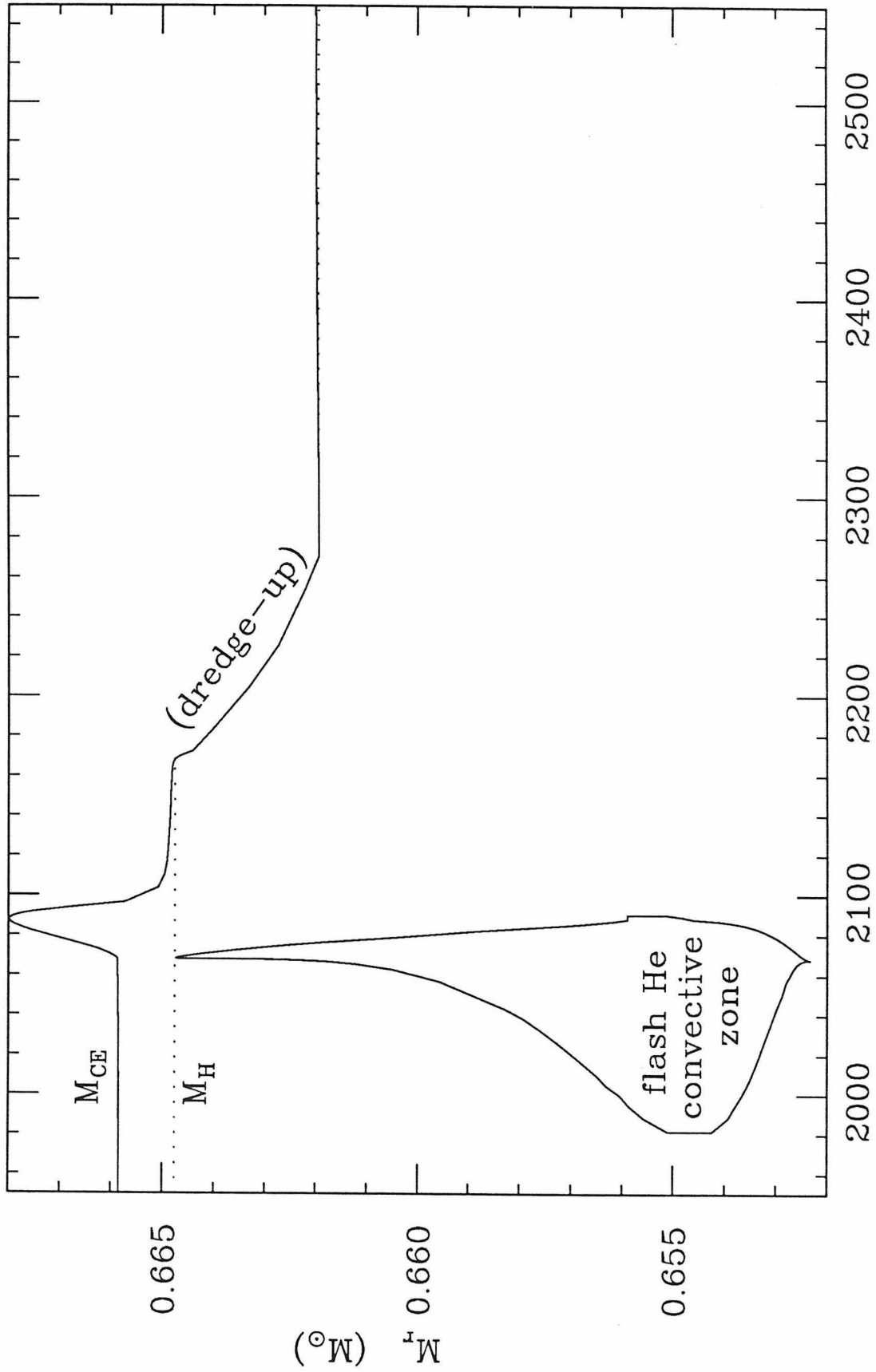


Fig. 12

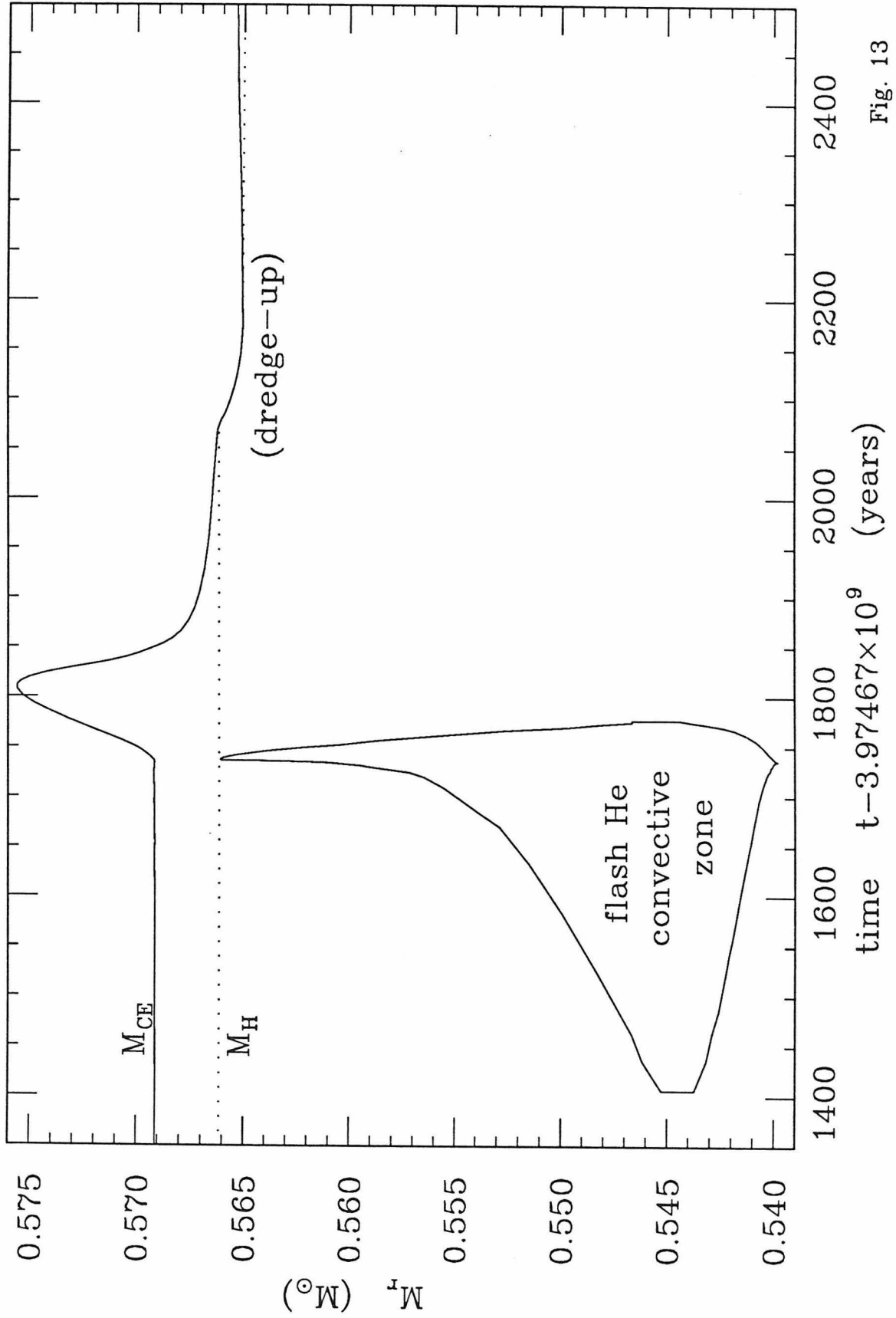


Fig. 13

CHAPTER 5.

On the Origin of the Solar System *s*-Process Abundances

Robert A. Malaney and Arnold I. Boothroyd

W.K. Kellogg Radiation Laboratory 106-38

California Institute of Technology, Pasadena, CA 91125

ABSTRACT

In the search for the origin of the solar system *s*-process abundances, much attention has been focused on the intershell zones of thermally pulsing AGB stars. It has recently been suggested that, relative to the poor fits obtained from intermediate-mass AGB models, low-mass AGB models may result in much better fits to the observed solar system abundances. This suggestion was motivated by the high intershell base temperatures indicated by recent low-mass AGB calculations. Using new data, presented for the peak intershell base temperature in such stars, the *s*-process enhancements occurring in the intershell zones of low-mass AGB stars are calculated. A non-solar distribution of *s*-process abundances is reported for all realistic AGB models studied. Other possible astrophysical sites for the origin of the solar system *s*-process abundances are discussed.

Subject Headings: nucleosynthesis — solar system: abundances — stars:

thermal pulses

I. INTRODUCTION

Since the pioneering study of Burbidge, Burbidge, Fowler, and Hoyle (1957), the origin of the solar system *s*-process abundances has been identified with some form of neutron production occurring in the interiors of red giant stars. It was clear from early analyses (Clayton, Fowler, Hull, and Zimmerman 1961) that the fraction of seed *s*-process nuclei irradiated by neutrons had to be a smoothly decreasing function of the total neutron exposure. Seeger, Fowler, and Clayton (1965) showed how an exponential form for this function resulted in a good fit to the observed solar system *s*-process abundances.

Ulrich (1973) showed how an exponential exposure distribution could arise quite naturally in a single star, as a result of periodic neutron exposures interspersed by removal of material from the irradiated zone. The work of Iben (1975*a, b*; 1977) identified the site for such a mechanism with the intershell zones of thermally pulsing asymptotic giant branch (AGB) stars of intermediate mass. Iben showed how the advance of the intershell zone, as the star evolves, allows for both the removal of matter from the irradiated region and the replenishment of the neutron source at each thermal pulse. The advancement of the intershell allows fresh ^{14}N to enter the intershell at each pulse; ^{22}Ne is then formed via a series of alpha captures. The peak temperatures found to occur at the bottom of the intershell zones of intermediate-mass AGB stars, typically $350 \times 10^6 \text{ K}$, allow for the production of neutrons via the $^{22}\text{Ne}(\alpha, n)^{25}\text{Mg}$ reaction. During the subsequent expansion phase of the pulse the convective envelope extends into the irradiated matter and this “dredge-up” brings *s*-processed material to the surface.

Although these intermediate-mass AGB stars provided the required distribution of neutron exposures necessary to reproduce the solar system *s*-process abundances, it was found from detailed *s*-process calculations (Howard *et al.* 1986) that a non-solar distribution of *s*-process abundances was formed. The problem in reproducing a solar system distribution lay with the high values of the average neutron density, typically 10^{11} – 10^{12} cm^{-3} , associated with the ^{22}Ne neutron source in these stars. Such high neutron densities can be compared with the $\sim 10^8$ cm^{-3} neutron density under which the solar system *s*-process abundances are believed to have been synthesized (Ward, Newman, and Clayton 1976; Käppeler *et al.* 1982; Howard *et al.* 1986). The calculations by Howard *et al.* (1986) had taken into account the suggestion by Cosner, Iben and Truran (1980) that the time dependence of the neutron density might help to alleviate the situation. These latter authors showed how the decline in the neutron density in the late phases of the thermal pulse could enable the last few neutron captures to occur under low-neutron density conditions. This late addition could then result in a redistribution of the nuclides, such that a more compatible fit with the solar system values are found. However, even after allowing for this effect, the overall fit remained somewhat poor. An underproduction of some *s*-process “only” isotopes was found, coupled to an overproduction of some *r*-process isotopes. In addition to these problems, observations of AGB stars in the Magellanic Clouds (e.g., Aaronson and Mould 1985) suggest that intermediate-mass AGB stars cannot produce *any* *s*-process elements since they lose their entire stellar envelopes before the onset of thermal pulses.

Recently, Mathews *et al.* (1986) have shown how the *s*-process production in low-mass AGB stars may resolve the situation. These authors pointed out that the calculations of Becker (1981, 1986) indicate that the peak base temperature T_b of the intershell zone in low-mass AGB stars is higher than originally believed. Hitherto, the low values of T_b associated with these low-mass stars resulted in negligible neutron production from the $^{22}\text{Ne}(\alpha, n)^{25}\text{Mg}$ reaction. However, a higher value for T_b could allow significant production of neutrons and *s*-process isotopes.

The purpose of this paper is to closely examine the production of *s*-process isotopes in AGB stars of low core mass M_c , using new low-mass AGB evolutionary calculations to determine the $M_c - T_b$ relation for such stars. (M_c is as usual identified with the mass M_H interior to the hydrogen-helium discontinuity at the base of the hydrogen-burning shell.)

II. THE $M_c - T_b$ RELATION FOR AGB STARS

Based on the then available calculations, Iben and Truran (1978) gave the following formula for the $M_c - T_b$ relation,

$$T_b = 310 + 285(M_H - 0.96), \quad (1)$$

where T_b is in units of $10^6 K$ and $M_H \equiv M_c$ is in solar mass units. This relation is plotted as the full line in Figure 1. The squares, taken from the calculations of Iben (1977), indicate some of the data points employed by Iben and Truran in constructing equation (1). Also plotted are more recent calculations of T_b for low core mass AGB models. The crosses are the calculations of the present work, the

circles those of Becker (1986), and the crossed circle corresponds to the low-mass stellar model of Iben and Renzini (1982). It can be seen that the $M_c - T_b$ relation differs significantly from the Iben and Truran relation for core masses less than about $1.0 M_\odot$. For such core masses, the following relation gives a better representation of the available calculated data:

$$T_b = \begin{cases} 290 + 67(M_H - 0.65), & 0.65 < M_H < 1.0 \\ 250 + 305(M_H - 0.53), & M_H < 0.65. \end{cases} \quad (2)$$

The dashed track of Figure 1 represents this relation.

All of the points plotted in Figure 1 are for full amplitude thermal pulses. The scatter of the points can be mainly attributed to the different stellar models employed. The high- T_b Becker value corresponds to a $3.0 M_\odot$, $Z = 0.01$ model, with the remaining two Becker points of lower T_b corresponding to a $2.25 M_\odot$, $Z = 0.01$ model. The Iben and Renzini model had a mass of $0.7 M_\odot$ and $Z = 0.001$. With regard to our own calculations, the $T_b = 270$, $M_H = 0.57 M_\odot$ point corresponds to a $1.2 M_\odot$, $Z = 0.001$ model; the $T_b = 298$, $M_H = 0.66 M_\odot$ point corresponds to a $2.0 M_\odot$, $Z = 0.001$ model; and the remaining points correspond to a $3.0 M_\odot$, $Z = 0.02$ model. The main point we wish to make in this section is that for the stellar models we have investigated we find no evidence for T_b values significantly higher than those given by equation (2). Of particular importance for what is to follow, is that no stellar model resulted in an AGB core mass of $0.65 M_\odot$ having a T_b value in excess of 300.

Details of the models presented in Figure 1 as well as details of other low-mass AGB models are given in Boothroyd and Sackmann (1987: Paper III). It should

be noted here, however, that the presence of a stellar wind can prevent some low-mass AGB models from reaching full pulse amplitude. For example, we find for a main-sequence model with an initial mass of $1.0 M_{\odot}$ and metallicity $Z = 0.001$, the presence of a stellar wind, given by Reimers' (1975) formula with $\eta = 0.4$ (Kudritzki and Reimers 1978), results in a core mass of $0.52 M_{\odot}$ and an envelope mass of $0.19 M_{\odot}$ at the onset of the first thermal pulse. After five pulses, at which point T_b and M_H had only attained values of 260 and $0.54 M_{\odot}$ respectively, the stellar envelope had been completely removed. Such a model can play no role in solar system *s*-process nucleosynthesis.

III. *s*-PROCESS ABUNDANCE CALCULATIONS

Using equation (2), the *s*-process enhancements in the intershell zones of low-mass, thermally pulsing AGB stars were calculated as a function of AGB core mass. A full description of the method employed for carrying out such calculations, and of the nuclear reaction network employed, can be found in Malaney (1986*a*).

Figure 2 plots the σN values for the solar system *s*-process isotopes, where σ is the Maxwellian neutron absorption cross section taken from Bao and Käppeler (1986), and N is the solar system abundance taken from Anders and Ebihara (1982). Only the *s*-process isotopes completely shielded from an *r*-process contribution are shown. Also plotted are the calculated distributions for the same isotopes, using different AGB models. To aid the eye, a curve is drawn through these calculated distributions. The structure between each plotted isotope is not shown. The curves correspond to an AGB star of $M_H = 0.65 M_{\odot}$, with the full and dotted curves

corresponding to T_b values of 290 and 300, respectively. (This latter value of T_b represents an upper limit for this core mass, as discussed shortly). It can be seen that neither of these two curves results in a very satisfactory fit to the observed solar system values. Other AGB models with different core masses and with T_b given by equation (2) did not result in fits to the observed data significantly better than the full line curve of Figure (2). These poor fits are a result of the high neutron densities associated with the higher core masses, and the low total neutron exposures found for the low core mass models. The dashed curve of Figure 2 is an “artificial” $T_b = 310$, $M_H = 0.65 M_\odot$ model. As pointed out by Mathews *et al.* (1986), using this model a reasonable fit to the observed data can be found. As discussed earlier, however, such a high value of T_b is not compatible with present AGB evolution calculations.

On a more formal basis, Table 1 lists the normalized χ^2 values for three of the different core mass models studied. The normalized value of χ^2 is calculated from

$$\chi^2 = \frac{(\sigma N_{\text{exp}} - \sigma N_{\text{calc}})^2}{\Delta^2(\sigma N)(n - 1)}, \quad (3)$$

where n is the number of isotopes and $\Delta^2(\sigma N)$ is the variance (square of the experimental error). In order to account for uncertainties associated with equation (2), the low-mass AGB calculations were also carried out for higher T_b values than those obtained from the use of equation (2). These additional models are indicated by an asterisk in Table 1. T_b values of 300 and 310 for the $M_H = 0.65 M_\odot$ and $M_H = 0.8 M_\odot$ models, respectively, represent such upper limits. The $M_H = 0.65 M_\odot$ model with $T_b = 310$ and an intermediate-mass AGB model with a core mass of

$M_{\text{H}} = 1.16 M_{\odot}$ are listed for comparison. This latter model was the best fit model obtained for an intermediate-mass AGB star. The χ^2 is calculated only for the s -only isotopes with atomic mass A in the range $90 < A < 200$. The motivation for this separation of the isotopes comes from the suggestion of Truran and Iben (1977) that the intershell zones of AGB stars are likely to be the main contributors to the solar system s -process isotopes only for isotopes in this heavier mass range, with the lighter isotopes produced in the helium-burning cores of massive ($> 10 M_{\odot}$) stars (Peters 1968). Analyses of the solar system s -process abundances have also led other authors to the same conclusion, that different neutron exposure environments for different mass ranges are necessary in order to reproduce the entire observed s -process spectrum (Ward, Newman, and Clayton 1976; Käppeler *et al.* 1982; Beer 1986).

For a good fit, a normalized χ^2 of order 1 should be found. From Table 1 it can be seen that none of the realistic stellar models results in an adequate fit to the observed data. For the low core mass models in which the T_b values are given by equation (2), the probability of random errors in the σN 's reconciling the calculations with the observed data is negligibly small. Similar remarks apply to those additional models in which upper limit T_b values are employed. Although an improvement is found using these additional models, a fit to the observed data is still not achieved. In order to obtain a good fit to the observed data, high values of T_b (not indicated by the stellar models) are required. This can be seen from the $M_{\text{H}} = 0.65 M_{\odot}$, $T_b = 310$ model.

It is concluded that the ^{22}Ne neutron source in thermally pulsing AGB stars of low mass results in poor fits to the solar system s -process abundances, as was previously found for intermediate-mass AGB stars.

IV. DISCUSSION

The possibility of reconciling AGB s -process production with the observed solar system s -process abundances will now be briefly discussed. The simplest manner in which this could be achieved is for further low-mass AGB evolution calculations to result in higher T_b values than those indicated here. Due to the paucity of data points in the core mass range of $0.7 - 0.9 M_\odot$, and the fact that none of our own models were evolved much further than a core mass of $0.65 M_\odot$, this could be a possibility. However, even if this were to be the case, another theoretical difficulty would have to be overcome if low-mass AGB stars were to be considered as significant s -process contributors to the solar-system abundances. As discussed earlier, intermediate-mass AGB stars dredge-up irradiated matter from the intershell into the stellar envelope. However, dredge-up is inhibited by small envelope masses and low core masses, as well as by higher stellar metallicities (Iben 1983; Lattanzio 1987; Boothroyd and Sackmann 1987): although dredge-up has been found in low-metallicity stellar models having core masses of order $0.65 M_\odot$ and total masses of order $1.5 M_\odot$, it is much harder to produce dredge-up in a models of lower core mass and smaller total mass that have physically reasonable input parameters. This finding is in agreement with the trends found by Wood (1981) which show that for low core masses, large envelope masses are required in

order for dredge-up to occur (although Iben 1983 has shown that low-mass AGB models with core masses in the range $0.6 - 0.65 M_{\odot}$, and in a limited parameter space, can undergo some dredge-up). Thus it appears that even if a solar system distribution of s -process isotopes could be produced in the intershells of low-mass AGB stars from the ^{22}Ne neutron source, they would not always be transferred to the stellar envelope (at least not in significant quantity) where they could be subsequently ejected into the interstellar medium. Of course it could be that a mixing mechanism other than classical dredge-up could be involved. However, as now discussed the most likely alternative mixing mechanism is unlikely to result in a solar system distribution of s -process abundances.

Iben and Renzini (1982*a, b*) have proposed an alternative neutron production and mixing mechanism for low-mass AGB stars in which the $^{13}\text{C}(\alpha, n)^{16}\text{O}$ reaction becomes the principal neutron producing reaction. This mechanism is based on the opacity change, and its subsequent effect on the convection properties, in the cool carbon-rich material at the top of the intershells in low-mass AGB stars (Sackmann 1980). The potency of the ^{13}C neutron source in low-mass AGB stars is sensitive to a number of stellar parameters (Iben 1983), and a detailed study of the s -process enhancements arising from Iben and Renzini's mixing mechanism may be of importance with regard to the production of a solar system s -process distribution. It should be noted, however, that even though the $^{13}\text{C}(\alpha, n)^{16}\text{O}$ reaction proceeds at the relatively low temperature of $\sim 150 \times 10^6 K$ for this mechanism (Iben and Renzini 1982*b*), the high reaction rate associated with this reaction (Caughlan *et al.* 1985) still results in neutron densities at least two orders of magnitude higher than

those required for production of the solar system *s*-process abundances (Iben 1983; Malaney 1986*a, b*). In addition, it has been argued (Truran and Iben 1977) that the low neutron absorption cross section of ^{16}O makes ^{13}C an unlikely neutron source for the solar system *s*-process abundances.

As discussed in the introduction, a key to reproducing the solar system *s*-process abundances is the requirement of an exponentially weighted distribution of neutron exposures. What about alternative astrophysical sites for the production of such neutron exposures? It was originally suggested that an exponential distribution of exposures would result from considering the recycling of neutron exposed material from one stellar generation to the next (Seeger, Fowler, and Clayton 1965). Due to the discovery that single stars by themselves could produce a distribution of exposures, this idea became less topical. It could be time to re-examine this original proposal.

Peters (1968) has shown how the contraction of an evolving helium-burning core in massive stars ($> 10 M_{\odot}$) leads to a distribution of neutron exposures. However, in these models the neutron source, ^{22}Ne , is not continually replenished as in the AGB models, and as such it was found that an insufficient number of neutrons were produced for synthesis of the heavier *s*-process abundances.

Convection in stellar interiors can also lead to neutron exposure distributions. Convective mixing in neutron-exposed regions has been discussed by Despain (1977). This author investigated the *s*-process production in a convective region, which extended from the helium-burning shell of a red giant all the way to the stellar

surface. However, again a non-solar distribution of *s*-process abundances was found. The inclusion of expansion and cooling effects in an energy producing convection zone, hitherto not included in any calculation, may be of importance. A study of the distribution of neutron exposures in an evolving convection zone would be useful.

In summary, it has been found that AGB stars in which the ^{22}Ne neutron source operates do not adequately reproduce the solar system *s*-process abundances. With regard to the origin of these abundances, alternative astrophysical sites should be more closely examined.

The authors are very grateful to Dr. S. A. Becker for making available to them his unpublished stellar evolution calculations. An allocation of computer time at the San Diego Supercomputing Center is gratefully acknowledged. This work was partly supported by National Science Foundation Grant PHY85-05682. R. A. M. acknowledges the financial support of an SERC/NATO Fellowship (U.K.).

REFERENCES

- Aaronson, M., and Mould, J. 1985, *Ap. J.*, **288**, 551.
- Anders, E., and Ebihara, M. 1982, *Geochim. Cosmochim. Acta*, **46**, 2263.
- Bao, Z. Y., and Käppeler, F. 1986, preprint.
- Becker, S. A. 1981, in *Physical Processes in Red Giants*, ed. I. Iben, Jr., and A. Renzini (Dordrecht: Reidel), p. 141.

- Becker, S. A. 1986, private communication.
- Beer, H. 1986, in *Nucleosynthesis and its Implications on Nuclear and Particle Physics*, ed. J. Audouze and N. Mathieu (Dordrecht: Reidel), p. 263.
- Boothroyd, A. I., and Sackmann, I.-J. 1987 (Paper III).
- Burbidge, G. R., Burbidge, E. M., Fowler, W. A., and Hoyle, F. 1957, *Rev. Mod. Phys.*, **29**, 547.
- Caughlan, G. R., Fowler, W. A., Harris, M. J., and Zimmerman, B. A. 1985, *At. Nucl. Data Tables*, **32**, 197.
- Clayton, D. D., Fowler, W. A., Hull, T. E., and Zimmerman, B. A. 1961, *Ann. Phys.*, **12**, 331.
- Cosner, K., Iben, I., Jr., and Truran, J. W. 1980, *Ap. J. (Letters)*, **238**, L91.
- Despain, K. H. 1977, *Ap. J.*, **212**, 774.
- Howard, W. M., Mathews, G. J., Takahashi, K., and Ward, R. A. 1986, preprint.
- Iben, I., Jr. 1975*a*, *Ap. J.*, **196**, 525.
- . 1975*b*, *Ap. J.*, **196**, 549.
- . 1977, *Ap. J.*, **217**, 788.
- . 1983, *Ap. J. (Letters)*, **275**, L69.
- Iben, I., Jr., and Renzini, A. 1982*a*, *Ap. J. (Letters)*, **259**, L79.
- . 1982*b*, *Ap. J. (Letters)*, **263**, L23.
- Iben, I., Jr., and Truran, J. W. 1978, *Ap. J.*, **220**, 980.
- Käppeler, F., Beer, H., Wisshak, K., Clayton, D. D., Macklin, R. L., and Ward, R. A. 1982, *Ap. J.*, **257**, 821.
- Kudritzki, R. P., and Reimers, D. 1978, *Astron. Astrophys.*, **70**, 227.

- Lattanzio, J. C. 1987, *Ap. J. (Letters)*, **313**, L15.
- Malaney, R. A. 1986a, submitted to *Ap. J.*
- .1986b, *M. N. R. A. S.*, in press.
- Mathews, G. J., Ward, R. A., Takahashi, K., and Howard, W. M. 1986, preprint.
- Peters, J. G. 1968, *Ap. J.*, **154**, 225.
- Reimers, D. 1975, in *Problems in Stellar Atmospheres and Envelopes*, ed. B. Baschek, W. H. Kegel, and G. Traving (New York: Springer-Verlag), p. 229.
- Sackmann, I.-J. 1980, *Ap. J. (Letters)*, **241**, L37.
- Seeger, P. A., Fowler, W. A., and Clayton, D. D. 1965, *Ap. J. Suppl.*, **11**, 121.
- Truran, J. W., and Iben, I., Jr. 1977, *Ap. J.*, **216**, 797.
- Ulrich, R. K. 1973, in *Explosive Nucleosynthesis*, ed. D. N. Schramm and W. D. Arnett (Austin: University of Texas Press), p. 139.
- Ward, R. A., Newman, M. J., and Clayton, D. D. 1976, *Ap. J. Suppl.*, **31**, 33.
- Wood, P. R. 1981, in *Physical Processes in Red Giants*, ed. I. Iben, Jr. and A. Renzini (Dordrecht: Reidel), p. 135.

Table 1

χ^2 Values for Different AGB Models

Core Mass (M_{\odot}):	0.65			0.8		1.16
T_b ($10^6 K$):	290	300*	310*	300	310*	350
χ^2 :	34.5	17.0	3.1	34.9	16.0	27.7

FIGURE CAPTIONS

Fig. 1.—The $M_c - T_b$ relation for AGB stars. The full line corresponds to eq. (1) and the dotted line to eq. (2). It can be seen that eq. (2) is a better fit to the data for low core mass AGB stars.

Fig. 2.—The observed solar system σN values are plotted along with the σN calculated values for a $0.65 M_\odot$ core mass model with T_b values of 290 (full curve), 300 (dotted curve), and 310 (dashed curve). The curves are normalized by dividing the σN values by the factor which minimizes χ^2 .

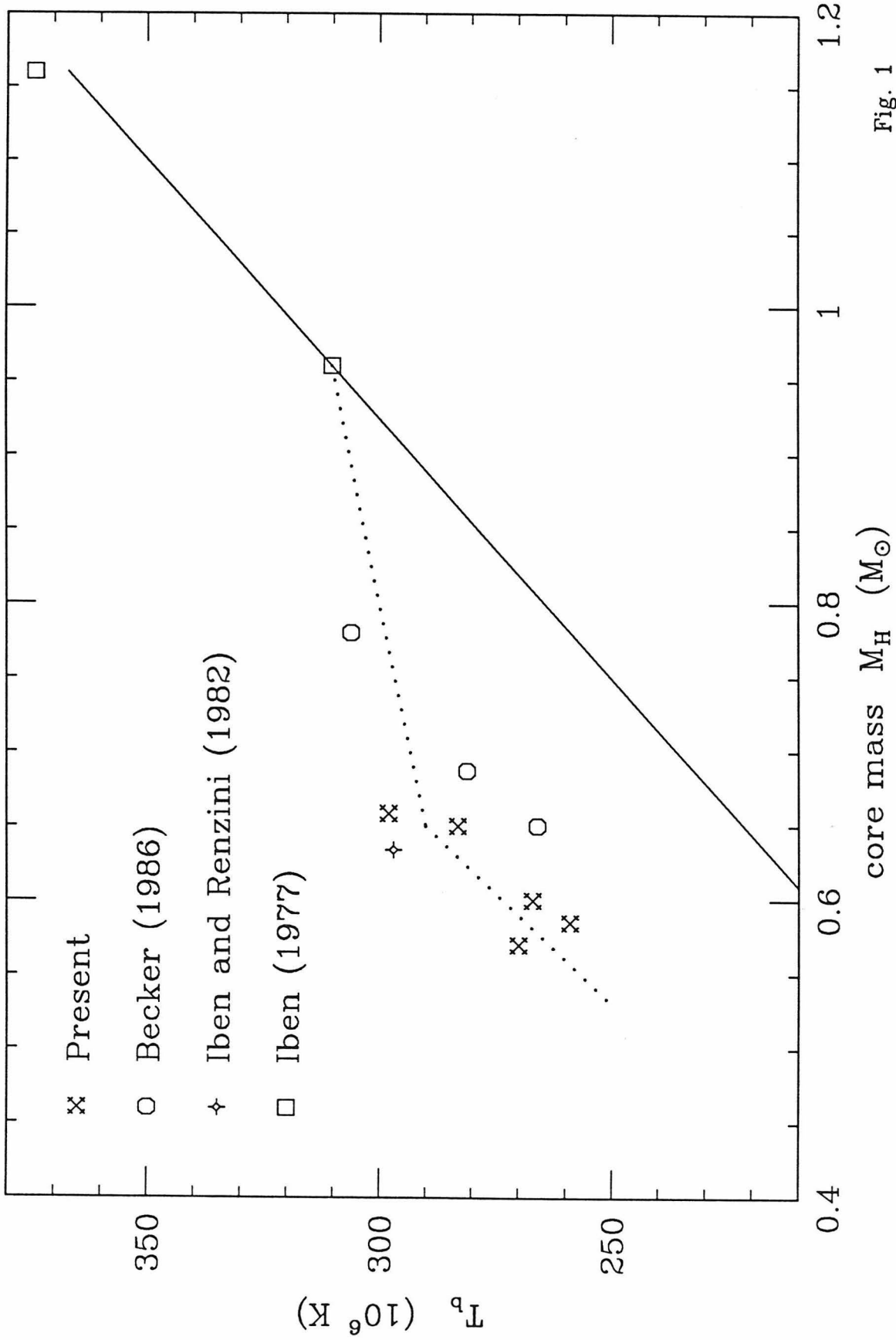


Fig. 1

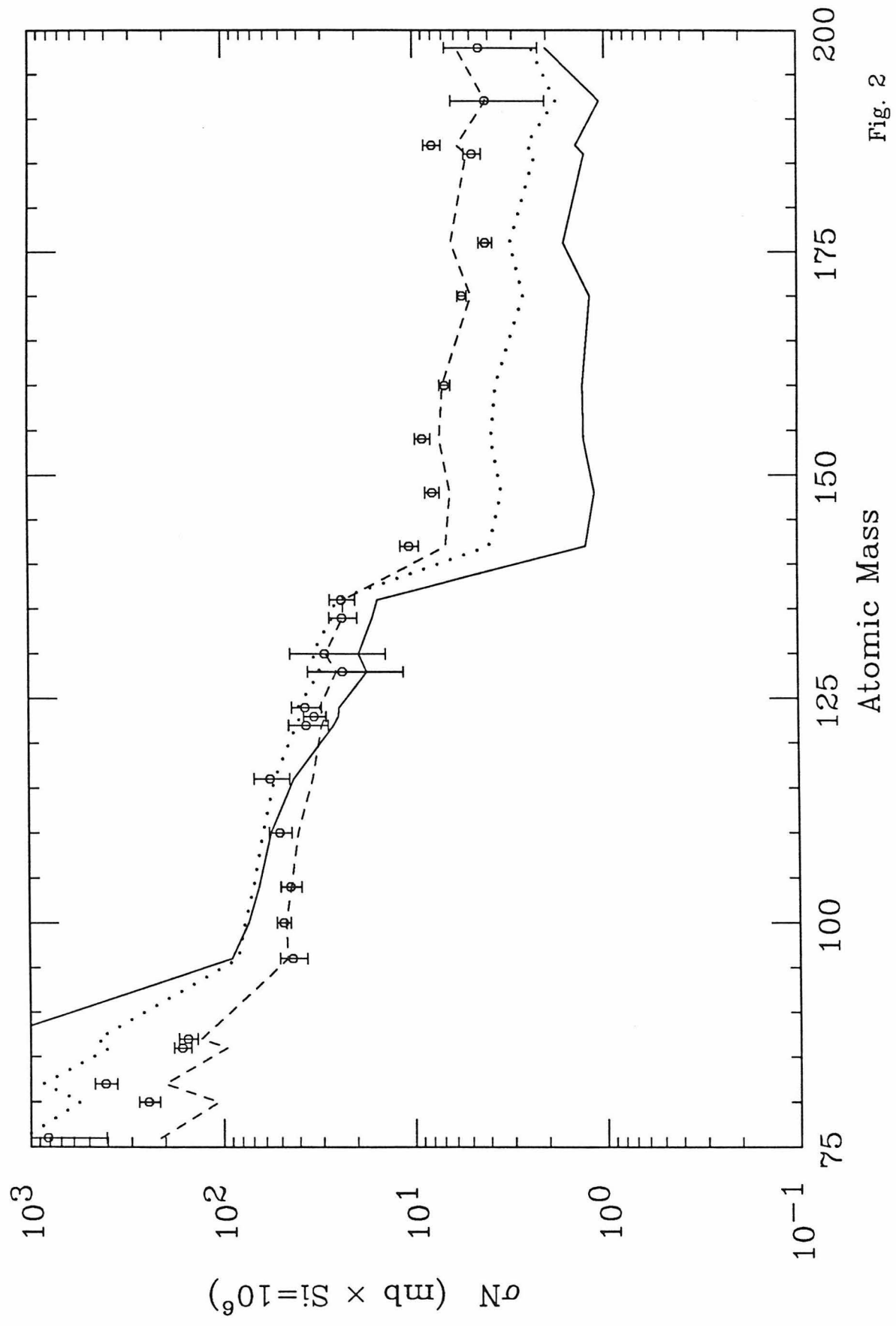


Fig. 2

CHAPTER 6.

Neutron Exposures in Time-dependent Stellar Convective Regions

Robert A. Malaney, Martin J. Savage, and Arnold I. Boothroyd

W.K. Kellogg Radiation Laboratory 106-38

California Institute of Technology, Pasadena, CA 91125

ABSTRACT

Hitherto, only one mechanism for producing an exponentially weighted distribution of neutron exposures within a stellar interior has been shown to be successful. In this letter a second mechanism is proposed, based on consideration of the time-dependence of the temperature, and consequently of the neutron production, in a stellar convective region. A wide range of mean neutron exposures, encompassing that necessary to form the solar system *s*-process abundances, can be produced by this new mechanism.

I. INTRODUCTION

In the early investigations into the origin of the solar system *s*-process abundances it became clear that, in order to reproduce the observed *s*-process elements in their solar system proportions, the fraction of material that undergoes a neutron

exposure τ^\dagger would have to follow some form of smoothly decreasing function of τ (Clayton, Fowler, Hull and Zimmerman 1961). It was subsequently discovered that an exponential form for this function, i.e., $\phi(\tau) \propto \exp(-\tau/\tau_0)$, with $\tau_0 \approx 0.26 \text{ mb}^{-1}$ gave the best fit to most of the observed data (Seeger, Fowler, and Clayton 1965; Käppeler *et al.* 1982; Howard *et al.* 1986; Beer 1986). The constant of the neutron distribution, τ_0 , is often referred to as the mean neutron exposure.

Since this discovery, attempts have been made to model such a decreasing function of neutron exposures from processes occurring in stellar interiors. Peters (1968) investigated the evolving cores of massive stars ($> 10 M_\odot$) and found that, although the contraction of such cores leads to a distribution of neutron exposures, the number of neutrons synthesized was insufficient with regard to heavy element production. Ulrich (1973, 1982) indicated how an exponential distribution of neutron exposures could arise in the intershell zones of asymptotic giant branch (AGB) stars as a consequence of coupling repeated neutron exposures to the radial advancement of such zones. The work of several investigators (Iben 1975*a, b*, 1977; Truran and Iben 1977; Cosner, Iben and Truran 1980) then identified the $^{22}\text{Ne}(\alpha, n)^{25}\text{Mg}$ neutron source in intermediate-mass AGB stars as the source of the solar system *s*-process abundances. More recently, however, objections have been raised against this scenario (Aaronson and Mould 1985; Howard *et al.* 1986; Malaney and Boothroyd 1987), and at the present time it is not clear how much this process contributes to the solar system *s*-process abundances.

[†] $\tau \equiv \int_0^t N_n v_t dt$, where N_n is the neutron density, v_t is the neutron thermal velocity, and t is the total time of irradiation.

The purpose of this letter is to point out another manner in which an exponential distribution of neutron exposures can occur within the interior of a single star. We find that such a distribution can arise when the time-dependence of the parameter grid (i.e., temperature, mass density, and pressure) of a stellar convective region is taken into account. Although we investigate only one particular case, similar conclusions can be drawn for any scenario in which the convective mixing time is a significant fraction of the lifetime of the convective region.

The particular scenario we investigate here is when the convective intershell zone and convective envelope (both present following a helium shell flash) of an AGB star are coupled together in such a way that a convective region extending from the helium-burning shell to the stellar surface is formed. The resulting injection of hydrogen into the stellar interior can give rise to substantial neutron fluxes via the $^{12}\text{C}(p, \gamma)^{13}\text{N}(, e^+\nu)^{13}\text{C}(\alpha, n)^{16}\text{O}$ sequence of nuclear reactions (cf. Malaney 1986a and references therein). Despain (1977) has investigated the heavy element synthesis arising from such a situation using a time-independent grid. Although current calculations indicate that such a scenario is not possible while the star remains on the AGB due to the existence of an entropy barrier at the hydrogen-burning shell (Iben 1975), it does become possible at the post-AGB phase once the stellar envelope mass has been substantially reduced (Fujimoto 1977; Schönberner 1979; Renzini 1979, 1981; Malaney 1986b).

The problems in properly accounting for energy generation from rapid envelope mixing are formidable and are well beyond the scope of the present investigation.

Although the model we work from is simplistic and ignores several important effects, such as envelope expansion and intershell splitting (Sweigart 1974), it is sufficient to demonstrate the main point of this letter: the inclusion of a time-dependent convective parameter grid can lead to a smoothly decreasing distribution of neutron exposures which can be adequately described by an exponential law.

II. STELLAR MODEL AND CONVECTIVE DIFFUSION

For the intershell region we adopt the parameter grid from the stellar model of initial mass $1.0 M_{\odot}$ ($Z = 0.001$) of Boothroyd and Sackmann (1987), during and just following the 5th helium shell flash. At the time of the flash the stellar model had a total mass of $0.55 M_{\odot}$ (due to mass loss), an envelope mass of $0.014 M_{\odot}$, and a radius of $\sim 200 R_{\odot}$. The dependence of the neutron density N_n as a function of time t and mass coordinate M_r (r is the distance from the stellar center) for the neutron-rich portion of the intershell region is shown in the three dimensional plot of Figure 1. Similar plots can be constructed for other parameters such as pressure $\mathcal{P}(r)$, the temperature $T(r)$, the mass density $\rho(r)$, and the convective mixing length $\lambda(r)$. The mixing length is set equal to the pressure scale height, that is,

$$\lambda(r) = \left[\frac{1}{\mathcal{P}} \frac{d\mathcal{P}}{dr} \right]^{-1}. \quad (1)$$

For the stellar envelope we simply add a constructed polytropic envelope of radius $50 R_{\odot}$ to the top of the intershell region. A relationship can be formed giving the mass of the stellar envelope, for a given value of the stellar radius, in terms of

the boundary conditions at the intershell-envelope interface. Using the boundary conditions from the intershell region employed, we find that for a stellar radius of $50 R_{\odot}$ the stellar envelope mass is approximately $10^{-2} M_{\odot}$. It can also be shown from polytrope theory that the mixing length in a polytropic envelope is given by $\lambda(r) = r/x$, where the value of x depends on the polytropic index. For our purposes the value of x is set so that the mixing length varies smoothly across the intershell-envelope interface ($x = 10$). If our present understanding of AGB theory is correct, then the coupling of the intershell and envelope convective regions can only proceed at a smaller envelope mass than that chosen here. However, we find our conclusions unchanged for smaller values of envelope mass consistent with current AGB theory. The main result is also found to be invariant to a range of x and of stellar radius.

Convective motions in the stellar interior lead to the turbulent diffusion of matter within the convective region. This diffusion of matter is usually followed by means of the turbulent diffusion equation, i.e.,

$$\frac{dN}{dt} = \frac{1}{\rho r^2} \frac{\partial}{\partial r} \left(\rho r^2 D \frac{\partial N}{\partial r} \right), \quad (2)$$

where N is the abundance of a particular nuclide and D is the diffusion coefficient. This equation is only valid at distances greater than many mixing lengths and is not well defined at shorter distances. Within the intershell, however, the neutron density can vary significantly over a mixing length, and therefore equation (2) cannot be used to determine accurately the neutron exposure undergone by a group of diffusing particles. To overcome this difficulty we calculate the total neutron exposure experienced by a series of test particles by explicitly following the random radial

walk of each test particle through the star by the use of Monte Carlo techniques. This is done by randomly choosing the initial position of the particle weighted according to the initial mass density $\rho(r)$. An initial direction, either radially inwards or outwards, is then randomly chosen. Now the probability $P(r)$ of a test particle *not* interacting after a distance $|r - r_0|$ can be written as

$$P(r) = \exp \left[- \int_{r_0}^r \frac{dr}{\lambda(r)} \right], \quad (3)$$

where r_0 is the initial starting position. Discretizing the distance $|r - r_0|$ into n units, we can write

$$\begin{aligned} P(r) &= \exp \left[- \sum_{i=0}^{n-1} \int_{r_i}^{r_{i+1}} \frac{dr}{\lambda(r)} \right] \approx \exp \left[- \sum_{i=0}^{n-1} \frac{(r_{i+1} - r_i)}{\lambda(r_i)} \right] \\ &\approx \prod_{i=0}^{n-1} \left[1 - \frac{(r_{i+1} - r_i)}{\lambda(r_i)} \right]. \end{aligned} \quad (4)$$

The probability of the particle interacting and reversing its direction before the point r is then given by $\frac{1}{2}[1 - P(r)]$, where the factor of $\frac{1}{2}$ arises from the fact that following an interaction it is possible that the particle may not reverse its direction. By setting the step size of the grid to $\frac{1}{10}$ of a mixing length we then calculate the probability of reversing the particle's direction at each of these grid points. The direction of the particle at each point is randomly chosen according to this probability. By this method the random walk of the test particle through the star is followed.

The calculation of $\lambda(r)$ at each step is actually modified from that given by equation (1). Such a modification is required because of the constraint of mass

conservation at each value of r . From the mass conservation equation we have

$$\begin{aligned} \rho(r + dr)v_c(r + dr) \left[1 - \frac{dr}{\lambda_e^-(r + dr)} \right] \\ = \rho(r - dr)v_c(r - dr) \left[1 - \frac{dr}{\lambda_e^+(r - dr)} \right], \end{aligned} \quad (5)$$

where v_c is the convective velocity, and λ_e is an “effective” mixing length with the “+” or “-” superscript applying to motion radially outwards or inwards, respectively. The right hand terms (in the square brackets) of equation (5) arise from consideration of mass conservation. From consideration of the moments of equation (5) we have

$$\frac{1}{\lambda_e^-} - \frac{1}{\lambda_e^+} = \frac{2}{\rho v_c} \frac{d}{dr}(\rho v_c) \equiv 2\nabla \ln(\rho v_c). \quad (6)$$

Defining $\mu \equiv \nabla \ln(\rho v_c)$, we find after some algebra that the effective mixing length is given by

$$\frac{1}{\lambda_e^\mp(r)} = \frac{1}{2\lambda(r)} \pm \mu + \sqrt{\mu^2 + \left(\frac{1}{2\lambda(r)}\right)^2}. \quad (7)$$

The effective mixing length $\lambda_e(r)$ replaces the normal mixing length $\lambda(r)$ in the random walk calculation of each test particle. Typically, $\lambda_e(r)$ is about a factor of two different from $\lambda(r)$.

As the test particle randomly walks through the convective region of the star, it will experience differing values of the neutron density depending on its radial position r . The neutron density at each value of r is given by $N_n = Af(T_9)$, where $f(T_9)$ is taken from the $^{13}\text{C}(\alpha, n)^{16}\text{O}$ reaction rate of Fowler, Caughlan, and Zimmerman (1975): T_9 is the temperature at r in units of $10^9 K$, and A is

a normalizing factor such that the peak neutron density is $\sim 10^{12} \text{ cm}^{-3}$, in agreement with the calculations of Malaney (1986a). (It should be noted that, due to the time-dependence of the neutron density, the stellar material actually experiences an average neutron density roughly three orders of magnitude smaller than the peak density. This lower *mean* neutron density is substantially lower than presently predicted by intermediate-mass AGB stellar models, but is more nearly consistent with both stellar and solar *s*-process observations: see Malaney [1987] and references therein.) At each timestep (i.e., at each $\frac{\lambda(r)}{10}$ position) the neutron exposure experienced by the test particle in moving the distance $\frac{\lambda(r)}{10}$ is given by $\Delta\tau = N_n v_t \Delta t$, where Δt is the time taken to travel $\frac{\lambda(r)}{10}$. The net exposure experienced by the test particle is then simply the summation $\sum^q \Delta\tau$ of all the $\Delta\tau$ values calculated at each timestep (where q is the number of timesteps). A processing time of about one second on a Cray X-MP/48 is required in order to calculate the net exposure of one test particle.

A histogram giving the distribution of 1000 test particles is shown in Figure 2. The dashed curve (bottom exposure scale) corresponds to an exposure distribution function $\phi(\tau) \propto \exp(-\tau/0.26)$. The dotted curve (top exposure scale) corresponds to the histogram outline of a similar calculation except that, in this case, the time-dependence of the parameter grid following the shell flash is removed. In this case a peak in the distribution of neutron exposures is found, although a significant fraction of the stellar material still experiences a wide range of neutron exposures. Additional calculations in which the convective zone was strictly confined to the

intershell region of the star resulted in a very narrow peak in the exposure distribution. This latter finding is in agreement with the assumption that, during each thermal pulse of an AGB star, all the matter within the intershell region experiences a single *unique* neutron exposure.

It can be seen from Figure 2 that the inclusion of time-dependent effects can result in a distribution of neutron exposures that resembles a decreasing exponential distribution. A more accurate representation of the exposure distribution could of course be obtained by employing two exponentials with different τ_0 values (the solar system *s*-process seeds are in fact believed to have been exposed to more than one exponential distribution, cf. Beer 1986). However, our statistics and the simplicity of our model do not warrant a more detailed analysis of Figure 2.

The value of τ_0 arising in a convective region depends critically on the amounts of the neutron-producing nuclei present in the region, and to a lesser extent on the properties of the convective region. In the scenario depicted here, the former criterion is largely influenced by the amount of envelope material engulfed into the hot, neutron producing regions of the stellar interior. Since the amount of such mixing will be determined by a number of factors, a wide range of τ_0 values can be expected. For example, a value of $\tau_0 = 0.5 \text{ mb}^{-1}$ could be obtained from our model by employing a slightly higher peak neutron density of $2 \times 10^{12} \text{ cm}^{-3}$.

III. CONCLUSIONS

We have shown that seed nuclei in a stellar convective region can experience a distribution of neutron exposures that can be described by a decreasing exponential

law, when the time-dependence of the neutron production within the region is taken into consideration. Although we have employed a simplistic convective model and describe here in detail only one particular case, this main result remains valid for a range of different stellar models. The key requirement is simply that the timescale for mixing matter throughout the convective region be a significant fraction of the lifetime of the convective region.

The authors are grateful to S. Braunstein for enlightening discussions regarding stochastic diffusion processes, and to C. A. Barnes and W. A. Fowler for their comments on the manuscript. An allocation of computer time at the San Diego Supercomputing Center is gratefully acknowledged. This work was partly supported by National Science Foundation Grant PHY85-05682. R. A. M. acknowledges the financial support of an SERC/NATO Fellowship (U.K.), and M. J. S. the financial support of a UGC Postgraduate Scholarship (New Zealand).

REFERENCES

- Aaronson, M., and Mould, J. 1985, *Ap. J.*, **288**, 551.
- Beer, H. 1986, in *Nucleosynthesis and its Implications on Nuclear and Particle Physics*, ed. J. Audouze and N. Mathieu (Dordrecht: Reidel), p. 263.
- Boothroyd, A. I., and Sackmann, I.-J. 1987 (Paper III).
- Caughlan, G. R., Fowler, W. A., Harris, M. J., and Zimmerman, B. A. 1985, *At. Nucl. Data Tables*, **32**, 197.

- Clayton, D. D., Fowler, W. A., Hull, T. E., and Zimmerman, B. A. 1961, *Ann. Phys.*, **12**, 331.
- Cosner, K., Iben, I., Jr., and Truran, J. W. 1980, *Ap. J. (Letters)*, **238**, L91.
- Despain, K. H. 1977, *Ap. J.*, **212**, 774.
- Fujimoto, M. Y. 1977, *Publ. Astr. Soc. Japan*, **29**, 331.
- Howard, W. M., Mathews, G. J., Takahashi, K., and Ward R. A. 1986, *Ap. J.*, submitted.
- Iben, I., Jr. 1975*a*, *Ap. J.*, **196**, 525.
- . 1975*b*, *Ap. J.*, **196**, 549.
- . 1977, *Ap. J.*, **217**, 788.
- Käppeler, F., Beer, H., Wisshak, K., Clayton, D. D., Macklin, R. L., and Ward, R. A. 1982, *Ap. J.*, **257**, 821.
- Malaney, R. A. 1986*a*, *M. N. R. A. S.*, **223**, 683.
- . 1986*b*, *M. N. R. A. S.*, **223**, 709.
- . 1987, *Ap. J.*, in press.
- Malaney, R. A., and Boothroyd, A. I. 1987, *Ap. J.*, in press.
- Peters, J. G. 1968, *Ap. J.*, **154**, 225.
- Renzini, A. 1979, in *Stars and Star Systems*, ed. B. E. Westerlund (Dordrecht: Reidel), p. 155.
- . 1981, in *Effects of Mass Loss on Stellar Evolution*, ed. C. Chiosi and R. Stalio (Dordrecht: Reidel), p. 319.
- Schönberner, D. 1979, *Astron. Astrophys.*, **79**, 108.
- Seeger, P. A., Fowler, W. A., and Clayton, D. D. 1965, *Ap. J. Suppl.*, **11**, 121.

Sweigart, A. V. 1974, *Ap. J.*, **189**, 289.

Truran, J. W., and Iben, I., Jr. 1977, *Ap. J.*, **216**, 797.

Ulrich, R. K. 1973, in *Explosive Nucleosynthesis*, ed. D. N. Schramm and
W. D. Arnett (Austin: University of Texas Press), p. 139.

———. 1982, in *Essays in Nuclear Astrophysics*, ed. C. A. Barnes, D. D. Clayton,
and D. N. Schramm (New York: Cambridge University Press), p. 301.

FIGURE CAPTIONS

Fig. 1.—Neutron density N_n (in cm^{-3}) as a function of mass coordinate M_r (in M_\odot) and time t (in years).

Fig. 2.—Histogram of exposures undergone by test particles for the time-dependent calculation, using a bin size of 0.02 mb^{-1} . $\phi(\tau)d\tau$ is the number of particles which experience a neutron exposure between τ and $d\tau$. The dashed curve (bottom exposure scale) corresponds to $\phi(\tau) \propto \exp(\tau/0.26)$, and the dotted curve (top exposure scale) corresponds to a time-independent calculation in which the parameter grid was held at its initial values.

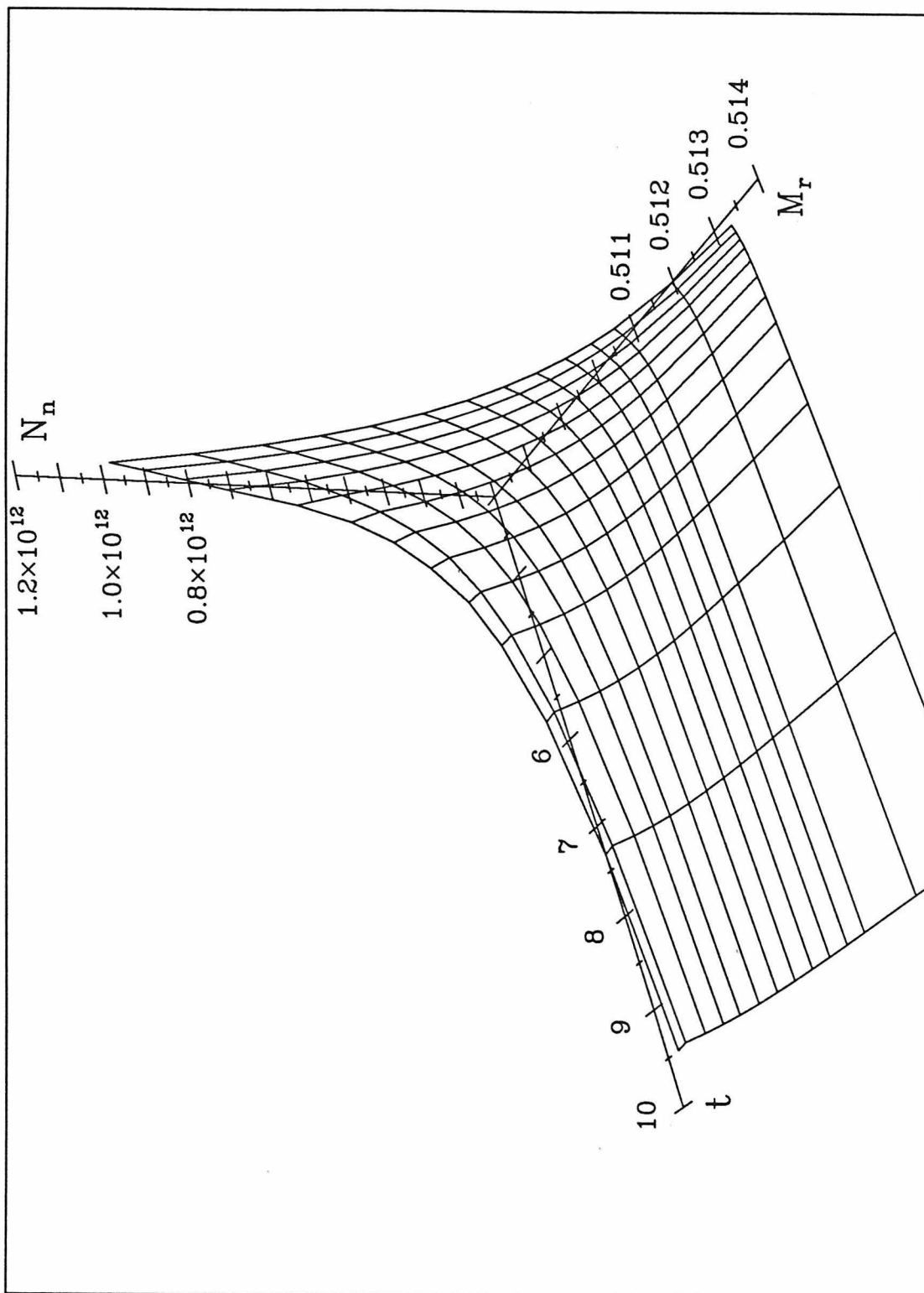


Fig. 1

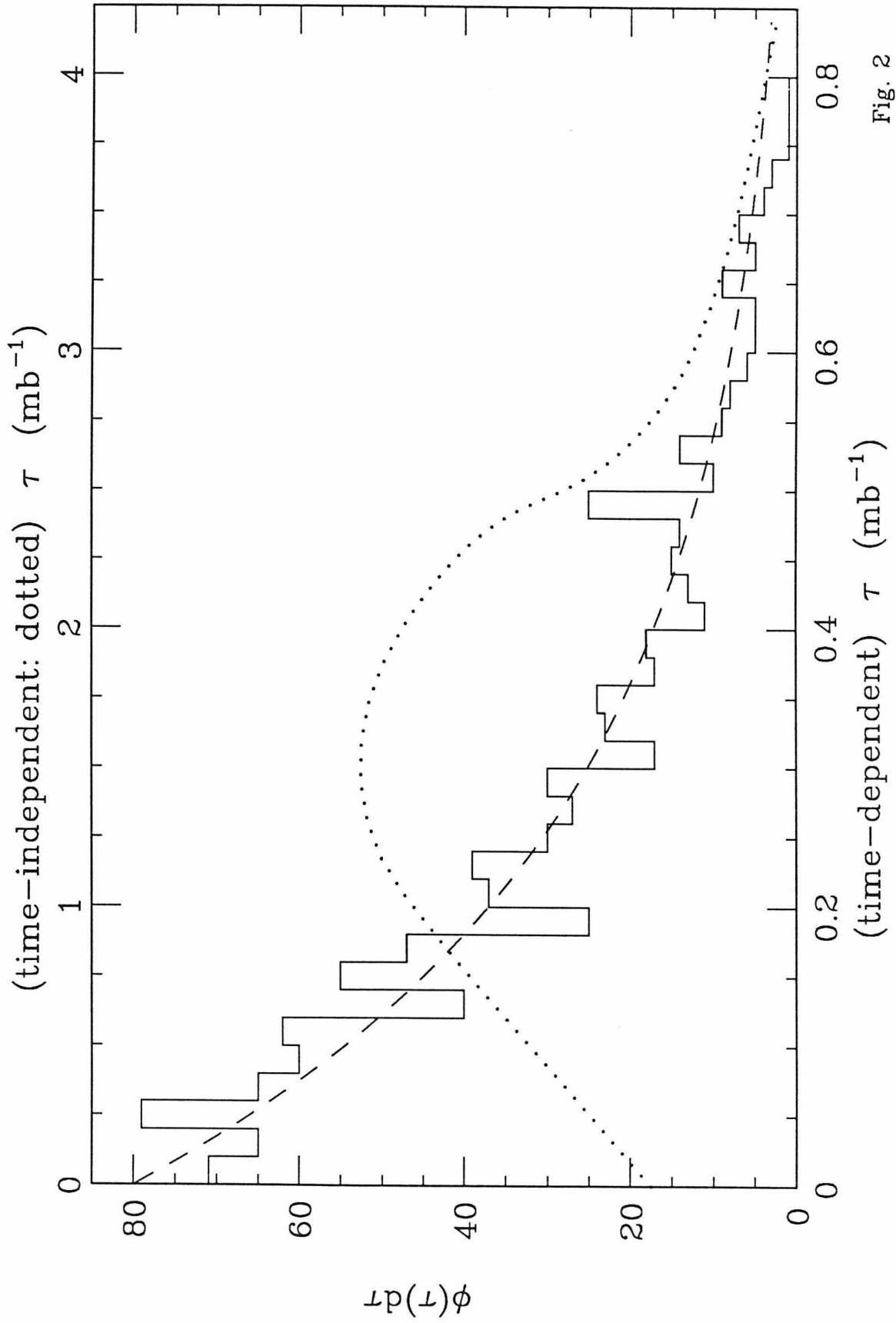


Fig. 2

CHAPTER 7.

SUMMARY AND CONCLUSIONS

Static stellar *envelopes* were computed, using new Los Alamos opacities (including low-temperature carbon and molecular opacities) and including the effects of carbon ionizations, to investigate the effects of large carbon enrichments in the envelope. It was found that the effects of carbon were complicated: it could either increase or decrease the opacity and the depth of convection. For this reason, full stellar evolutionary runs (described below) were necessary to make final statements about the effect of carbon on the depth of envelope convection. On the other hand, it *was* possible to conclude that the effects of carbon are not minor: large shifts in the H-R diagram could be produced.

Detailed stellar evolutionary computations were carried out for a *metal-poor* case ($Z = 0.001$) for stars of initial masses $M_i = 0.8 M_\odot, 1.0 M_\odot, 1.2 M_\odot, 2.0 M_\odot,$ and $3.0 M_\odot$, and for a *solar metallicity* case ($Z = 0.02$) for stars of $M_i = 1.2 M_\odot$ and $3.0 M_\odot$. The stars were evolved from the main sequence through the red giant branch (RGB), including the helium core flash that occurs in stars of $M_i \lesssim 2 M_\odot$, through core helium-burning on the horizontal branch, and finally through a number of helium shell flashes (thermal pulses) on the asymptotic giant branch (AGB). Mass loss via a Reimers-type stellar wind was included on the RGB and the AGB. The most up-to-date Kellogg nuclear reaction rates were used, with screening corrections at high densities. The latest Los Alamos opacities were used, including low

temperature carbon opacities and some molecular opacities; thermodynamic effects of carbon and oxygen ionizations were taken into account. A detailed treatment of convection and semiconvection was included.

Breathing pulses were found during core helium-burning on the horizontal branch, in which the central convective core rapidly engulfs a large amount of the surrounding helium-rich region, resulting in a sudden large increase in the central helium abundance and a rapid loop in the H-R diagram. On the AGB at the height of the post-flash expansion, a semiconvective region was found to be associated with the tip of the flash-produced intershell carbon pocket (in the low- Z stars) that could be capable of mixing small amounts of hydrogen downward. This would result in ^{13}C -production; since relatively small amounts of hydrogen would be present in a carbon-rich region, much of the ^{13}C produced by the $^{12}\text{C}(p, \gamma)^{13}\text{N}(, e^+\nu)^{13}\text{C}$ reaction would *not* be destroyed by the $^{13}\text{C}(p, \gamma)^{14}\text{N}$ reaction. (Note that the CNO-equilibrium $^{13}\text{C}/^{12}\text{C}$ ratio is roughly $\frac{1}{4}$.) When this ^{13}C was mixed down into the next flash-driven intershell convective region, some s -processing could take place via the $^{13}\text{C}(\alpha, n)$ neutron source (although not very much, unless rather more hydrogen were mixed down by semiconvection than seems probable from our results).

The most up-to-date Kellogg nuclear reaction rates were used, including the new $^{12}\text{C}(\alpha, \gamma)^{16}\text{O}$ rate (increased by a factor of 3): this resulted in carbon-poor, oxygen-rich cores ($C \sim 20\%$, $O \sim 80\%$), but had little effect on the abundances in the flash-produced carbon pocket ($C \sim 20\%$, $^{16}\text{O} \sim 2\%$), nor did the increased ^{16}O production result in any significant ^{20}Ne -production via the $^{16}\text{O}(\alpha, \gamma)^{20}\text{Ne}$ reaction.

Note that the ^{13}C -production mentioned in the previous paragraph would *not* be prevented by ^{18}O grabbing all the mixed-down hydrogen, since it was found that most of the ^{18}O produced during the flash from ^{14}N was converted to ^{22}Ne .

Another recently revised nuclear reaction rate was that of the $^{14}\text{N}(p, \gamma)^{15}\text{O}$ reaction, the basic rate-determining reaction of the CNO-cycle. Most of the stellar evolutionary runs were performed with a rate *reduced* by a factor of 2; but more recent information indicated an *additional increase* of a factor of 3 to 4 superimposed on this at astrophysical energies (leading to an increase of a factor of 1.5 to 2 over the *original* rate). One evolution (namely $M_i = 3.0 M_\odot$, $Z = 0.02$) was carried out with the latter new, increased $^{14}\text{N}(p, \gamma)^{15}\text{O}$ rate; this turned out to have surprisingly little effect, yielding changes of no more than a few percent in the star's evolution as compared to evolution using the low $^{14}\text{N}(p, \gamma)^{15}\text{O}$ rate. The *most recent* information, received after all computations of the present had been completed and analyzed, indicates that the *correct* $^{14}\text{N}(p, \gamma)^{15}\text{O}$ rate is actually very close to the original rate.

The Reimers wind produced major mass loss on the RGB for all low mass stars ($M_i \lesssim 1.2 M_\odot$), namely 41%, 24%, and 14% for stars of $Z = 0.001$ with $M_i = 0.8 M_\odot$, $1.0 M_\odot$, and $1.2 M_\odot$ respectively, and 29% for a star of $M_i = 1.2 M_\odot$, $Z = 0.02$; with the mass loss rate used in this work, the $0.8 M_\odot$, $Z = 0.001$ star left the RGB to become a white dwarf, without ever encountering the core flash and subsequent helium burning stages. The above amounts of mass loss were obtained using mass loss normalization $\eta = 0.4$ with mixing length parameter $\alpha = 1.0$, and

turn out to be an overestimate by nearly a factor of 2: the *correct* choice of the value of η turns out to depend strongly on the choice of α (namely, $\eta \propto 1/\alpha$) and on the stellar opacities, since these affect the stellar radius and thus the mass loss rate.

The Reimers wind produced major mass loss during the helium shell flash AGB stage for stars of *all* masses. For stars of $M_i < M_{WK}$, even the *corrected* Reimers wind (reduced by a factor of about 2) was found to be sufficient to account for the entire mass loss needed to satisfy the initial–final mass relation discovered by Weidemann and Koester: $M_{WK} \sim 1.5 M_\odot$ for $Z = 0.001$, but for $Z = 0.02$ the value of M_{WK} is only constrained to lie in the interval $1.2 M_\odot < M_{WK} < 3 M_\odot$ by the results of the present work. For higher mass stars ($M_i > M_{WK}$), additional mass loss such as a superwind must be invoked.

For low mass stars, the onset of the helium shell flashes takes place at a considerably lower core mass and luminosity than obtained from the interpolated Iben and Renzini relation, by as much as $\Delta M_{\text{bol}} \sim 1.5$ for $Z = 0.02$. For $Z = 0.001$, flashes began at higher luminosity than for $Z = 0.02$, but still at lower luminosity than indicated by the Iben and Renzini relation. This earlier flash onset allows flashes time to build up before the star reaches a luminosity where observations indicate that it should become a carbon star. In addition, the point at which flashes begin varies much less steeply with the initial stellar mass for high- Z stars than for low- Z stars.

It was shown that the previously-established core mass–luminosity ($M_c - L$) relations could *not* be extended to the low mass stars, as is frequently done. For the

helium shell flash AGB stage, the $M_c - L$ relation for the case of solar metallicity ($Z = 0.02$) was $L = 52000(M_c - 0.456)$ for $0.52 M_\odot \lesssim M_c \lesssim 0.7 M_\odot$. It was also noted that the $M_c - L$ relation is composition-dependent; namely $L \propto \mu^3 (Z_{\text{CNO}})^{1/25}$. The RGB also has an $M_c - L$ relation, namely $L = (6.86 M_c)^7$ for $Z = 0.02$ and $0.3 M_\odot \lesssim M_c \lesssim 0.45 M_\odot$, with a composition dependence $L \propto \mu^7 (Z_{\text{CNO}})^{1/12}$. It was found that the core mass–interflash period relation was also composition dependent, differing by about a factor of 2 between the two compositions.

On the AGB, helium shell flashes cause the star to spend as much as 20–30% of its time at a luminosity a factor of 2 lower than that given by the $M_c - L$ relation. They also cause a relatively short-lived luminosity increase by a factor of 2; this could cause the star to encounter dynamic envelope instability and envelope ejection at a core mass lower by $\Delta M_c \sim 0.1 M_\odot$ than would otherwise be the case. Radius variations of the same size also occur, in phase with the luminosity variations; the fastest of these variations (timescales of years to decades) are perhaps on the verge of being observable, but would be exhibited by fewer than one AGB star in a thousand.

The helium flash strength $L_{\text{He}}^{\text{max}}$ grows much faster and reaches much higher flash strengths ($L_{\text{He}}^{\text{max}} \sim 10^8 L_\odot$) for low metallicity stars, as compared with stars of solar metallicity. $L_{\text{He}}^{\text{max}}$ grows linearly with core mass for each star, showing *no* signs of leveling off even after 10 or 20 flashes: there is *no* evidence of any universal curve giving $L_{\text{He}}^{\text{max}}$ as a function of core mass M_c , even at a fixed metallicity. This means that *misleading* results can be obtained if one arbitrarily adds or subtracts mass to

the envelope of a given stellar model in the hopes of simulating the behavior of a star with a *different initial mass* without going through its prior evolution: such a short-cut has frequently been employed, by a number of investigators.

The maximum temperature T_b^{\max} at the base of the flash-driven intershell convective region is crucial for *s*-process nucleosynthesis. An $M_c - T_b^{\max}$ relation was obtained for low core masses M_c ; previous extrapolations to low M_c turned out to be inappropriate. Malaney's associated calculations based on this new relation indicate that neither the $^{22}\text{Ne}(\alpha, n)$ nor the $^{12}\text{C}(\alpha, n)$ neutron source yields a solar system *s*-process abundance distribution in a star of $M_c \lesssim 0.7 M_\odot$. They also demonstrate that time variation of temperature and density during a single flash (from the present work) *could* produce an exponentially weighted distribution of neutron exposures via $^{12}\text{C}(p, \gamma)^{13}\text{N}(, e^+\nu)^{13}\text{C}(\alpha, n)$, if a case occurred where the *last* shell flash causes the remaining hydrogen-rich envelope to be engulfed by flash convection. (Normally this observationally-required exponentially-weighted distribution can only be obtained via repeated flashes.)

Two *low-luminosity carbon stars* were achieved, in good agreement with observations; the mechanism turned out to be *classical third dredge-up*. One star of initial mass $M_i = 2.0 M_\odot$ and $Z = 0.001$ first encountered dredge-up after the 11th flash (of strength $L_{\text{He}}^{\max} = 7 \times 10^7 L_\odot$); the dredged-up carbon immediately resulted in a carbon star, increasing the envelope metallicity Z by 70%. The pre-flash luminosity was $\log(L/L_\odot) = 3.95$ (i.e., $M_{\text{bol}} = -5.11$); the long-lived post-flash luminosity dip reduced it to $\log(L/L_\odot) = 3.78$ (i.e., $M_{\text{bol}} = -4.68$). The current total mass was

$M_{\text{tot}} = 1.72 M_{\odot}$ with core mass $M_c \equiv M_{\text{H}} = 0.665 M_{\odot}$; the mixing length parameter was $\alpha \equiv l/H_p = 1.5$, producing $\log T \approx 6.5$ at the base of the convective envelope during dredge-up. The other star, of $M_i = 1.2 M_{\odot}$ and $Z = 0.001$, first encountered dredge-up after the 6th flash ($L_{\text{He}}^{\text{max}} = 3 \times 10^7 L_{\odot}$), increasing envelope Z by 120%. The pre-flash luminosity was $\log(L/L_{\odot}) = 3.65$ (i.e., $M_{\text{bol}} = -4.35$); the post-flash dip reduced this to $\log(L/L_{\odot}) = 3.34$ (i.e., $M_{\text{bol}} = -3.59$). The current mass was $M_{\text{tot}} = 0.81 M_{\odot}$ with $M_c = 0.566 M_{\odot}$; for this star, a value of $\alpha = 3.0$ was required to obtain dredge-up (and $\log T \approx 6.5$ at the base of the convective envelope), no dredge-up being found for $\alpha \leq 2.0$. Neither star experienced a second dredge-up episode, due to the large increase in envelope metallicity and the reduction of the envelope mass due to the stellar wind.

All of the evolutionary runs initially had $\alpha = 1.0$, and *no* carbon dredge-up was ever found using this value of α . A value of $\alpha \gtrsim 1.5$ appeared to be a *necessary* condition to produce the observed low-luminosity carbon stars via dredge-up in low mass stars. An increased value of α made dredge-up easier by causing the envelope convection to reach inward to higher temperatures. Other conditions that we found to be favorable to dredge-up and carbon star formation are (i) *a relatively large envelope mass*, which caused envelope convection to reach inward to higher temperatures; (ii) *a low metallicity*, which had a similar effect on the depth of envelope convection, as well as causing stronger flashes; and (iii) *high flash strength*, which caused expansion of the carbon pocket out to cooler temperatures. We found that *mass loss opposed dredge-up*, by reducing the envelope mass and by severely limiting total number of flashes that could occur. Both wind mass loss and the

increase in metallicity due to dredge-up acted to reduce the number of *repeated, successive* dredge-up episodes that could occur. Finally, for $Z = 0.001$, it was found that only stars of $M_i \lesssim 2 M_\odot$ experienced flashes at a low enough core mass to become carbon stars while still satisfying the observational initial–final mass relation discovered by Weidemann and Koester. In other words, this relation implied that stars of $Z = 0.001$ of initial mass $M_i \gtrsim 3 M_\odot$ must lose their entire envelopes and leave the AGB at a time when they have encountered only a few flashes or none at all: such stars thus would *not* become high-luminosity carbon stars.